EQUILIBRIUM ANALYSIS OF MASONRY DOMES

by

Wanda W. Lau

B.S., Civil Engineering
Michigan State University, 2002

Submitted to the Department of Architecture
in Partial Fulfillment of the Requirements for the Degree of

Master of Science in Building Technology

at the

Massachusetts Institute of Technology

June 2006

Signature of Author.....
Department of Architecture
May 25, 2006

Certified by .....
John A. Ochsendorf
Assistant Professor of Building Technology
Thesis Supervisor

Accepted by .....
Yung Ho Chang
Chair of the Committee on Graduate Students

EQUILIBRIUM ANALYSIS OF MASONRY DOMES

by

Wanda W. Lau

Submitted to the Department of Architecture
on May 25, 2006 in partial fulfillment of the
requirements for the Degree of Master of Science in
Building Technology

ABSTRACT

This thesis developed a new method to analyze the structural behavior of masonry domes: the modified thrust line analysis. This graphical-based method offers several advantages to existing methods. It is the first to account for the ability of domes to achieve a range of internal forces, gaining potentially an infinite number of equilibrium solutions that could not be derived otherwise. This method can also analyze non-conventional axisymmetrical dome geometries that are difficult or impossible to analyze with existing methods.

Abiding by limit state conditions and the principles of the lower bound theorem, the modified thrust line method was used to ascertain the theoretical minimum thrust of spherical and pointed domes, a parameter that was previously unsolved. Several methods to estimate minimum thrust-to-weight ratio were provided. For spherical domes, this ratio may be estimated as $-0.583\alpha + 1.123$; for pointed domes, the estimated ratio is $0.551\delta - 1.061\delta/\alpha - 0.615\alpha + 1.164$, where α and δ are the embrace and truncating angles, respectively. From the results, salient relationships between minimum thrust and dome geometry were derived, including an inverse relationship between the minimum thrust and the thickness-to-radius ratio, angle of embrace, and, for pointed domes, the truncation angle of the crown for a constant angle of embrace.

The capabilities of the modified thrust line method were demonstrated in two masonry dome case studies that existing methods could not successfully analyze. The potential of this method to predict the ultimate load capacity of masonry domes was also explored. The method over-predicted the capacity of two small-scale masonry domes loaded to failure by a concentrated applied load at the crown; however the small size of the domes compared to real-world domes suggested that scale effects may have influenced their behavior.

Finally, interactive geometry programs of the modified thrust line method and other existing graphical analysis methods were created to disseminate these illustrative tools to understanding the structural behavior of masonry domes.

Thesis Supervisor: John A. Ochsendorf

Title: Assistant Professor of Building Technology

Acknowledgements

I am grateful to many people without whom this thesis would be incomplete and nowhere as long.

First, to my graduate adviser, instructor and mentor, John Ochsendorf, whose guidance, expertise, and enthusiasm inspired me to continually strive for more answers and subsequently more questions. His passion in his work and in life is a paradigm for those around him.

I thank two former graduate student colleagues, Michael Ramage and Barbara Cipriani. Michael's interests in timbrel vaults and his initiative provided me the wonderful opportunities to collaborate on masonry dome projects both in England and in MIT. Barbara, who has detailed knowledge and resources in Mamluk dome architecture, in addition to a unique sense of humor, was invaluable to my research in pointed domes.

To Jack Germaine and Steve Rudolph, I am grateful for their patience and generosity in providing the use of the space and test equipment in the civil engineering laboratory and machine shop, and for their advice and knowledge in all things pragmatic.

I am grateful to Patrick Underhill, without whom I would not have a properly placed recursive function.

In addition, I thank my colleagues in the Building Technology Research Laboratory, who made the long hours much more fun. In particular, I thank Phillipe Block, who introduced me to the world of *Cabri*, and Matthew Hodge, whose assistance and company in the second AAC dome construction, made the time pass faster.

To my parents, Ying and Choi Lau, and my sister, Miranda, I thank them for their love, support, and continual correspondence.

Finally, I thank Michael Rappel for providing me the shoulders on which to climb and see the view from above.

Biographical Note

Born and raised in southeast Michigan, I attended Michigan State University in East Lansing, Michigan, between 1998 and 2002. In 2000, I published my first paper in *The Michigan Academician* written under the supervision of Joanne Westphal. In May 2002, I graduated with high honors with a Bachelor of Science in civil engineering. From June 2002 to 2004, I worked as a consulting engineer for Simpson Gumpertz and Heger, Incorporated, currently based in Waltham, Massachusetts. In September 2004, I began my graduate studies in the Building Technology department at the Massachusetts Institute of Technology in Cambridge, Massachusetts, under the advisement of John Ochsendorf. At MIT, I was granted a Presidential Fellowship, and I was a teaching assistant to graduate students. In 2006, I co-authored a conference paper that is published in *Proceedings of the Second International Congress on Construction History*.

Table of Contents

Preface

Dome of Farag Ibn Barquq, Cairo, Egypt Photograph courtesy of the Egyptian Council of Antiquities (c. 1970)

In northeast Cairo, the dome of the Mausoleum of Farag Ibn Barquq has stood over the city for the past 600 years—but no one has explained how. Constructed of intricately carved stone masonry, the dome spans an astounding 47 ft at its base and has a thickness of less than 15 in. Its structural elegance is further accentuated by the 20-ft high cylindrical wall of equal slenderness on which the dome sits. The dome has no metal reinforcing despite the insistence of existing structural analysis methods that tensile reinforcement is critical to the dome's stability. Yet the dome stands.

This thesis describes a new method of masonry dome analysis that explains *how*.

Chapter 1. Introduction

A curve rotated about a central axis to form a surface typically used as a roof creates a dome. The curve may assume an infinite number of shapes with different geometric parameters, such as its span, rise, center(s) of curvature, and radius and direction of curvature. Though it has potential application to domes of unconventional geometries, this thesis primarily considers domes with one or two centers of curvature, and positive Gaussian curvature[1].

Dome vaults made possible construction beyond the orthogonal or rectilinear roof plan, creating high, clear spaces with open floor plans. The first known dome constructions, dating back to fourteenth and twelfth centuries B.C., are located in disparate regions around the world in what is today Greece, China, Egypt, and India. Often integrated with the natural terrain, these ancient structures were constructed from cutout rock, sun-dried mud, or stone, and had funerary or utilitarian purposes such as defense, shelter, storage and kilns (Melaragno 1991).

One of the first known domes, the Treasury of Atreus, Mycenae (c. 1325 B.C.), features corbel construction in which masonry courses are dry laid in concentric rings from the base to crown with horizontal bed joints and vertical head joints without centering (Fig. 1.1).

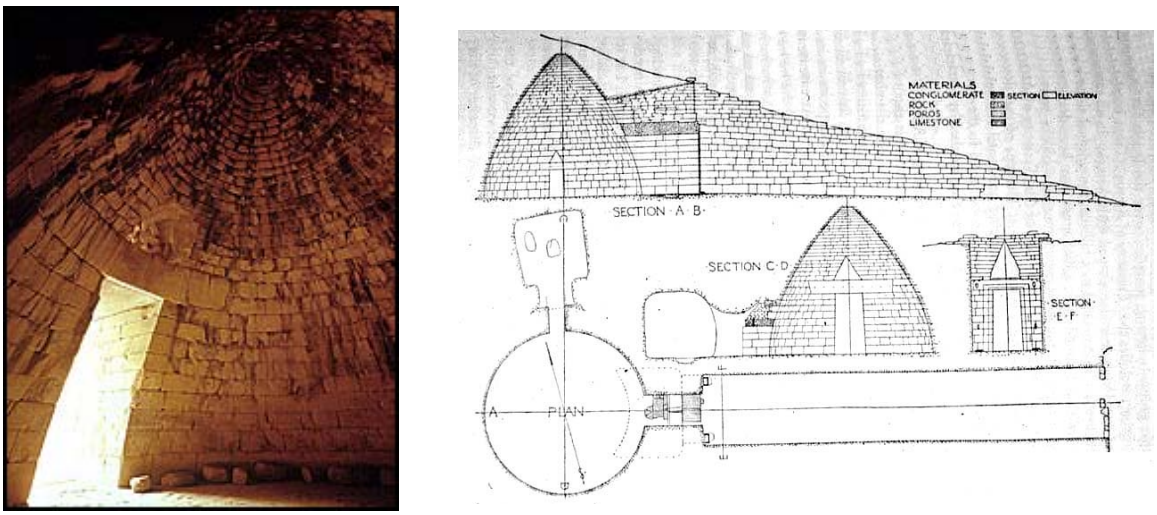

Figure 1.1. The corbel dome of the Treasury of Atreus in Mycenae is one of the oldest remaining domes. Left: figure from Walling (2006). Right: figure modified from Hanser (2003).

[1] Gaussian curvature is the product of the principal curvatures, $k_1 k_2$, of a surface. A surface with positive Gaussian curvature signifies that a tangent plane intersects the surface at only one point, as in the case of a sphere. A surface with negative curvature signifies a tangent plane would intersect the surface, as in a saddle curve.

Prior to the turn of the first century, bed joints in the concentric rings in trulli, stone structures covered with pointed stone domes in southern Italy, began to incline inward with the geometry of the curve (Melaragno 1991). As dome construction continued to evolve, techniques such as "cohesive" masonry construction, reinforced concrete, double shell, and thin shell construction made possible the magnificent domed structures later constructed (Fig. 1.2).

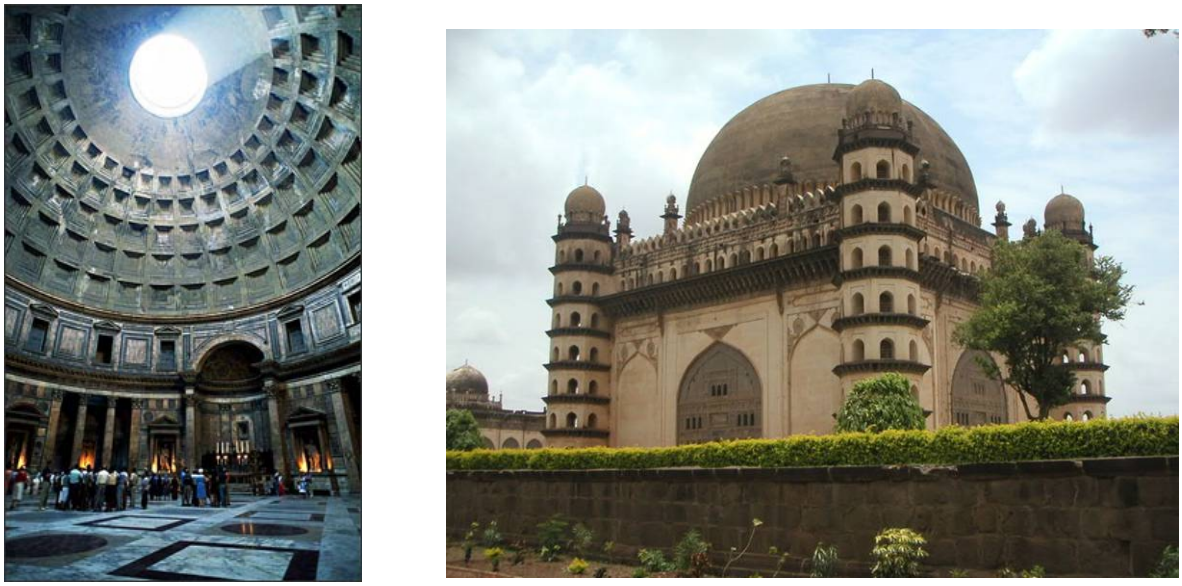

Figure 1.2. Left: Interior of the Pantheon in Rome (120 – 124 A.D.) (photograph by Ruggero Vanni); Right: Exterior of Gol Gumbaz, the Tomb of Muhammad Adil Shah, in Bijapur, India (1627 – 1656 A.D.) (photograph from Crave Services)

1.1. Fundamental Structural Behavior

Dome structures must provide strength, stiffness, and stability (Heyman 1995). They must be capable of supporting applied loads and self weight without excessive deflection and unstable displacements. Similar to an arch, a dome develops internal meridional forces that transfer loads to a support structure at its base. These forces are compressive and increase in magnitude from the crown to the base for any dome loaded axisymmetrically by self weight (Fig. 1.3).

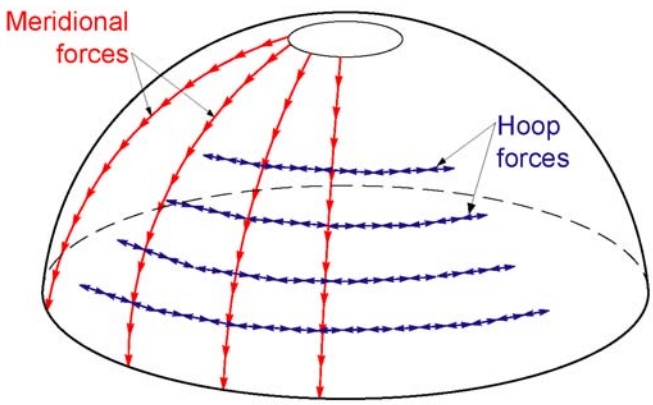

Figure 1.3. Domes develop internal meridional forces and hoop forces.

Unlike an arch, a dome can resist out-of-plane bending of the meridians by developing internal hoop forces that act in the latitudinal direction as parallel rings. Hoop forces allow ring-by-ring construction of a dome without centering, an unfeasible task for an arch. As a result, though an arch is unstable without its keystone, a dome with an oculus is perfectly stable, as evidenced by the "incomplete" domes around the world, such as the Pantheon in Rome.

The line of thrust, or funicular polygon, is the path on which internal forces in a structure transport external loads to the supports. The funicular polygon represents the line of thrust in which internal forces are axial; this may be envisioned as a string loaded with weights corresponding to the loads of the structure. For traditional masonry domes, the predominant applied load is self weight; thus this thesis primarily considers domes loaded only by gravity loads. When inverted, this hanging string model may represent the line of thrust in compression for an upright arch or dome structure as Poleni demonstrated in 1748 (Fig. 1.4).

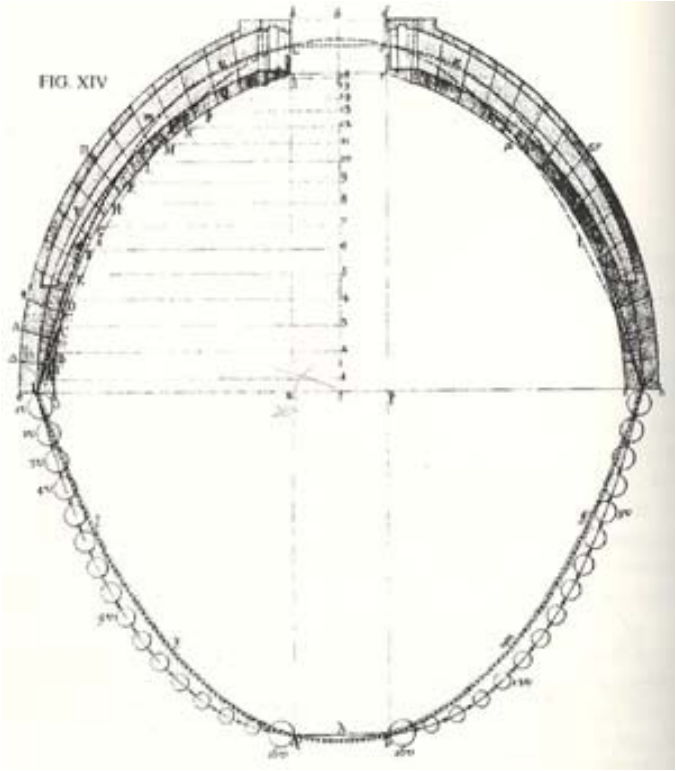

Figure 1.4. Poleni illustrated that the line of thrust is a funicular polygon that may be envisioned as an inverted string loaded with weights for the dome of St. Peter, Rome (from Heyman 1996).

At the base of a dome, the support structure must resist the inclined loads from the dome with equal and opposite reactions (Fig. 1.5). The support structure typically resists the vertical component of the inclined force with ease. However, the dome and support structure must also resist the horizontal component, the outward thrust, particularly near the base of the dome where total thrust is greatest. External means of resistance may be employed, such as massive support structure walls, as used in the Roman Pantheon, or a metal tension ring around the dome's base.

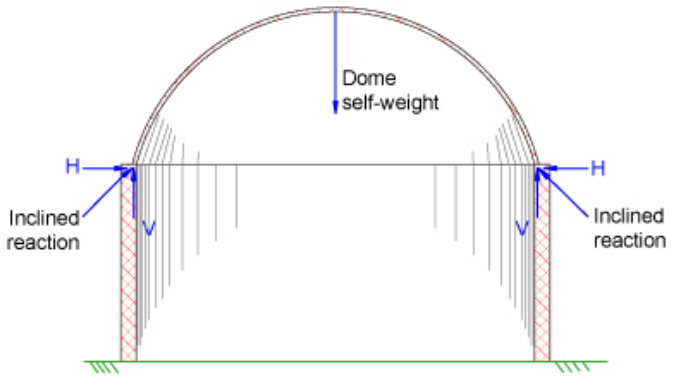

Figure 1.5. The support structure must resist applied and gravity loads with equal and opposite reactions.

Though the methods it describes could be applied to steel or reinforced concrete domes, this thesis focuses on new ways to analyze masonry domes, and abides by the classical Heyman (1995) limit analysis conditions:

1. Masonry has no tensile strength.
2. Masonry has virtually infinite compressive strength compared to the low internal stresses that a structure develops relative to the failure strength of masonry.
3. Sliding failure does not occur.

The upper bound for masonry is defined by the uniqueness theorem:

> If a line of thrust can be found which represents an equilibrium state for the structure under the action of the given external loads, which lies wholly within the masonry, and which allows the formation of sufficient hinges to transform the structure into a mechanism, then the structure is on the point of collapse; … the value of [the] load factor at collapse is unique. (Heyman, 1996, p. 6)

Local or comprehensive failure of domes may result from the masonry's inability to resist tensile or bending forces that develop due to unanticipated loads on the dome. A typical failure or collapse mechanism consists of: first, the formation of radial cracks along its meridians that divide the dome into lunes, or pie-shaped arches (Fig. 1.6).

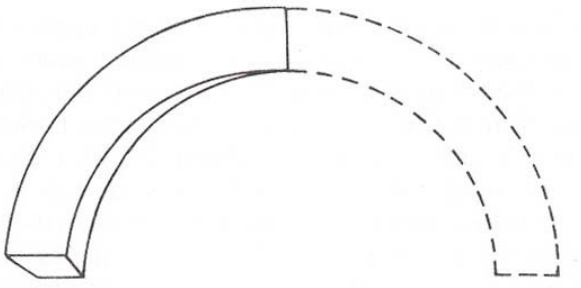

Figure 1.6. The dome may be considered as a radial series of lunes that comprise the dome (from Heyman 1977).

Second, two hinge circles form in the dome mid-section, with a third hinge circle formation at or near the base. The cap of the dome will fall straight down, while the base of the lunes, as defined by the radial cracks, will rotate outward (Fig. 1.7).

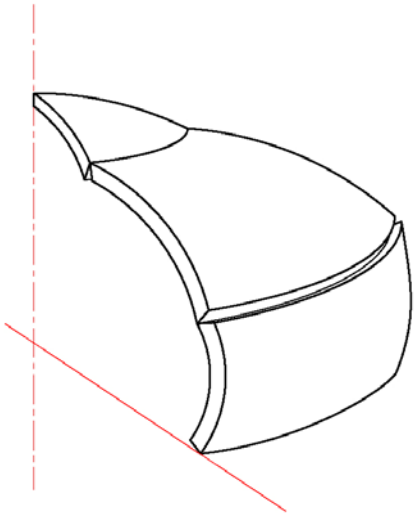

Figure 1.7. Typical collapse mechanism for a dome

1.2. Literature Review

In the mid-eighteenth century, Poleni was one of the first recorded to formally analyze domes when he used static analysis to assess meridional cracks in the dome of St. Peter's, Rome. Applying Robert Hooke's discovery that a hanging chain model represents an inverted force line of a structure in compression, Poleni correctly concluded that the line of thrust for the dome's load conditions remained within the effective thickness of the structure, rendering the dome as safe (Fig. 1.4). However, this lower bound approach was conservative because the hanging chain represented forces in only two dimensions: hoop forces in the third dimension would have further assured the dome's stability.

In 1866, Johann Schwedler presented the membrane theory, which provided the basis for preliminary mathematical equations later published by other authors, including Rankine (1904). The membrane theory makes four primary assumptions (Billington 1982):

1. Applied loads are resisted by internal forces within the surface, which has no stiffness against bending; therefore internal forces are either pure tension or pure compression.
2. On a symmetrically and uniformly loaded dome, internal forces act perpendicularly to each other in the meridional and latitudinal, or hoop, directions.
3. Internal forces are coplanar; that is, the membrane has zero thickness.

4. The membrane plane is located along the centerline of the dome's effective thickness; thus the lines of thrust must also lie on this median surface.

The latter two assumptions, which constrain the location of the thrust line to the median radius and reduce the dome's thickness to zero, limit hoop force values to those needed to equilibrate meridional forces; as a result, the membrane solutions tend to underestimate the dome's ability to attain stability. In addition, the equations, limited in versatility, are difficult to apply to domes with unconventional geometries and conditions. This thesis elaborates further on these limitations in later chapters.

Around the turn of the twentieth century, engineers and architects used graphical analysis methods in conjunction with basic equilibrium equations to design and analyze domes. In 1877, Eddy published a method of graphical analysis specifically for masonry domes based on the funicular polygon, detailed in Section 2.1. Eddy identified that, for a hemispherical dome loaded axisymmetrically, the transition between compressive hoop forces near the crown and tensile hoop forces near the base occurs at 51°49' from the axis of rotation. Below the "point where the compression vanishes (and) we shall not assume that the bond of the masonry is such that it can resist the hoop tensions which is developed," Eddy limited the thrust line to lie within the middle third in order for the "upper part of the dome [to] be then carried by the [lower part] as a series of masonry arches standing side by side" (Eddy 1877, pp. 56-57).

The middle-third rule states that a satisfactory design is obtained when the thrust line lies within the middle third of a structure's effective thickness. Should the thrust line pass outside this region, the elastic bending theory assumes that the section will experience tensile forces that may separate the masonry voussoirs (Heyman 1982). Though it remains a built-in safety factor in masonry construction today, the rule presumes purely linear-elastic behavior of the masonry. In actuality, the state of a structure constantly changes due to environmental factors or settlement, and thus "the imperfections of the real world … would make it … unlikely that linear elastic behavior will actually occur" (Heyman 1982, p. 24). Thus elastic analyses, including one posed by Navier in the mid-nineteenth century, are inaccurate in gauging masonry dome behavior. For example, the membrane theory, a lower bound method within the framework of limit analysis,

makes no assumptions about the elastic properties of the material (Heyman 1995). As a result, Eddy's method is conservative in exploring the theoretical possibilities of masonry domes.

Wolfe (1921) published a graphical method similar to Schwedler's membrane theory-based graphical method that, like the membrane theory, is conservative due to its constraint of the thrust line to the dome's median radius. Section 2.2 describes this method further.

Heyman's limit state assumptions initiated contemporary work in masonry structures using plastic methods of analysis that consider a design satisfactory when the thrust line is contained anywhere in the entire effective thickness of the structure per the safe theorem:

> If a line of thrust can found which is in equilibrium with the external loads and which lies wholly within the masonry, then the structure is safe. …[T]he line of thrust found in order to satisfy the safe theorem need not be the actual line of thrust[.] (Heyman, 1996, p. 6)

However, in a study of the theoretical minimum thickness of masonry domes, Heyman (1977) neglected internal hoop forces to simplify the study, a simplification that later studies also made. Heyman derived the minimum thickness-to-radius ratio, *t/R*, by simplifying the lune analysis to two dimensions and assuming no hoop force transfer between individual lunes (Fig. 1.8). By assuming the dome acts as a radial series of arches, Heyman eliminated the dome's ability to develop stability with its hoop forces anywhere below the dome cap, which may result in a conservative solution.

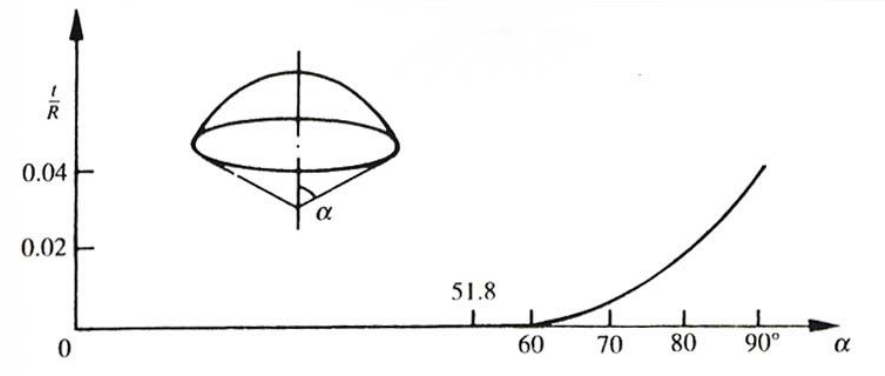

Figure 1.8. The minimum thickness-to-radius of curvature ratio versus angle of embrace for an unreinforced masonry dome structure (Heyman 1995)

Oppenheim et al. (1989) also assumed zero hoop stresses in their derivation of a thrust line surface for a hemispherical and pointed dome under axisymmetrical loading. The resulting thrust line surfaces were not based on the membrane theory, and thus:

> For limit state analysis of masonry shells the admissible membrane force surface should be required only to lie within the shell thickness and admit only compressive forces. There can be more than one such thrust surface, and these in general will differ from the middle surface of the shell. (Oppenheim et al., 1989, pp. 871-872)

Oppenheim et al. used static equilibrium equations to ascertain the minimum *t/R* by assuming the locations of the three hinge points through which the thrust line passes prior to collapse. Using a thickness-to-radius of curvature ratio of 0.05, Oppenheim et al. found a satisfactory thrust surface for hemispherical domes but not for pointed domes (Fig. 1.9).

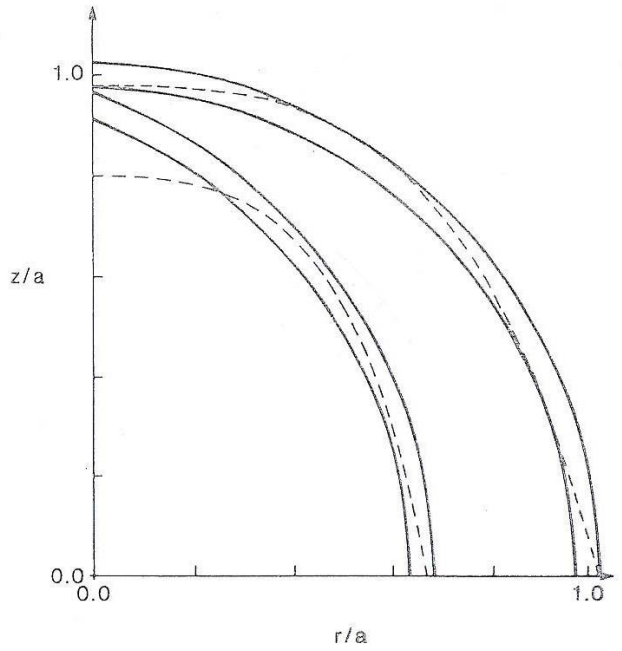

Figure 1.9. Without hoop forces, the thrust line exits the ogival, or pointed, dome section (Oppenheim et al. 1989).

As a side note, the *t/R* ratio for the dome of Farag Ibn Barquq, discussed in the opening paragraph, is less than 0.05. Oppenheim et al. acknowledged the importance of hoop forces in domes, but argued the magnitudes of these forces are very low. Thus, a unified method to establish the minimum thickness of masonry domes with any shape remains unknown to date.

O'Dwyer (1999) used linear programming and geometric constraints to model a masonry dome as a three-dimensional discrete network of forces applied at nodes. However, he limited his discussion to the analysis process, and less on new insights arising from his methodology or detailed analyses of specific dome case studies.

D'Ayala (2001) explored the role of friction-induced tensile strength in masonry domes by investigating the minimum *t/R* for a hemispherical dome under self-weight. She assumed tensile resistance from friction due to internal forces developed between the faces of the masonry voussoirs. Though voussoirs likely develop some friction at their interfaces, the presence of masonry cracks limits the reliability of this resistance. This thesis concentrates instead on the structural limits of domes with minimal or no reliance on direct or indirect tensile strength.

The current prevalent method to design and analyze thin-shell and domes structures is numerical finite element modeling (FEM) computer software. Though several recent studies have attempted to analyze historic masonry structures through FEM, these computer programs tell little more than what the basic membrane and bending theories reveal. For example, Robison (1988) conducted a study on St. Peter's dome using FEM that reaffirmed the stability of the dome: something Poleni demonstrated through his hanging string model.

In addition, the input process for these programs, which may assume nonlinear behavior with either plastic or elastic behavior, is typically laborious, particularly for nonlinear models. Meanwhile the solution is limited in its demonstration of structural behavior, and often includes tensile internal forces, which are inapplicable to masonry construction. Linear elastic results say nothing about potential collapse states. The results can be difficult to interpret correctly while remaining mindful of the associated risks and downfalls of the analysis methods. Too often a solution produced from FEM is quickly accepted as the singular solution when the stresses predicted by linear elastic FEM do not occur in reality.

Methods for finding the upper bound limits of masonry domes remain largely unproven. Through analytical and computational means, several past authors have attempted to estimate upper bound limits of domes by conducting an equilibrium analysis of a structure at incipient collapse. Hodge and Lakshmikantham (1963) assumed limit analysis theorems and the applicability of virtual

work to predict the theoretical yield-point load of rigid, perfectly plastic, axisymmetrical shallow shells; however, their work assumed ductile material behavior that yields in a plastic manner, which is not representative of masonry behavior. Livesley (1992) also used linear programming to model the collapse mode of three-dimensional masonry structures by examining the sliding, twisting and hinging mechanisms of discrete blocks due to foundation movement, but did not examine the limits of applied loads on the dome surface itself.

Save, Massonnet and de Saxce (1997) derived equations through energy balance methods to calculate the critical uniformly distributed load over a horizontal projection of a spherical reinforced concrete shell. Again, their assumption of ductile material behavior limits the equations' use in analyzing masonry structures. In addition, the authors do not discuss the applicability of their method to domes of other shapes, materials and load conditions.

Anselmi et al. (2005) used numerical programming methods to predict the "load collapse multiplier" for masonry structures under limit analysis theorems. They achieved a multiplier for an axisymmetrical dome subjected to dead load, but revealed little about upper bound limits of domes under applied loads, a more relevant scenario for masonry domes. Typically, masonry domes have little problem carrying their own weight if limit state conditions are satisfied.

1.3. Research Objectives

Despite the myriad of existing structural analysis methods and theories, the structural behavior of masonry domes remains relatively obscure. Masonry domes, particularly those with non-spherical geometries, lack a versatile and comprehensive analysis method that fully accounts for their ability to develop forces in three dimensions, and explains the stability of domes that have stood for centuries. Though several studies have explored acceptable dome configurations using the thickness-to-radius parameter, the relation between dome geometry and other theoretical structural limits, including minimum thrust values and safe limits, has been ignored.

The research objectives of this thesis are manifold. First, this thesis introduces a new method of structural analysis developed for masonry domes that has the potential to analyze most, if not all, axisymmetrical dome geometries, including spherical, pointed, and non-conventional geometries.

Chapter 2 describes this new approach, called the modified thrust line method, which has bases in limit analysis, thrust line analysis, and existing graphical analysis methods. The modified thrust line method explores the role of variable internal meridional and hoop forces, in contrast to the fixed values calculated by existing methods, in the behavior and theoretical limits of dome structures.

Second, this thesis derives the minimum thrust of a dome, a structural limit of masonry domes that is currently unsolved. This thesis establishes general characteristics of structural behavior based on geometry by analyzing hundreds of dome geometries with the modified thrust line method. These results have numerous applications, such as the minimum thrust of half-dome buttresses and the stability of a dome's support structure. Chapter 3 discusses these results and notable applications for spherical dome geometries, and Chapter 4 concentrates on pointed dome geometries. Chapter 5 further demonstrates the application of this research by analyzing two specific case studies: the Mamluk dome of Farag Ibn Barquq in Cairo, Egypt, and the domes of the Pines Calyx in Dover, England.

Third, this thesis attempts to establish the modified thrust line analysis as a method to predict upper bound limits of masonry domes of variable geometry and load conditions. Chapter 6 discusses the analysis's potential in the prediction of theoretical upper bound limits for two small-scale masonry dome constructions loaded to failure.

Finally, in conjunction with the above objectives, the author created computer programs, which may be accessed worldwide, to conduct the existing and new graphical analysis methods in real-time. These interactive geometry programs hope to encourage users unfamiliar with the structural analysis of curved masonry surfaces to learn the potential of dome vaults. Targeting the fields of architecture and historic conservation, these programs are an alternative to the complex analysis programs structural engineers primarily use today. To reduce the potential of human error in the interactive programs, the author also created spreadsheet programs that conduct multiple analyses with the new methodology developed herein.

To summarize, this work explores the potential of geometry and structural equilibrium to address lingering questions on the behavior and capabilities of masonry domes.

Chapter 2. Lower Bound Analysis Methods

This chapter begins by explaining the methodology of existing graphical analysis techniques that utilize thrust line principles in masonry dome analysis. The derivation and implementation of these methods, particularly those described in Eddy (1877) and Wolfe (1921), formed the bases for the new structural analysis procedure for masonry domes. The last section of this chapter discusses the assumptions, derivation, and methodology of the modified thrust line method.

2.1. Graphical Analysis of a Dome as a Series of Lunes with No Hoop Forces

In 1877 Eddy published *New Constructions in Graphical Statics*, perhaps the first text in English that included a graphical analysis method specifically for masonry domes. Though Eddy acknowledged the development of internal hoop forces in regions between the dome's crown and base, his method simplified hoop forces to a single value representing the "greatest horizontal thrust which … is possible for any segment of the dome (between the crown and 51°49' from the crown) to exert upon the part below it" (Eddy 1877, p. 56). However, in doing so, Eddy limited internal forces to only two dimensions, and essentially analyzed the dome as an arch. In addition, Eddy's use of the term, "greatest horizontal thrust," is misleading because his method does not calculate the maximum thrust possible in a masonry dome, which theoretically could be infinite. Rather, Eddy calculated a thrust value that is greatest relative to the particular thrust line derived; that is, no other parts of the dome will experience a thrust higher than the value determined in the force polygon corresponding to the particular thrust line. Albeit limited, Eddy's method provided early insight on dome stability and thrust, thrust line geometry, and internal meridional forces.

Due to symmetry, Eddy simplified the analysis to consider only a lune, a representative piece of the dome; this simplification is common in dome analysis, including the one developed in this thesis. To calculate the weight of the lune, Eddy assumed the lune as a series of cones with bases that form the outer surface of the lune and whose heights represent the radius of curvature. If the surface is divided into equal areas, then each cone has the same volume and weight. As a result, the voussoirs into which Eddy further divided the lunes comprise different arc lengths of the dome surface, but have equal weights (Fig. 2.1).

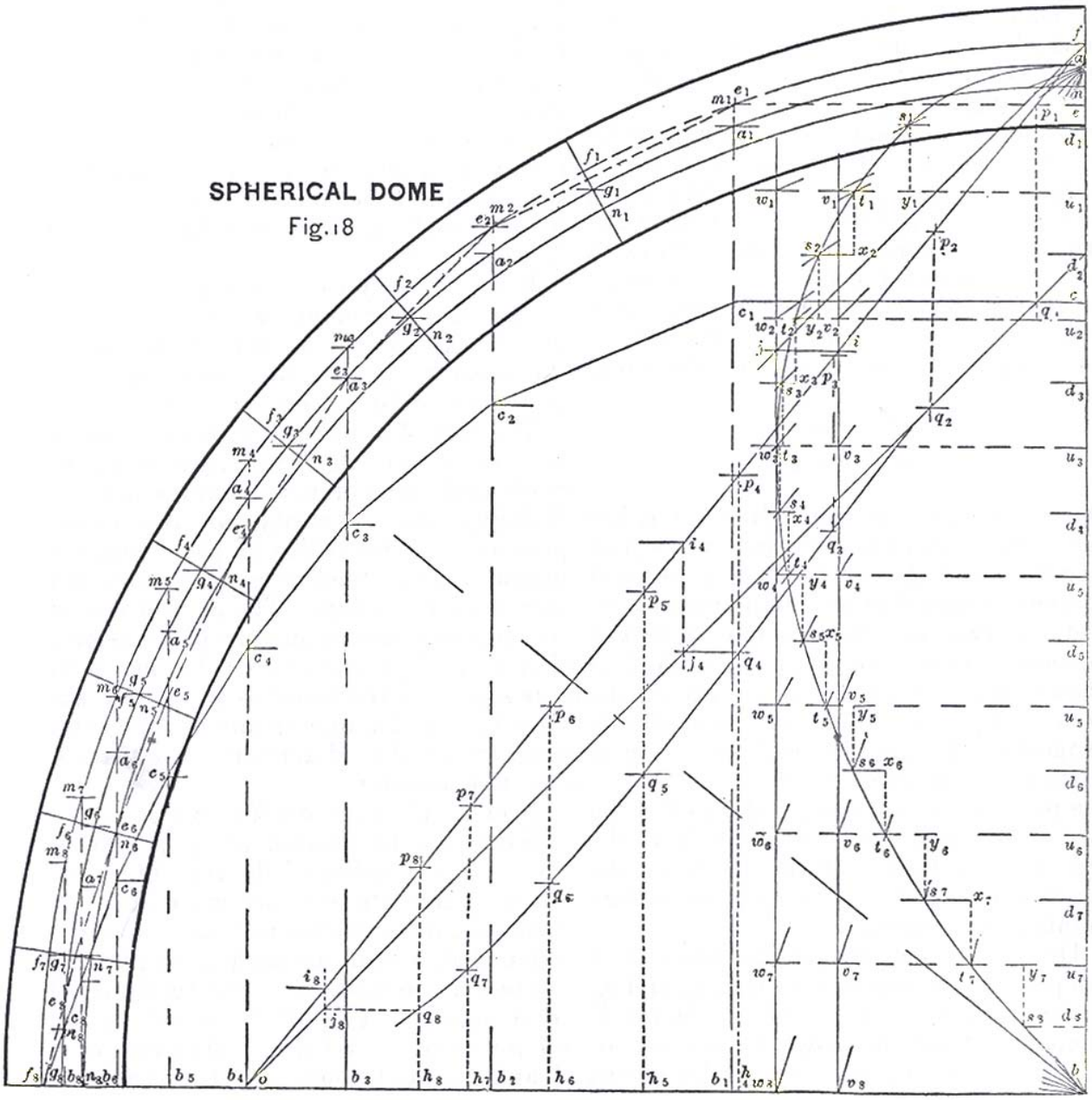

Figure 2.1. Graphical analysis construction by Eddy. The final thrust line curve, *e1e8*, is determined by parallel segments radiating from the pole, *a*, to the final position of the weight line, *w1w8* (from Eddy 1877).

The procedure for conducting the analysis using Eddy's method is straightforward but cumbersome to perform by hand:

1. Draw the lune section and divide it into *n* voussoir divisions; to an extent, the higher the *n*, the more accurate the analysis. Locate the centers of gravity, g_i, of each voussoir *i*.

2. Assume an initial horizontal distance between pole a, at the intersection of the lune's median radius and vertical axis of revolution, and the weight line w_1w_n. This distance represents the magnitude of the horizontal thrust exerted by the lune. Points w_i are collinear with points g_i, and are parallel to the dome's axis of rotation.

3. Draw vertical lines b_ig_i through each voussoir's center of gravity.

4. Connect the pole a and the weight line with segments aw_i. Starting from point f_n at the exterior middle-third of the section at the base, construct the initial funicular polygon cc_n with segments parallel to aw_i between consecutive vertical dividers b_ig_i and $b_{i+1}g_{i+1}$.

5. To estimate the ratio by which to scale the initial thrust line curve cc_n to lie within the middle third of the section "to ensure stability," construct line fo oriented 51.8° from the horizontal, starting at the outer middle-third curve at the dome base (Eddy 1877, p. 57).

6. Draw points m_i at the intersections of the outer middle-third curve and lines b_ig_i. Draw horizontal segments m_ip_i, where points p_i are on line fo.

7. Draw points q_i at the intersections of a horizontal line through c_i and vertical line through p_i. Connect the points to draw curve qq_n and tangent line oq_n.

8. Draw line fj parallel to line oq_n through line w_1w_n. Then draw point i at the intersection of line fo and a horizontal line through point j.

9. Translate the position of the weight line w_1w_n horizontally until it aligns with point i. Construct a new thrust line curve, ee_n, using the revised slopes between the pole a and the revised weight line v_1v_n in a similar manner to the construction of line cc_n. Verify this curve lies within the middle third of the lune's section.

10. Determine the magnitude of the horizontal thrust by multiplying the horizontal distance between pole a and the line v_1v_n by the scale equal to the weight of the lune divided by the length of the weight line.

This method, which was made popular in the early twentieth century by Dunn (1904), was employed by some dome designers, such as Rafael Guastavino, Jr. (Huerta 2003). As an exercise

in the study of existing graphical analysis methods, the author created a program[2] based on Eddy's method using interactive geometry-based computer software[3], thus automating the method's painstaking aspects. The program also reduces human error in constructing the drawings, permits interactive definition of the dome section, and allows the analyst to move, in real-time, the weight line $w_1 w_n$ from the pole a, and see the resulting shape of the thrust line.

2.2. Graphical Analysis using the Membrane Theory

In the 1920s, around the time J. W. Geckeler published a simplified form of the membrane theory equations, Wolfe (1921) published a graphical method for masonry domes in *Graphical analysis: A text book on graphic statics* (Billington 1982). This method, effectively a graphics-based version of the membrane theory, was similar to Schwedler's graphical analysis method published 70 years prior. It fixed internal hoop forces to the values needed to equilibrate the meridional forces and constrain thrust line to the median surface of the dome's thickness. What was significant about Wolfe's approach was its development of a zero-hoop force thrust line path that deviated from the median surface thrust line when tensile strength in the masonry is required. However, this method remains a conservative predictor of dome behavior due to its partial constraint of the thrust line to the median radius.

Like Eddy, Wolfe analyzed the dome as a radial series of lunes; however, Wolfe differentiates the internal force values in the lune through force polygons drawn to scale. The lune is subdivided into n voussoirs a, b, …, x with equal section areas, where x is the n^{th} letter of the alphabet; due to the increasing width of the lune, the weight of each voussoir increases from crown to base. Assuming the dome is loaded axisymmetrically by only self weight, each voussoir experiences five forces: self weight, compressive meridional forces on its top and bottom faces, and coplanar equal and opposite hoop forces on its lateral faces (Fig. 2.2).

[2] Program is available for public use at http://masonry.mit.edu.
[3] *Cabri II Plus*, a graphics-based computer software developed by Cabrilog, is available at www.cabri.com.

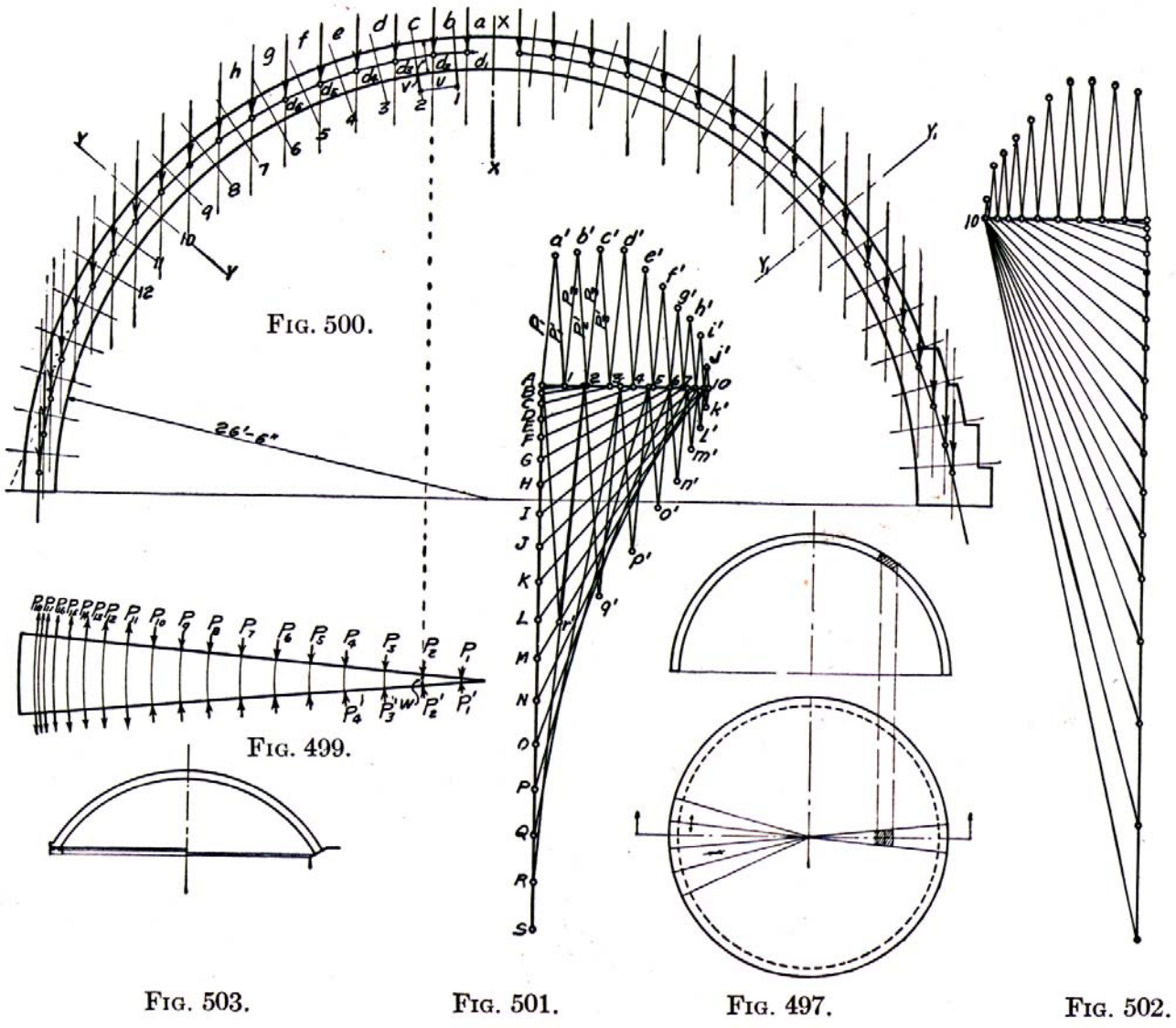

Figure 2.2. Wolfe's graphical analysis method for domes (Wolfe 1921). "Fig. 501" is a force polygon for a lune constructed of material with tensile capacity, such as metal. "Fig. 502" is a force polygon modified for a lune with zero tension capacity.

The procedure to conduct Wolfe's analysis follows:

1. Determine the weight of each voussoir. Assuming the weight acts as a "concentrated force at the centroid of each division," construct the load line of the force polygon with consecutive and joined vertical segments *AB, BC, … , XX*, of lengths scaled proportionally to the voussoir weights and oriented downward to match the direction of gravity loads (Wolfe 1921, p. 251).

2. On the force polygon, draw a horizontal ray through point *A*, which represents the zero vertical load and unknown horizontal reaction at the crown.

3. Draw the median radius of curvature through the lune section.

4. Draw vertical lines through each voussoir's center of gravity. For an angle of the lune in plan less than 15 degrees, the centroids may be approximated to lie on the median surface.

5. On the force polygon, draw segments parallel to the slope of the median surface between consecutive vertical lines through the voussoirs' centroids. The orientation of these segments represents the orientation of the meridional force vectors at the top and bottom faces of the voussoirs.

6. On the force polygon, extend the angled segments from the load line to the horizontal ray through *A* to intersect at points *1, 2, ..., n*. The horizontal distance between consecutive points represents the net horizontal component of the hoop force at each voussoir.

7. Determine the magnitude of the hoop force by assuming the hoop forces act perpendicularly to the meridians. On the dome plan, draw lines perpendicular to the lateral faces of the lune.

8. On the horizontal ray on the force polygon, draw lines parallel to these lines through points *1, 2, ..., n* that intersect at points *a*', *b*', …, *x*'. The final hoop force segment should intersect the pole, *A*, rendering the section in equilibrium.

The length of the vertical load line in the force polygon represents the total weight of the lune. The length of the horizontal ray through *A* represents the total thrust of the lune that must be resisted at its base by the material or through external means, such as a continuous metal ring. Meridional and hoop force values may be calculated directly from the segment lengths on the force polygon using the analyst-defined scale.

For an axisymmetrical spherical dome loaded only by self-weight, and with an angle of embrace greater than 51.8 degrees from the center axis of revolution, this method requires tensile hoop forces in the structure to establish equilibrium. For a masonry dome with little or no tension resistance, Wolfe's method may be modified by assuming the structure acts as a compressive cap

supported by a series of radial arches, as Eddy attempted to convey in his method. Where the analysis predicts tensile hoop forces, which is indicated on the force polygon when succeeding angled segments are steeper than their precedents, alternative meridional segments may be drawn from the terminal of the horizontal ray to the remaining points on the load line. On the dome section, a revised thrust line may be constructed using the slopes of these new segments for the lower dome portion. If this revised thrust line exits the dome section, then the analysis concludes that the dome must be modified to accommodate the thrust line. Increasing the section thickness at the base or installing tensile reinforcement are two plausible modifications.

Wolfe's graphical method made some improvements over Eddy's method by allowing one to calculate the progressing internal meridional and hoop forces at each voussoir between the crown and base. The piecewise construction of the no-tension thrust line served as an alternative solution for masonry dome designs, which early twentieth-century designers utilized (Huerta 2003). However, while Eddy constrained portions of the thrust line to the middle-third of the lune section, Wolfe constrained the initial thrust line location to the median radius. Therefore, his method was also conservative in ascertaining the stability of dome geometries.

As an exercise in understanding this method, the author created a computer program[4] to conduct this analysis as published by Wolfe, with the interactive geometry software cited previously. The program reduces the risk of human error in constructing the analysis, and allows for real-time exploration of internal force values and corresponding thrust line results.

2.3. The Membrane Theory

At some point in the mid-twentieth century, as architects and structural engineers became distinct and disparate professions, engineers began to favor analytical analysis methods over graphical methods, and virtually relegated the latter into obscurity. The membrane theory, which served as the basis of Wolfe's method and remains in use today, provides a lower bound, or safe, analysis for axisymmetrical thin-shell domes through equilibrium equations. Shells are considered thin if their thickness is less than 5% of the local radius of curvature, or $t/R < 0.05$ (Heyman 1995).

[4] Program is available for public use at http://masonry.mit.edu.

However, this thesis extends the application of the membrane theory to non-thin shell domes with $t/R \geq 0.05$ for comparison to results from graphical methods, whose applicability is generally independent from thickness.

Figure 2.3 defines the geometric parameters of a dome used in this thesis.

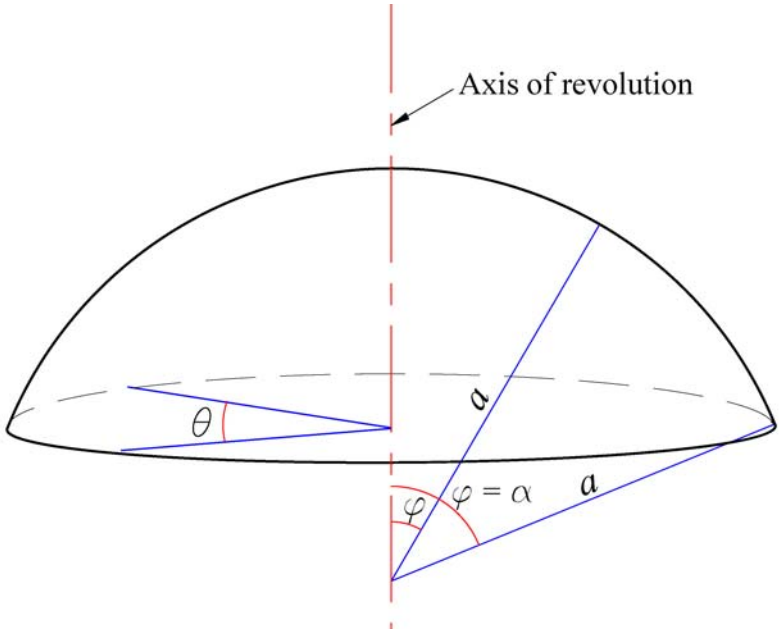

Figure 2.3. Parameter definitions for a spherical dome

This theory is based on three main principles (Heyman 1996):

1. The structure must be permanently in equilibrium and stable for statics to apply, though in actuality, the state of the structure may vary.
2. The material is rigid in compression, and the structure does not behave elastically.
3. Compatibility equations of deformation are not applied.

As mentioned before, the membrane theory assumes the dome has zero thickness, and that internal stresses only occur on a membrane surface at the median radius, a, of a dome. The membrane theory equations are derived by considering equilibrium of either an infinitesimal element of the dome or the entire dome structure (Fig. 2.4). Refer to Appendix A for derivation of the equations.

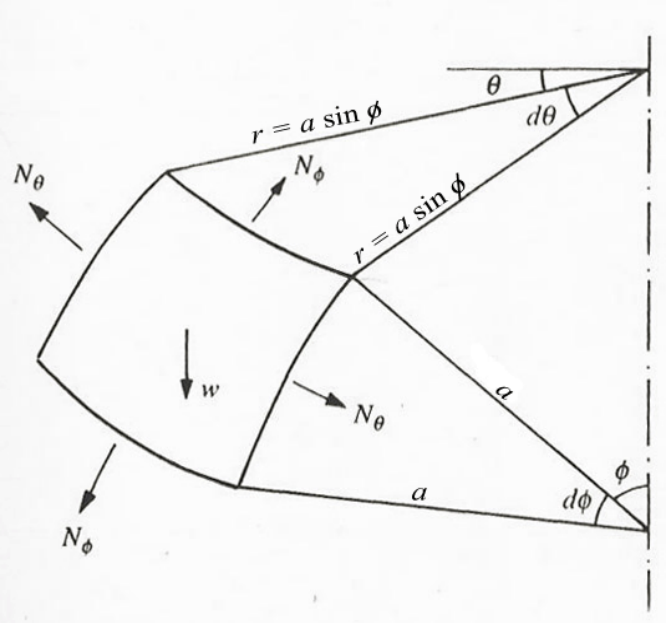

Figure 2.4. The membrane theory considers equilibrium of an infinitely small particle on the median radius of a dome (modified from Heyman 1977).

Equations 2.1 and 2.2 calculate the internal meridional and hoop stress resultants, N_φ and N_θ, respectively, in units of force per length.

$$N_\phi = -\frac{wa}{1+\cos\phi} \tag{2.1}$$

$$N_\theta = wa\left[\frac{1}{1+\cos\theta} - \cos\phi\right] \tag{2.2}$$

The self-weight of the element, w, is in units of force per area. Shear stresses are negligible due to axisymmetrical loading. Negative values indicate compressive forces.

For pointed domes, the internal meridional and hoop stress resultants are similarly derived and are given by Eqs. 2.3 and 2.4, respectively (Billington 1982):

$$N'_\phi = -aw\frac{\cos\delta - \cos\phi - (\phi-\delta)\sin\delta}{\sin\phi(\sin\phi - \sin\delta)} \tag{2.3}$$

$$N'_\theta = -\frac{aw}{\sin^2\phi}\left[(\sin\phi - \sin\delta)\sin\phi\cos\phi - (\cos\delta - \cos\phi) + (\phi - \delta)\sin\delta\right] \tag{2.4}$$

where δ is the initial, or truncating, angle of the arc of a pointed dome (Fig. 2.5)

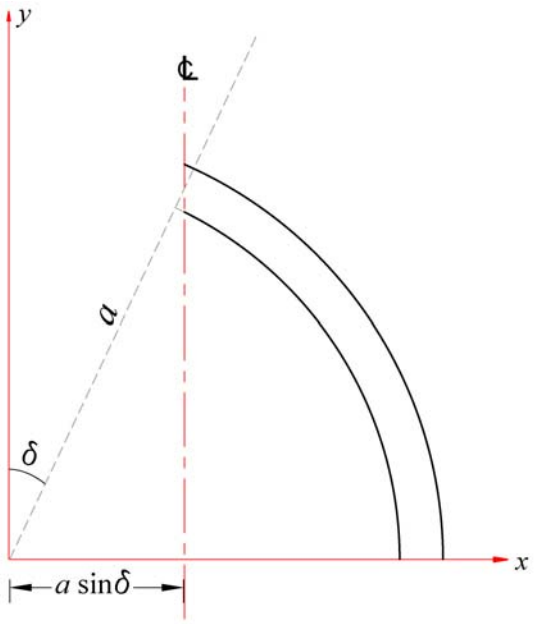

Figure 2.5. The truncation angle from the axis of curvature to the pointed crown of the dome is identified as δ.

For domes of other geometries and load conditions, such as an oculus or a cupola at the crown, derivations and formulae are available in Billington (1982). Ordinary differential equations, which may be solved analytically or numerically, assess the structural behavior of domes under asymmetrical loads, but are not discussed in this thesis (Farshad 1992).

The membrane theory assumes the dome is supported tangential to the meridians at its base. In the real world, most domes are supported vertically, which causes bending forces and small displacements at its edge that quickly dissipate upward into the dome. The membrane theory and force method of analysis may be used to analyze edge effects at these boundary conditions with the bending theory. Because analytical and empirical analyses have shown that the influence of edge effects becomes negligible when a φ-distance of 20 degrees is attained from dome base, and that the influence of high bending stresses in these localized areas does not greatly impact the overall strength of the dome, this thesis does not elaborate on the bending theory and edge effects (Rotter 2002; Farshad 1992).

2.4. The Modified Thrust Line Method

With bases in graphical statics and the analysis methods by Eddy and Wolfe, the modified thrust line method is a new approach to analyze masonry domes. The method is distinct from existing methods in several aspects:

- Internal forces may assume a range of values in compression and tension, if applicable.
- The thrust line may occupy the entire effective thickness of the structure from crown to base.
- Domes with any axisymmetrical geometry, including spherical, pointed, and irregular curves with positive and negative Gaussian curvature, may be analyzed.

By varying internal hoop and meridional forces values, this method can identify satisfactory thrust line solutions in domes that existing methods cannot find. Again, the membrane theory calculates hoop force values by requiring that the theoretical thrust surface at the dome's median radius is in equilibrium, which results in compressive or tensile fixed hoop force values.

In reality, only the values of the dome's external loads are known and fixed. Both internal meridional and hoop forces can assume a range of values; different combinations of values result in different thrust line configurations, many of which deviate from the median surface of a dome.

Per the lower bound theorem, the structure is safe if one satisfactory equilibrium state is found. For a masonry dome evaluated as a series of lunes, if a thrust surface is found that lies within one lune, then stability is satisfied for the "original undivided structure" (Heyman 1977, p. 109).

This method makes several assumptions regarding thrust line and internal force behavior, several of which have been discussed. In addition, the method assumes that the thrust line may touch the dome surfaces at no more than two hinge locations per lune; additional contact points put the structure at incipient collapse. A dome axisymmetrically loaded by self-weight experiences only axial forces. Under these conditions, the method also assumes that the slope of the thrust line increases in magnitude from the crown to base with no major aberrations in the thrust line curvature, which isolated point loads would create. Hoop forces are greatest near the crown

where masonry units push against adjacent units to prevent self collapse and inward rotation; hoop forces decrease or become zero toward the dome base. Conversely, meridional forces are zero at the crown and increase toward the base of the dome. As a result, the initial slope of the thrust line is zero at the crown, or $y_{TL_{i=1}} = y_{TL_{i=0}}$, and $x_{TL_{i=0}}$, the start point of the thrust line, lies on the dome's axis of revolution (Fig. 2.6).

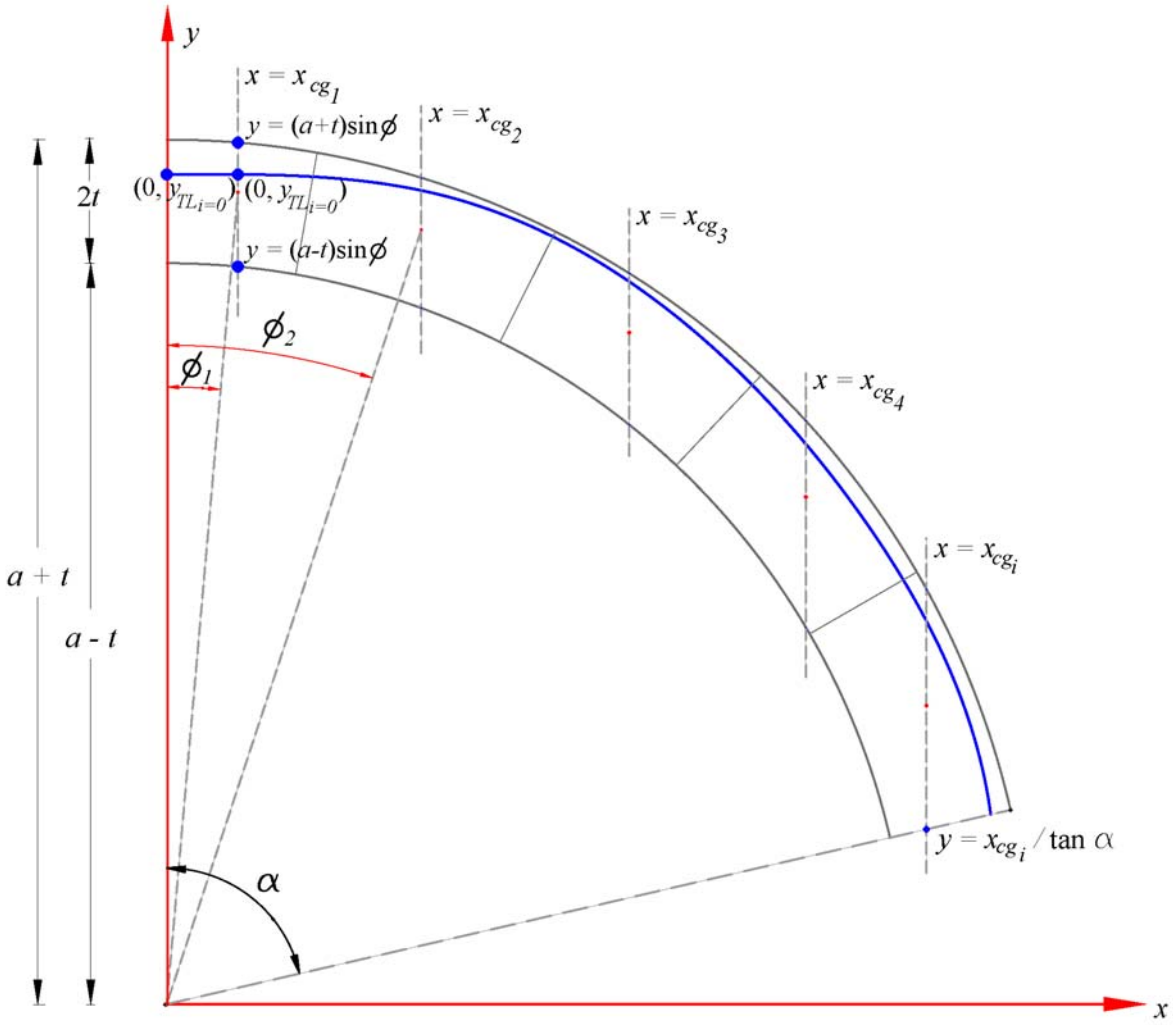

Figure 2.6. Parameter definitions for the modified thrust line analysis

Internal meridional and hoop forces must be within material strength limits; typically this requirement is easily met due to low internal stresses in masonry domes relative to material crushing strength (Heyman 1995).

The modified thrust line program currently exists in two program formats. The first program, written in Microsoft Corporation's *Visual Basic for Applications with Excel 6.3*, conducts the analysis with user input only in defining dome geometry and material properties, and runs multiple simulations consecutively. The second program, developed using *Cabri II Plus* by Cabrilog, relies on user interaction to conduct the graphical analysis. The analyst must graphically define the dome section and locate a satisfactory thrust line through trial-and-error via the user interface. The latter program permits analysis of geometries beyond conventional dome shapes, and its visual and interactive nature clearly illustrates the force behavior in domes. The *Visual Basic* program currently analyzes domes only with uniform thickness, although custom geometries are entirely plausible with some program modifications. Descriptions of both program versions follow.

The *Visual Basic* program considers a lune with $0° \leq \theta \leq 90°$ divided into n voussoir free bodies defined by the cuts along the meridional planes at its lateral faces, and cuts through the dome's center of curvature at angles β and γ (Fig. 2.7).

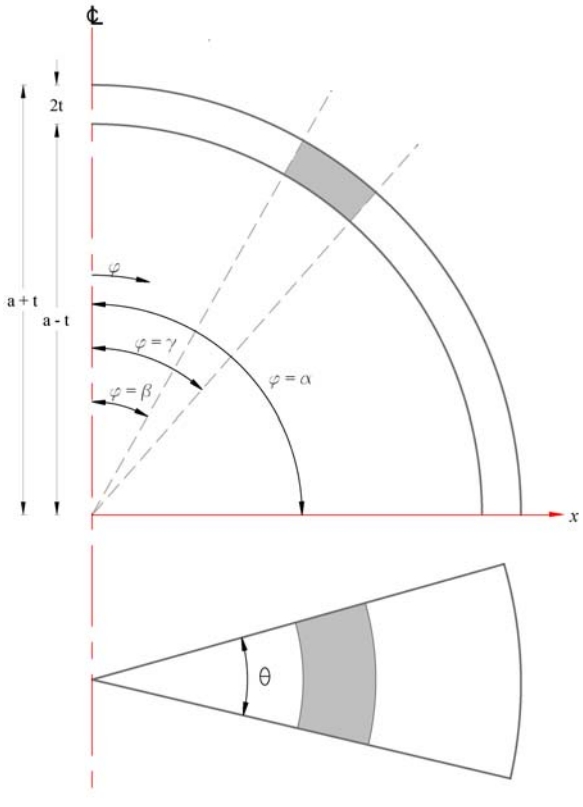

Figure 2.7. General parameters for lune in section and plan

The weight of a section of dome, or individual voussoir *i*, is:

$$w_i = \frac{\theta \cdot \rho \cdot \left(r^3 - r'^3\right)}{3}\left[\cos\beta - \cos\gamma - (\gamma - \beta)\cdot \sin\delta\right] \tag{2.5}$$

where $r = a + t$, $r' = a - t$, ρ is the material unit weight, and δ is the initial φ-angle from the radius of curvature at the crown for a pointed dome ($\delta = 0$ for spherical domes). Thus the length of the load line of the force polygon representing the dome's self weight, is known.

The weight of the voussoirs is assumed to act at the volume centroid of each voussoir. The horizontal distance from the axis of revolution to the centroid of voussoir *i* is defined by:

$$x_{cg_i} = \frac{3\left(r^4 - r'^4\right)}{8\left(r^3 - r'^3\right)}\cdot\frac{\sin\frac{\theta}{2}}{\theta}\left[\frac{(\gamma-\beta)\left(2+4\sin^2\delta\right)+(8\sin\delta)(\cos\gamma-\cos\beta)-\sin 2\gamma+\sin 2\beta}{\cos\beta-\cos\gamma+(\beta-\gamma)\sin\gamma}\right] \tag{2.6}$$

On the force polygon, horizontal lines intersecting the load line represent the cumulative thrust of the dome at voussoir *i*. These lines also represent the horizontal component of the meridional force (Fig. 2.8). The difference between consecutive horizontal segments on the force polygon represents the net outward component of the equal and opposite hoop forces, shown in Fig. 2.8 "Plan View of Lune". The analyst can modify the lengths of these horizontal segments, or the horizontal thrust in each voussoir, to achieve different internal force combinations and, subsequently, different thrust lines.

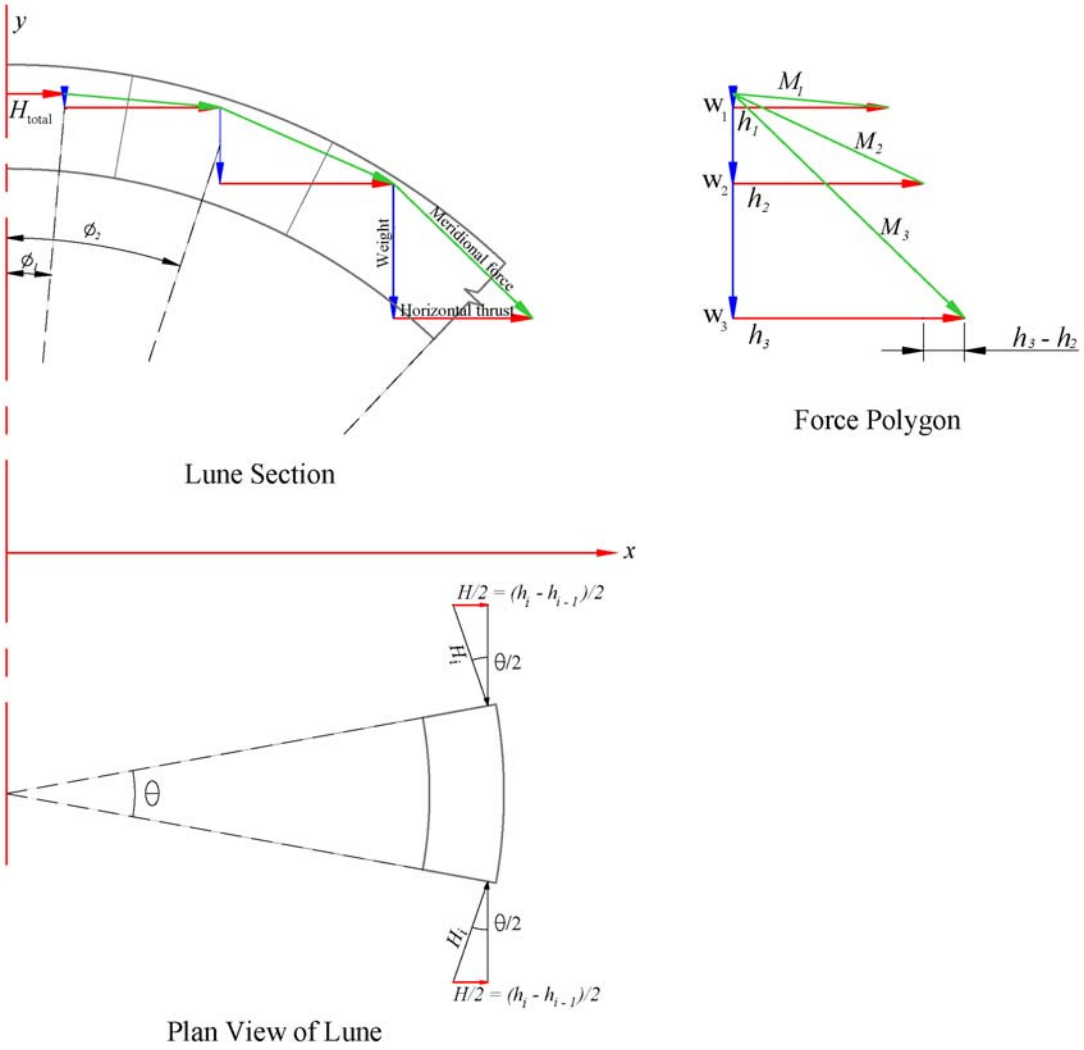

Figure 2.8. Parameters relating the internal forces in the lune section with the force polygon. The cumulative force polygon on the right consists of individual equilibrium polygons within each voussoir division of the lune. The slope of the thrust line is equal to the slope of the meridional force vectors comprising the force polygon.

Starting at the crown, the force polygon contains individual equilibrium polygons for each voussoir composed of vectors representing the meridional force, horizontal thrust, and cumulative weight from the crown to voussoir *i* at $\varphi = \gamma_i$. From the force polygon, the meridional force at voussoir *i* is (positive force values indicate compression):

$$M_i = \sqrt{W_i^{\,2} + h_i^{\,2}} \tag{2.7}$$

where W is the cumulative weight of the lune portion above $\varphi = \gamma_i$, and h is the total length of the horizontal thrust vector defined by the user or the program. Meridional stress is thus defined as:

$$\sigma_M = \frac{M}{2 \cdot t \cdot a \cdot \theta \cdot (\sin\gamma - \sin\delta)} \tag{2.8}$$

The internal hoop force and hoop stress at $\varphi = \gamma$ are defined, respectively, as:

$$H_i = \frac{(h_i - h_{i-1})}{2 \cdot \sin\left(\frac{\theta}{2}\right)} \tag{2.9}$$

$$\sigma_H = \frac{H}{2\,t\,a(\gamma - \beta)} \tag{2.10}$$

For the first ($i = 0$) and last ($i = n$) voussoirs at the crown and base of a spherical dome, Eq. 2.10 is multiplied by a factor of 2 because the effective section areas, taken between consecutive centers of gravity, of these voussoirs are one-half the areas of other voussoirs. For pointed domes, the section area of the 0^{th} voussoir at the pointed crown will slightly differ from the denominator of Eq. 2.10 due to an assumption of an angled top face of the voussoir when it is actually flush with the dome's centerline (Fig. 2.5).

At the base of the dome, the total horizontal thrust of the lune is simply the length of the segment h_n. The total weight of the lune, W_n, is represented by the total length of the load line.

With the horizontal or x-coordinates of the thrust line known with Eq. 2.6, only the y-coordinates remain unknown. From the force polygon, the y-coordinates are determined as:

$$y_{TL_i} = -\frac{W_{i-1}}{h_{i-1}}\left(x_{cg_i} - x_{cg_{i-1}}\right) + y_{TL_{i-1}} \tag{2.11}$$

For $0 \le i \le n$, y_{TL_i} must lie between the dome's intrados and extrados at every x_{cg_i}:

$$(a-t)\cos\left[\sin^{-1}\left(\frac{x_{cg_i}}{a-t}\right)\right] \le y_{TL_i} \le (a+t)\cos\left[\sin^{-1}\left(\frac{x_{cg_i}}{a+t}\right)\right] \tag{2.12}$$

For voussoirs in which $x_{cg_i} > (a-t)\sin\alpha$, then:

$$\frac{x_{cg_i}}{\tan\alpha} \le y_{TL_i} \le (a+t)\cos\left[\sin^{-1}\left(\frac{x_{cg_i}}{a+t}\right)\right]. \tag{2.13}$$

At the base of the dome, the *x*-coordinate of the final point of the thrust line, $(x_{TL_{n+1}}, y_{TL_{n+1}})$, assumed to lie on a line drawn from the dome's center of curvature at an angle $\varphi = \alpha$, must meet the following criteria:

$$r'\sin\alpha \le x_{TL_{n+1}} \le r\sin\alpha \tag{2.14}$$

where:

$$x_{TL_{n+1}} = \frac{y_{TL_n} + \frac{W_n}{h_n}\cdot x_{TL_n}}{\cot\alpha + \frac{W_n}{h_n}} \tag{2.15}$$

The final point of the thrust line may touch the extrados or intrados provided the thrust line has not touched the dome surface at two locations prior. If the thrust line meets all the above criteria, then it is a satisfactory solution that establishes equilibrium of the lune and subsequently, equilibrium of the masonry dome.

The graphics-based version of the modified thrust line method, also developed in *Cabri II Plus*, allows real-time computer-based execution of the methods described by Eddy and Wolfe, as well as the modified thrust line method. Relying primarily on geometric input from the analyst on the graphical user interface, the program graphically outputs the thrust line shape that corresponds to the user-defined internal forces. In addition, the program outputs the numerical values of the internal forces and horizontal thrust at the base of the dome (Fig. 2.9).

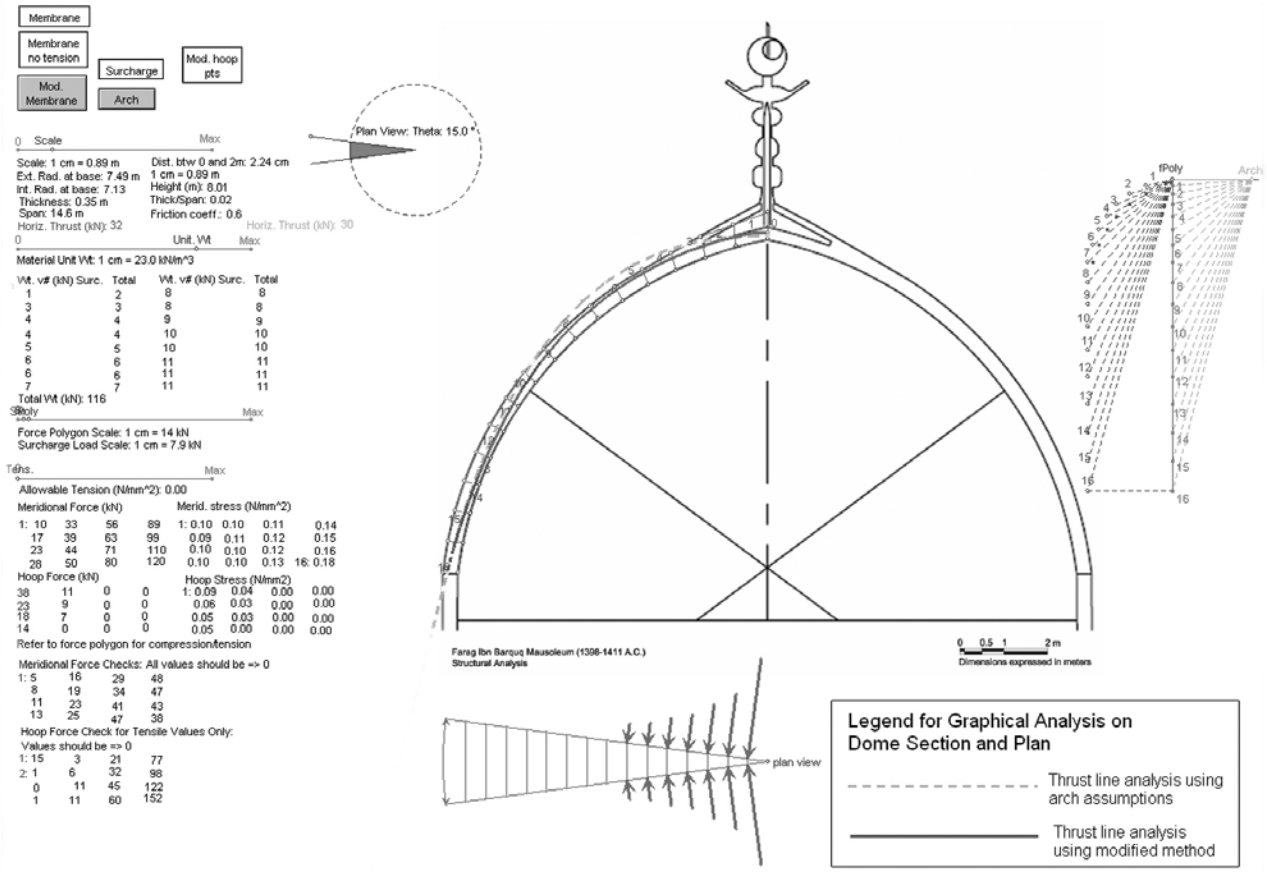

Figure 2.9. User interface for the graphics-based modified thrust line method comparing thrust lines determined by the membrane theory and the modified thrust line method. Analysis shown for the dome of Farag Ibn Barquq, Cairo (Cipriani and Lau 2006)

This program assumes the masonry dome acts as a rigid body with zero tensile capacity and no elastic deformations. Additional assumptions include axisymmetrical load conditions and geometry, tangential support structure at the dome's base, and the presence of a structure to counteract the horizontal thrust at its crown, such as the complementing lune. The program evaluates a representative lune with $\theta \leq 15°$, which is further divided into 16 wedge-shaped voussoirs. In the graphics-based program of this method, the user can also customize the dome geometry by altering the shape of the voussoirs comprising the lune (Fig. 2.10).

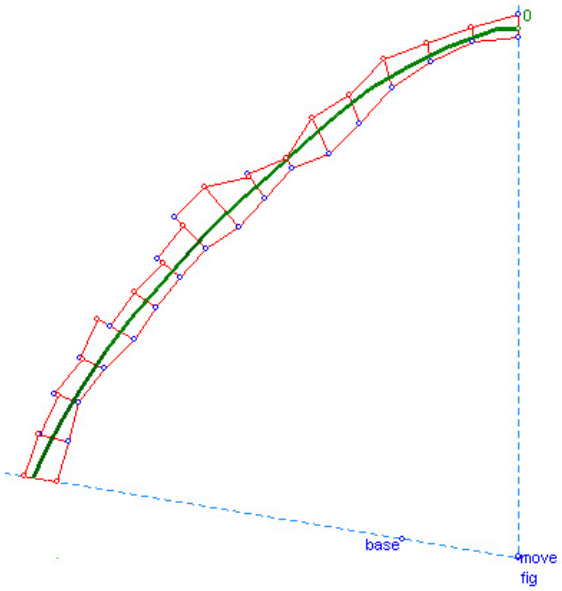

Figure 2.10. The interactive geometry program of the modified thrust line method can analyze non-conventional dome geometries.

Through geometry and user-input material density, the program determines and applies the external loads of each voussoir to its centroid, and constructs the force polygon to a user-defined scale. The vertical load line, representing the gravity loads of the structure, changes in length with response to changes to section geometry or applied loads in real-time. The resulting funicular polygon generates a thrust line that is displayed in the dome section, permitting exploration of possible thrust line geometries in the lune.

The analyst can choose whether to conduct the analysis under arch, or zero-hoop force, behavior, membrane theory conditions, or the modified thrust line method. The methods vary in their treatment of hoop forces, which may develop between lunes depending on the condition of the dome. For example, if the dome has extensive meridional cracks, the analyst will likely choose to analyze the dome as a radial series of independent arches. Under arch assumptions, the analyst controls the magnitude of the unknown horizontal thrust and starting point of the thrust line. Under membrane theory assumptions, the program conducts the analysis using Wolfe's method as described in Section 2.2. The program includes the option to append a no-tension thrust line construction to the original thrust line at the median radius of the section.

The modified thrust line analysis provides the greatest flexibility in defining hoop force values and subsequently, controlling the shape of the thrust line. By experimenting with the internal

force values at each voussoir in the lune, and the start point of the thrust line at the crown at the axis of rotation, the analyst can attain thrust line solutions that explore the entire effective thickness of the dome, and satisfy static equilibrium conditions.

2.5. Chapter Summary

Since the mid-nineteenth century, structural analysis methods for masonry domes have evolved from graphical techniques to the membrane theory equations, which remain in use today. While they are certainly acceptable, existing analysis methods incorporate conservative assumptions that underestimate the ability of the dome to develop internal forces in three directions, and limit the location of a thrust line in the dome's effective thickness. Using existing methods as a starting point, the author developed the modified thrust line method, a graphical statics-based technique to explore the dome's structural possibilities. The programmable methodology is invaluable in acquiring the general characteristics of dome structural behavior established in the next chapter.

Chapter 3. Theoretical Results and Applications of the Modified Thrust Line Method

Due to the versatility and flexibility offered by graphical analysis, the modified thrust line method is ideal for exploring the relationship between geometry, internal forces, and the stability of masonry dome structures. This chapter focuses on identifying the theoretical minimum thrust exerted by spherical domes, and its applications to real world questions. As discussed in previous chapters, existing analysis methods limit the number of thrust lines solutions in a dome by restricting the thrust line to a specific region, or by assuming internal forces as fixed values. In addition, the intent of these methods is to attain a single solution to the problem; thus, they tend to overlook the potentially infinite number of satisfactory lower bound solutions.

To abide by limit state assumptions and the characteristics of internal forces discussed in previous chapters, the combination of internal forces must meet the following requirements in the study of an axisymmetrical dome loaded only by self-weight:

- For any voussoir i, the cumulative horizontal thrust, h_i, is greater than h_{i-1}, where $\phi_{i-1} \leq \phi_i$.
- The absolute value of W_i/h_i is less than or equal to the absolute value of W_{i+1}/h_{i+1} where W_i is the cumulative weight of the dome from the crown to φ_i.

The modified thrust line method also assumes that for conventional dome geometries, under uniformly distributed loads, the thrust line cannot change from positive to negative Gaussian curvature; that is, the thrust line has no "kinks" that would suggest an isolated concentrated load on the dome. These requirements limit the acceptable force polygon configurations, internal force values, and thrust line shape in the modified thrust line method.

For a dome loaded by self-weight only, the membrane theory equations calculate that hoop forces decrease from maximum compression at the crown to a point of zero hoop force in mid-span, and increase to maximum tension at the base. In reality, masonry rings in the dome can likely assume higher or lower hoop forces than adjacent rings, in order to keep the line of thrust within the dome's thickness. Only the structure knows its true behavior, but, depending on the geometry in question, it is likely that the structure can experience oscillating hoop force values.

As discussed in Chapter 1, though past studies neglected hoop forces in ascertaining the structural limits of masonry domes, hoop forces are invaluable in this study of minimum thrust because they comprise thrust lines that otherwise could not be attained. Oppenheim et al. (1989) acknowledged the necessity of compressive hoop forces in the dome cap when their thrust surface solution for a pointed dome with $\alpha = 90°$, $\delta = 20°$, and $t/R = 0.05$ exited the dome section. Including hoop forces in the analysis, the modified thrust line program in *Cabri* generated a satisfactory no-tension thrust line for the same section (Fig. 3.1).

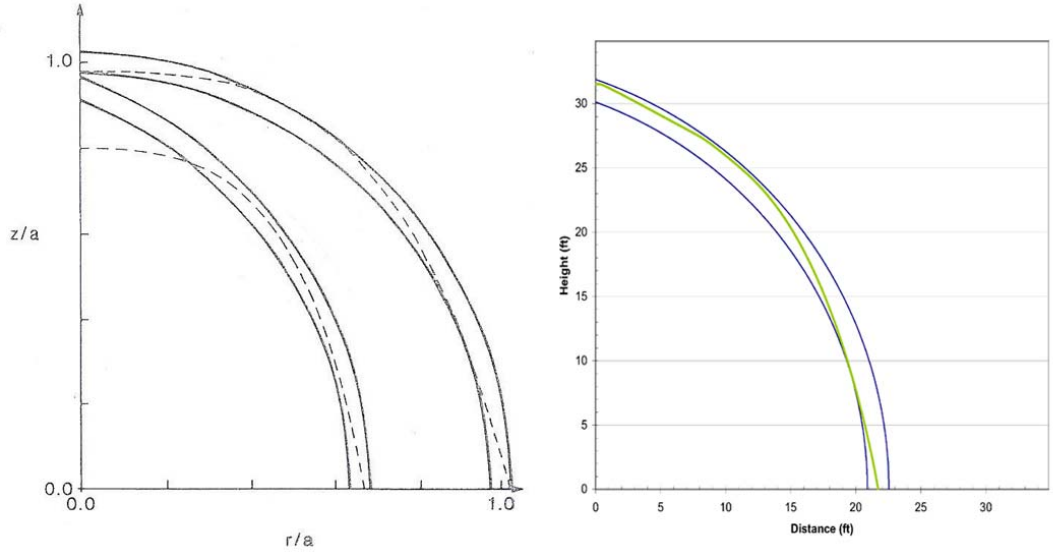

Figure 3.1. Right: The modified thrust line finds a satisfactory thrust line for the example discussed by Oppenheim et al. (1989). In this example, θ equals $1/a$, and the thrust line was permitted within $0.01a$ of the dome's extrados.

3.1. Minimum Thrust Results for Spherical Domes with One Center of Curvature

Using the modified thrust line method programmed in Microsoft's *Visual Basic for Applications in Excel*, the author attained minimum horizontal thrust-to-weight ratios for spherical domes with different thickness-to-radius of curvature ratios, t/R, and angles of embrace, α. Spherical dome geometries have one center of curvature that lies on the vertical axis of revolution. This study compares results for domes in which compressive hoop forces can develop between lune segments (e.g., an intact dome), and domes in which hoop forces cannot develop (e.g., a dome with meridional cracks from crown to base).

Due to the infinite permutations of geometric parameters that define the shape of a spherical dome, this work limited its investigation to domes with the following parameters:

- Thickness-to-radius ratios of 0.001, 0.01, 0.02, 0.03, 0.04, 0.05, 0.10, 0.15, and 0.20
- Angles of embrace between 20 degrees and 90 degrees in intervals of 10 degrees[5]
- Lune segments with angles in plan equal to 1, 22.5, and 45 degrees.

The program assumed a radius of curvature of 33 ft and a material unit weight of 100 pcf; these values and units become irrelevant because the ultimate result, the horizontal thrust-to-weight ratio, *H/W*, is dimensionless. Each lune was subdivided into the larger of 30 or $\alpha°$ voussoirs. The thrust line resembles more of a smooth curve than a polygon when the number of voussoir divisions is large. The author experimented with the number of voussoirs, but changes in *H/W* values were minor at less than 5%.

Initially the program tested all acceptable combinations of internal force values meeting the aforementioned assumptions and limit state conditions when searching for the thrust line with the minimum thrust. However, the time to complete one simulation at times exceeded several days, which was not favorable for this study of almost 500 different dome geometries.

To reduce the solution time, the author made assumptions to simplify the algorithm. The program assumed the desired thrust line would be closer to the extrados than the intrados at the dome crown; for the thrust line's starting point, the program first tried a distance about *a*/3000 below the extrados, and if needed, gradually moved the thrust line toward the intrados in increments between *a*/3000 and *a*/300. The program allowed the thrust line to approach within *a*/3000 of the extrados in the remainder of the dome, but not touch either surface. The virtually zero tolerance of the thrust line to the dome's surface was chosen to immediately pinpoint the thrust line with the minimum thrust. Analyses using different tolerance values and start point locations produced differences in the *H/W* of about 5% or less.

Figures 3.2 to 3.5 plot the minimum thrust for lunes with $\theta = 1°$, 22.5° and 45°, respectively, and assume hoop forces are transferred between lunes.

[5] This work does not include minimum thrust results for domes with $0° \leq \alpha < 20°$ because of the infrequency of these shallow embrace angles in existing dome structures.

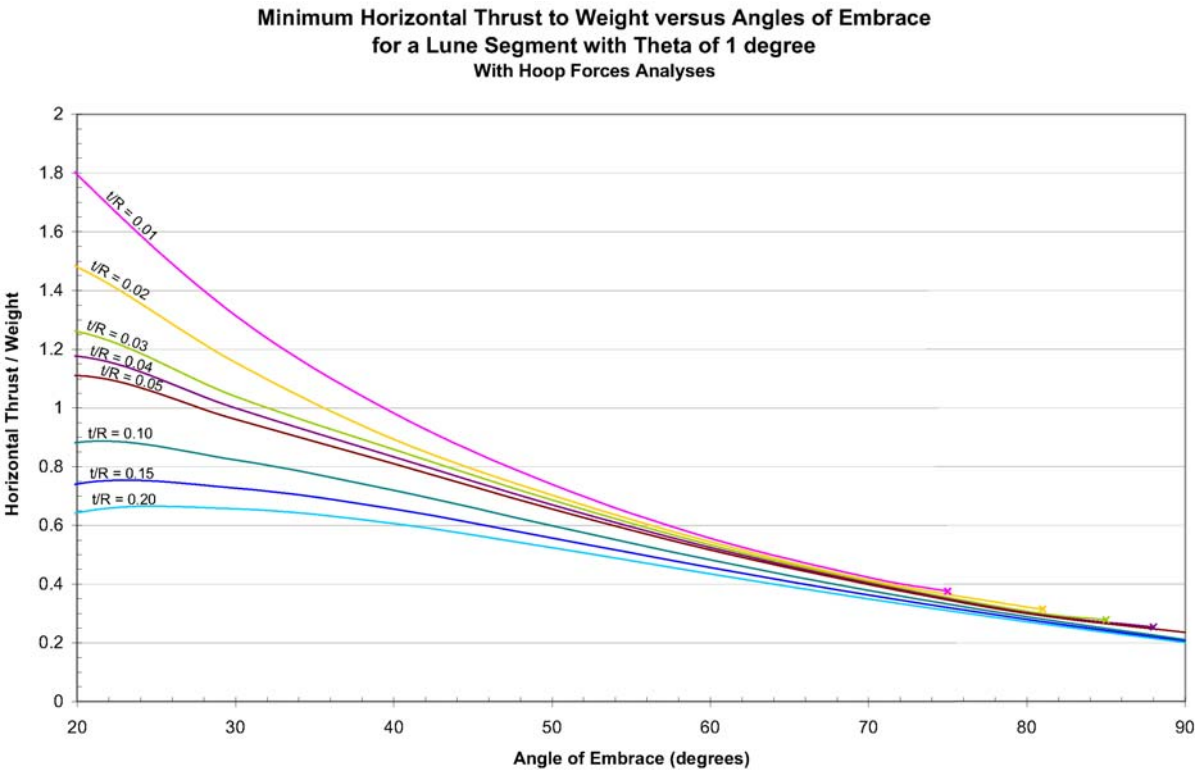

Figure 3.2. Minimum horizontal thrust for a lune with $\theta = 1°$ of a spherical dome with hoop forces

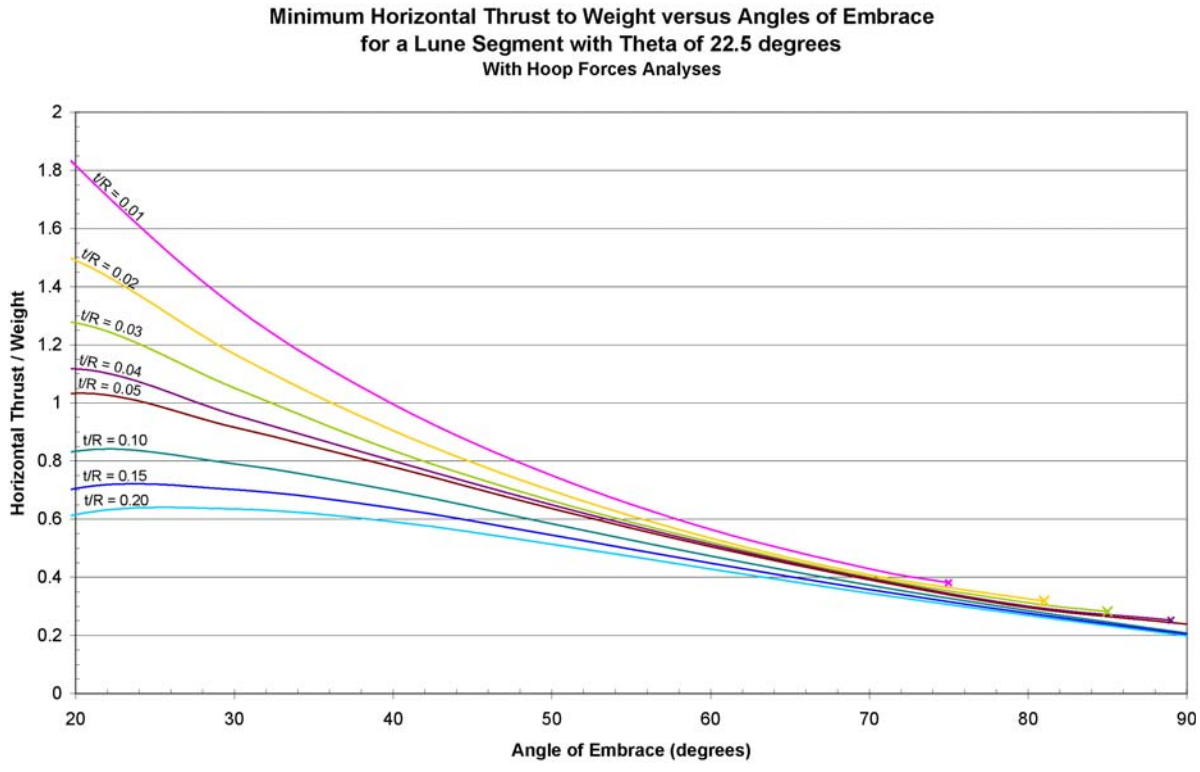

Figure 3.3. Minimum horizontal thrust for a lune with $\theta = 22.5°$ of a spherical dome with hoop forces

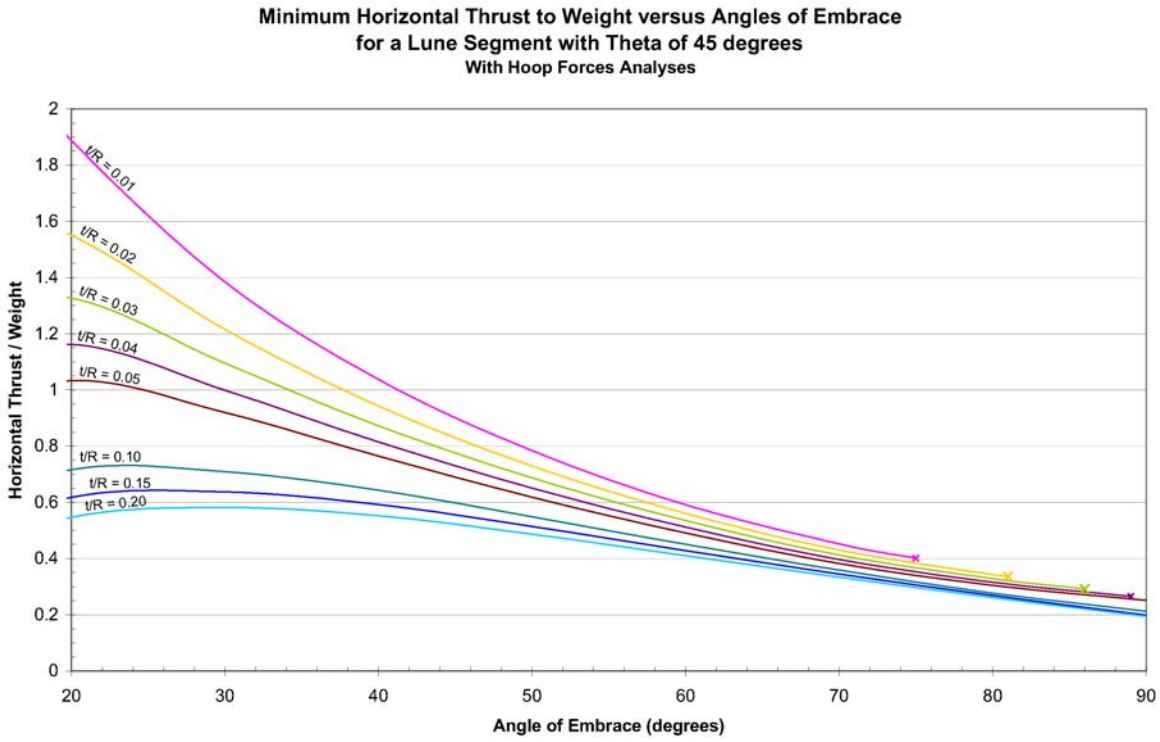

Figure 3.4. Minimum horizontal thrust for a lune with $\theta = 45°$ of a spherical dome with hoop forces

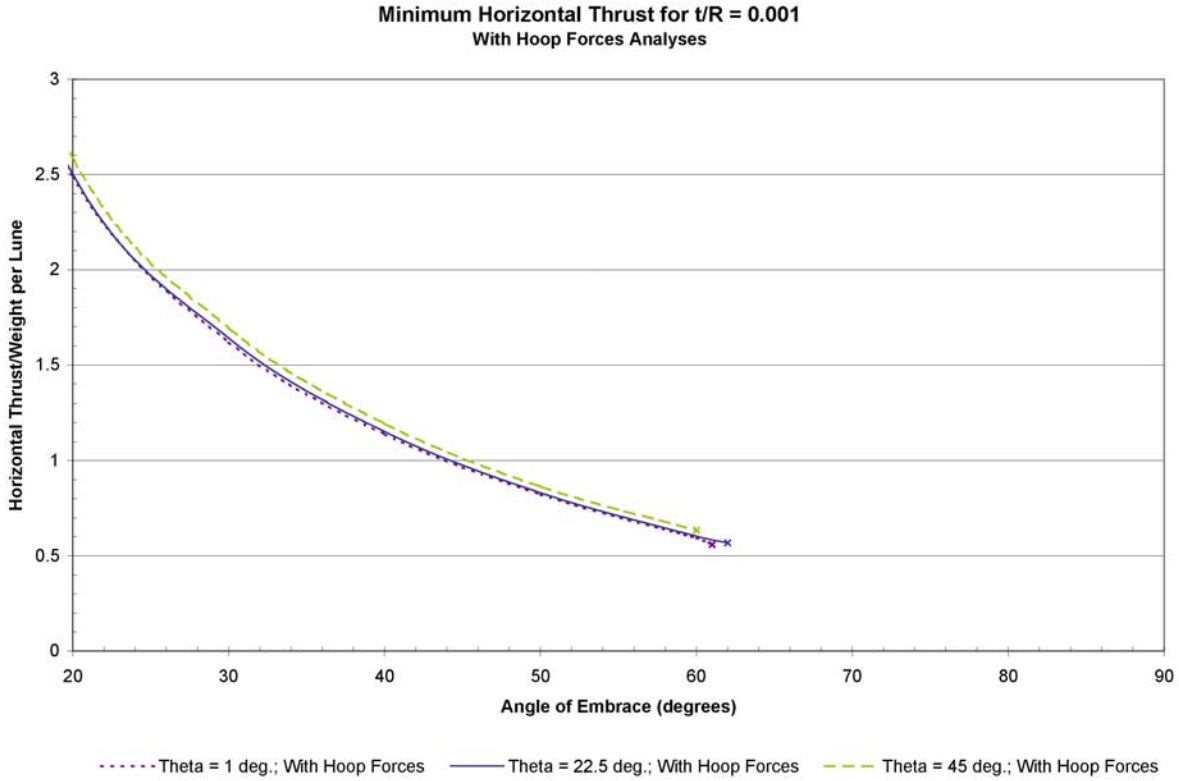

Figure 3.5. Minimum horizontal thrust for $t/R = 0.001$ for a spherical dome with hoop forces

For masonry domes with hoop forces, the following trends from these figures are salient:

- The minimum thrust is inversely related to t/R and to α.
- The range of H/W values, regardless of t/R and θ, decreases as α increases. For example, for $\alpha = 60°$, H/W values are within 10% of each other; for $\alpha = 90°$, the range is 5%.
- For $\alpha \geq 60°$, the relationship between α and H/W is approximately linear.
- The plan angle of the lune, θ, has little impact on H/W; for a lune with $\theta = 1°$, 22.5°, or 45°, the minimum thrust values are within 5% for a constant t/R and α.
- As t/R increases, the range of embrace angles that equate to stable dome geometries increases to include deeper and eventually hemispherical domes in which $\alpha = 90°$.
- Similar to the membrane theory, the modified thrust line analysis finds satisfactory equilibrium solutions for $\alpha \leq 51.8°$ for all t/R ratios considered in this study.
- For $t/R = 0.001$, the method finds a stable, no-tensile thrust line solution up to $\alpha = 61°$, whereas the membrane theory attains a no-tensile solution only up to $\alpha = 52°$.

Section 3.2 further discusses the significance of these trends. In all analyses, internal stresses, which depend on masonry unit weight, remained well under the crushing stress of masonry.

Figures 3.6, 3.7, and 3.8 plot the minimum thrust-to-weight ratios for a lune that does not develop hoop forces, thus acting as a wedge-shaped arch instead of a dome.

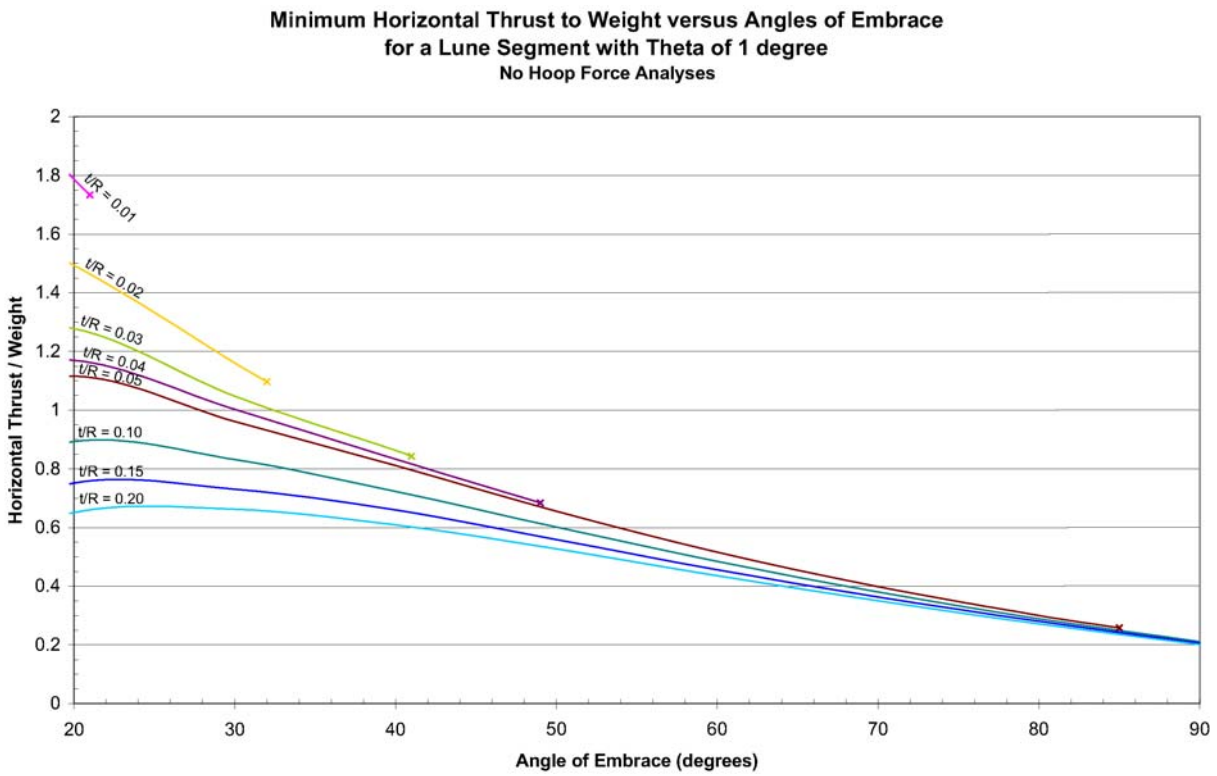

Figure 3.6. Minimum horizontal thrust for a lune with $\theta = 1°$ that acts as an independent arch

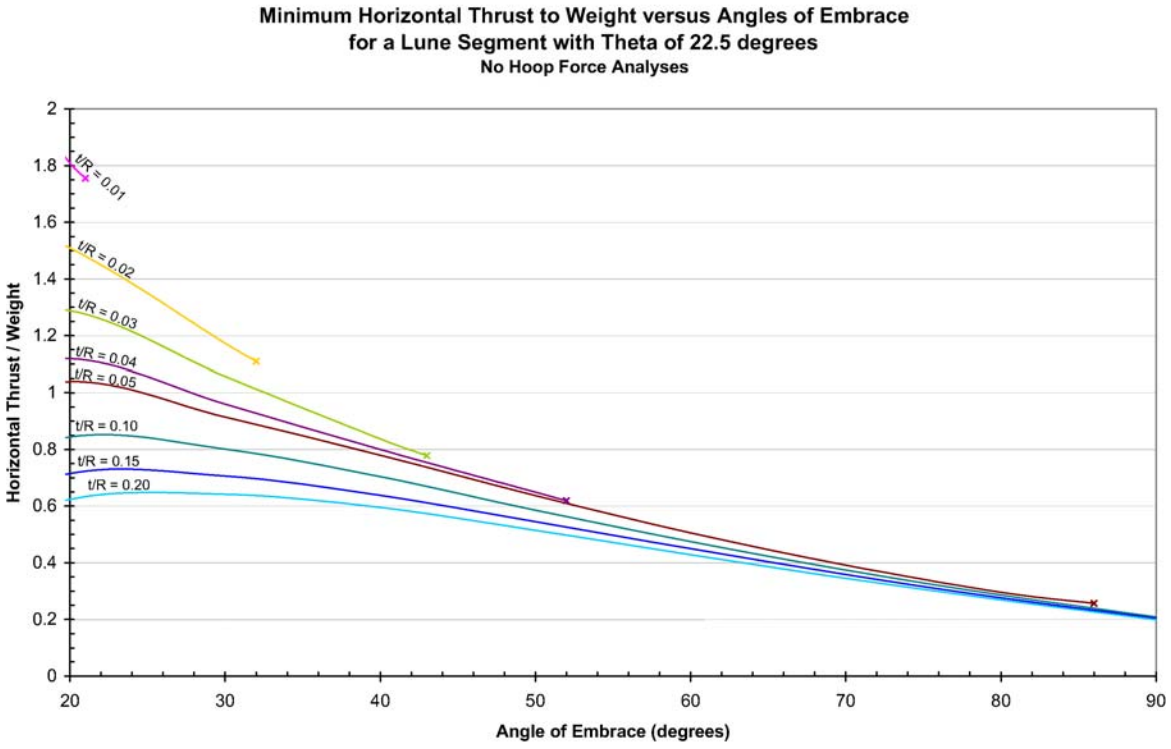

Figure 3.7. Minimum horizontal thrust for a lune with $\theta = 22.5°$ that acts as an independent arch

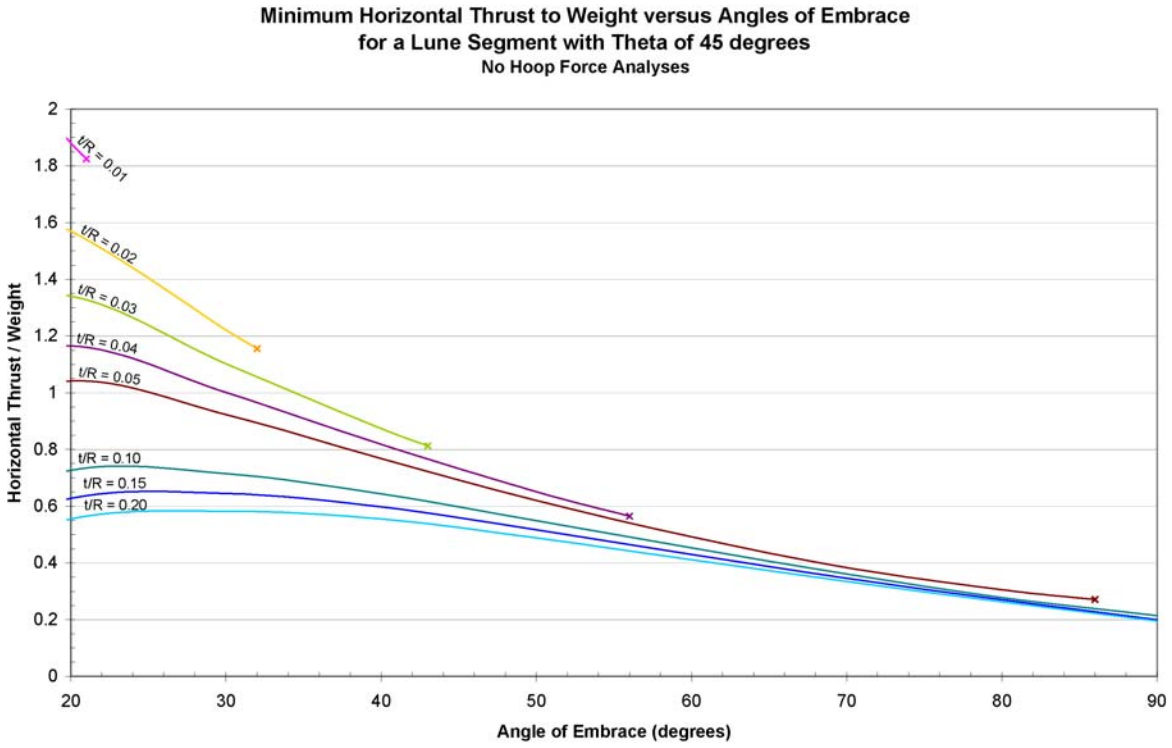

Figure 3.8. Minimum horizontal thrust for a lune with $\theta = 45°$ that acts as an independent arch

By excluding hoop forces in the analyses, the modified thrust line program did not find satisfactory thrust line solutions for $t/R = 0.001$ and $\alpha > 10°$; as a result, a figure for $t/R = 0.001$ is not shown. From Figs. 3.6 to 3.8, two observations are salient:

- For $t/R < 0.05$, the analyses did not find satisfactory thrust lines, for all values of α in which the previous analyses that incorporated hoop forces did find solutions. For $t/R = 0.05$, the program found a solution up to $\alpha = 86°$.
- H/W values for the no-hoop force analyses are within a few percent of H/W values for the with-hoop forces analyses. Thus, trends for the latter also relevant to this study.

3.2. Discussion of Results for Domes with One Center of Curvature

The minimum thrust-to-weight ratios from the modified thrust line analyses revealed several trends.

Minimum Thrust-to-Weight Ratio, *H/W*, and the Embrace Angle, α

The minimum thrust-to-weight ratio is larger for shallow domes, with small α values, than deeper domes. Similar to arches, shallow domes thrust more than deeper domes, relative to self weight, because the thrust line and the dome's bottom edge are oriented more horizontally. For a hemispherical dome with tensile capacity, the thrust line at the base could be vertical, indicating zero thrust, which is what the membrane theory calculates. Under limit analysis conditions, near the cap of a dome, the horizontal thrust accumulates with increasing α due to internal forces following the dome curvature. As the dome surface becomes more vertical toward the base, the increase in thrust becomes negligible, but the masonry lacks tensile capacity to resist the existing thrust generated in the upper portion of the dome; simultaneously, the weight of the lune continues to increase with α. As a result, *H/W* is inversely related to α.

For a lune of a hemispherical dome of sufficient thickness, the modified thrust line method estimates the minimum thrust to be about 20% of the lune's weight, regardless of θ and *t/R*.

Minimum Thrust-to-Weight Ratio, *H/W*, and Thickness-to-Radius Ratio, *t/R*

For the geometries studied, the modified thrust line analyses show an inverse relationship between *t/R* and *H/W* with or without the presence of hoop forces (Figs. 3.2 to 3.8). As the thickness of the dome increases, the center of gravity of the entire lune approaches the "toe" of the lune, where the intrados and base intersect (Fig. 3.9) (Oppenheim et al. 1989, p. 879).

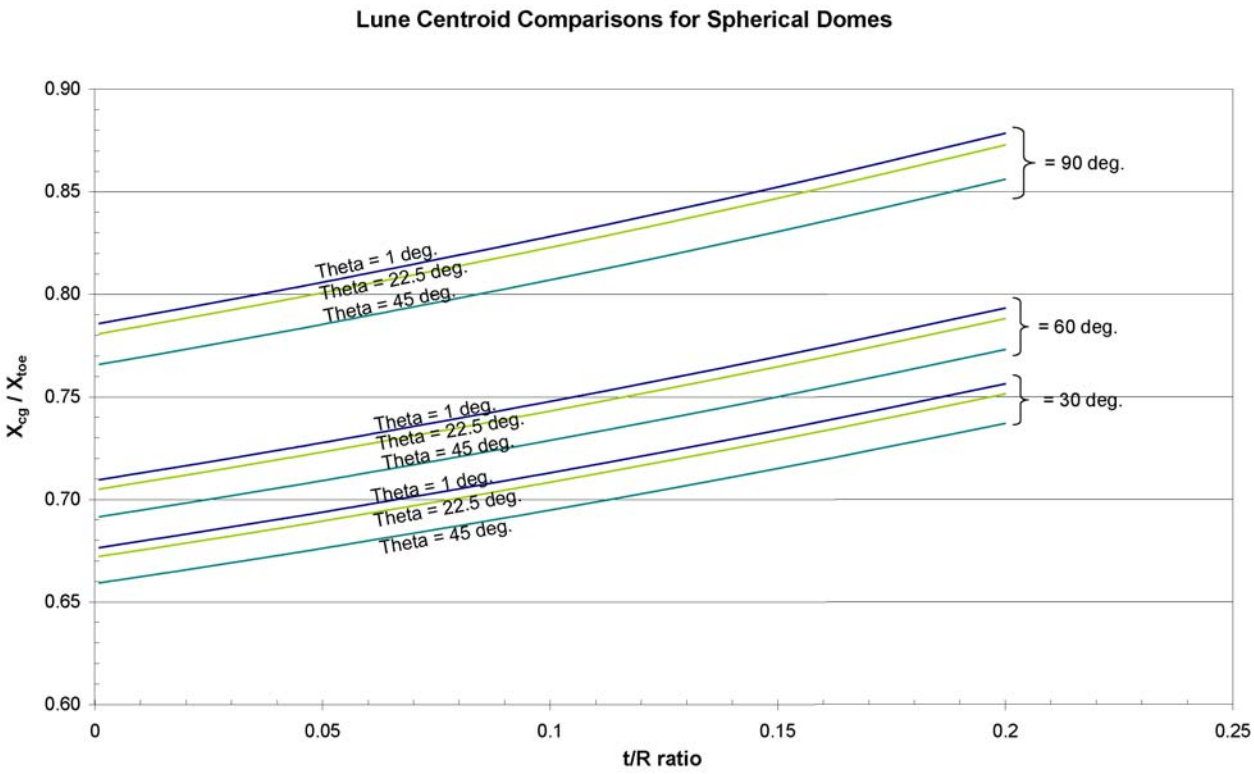

Figure 3.9. As *t/R* increases, the centroid of the lune approaches the intrados at the base of the dome.

As the centroid moves closer to the toe, the decrease in the horizontal reaction at the crown to prevent overturning of the lune is proportionally lower than the lune's increase in weight due to additional thickness; this horizontal reaction is equal to the *H* value. Thus *H* decreases while *W* increases for increasing *t/R*, generating an inverse relationship discussed below.

Minimum Thrust-to-Weight Ratio, *H/W*, and Angle in Plan, θ

For small *t/R* ratios, the minimum thrust-to-weight increases slightly with θ. Conceptually, as the center of gravity of the thin-shell lune moves closer to the center of the dome due to the "spreading" of its base, the horizontal reaction required to prevent inward rotation of the lune increases slightly faster than the self-weight of the thin-shell lune.

For larger *t/R* ratios, the inverse occurs: the horizontal reaction to prevent inward rotation of the lune increases slower than the lune's self-weight. As *t/R* increases and the lune becomes relatively thick and sturdy, the quarter-dome and, to a lesser extent, eighth-dome gain the ability to become freestanding, which negates the need for a counteracting horizontal reaction at the crown to develop for stability.

Intuitively, increasing θ should increase the horizontal thrust of the dome portion; however this increase may not manifest into an increase in the minimum thrust-to-weight ratio. Increasing θ is similar to abutting smaller individual lunes together. The contribution of the individual thrusts to the net thrust of the combined lune diminishes as the individual lunes fan out to form a half-dome to the point where the thrust of the complementing lunes at the edges cancel each other. Section 3.3 explores this concept further.

The Impact of Hoop Forces

This section discusses the significance of including hoop forces in the spherical dome analyses. While hoop forces were shown to have negligible impact on the magnitude of H/W, their importance is clear a comparison of geometries of lunes with and without hoop forces, for which the modified thrust line method found satisfactory thrust lines (Fig. 3.10).

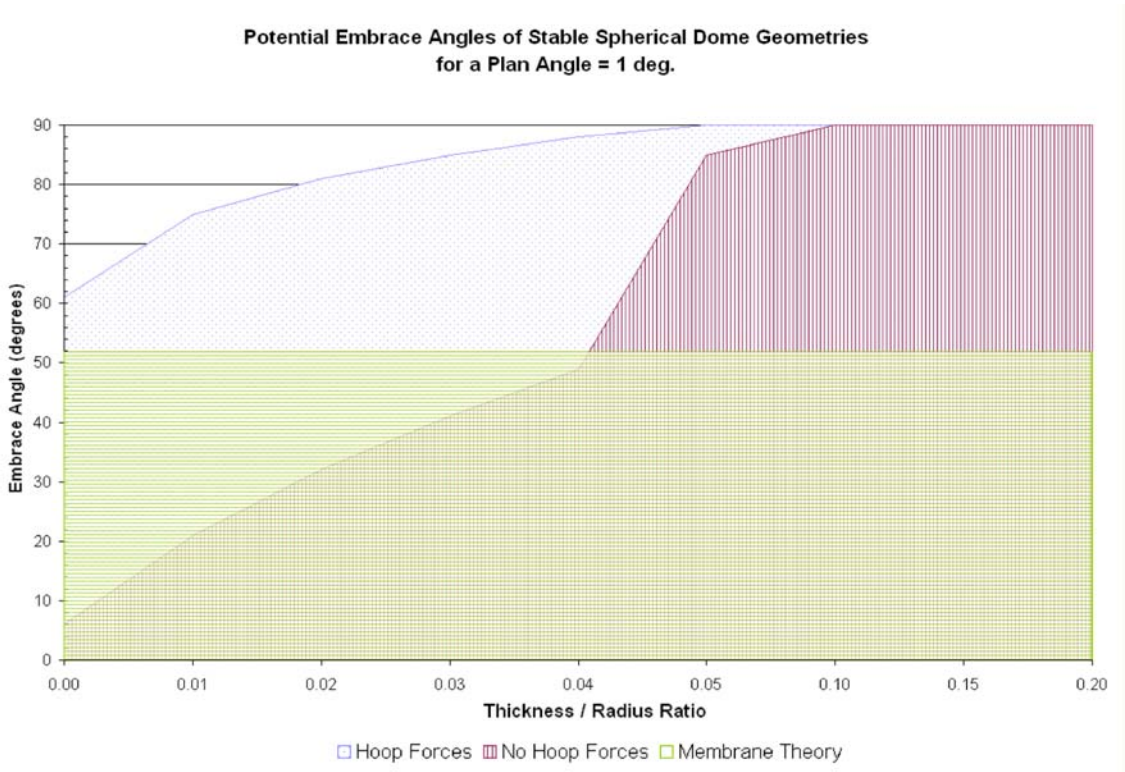

Figure 3.10. The modified thrust line method found that more spherical dome geometries are stable when hoop forces contribute to the dome's stability, than if the dome acted as a series of independent arches.

As the embrace angle increases in thin shells, the thrust line relies on compressive hoop forces to resist the horizontal reaction at the crown, hold the rings of individual masonry units together,

and retain the thrust line within the dome's thickness. At the crown, the horizontal force that the lune's structural counterpart exerts on the lune would tend to collapse the upper dome portion because individual masonry units are unable provide resistance without hoop forces as the dome curves down (Fig. 3.11).

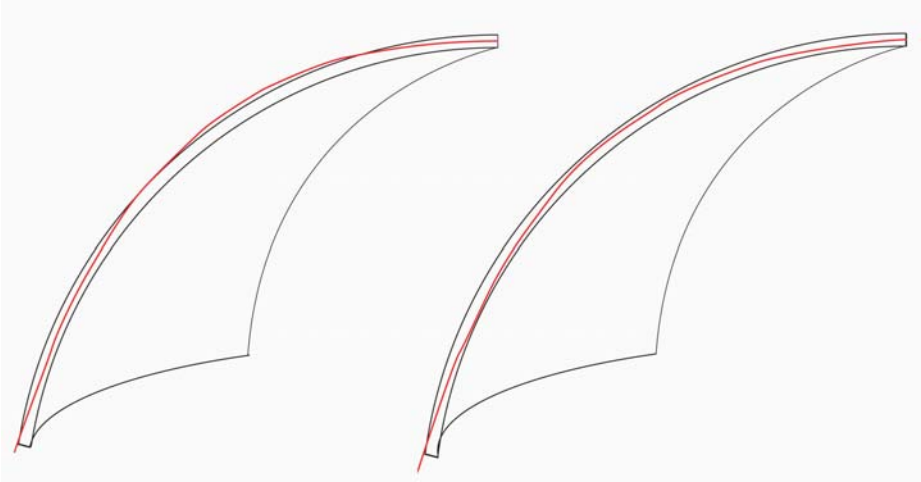

Figure 3.11. Thrust line comparison for lune with $t/R = 0.02$ and $\alpha = 80°$. Left: Without hoop forces, the thrust line exits the dome section as it curves downward. Right: With hoop forces, the thrust line remains within the section.

In very shallow dome geometries, hoop forces become less critical because the curvature of the line of thrust approaches a straight line. The horizontal thrust at the crown and base clamp the masonry units in place in the lune, similar to a flat arch, thus stabilizing the dome with minimal or no hoop forces (Fig. 3.12).

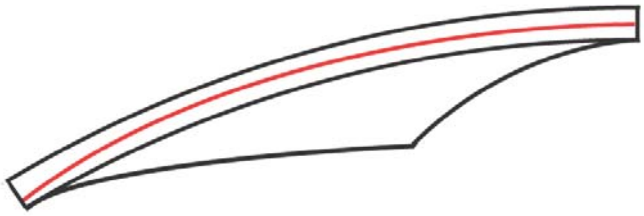

Figure 3.12. In very shallow domes, the line of thrust has low curvature; masonry units are clamped together like a shallow arch reducing the necessity of hoop force transfer between lunes. Here, $t/R = 0.02$ and $\alpha = 30°$.

Without hoop forces, the modified thrust line program predicts a minimum t/R ratio of 0.069 for a hemispherical dome, which is more conservative than Heyman's estimate of 0.042 (Fig. 1.8) (Heyman 1977). With hoop forces in domes with $60° < \alpha < 80°$, the modified thrust line analyses

calculated minimum *t/R* ratios between zero and 0.002 lower than Heyman's study (Fig. 3.13). For a hemispherical dome, the modified thrust line method predicts a minimum *t/R* of 0.041.

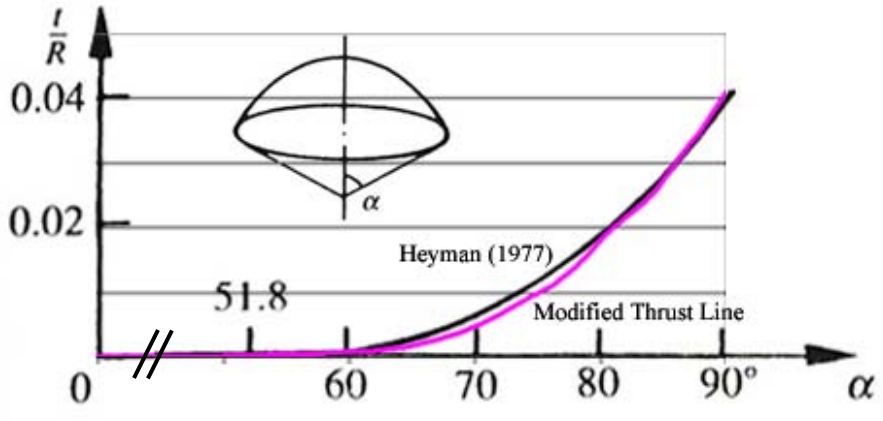

Figure 3.13. The minimum *t/R* versus the angle of embrace as determined by the modified thrust line method superimposed on the solution by Heyman (1995) (complete Heyman solution shown in Fig. 1.8)

From these small differences, the advantages of analyzing a dome as a dome and not as a series of independent lunes are not substantial for spherical domes. Heyman's analytical analysis was accurate under his assumptions, including the negation of hoop forces. His assessment of minimum *t/R* ratios, which were lower than the ratios calculated by the modified thrust line analyses without hoop forces, used thrust lines of domes at incipient collapse; however, the modified thrust line program's thrust line solutions were for stable dome geometries. This coupled with inherent discrepancies in a graphical analysis caused by the simplification of the structure and its loads, versus the precision of an analytical analysis led to the similarity between the results. However, the benefit of hoop forces is more evident in the study of pointed dome geometries examined in Chapter 4.

3.3. Applications of the Minimum Thrust in Spherical Domes

The minimum thrust-to-weight charts have several applications to the analysis and design of masonry domes. Clearly, one can use Figs. 3.2 to 3.5 to estimate the minimum horizontal thrust at the base, equivalent to the "propping" force required at the crown, that renders a dome or dome portion stable (Heyman 1977, p. 114). One may use Figs. 3.6 to 3.8 to estimate this force directly for a standalone lune without hoop forces. At the base of the dome, *h*, the horizontal thrust in units of force per length of circumference is given by:

$$h = \frac{H}{a\theta(\sin\alpha - \sin\delta)} \tag{3.1}$$

Interpolating and Extrapolating the Minimum Thrust

From the relatively linear relationship between *H/W* and α for $\alpha \geq 60°$ shown on Figs. 3.2 to 3.5, a simple linear equation may be written to approximate *H/W* within 20% of the value determined by the modified thrust line analysis, as a function of α in radians:

$$\frac{H}{W} = -0.583\alpha + 1.123 \qquad \text{for } \alpha \geq \frac{\pi}{3} \tag{3.2}$$

Assuming hoop forces occur, an incomplete dome with $\theta \leq 180°$ may be approximated as a collection of smaller lunes with plan angle θ', provided the structure against which the dome abuts can resist the compressive hoop forces at its lateral edges (Fig. 3.14). This resistance is critical at the crown where the greatest hoop forces are most likely to occur.

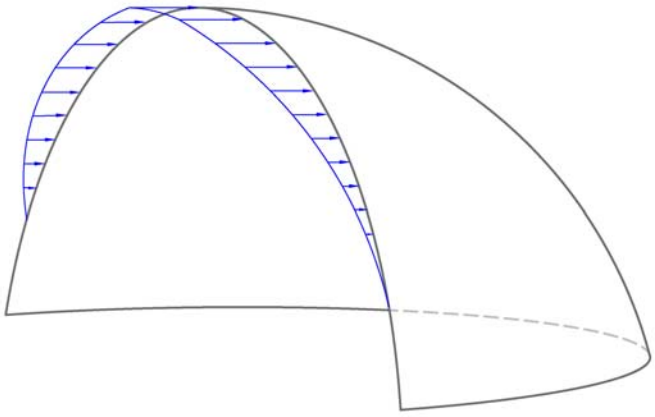

Figure 3.14. The support structure must provide a propping force and resist the compressive hoop forces at the lateral edges of the dome.

As stated previously, as θ increases, the lunes' individual contributions to net thrust diminish at the dome's edges (Fig. 3.15).

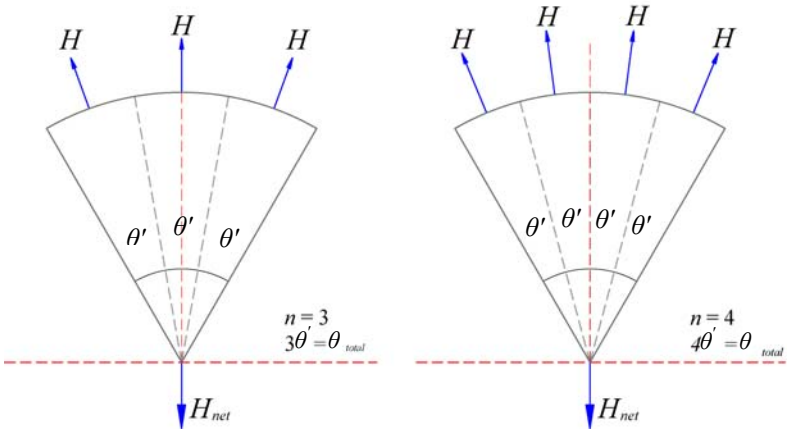

Figure 3.15. The contribution of thrust of the individual lunes to net thrust diminishes at the dome's edges.

For a lune with $\theta \leq 90°$, the net thrust, H_{net}, of an incomplete dome composed of n lunes may be estimated from Eqs. 3.3 and 3.4, provided that $n\theta' \leq 180°$:

For n odd: $H_{net} = H\left[1 + 2 \cdot \sum_{i=1}^{j} \cos(i \cdot \theta')\right]$ where $j = \dfrac{n-1}{2}$ (3.3)

For n even: $H_{net} = 2H \cdot \sum_{i=1}^{j} \cos\left[\dfrac{(2i-1)\theta'}{2}\right]$ where $j = \dfrac{n}{2}$ (3.4)

where H_{net} is the net minimum thrust of the incomplete dome with $\theta = n\theta'$.

Unlike horizontal thrust, the weight of the incomplete dome composed of n lunes with equal θ' values is directly proportional to n:

$$W_\theta = nW_{\theta'=\frac{\theta}{n}} \tag{3.5}$$

The differences in these rates of change for horizontal thrust and weight with respect to θ correlate with the inverse relationship between H/W and t/R demonstrated. For example, from Fig. 3.16, a lune with $\theta = 130°$ will have a net minimum thrust 110 times the minimum thrust of a lune with $\theta = 1°$. However the weight of the larger lune will be 130 times the weight of the smaller lune, and the H/W of the larger lune will be 110/130 = 0.85 times that of the smaller lune.

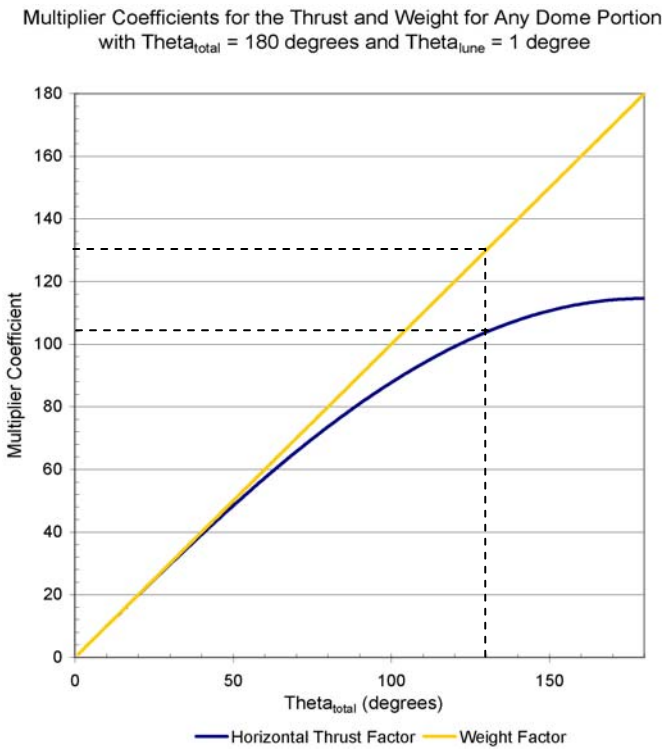

Figure 3.16. The horizontal thrust and weight of a dome consisting of individual lunes changes at different rates.

Using these coefficients, the author estimated the *H/W* of a lune with $\theta = 45°$ from a lune with $\theta = 1°$ (Appendix C). For $t/R \geq 0.10$, the error between this estimate and Fig. 3.4 was highest at about 20% for shallow domes and tapered to less than 5% for $\alpha \geq 60°$, a similar range of error generated by Eq. 3.2. For $t/R < 0.10$, the difference between the estimated and actual *H/W* was within 10% for $20° \leq \alpha \leq 90°$. Thus, extrapolation of the minimum thrust data for lunes with plan angles other than those provided in Figs. 3.2 to 3.5 will produce a reasonable approximation of *H/W* for near-complete domes and thin shell domes.

Estimating the Minimum Thrust through Equilibrium Equations

To a limited extent, one may use static equilibrium equations to approximate the minimum thrust. Assuming a pin support at the mid-point of the lune's bottom edge, and a vertical roller support at the dome's extrados at the centerline, the minimum horizontal reaction at the crown, *H*, to prevent inward rotation due to self-weight is:

$$H = \frac{W\left(a \sin \alpha - x_{cg\ lune}\right)}{(a+t)\cos\delta - a\cos\alpha} \tag{3.6}$$

where W is the weight of the lune (Eq. 2.5), $x_{cg\ lune}$ is the center of gravity of the lune (Eq. 2.6), and t is equal to half the dome thickness (Fig. 3.17).

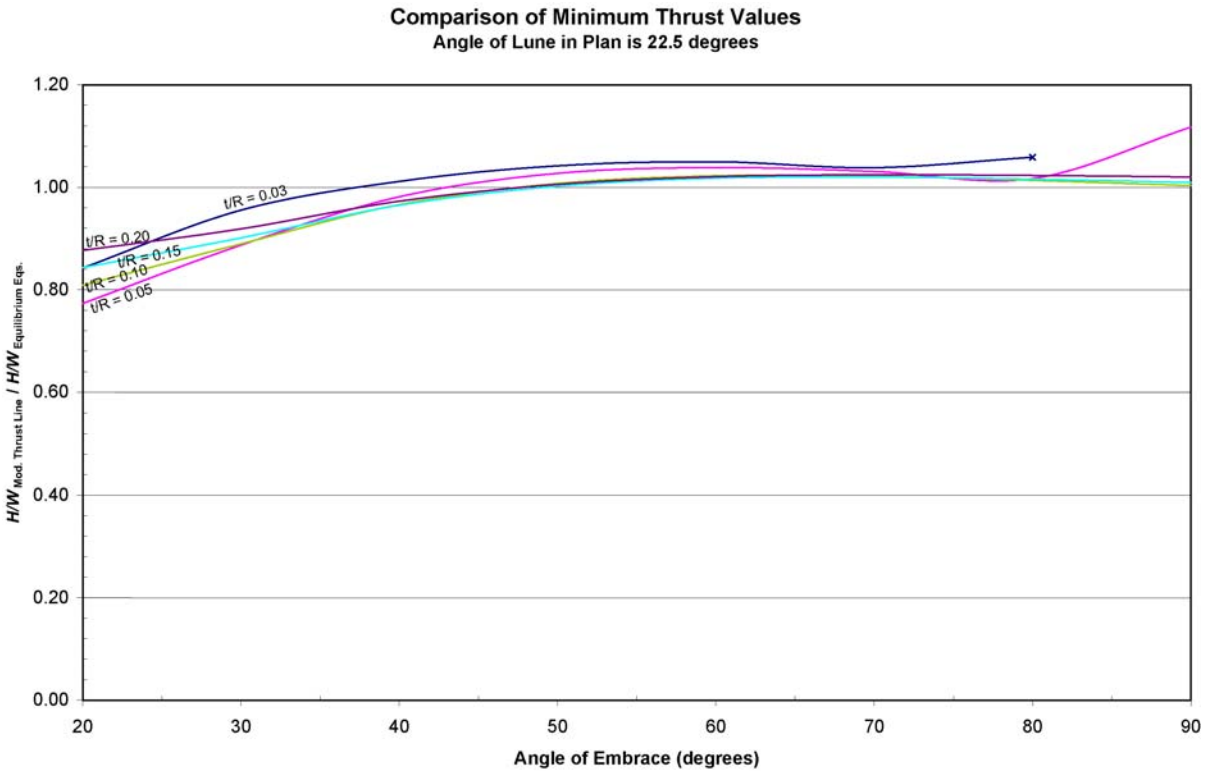

Figure 3.17. The difference between H/W determined from the modified thrust line method and from static equilibrium equations

In general, for domes with $\alpha < 40°$, the minimum thrust calculated by the modified thrust line analysis will be about 5 to 20% lower than that calculated with static equilibrium equations. As the embrace angle approaches 90 degrees, the thrust values from the two methods are, for the most part, within 5%, a good approximation for a wide range of embrace angles. However, one should be cautious in using equilibrium or other equations because they reveal nothing about the dome's stability. For example, the equations produce a thrust value for a dome with $t/R = 0.001$ and $\alpha = 90°$ when in reality, this geometry is stable only if the dome can resist tension forces.

The Half-Dome as a Buttress

The half-dome is frequently employed as a buttress against vertical bearing walls or at the base of a larger dome, such as the configuration at the Hagia Sophia. "The half-dome in fact can stand freely, and will also be stable when subjected to the out-of-balance horizontal force from the

lunes" (Heyman 1995, p. 43). This can be envisioned conceptually with Eq. 2.6, which locates the centroid of a half-dome at approximately half the span between the centerline and the intrados of the dome base. Thus either a distributed vertical reaction along the base at $0 \le x \le x_{cg}$, or a propping force, *H*, at the crown can prevent overturning of the dome (Fig. 3.18). The author estimated *H/W* of a half-dome using Fig. 3.4 and Eq. 3.4 where $n = 4$ (Fig. 3.19).

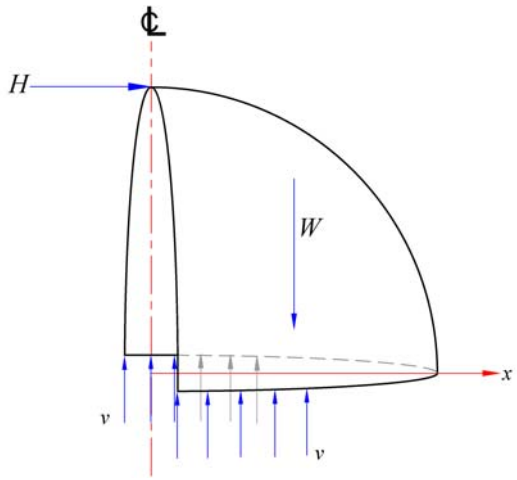

Figure 3.18. The half-dome is a stable structure due to horizontal and/or vertical reactions that resist its overturning.

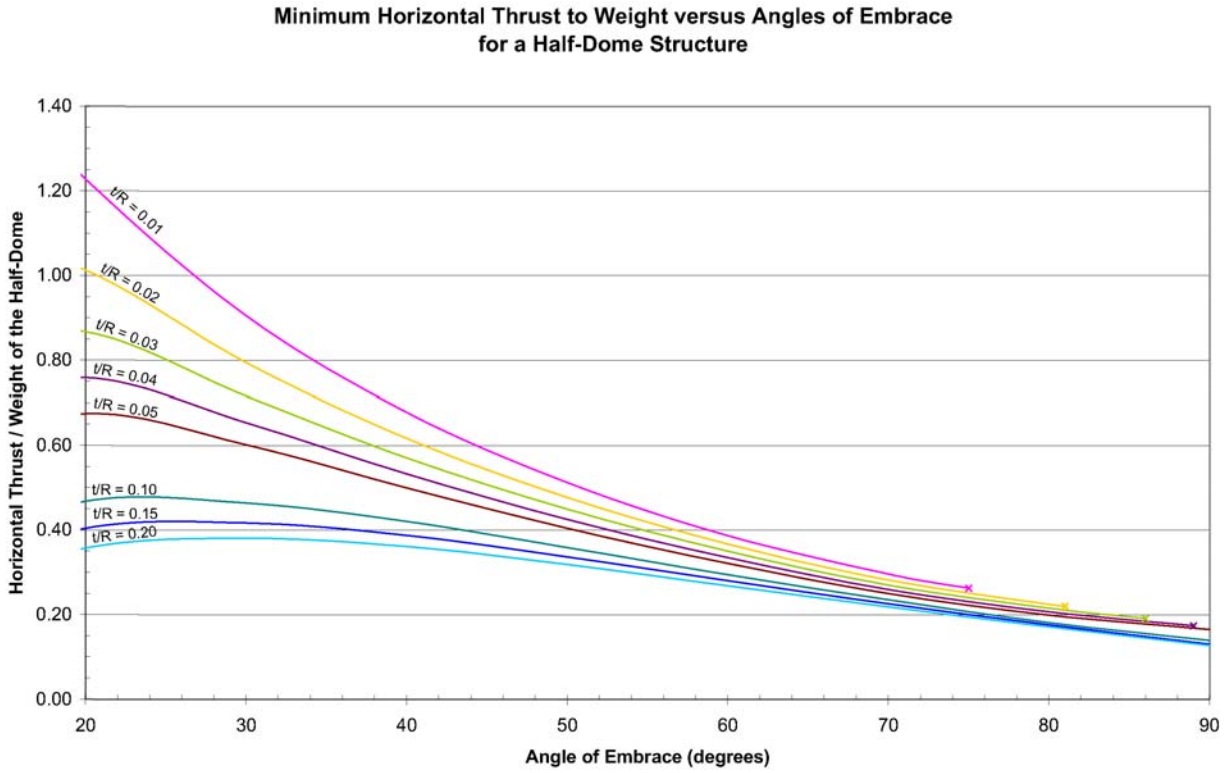

Figure 3.19. The minimum thrust for a half-dome as estimated by the modified thrust line analysis

For a half-dome with $\alpha = 90°$, *H/W* is between 0.12 and 0.18, which is comparable to Heyman's study of estimated thrust as $H = 0.068 \cdot W_{dome}$, where W_{dome} is the weight of a complete hemispherical dome or $2 \cdot W$, where W is the weight of the half-dome (Heyman 1977).

The author analyzed the minimum thrust of a half-dome as a structure composed of four lunes, each with $\theta = 45°$, instead of a single lune with $\theta = 180°$. In general, for $\theta > 45°$, the modified thrust line estimate will provide a conservative minimum thrust value because the stability of the wide lune likely relies on a thrust surface than a single thrust line.

Stability of the Support Structure

The *H/W* ratio also provides insight to the stability of the support structure under the dome. The inverse of the ratio, equivalent to the slope of the steepest satisfactory thrust line at the dome-support structure interface, may be used to calculate the height at which the thrust line exits the structure's walls, assuming the walls have no tensile resistance or reinforcement (Fig. 3.20).

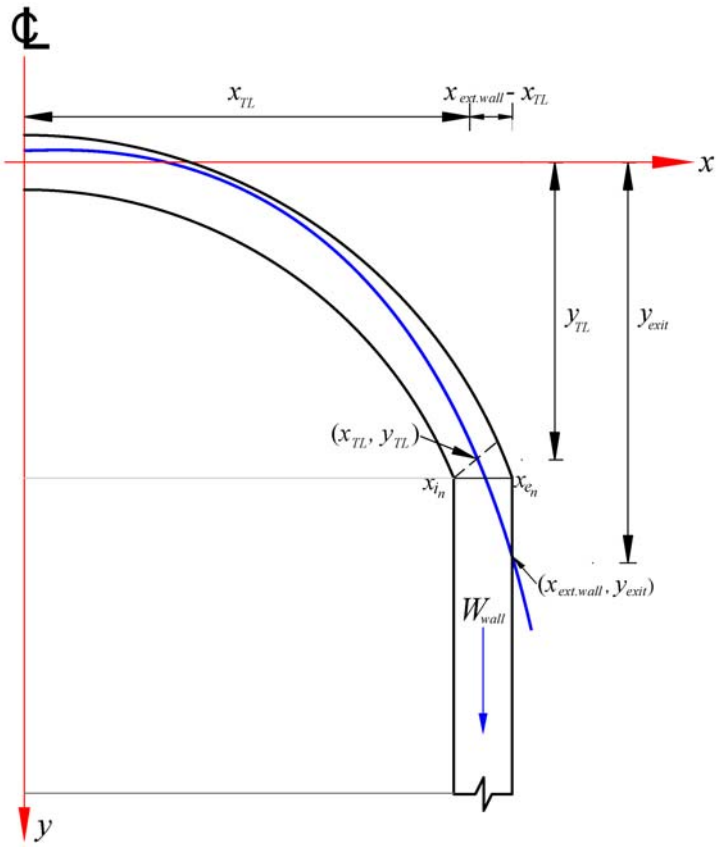

Figure 3.20. Parameters to locate the exit point of the thrust line in the support structure under the dome

The modified thrust line method assumes a tangential support at the dome's base. Two additional loads contribute to the weight of the "voussoir" representing the support structure, which may affect the slope of the thrust line as it enters the support structure:

1. The weight of the dome base not included in the original analysis if the dome terminates parallel to the horizontal (delineated as a triangle wedge in Fig. 3.20). This may be negligible relative to the weight of the entire structure.

2. The weight of the support structure with length $a\theta(\sin\alpha - \sin\delta)$, and thickness between x_{i_n}, the intrados of the dome at its base, and x_{e_n}, the extrados at its base.

The *x*-coordinate[6] of the initial point of the segment of the thrust line entering the support structure is given by Eq. 3.6 where $\beta = \alpha - \frac{\pi}{180}$ and $\gamma = \alpha$, in radians. The *y*-coordinate of the thrust line with respect to the median height of the dome is:

$$y_{TL} = k \cdot a(\cos\delta - \cos\alpha) \tag{3.7}$$

where *k* is given in Table 3.1 for a lune of $\theta = 1°$.

For example, for a spherical dome with $t/R = 0.04$, $\alpha = 60°$, $a = 25$ ft, the median height of the dome is $a(\cos\delta - \cos\alpha) = 25(\cos 0° - \cos 60°) = 12.5\,ft$. The estimated distance to the last point of the thrust line in the dome with respect to the median height of the dome at the crown is, from Eq. 3.7: $y_{TL} = 1.005 \cdot 25(\cos 0° - \cos 60°) = 12.56\,ft$. This point of the thrust line is slightly lower than the midpoint of the sloped bottom edge of the dome.

[6] Assuming the thicknesses of the support structure and dome base are equal. Otherwise, the thrust line with a slope of $-\left(\frac{H}{W}\right)^{-1}$ enters the support wall and changes slope only after $x_{TL} > x_{cg\ wall}$ to $-\left(\frac{H}{W+W_{wall}}\right)^{-1}$.

Table 3.1. Values of k, the vertical distance between the median height of the dome and last point of the thrust line segment in the dome, divided by the median height for a spherical lune with a = 33 ft and θ = 1°. Values in parentheses are the maximum stable embrace angle to be used in lieu of the angle shown in the first column.

	Thickness-to-Radius Ratio								
Angle of Embrace (deg.)	**0.001**	**0.01**	**0.02**	**0.03**	**0.04**	**0.05**	**0.10**	**0.15**	**0.20**
20	0.971	1.041	1.127	1.228	1.237	1.239	1.221	1.188	1.142
30	0.969	1.001	1.047	1.095	1.093	1.094	1.086	1.073	1.055
40	0.977	0.997	1.030	1.033	1.033	1.033	1.030	1.022	1.013
50	0.982	1.001	1.013	1.012	1.012	1.012	1.010	1.007	1.001
60	0.985	1.002	1.005	1.005	1.005	1.004	1.003	1.001	0.998
70	(62) 0.984	0.992	1.001	1.001	1.001	1.001	1.001	1.000	0.998
80		(75) 0.973	0.964	0.992	1.000	1.000	1.000	0.999	0.999
90			(81) 0.956	(85) 0.943	(88) 0.931	0.926	1.000	1.000	1.000

The thrust line exits the support wall at y_{exit}, the vertical distance with respect to the crown:

$$y_{exit} = -\frac{W_{lune} + W_{wall}}{W_{lune} \cdot c}\left(x_{ext.wall} - x_{TL}\right) + y_{TL} \tag{3.8}$$

where W_{lune} is the weight of the dome lune of θ = 1°, c is the minimum thrust-to-weight ratio, H/W, given in Figs. 3.2 and 3.5, W_{wall} is the weight of the support wall portion described above, and $\left(x_{ext.wall} - x_{TL}\right)$ is the distance between the exterior face of the support wall and the center of gravity of the lowest voussoir in the lune. A case study in Chapter 5 demonstrates this procedure to check the stability of the support structure.

Internal Force Comparison to the Membrane Theory

The membrane theory remains a common method with which to analyze the structural behavior of thin-shell masonry domes. However, the membrane theory equations cannot specify only non-tensile internal hoop force solutions; therefore, its solutions do not meet limit state conditions for domes with embrace angles greater than 52 degrees (Eqs. 2.1 and 2.2). However, internal hoop forces determined with the modified thrust line method may be limited to either compressive or zero, the latter signifying hoop forces are not required in the corresponding regions to stabilize the dome. Figure 3.21 plots the φ-angle at which the modified thrust line analysis predicts zero hoop forces from that point in the dome down to its base for a lune of θ = 1° and $t/R \leq 0.05$ under uniform axisymmetrical load conditions.

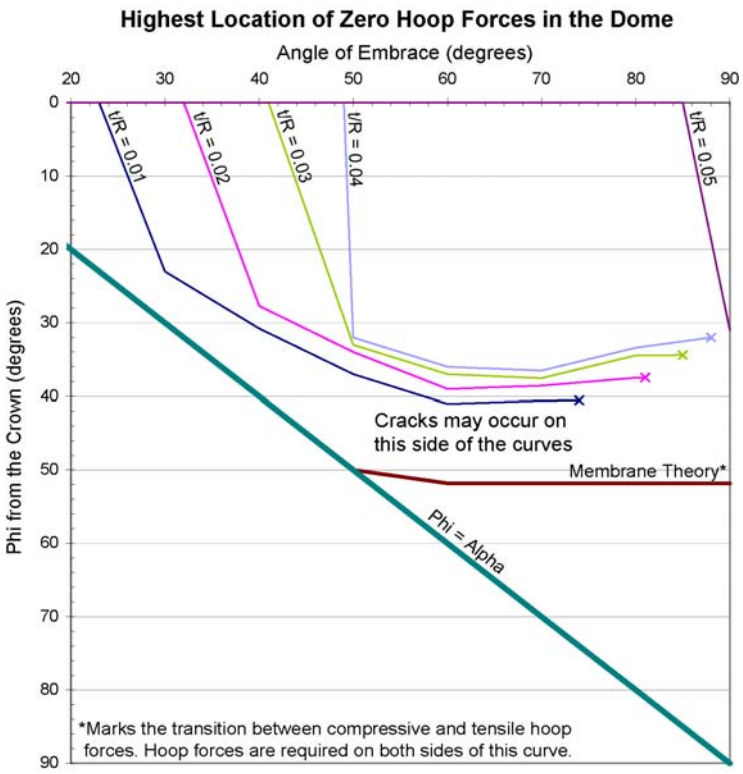

Figure 3.21. Hoop forces are not necessary between the modified thrust line curves and the "Phi = Alpha" line. The "Membrane Theory" curve marks only the transition point between compressive and tensile hoop forces.

In theory, a spherical dome with meridional cracks anywhere between the modified thrust line curves and the "Phi = Alpha" line shown in Fig. 3.21 will be stable. For instance, a dome with $t/R = 0.03$ and $\alpha = 42°$ with continuous meridional cracks from the base up to $\varphi = 10°$ would theoretically be stable. For domes in which $t/R > 0.05$, hoop forces are not required in the stability of the dome. Thus if the structure is reasonably intact, that is, with no missing voussoirs or substantial material deterioration, et cetera, then it is stable even with meridional cracks from crown to base.

In contrast, the "Membrane Theory" curve marks only the transition point at where hoop forces switch from compressive to tensile; hoop forces are necessary on both sides of this curve. Under the membrane theory, any meridional cracks, which preclude the development of hoop forces, render the dome as unstable. Thus, for domes with $t/R \leq 0.05$, the modified thrust line analyses provide insight on the impact of meridional cracks on the stability of spherical masonry domes, while the membrane theory provides no such information.

3.4. Chapter Summary

This chapter discussed the minimum thrust values of spherical masonry domes and their applications in structural behavior. The chapter also summarized and explained salient relationships between minimum thrust and dome geometry, as well as methods to estimate the minimum thrust for all spherical domes loaded only by self-weight, the dominant load that masonry domes carry. In addition, this chapter discussed a method to assess the stability of the support structure under the dome, and the impact of meridional cracks to the stability of spherical masonry domes. The next chapter will address these issues for an equally important and common dome geometry: pointed domes.

Chapter 4. The Modified Thrust Line Analysis and Pointed Domes

This chapter discusses the use of the modified thrust line method for pointed dome geometries to attain minimum thrust values, patterns of structural behavior, and structural limits that have not been solved before. Pointed domes considered here are formed by rotating two curves with the same radius of curvature about a vertical axis offset symmetrically from two centers of curvature by a horizontal distance, $a \sin \delta$, where δ is the angle that truncates the dome curve at the crown (Fig. 4.1).

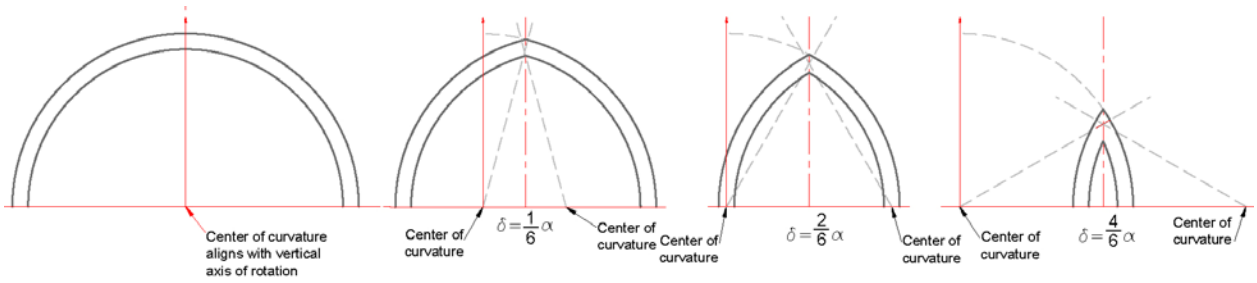

Figure 4.1. Comparison of dome sections with different truncation angles, δ, and equal radii of curvature

This study makes similar assumptions to those outlined in the spherical dome study: Meridional forces increase from the crown to the base of the dome, while hoop forces are generally highest in compression in the crown and lower in magnitude toward the base. Hoop force values may fluctuate between increasing and decreasing in adjacent dome rings. Finally, the slope of the thrust line always increases in magnitude, or becomes steeper, from crown to base if the dome experiences only uniform axisymmetrical loads.

As stated in Chapter 2, the weight and centroid of the voussoirs calculated by Eqs. 2.5 and 2.6 will slightly deviate from actual values depending on the "sharpness" of the crown (Fig. 2.5).

4.1. Minimum Thrust Results for Pointed Domes with Two Centers of Curvature

The maximum δ value evaluated in the spreadsheet program of the modified thrust line method was $\delta_{\max} = \sin^{-1}\left(1 - \frac{t}{R}\right)$, to satisfy the criteria that $a \sin \delta \le a - t$. The program analyzed domes with the following parameters:

- Thickness-to-radius ratios of 0.05, 0.08, 0.10, 0.15, and 0.20
- Angles of embrace of 30, 45, 60, 80, 85, and 90 degrees
- Truncating angles at the crown, δ, from 0 to $5\alpha/6$ in increments of $\delta_{max}/6$ degrees
- Lune segments with angles in plan of 1, 22.5, and 45 degrees.

The author limited the analyses to these parameters to study based on common geometries of existing pointed domes. The program assumed a radius of curvature of 33 ft and a material unit weight of 100 pcf, but, similar to the spherical dome study, the magnitude and units are factored out in the final result: the minimum horizontal thrust-to-weight ratio, *H/W*. The program subdivided each lune into the larger of 30 or $(\alpha - \delta)°$ voussoirs, and assumed the domes were axisymmetrically loaded by self-weight only. The modified thrust line program searched for the thrust line producing the minimum thrust by assuming it would be closer to the dome extrados at the crown, and then progressing toward the intrados in increments of *a/3000* until it found a satisfactory solution. The program kept the thrust line at least *a/3000* away from the extrados of the dome.

The author experimented with different numbers of voussoir divisions and thrust line tolerances to the dome's extrados, and also conducted simulations in which the program initially tested thrust lines in closer proximity to the dome's intrados. In a limited number of cases, this strategy produced a lower *H/W* ratio by a few percent at most; however, the thrust line originating closer to the extrados produced a lower *H/W* ratio for the majority of the cases analyzed.

The plots of the minimum thrust values for pointed domes show different fixed values and variables than the charts for the spherical dome results. In Figs. 4.2 to 4.10, the embrace angle, α, and angle in plan, θ, are constant while the thickness-to-radius ratio, *t/R*, and truncating or initial angle at crown, δ, vary. Due to large number of parameter combinations tested, only the summary charts for only the analyses using embrace angles of 30, 80 and 90 degrees are included in the main text of this thesis. Appendix D contains the summary charts for the minimum thrust-to-weight ratios for all pointed dome geometries analyzed in this study.

Figures 4.2 to 4.4 plot the minimum thrust-to-weight ratios versus δ for a pointed dome lune with $\theta = 1°$. Figures 4.5 to 4.7 plot the minimum thrust-to-weight ratios versus δ for a pointed dome lune with $\theta = 22.5°$. Figures 4.8 to 4.10 plot the minimum thrust-to-weight ratios versus δ for a pointed dome lune with $\theta = 45°$. These figures combine the analyses that included and neglected hoop forces between lunes because *H/W* results were or nearly were equal. The without-hoop force analyses are later shown separately to highlight the role of hoop forces in the stability of pointed domes.

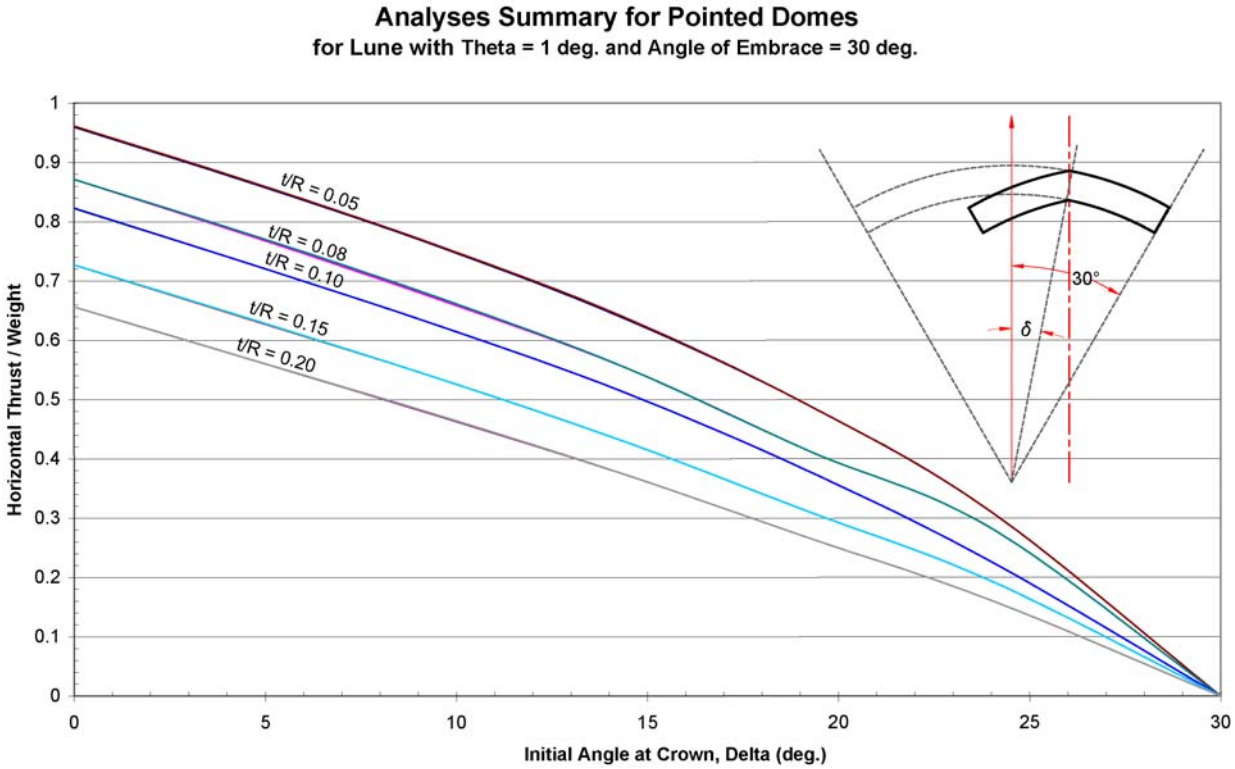

Figure 4.2. Minimum horizontal thrust for a pointed dome with $\theta = 1°$ and $\alpha = 30°$. The curves for the with- and without-hoop force analyses coincide due to the similarity of the results.

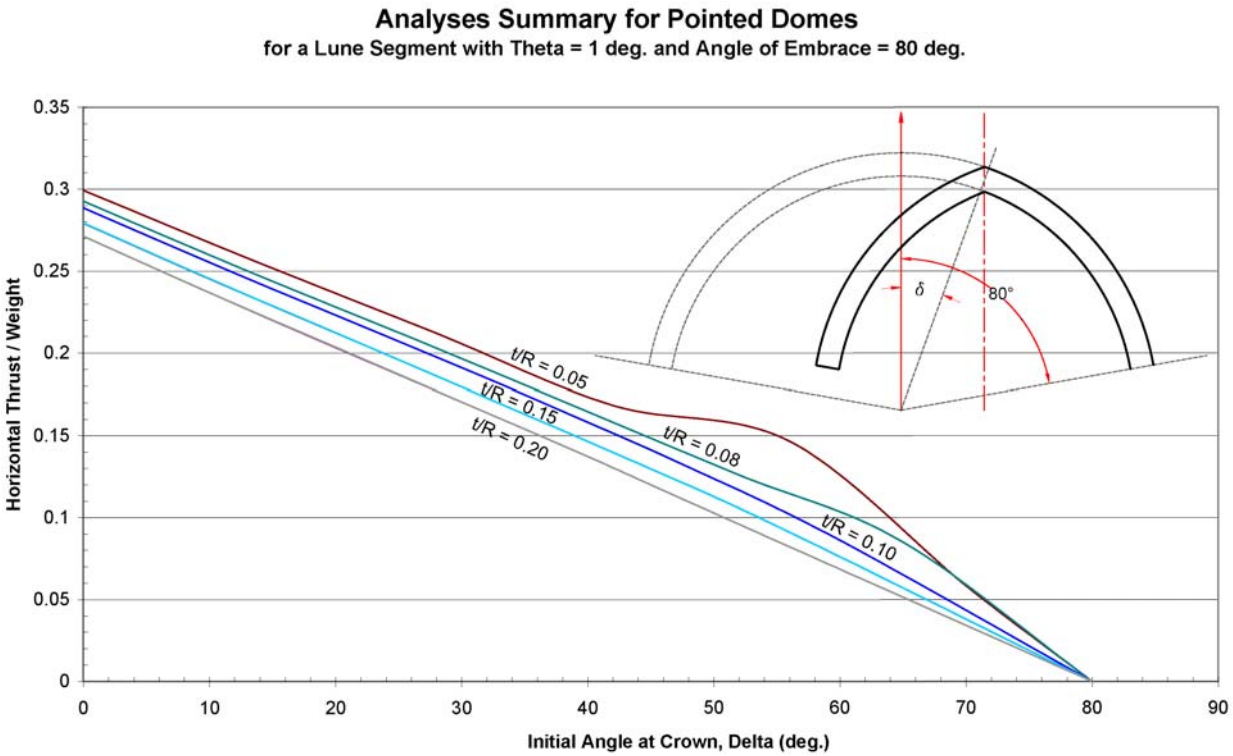

Figure 4.3. Minimum horizontal thrust for a pointed dome with $\theta = 1°$ and $\alpha = 80°$. The curves for the with- and without-hoop force analyses coincide due to the similarity of the results. The bump in the $t/R = 0.05$ curve is exaggerated due to the large scale of the y-axis.

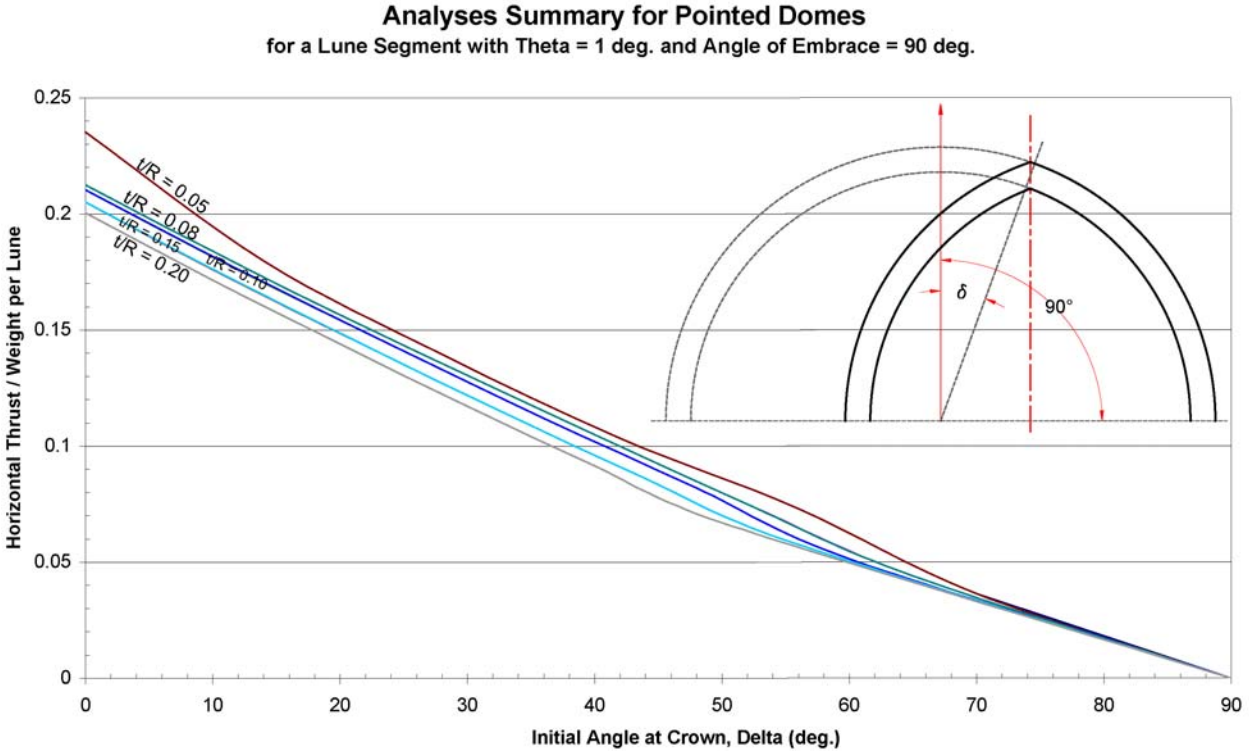

Figure 4.4. Minimum horizontal thrust for a pointed dome with $\theta = 1°$ and $\alpha = 90°$. The curves for the with- and without-hoop force analyses coincide due to the similarity of the results.

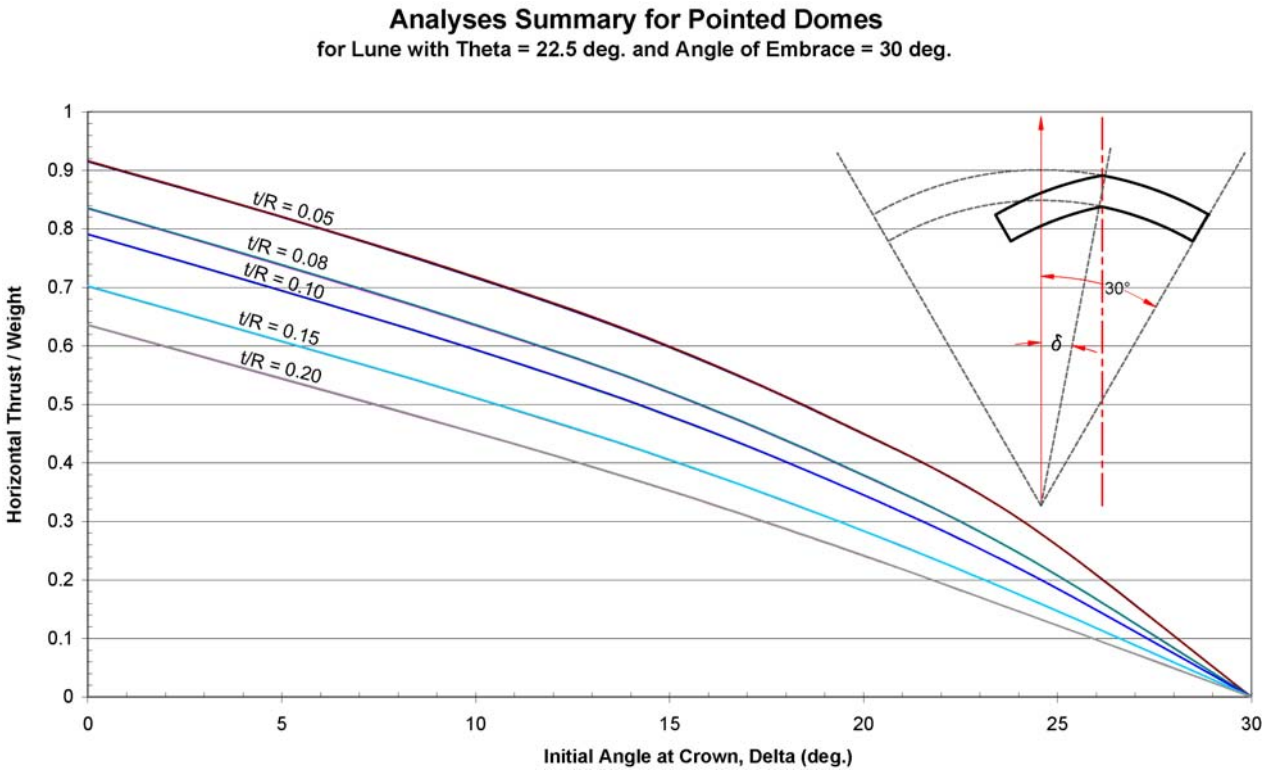

Figure 4.5. Minimum horizontal thrust for a pointed dome with $\theta = 22.5°$ and $\alpha = 30°$. The curves for the with- and without-hoop force analyses coincide due to the similarity of the results.

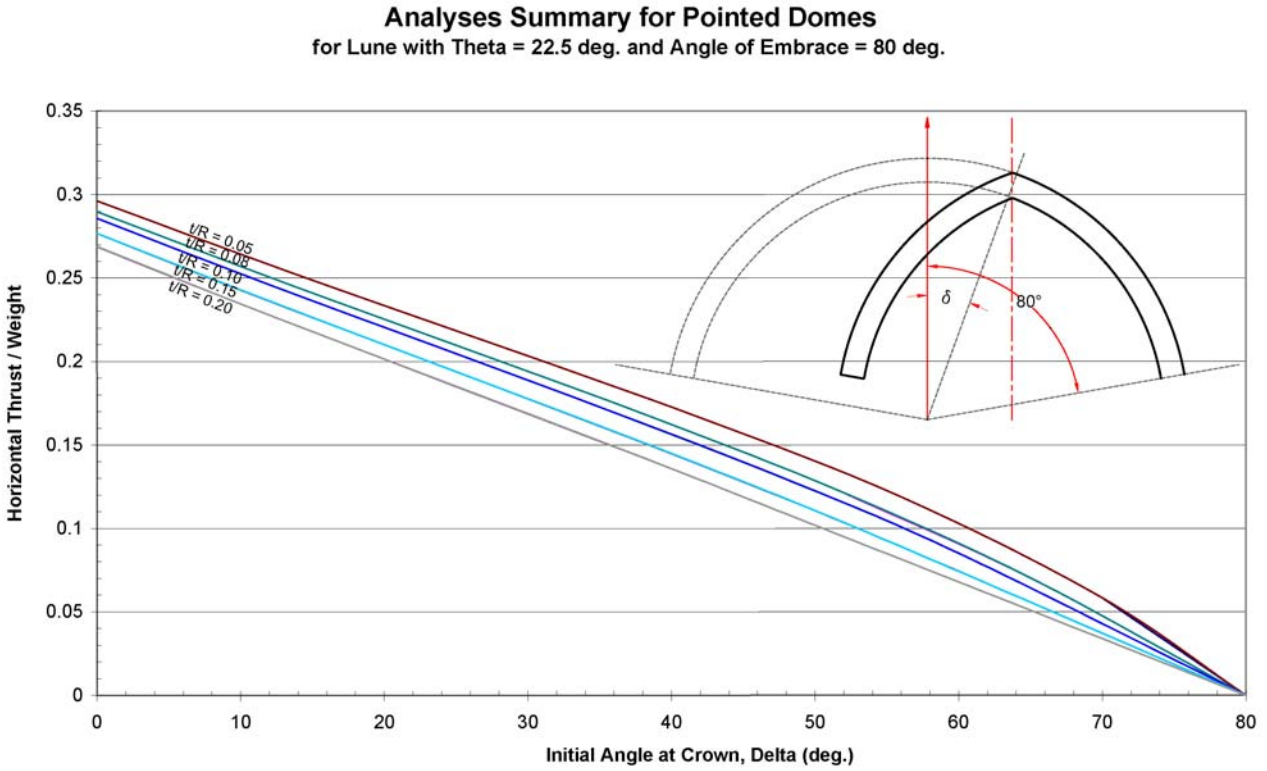

Figure 4.6. Minimum horizontal thrust for a pointed dome with $\theta = 22.5°$ and $\alpha = 80°$. The curves for the with- and without-hoop force analyses coincide due to the similarity of the results.

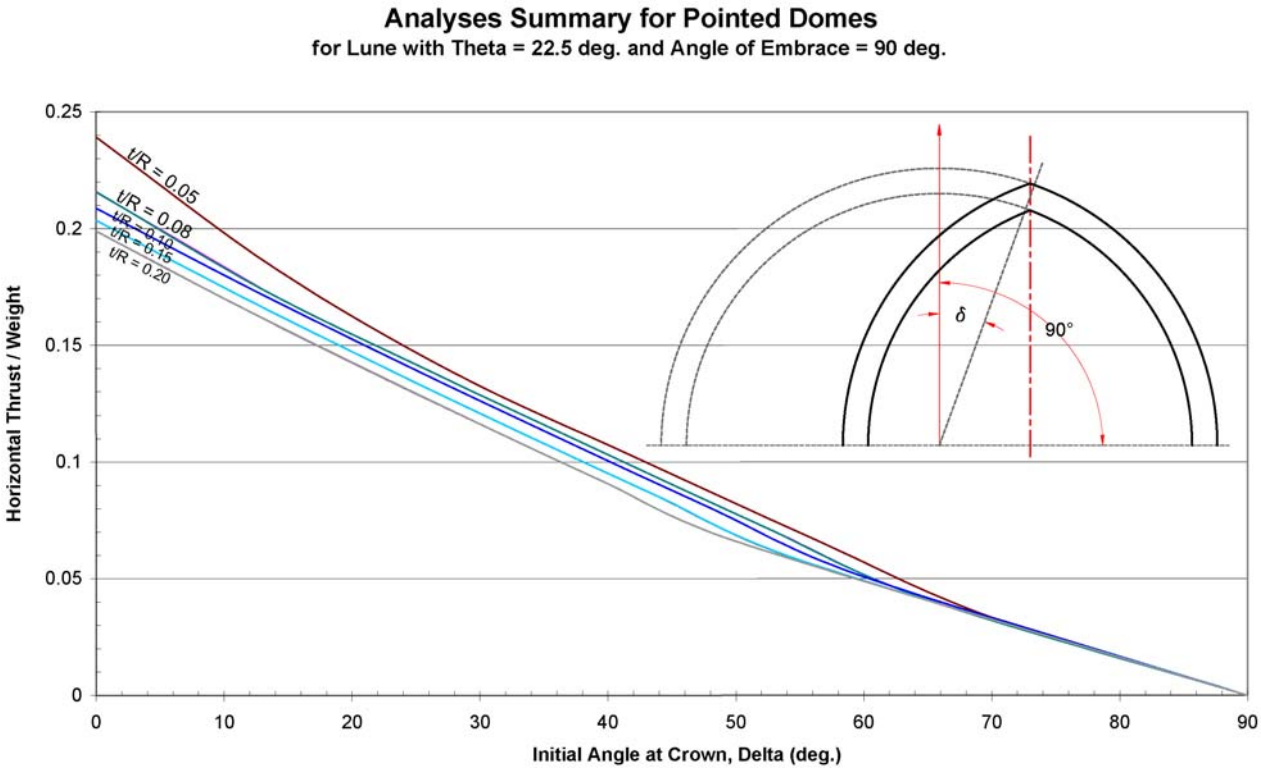

Figure 4.7. Minimum horizontal thrust for a pointed dome with $\theta = 22.5°$ and $\alpha = 90°$. The curves for the with- and without-hoop force analyses coincide due to the similarity of the results.

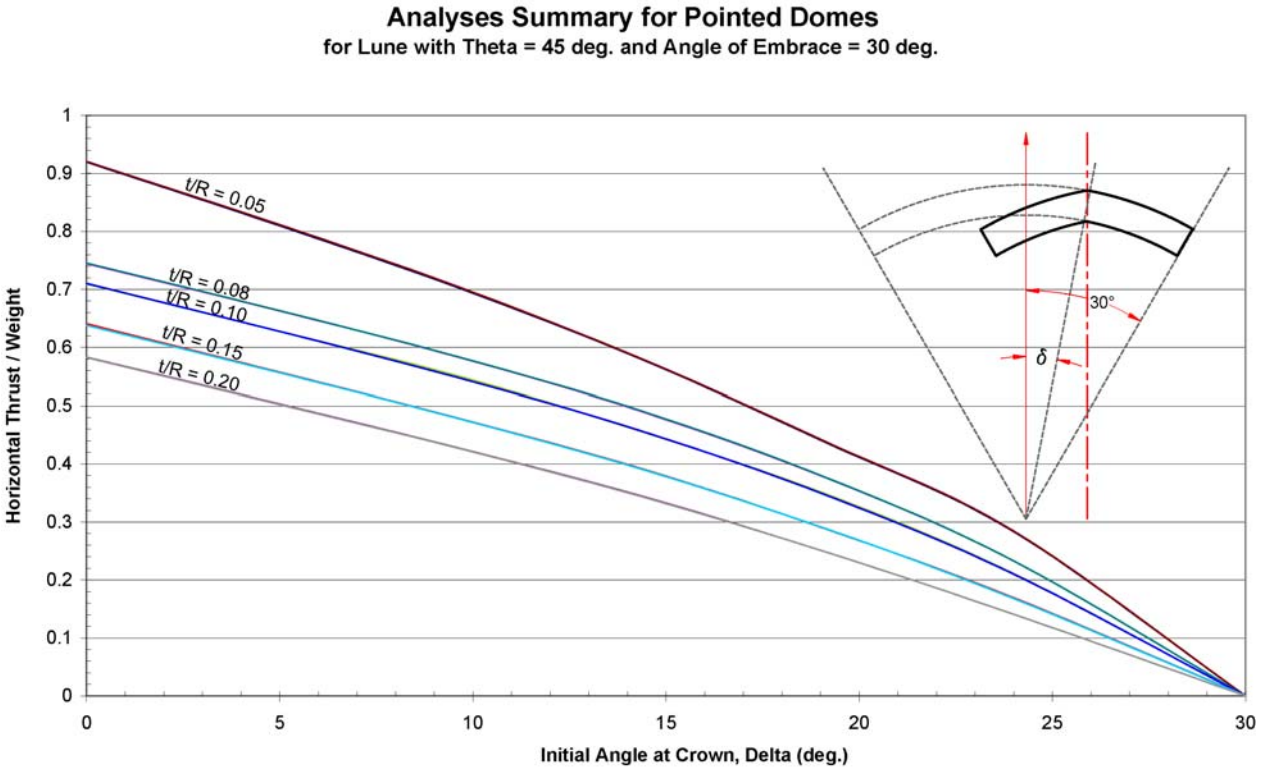

Figure 4.8. Minimum horizontal thrust for a pointed dome with $\theta = 45°$ and $\alpha = 30°$. The curves for the with- and without-hoop force analyses coincide due to the similarity of the results.

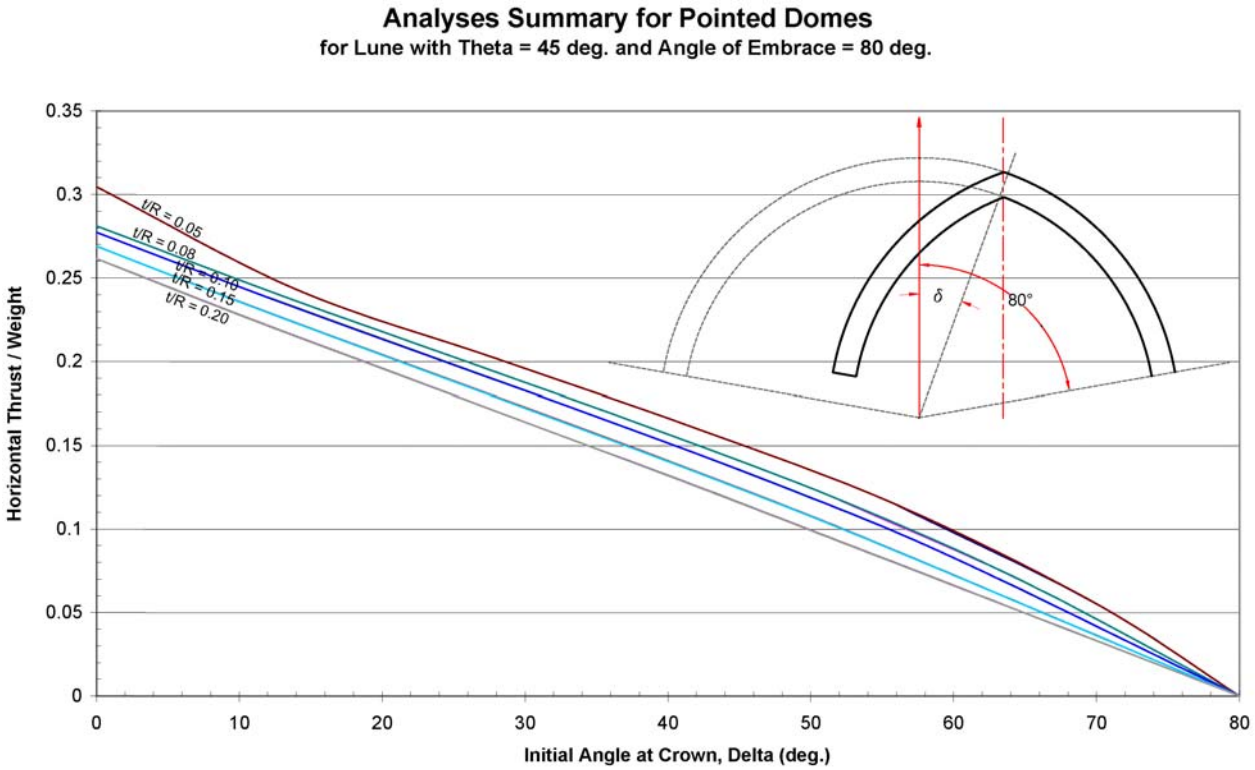

Figure 4.9. Minimum horizontal thrust for a pointed dome with $\theta = 45°$ and $\alpha = 80°$. The curves for the with- and without-hoop force analyses coincide due to the similarity of the results.

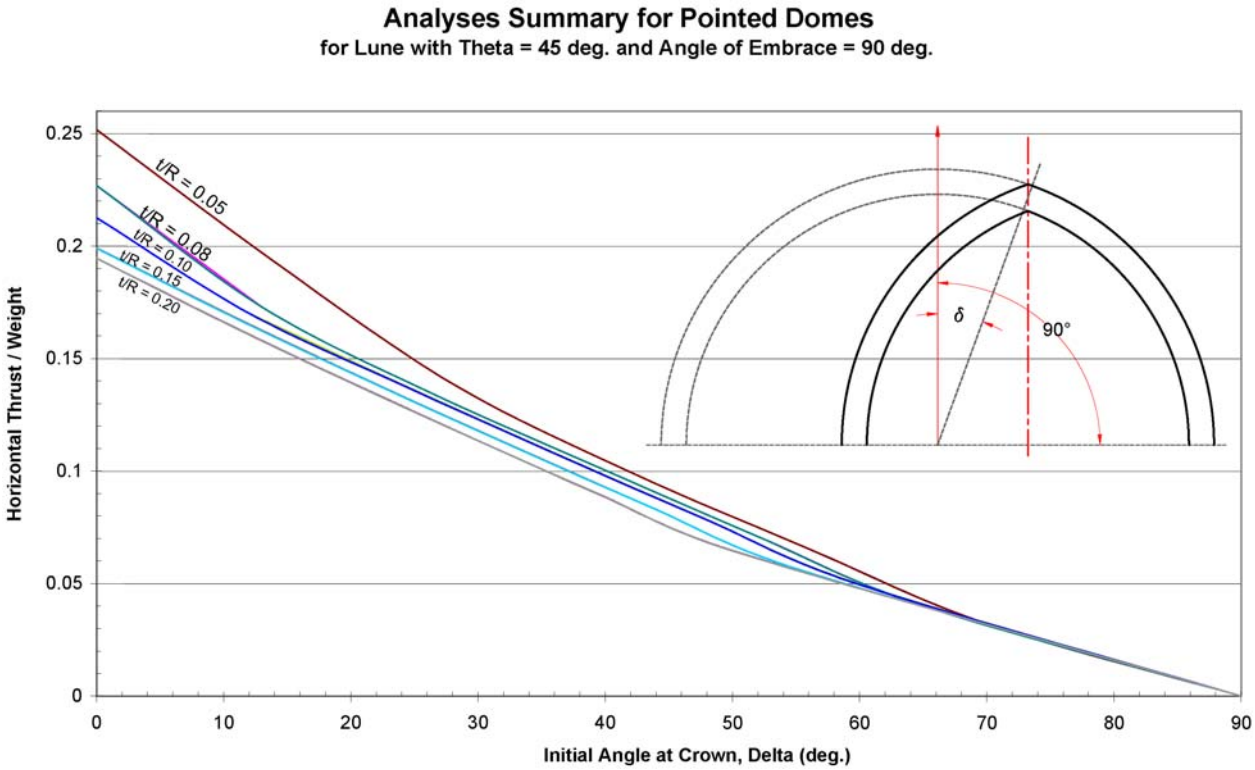

Figure 4.10. Minimum horizontal thrust for a pointed dome with $\theta = 45°$ and $\alpha = 90°$. The curves for the with- and without-hoop force analyses coincide due to the similarity of the results.

From the above figures, the following salient trends regarding the minimum thrust-to-weight ratio to pointed dome geometries are evident:

- The minimum thrust is inversely related to t/R and to α.
- In general, H/W and δ are linearly and inversely related. H/W decreases as δ approaches α; in other words, as the dome becomes steeper and the arc length between the crown and the base of the dome decreases, H/W decreases.
- For larger α values, the effect of t/R on the minimum thrust decreases. For example, for a dome with $\alpha = 30°$, H/W for $t/R = 0.05$ is about 30% lower than for $t/R = 0.20$; for $\alpha \geq 80$ degrees, H/W ratios between any t/R values are within 5%.
- The angle in plan, θ, has little impact on H/W. Minimum thrust values are within 5% for a constant t/R, δ, and α, and θ values of 1, 22.5, and 45 degrees.
- The inclusion of hoop forces in the analyses has no effect on the values of H/W; Figs. 4.2 through 4.10 plot both the with- and without-hoop force results, but their similarities preclude their distinction. However, incorporating hoop forces significantly increases the range of stable geometries for pointed domes with $t/R \leq 0.08$.

For all analyses, the internal stress values, which depend on masonry unit weight, are below the crushing stress for masonry.

4.2. Discussion of Results for Pointed Domes with Two Centers of Curvature

The minimum horizontal thrust-to-weight ratios from the modified thrust line method reveal several trends in the behavior of pointed dome structures.

Minimum Thrust-to-Weight Ratio, *H/W*, and the Embrace Angle, α

For a constant δ, as α increases, the thrust-to-weight ratio of a pointed dome decreases. Thrust developed in the upper portion of the dome, due to transfer of the masonry self-weight to the supports hoop forces, or the propping reaction force at the crown, is not resisted in the masonry. Descending from the crown to the base, the rate at which thrust increases gradually declines as

the dome curve becomes more vertical. While increasing the embrace angle adds little additional thrust to the dome, the weight of the dome does increase proportionally, resulting in a lower *H/W* ratio as α approaches 90 degrees.

Minimum Thrust-to-Weight Ratio, *H/W*, and the Truncating Angle, δ

For constant α, the minimum thrust is inversely related to δ. The thrust develops mostly in areas of near-horizontal orientation, such as the cap of a spherical dome, where masonry units must push against each other to resist inward rotation. For small values of δ, indicating a near-spherical dome, the thrust generated in the dome is large. As δ approaches α, and the pointed dome becomes steeper, the centroid of the lune approaches the toe of the lune, reducing the tendency of the voussoirs and the dome to overturn. As the arc length between the crown and the base decreases and the dome becomes steeper, the force path on which the dome's loads transfer to the supports becomes nearly vertical, resulting in small thrust values.

Minimum Thrust-to-Weight Ratio, *H/W*, and Thickness-to-Radius Ratio, *t/R*

For constant α and δ, the inverse relationship between *t/R* and *H/W* is similar to that for spherical domes discussed in Chapter 3. For larger *t/R* ratios, the centroid of the lune is closer to the toe about which the lune would rotate, and the propping force or thrust to counteract this moment decreases, while the weight of the lune increases. For shallow domes, the range of *H/W* ratios with respect to *t/R* is slightly larger than the range of values for deeper domes, but this is mostly due to the relationship between *H/W* and α discussed before.

Minimum Thrust-to-Weight Ratio, *H/W*, and Angle in Plan, θ

With all other parameters constant, in general, changing θ has little effect on *H/W*. Increasing the θ value of the lune will slightly decrease *H/W* by less than 5%; conceptually, though the weight of the lune increases proportionally with θ, the horizontal thrust increases at an equal or slightly slower rate due to the "fanning" out of the lunes around the axis of revolution. The low *H/W* ratios for domes with large embrace angles manifest in the reduced difference in *H/W* with respect to θ.

The Impact of Hoop Forces

For the dome geometries studied, the presence or absence of hoop forces has little impact on the *H/W* ratio as long as the modified thrust line method finds a satisfactory thrust line. With the exception of extremely steep domes where δ is within 20 degrees of α, compressive hoop forces are required in the dome cap for stability of thin pointed domes with $t/R = 0.05$ or 0.08.

As mentioned briefly above, the lune of a pointed dome with $t/R < 0.8$ that does not develop hoop forces has less potential to fail than a spherical dome for several reasons. Conceptually as the dome becomes steeper, the force path to the support structure becomes nearly vertical, reducing the need for hoop forces. For constant t/R, θ, and α, the centroid of a pointed dome lune is closer to its toe than the centroid of a spherical dome lune; depending on δ and α, the difference may be quite significant. As a result, the lunes of a pointed dome stand more readily as a radial series of independent arches. To illustrate, for a spherical dome of $t/R = 0.08$ and $\alpha = 90°$, the modified thrust line analysis estimates that its minimum thrust is 85% greater than the thrust for a pointed dome with $\delta = 13°$, and about 3000% greater than when $\delta = 52°$ (Fig. 4.11).

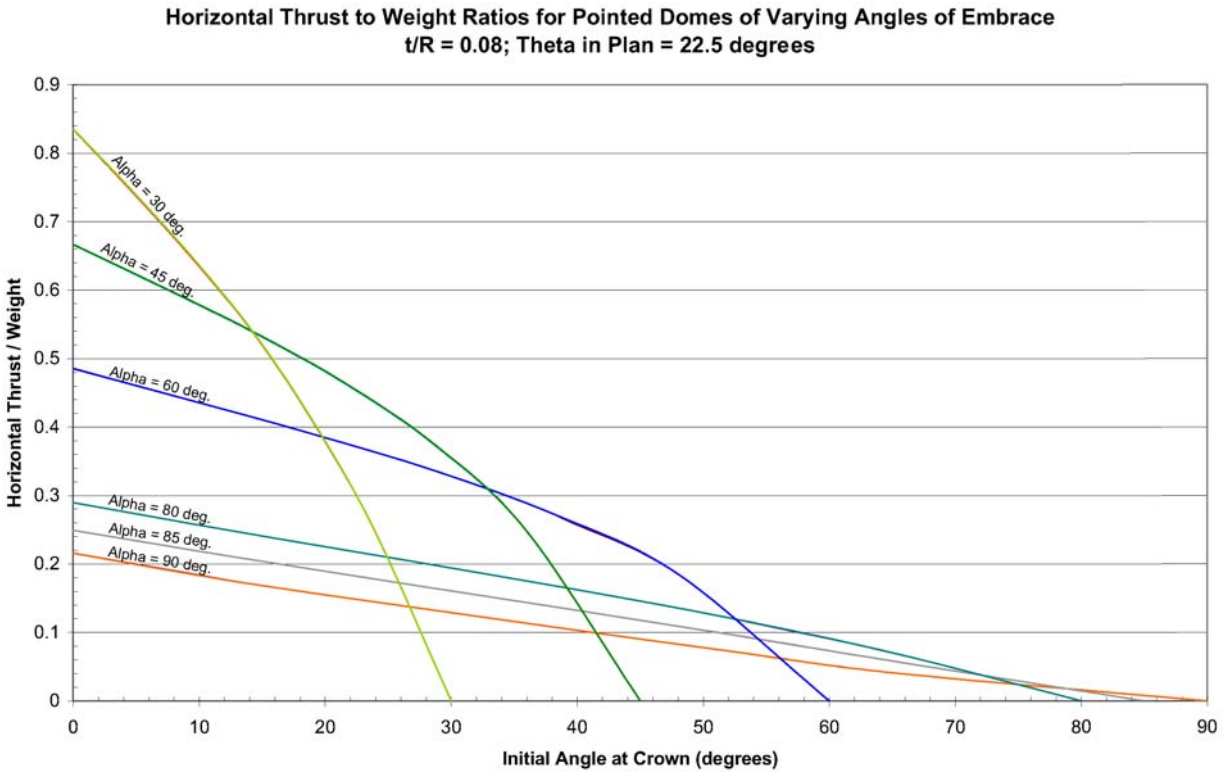

Figure 4.11. For a constant t/R and θ, H/W decreases as δ approaches α and the pointed dome becomes steeper.

Subsequently, the presence of hoop forces has little impact on the minimum thrust value because the lunes are able to resist the relatively small thrust at the dome crown without hoop forces.

Similar to spherical domes, hoop forces are significant in increasing the range of stable dome geometries. Figures 4.12 and 4.13 show the limited δ-values for which the modified thrust line method found satisfactory thrust lines if hoop forces do not develop in domes with $t/R = 0.05$ and $t/R = 0.08$, respectively.

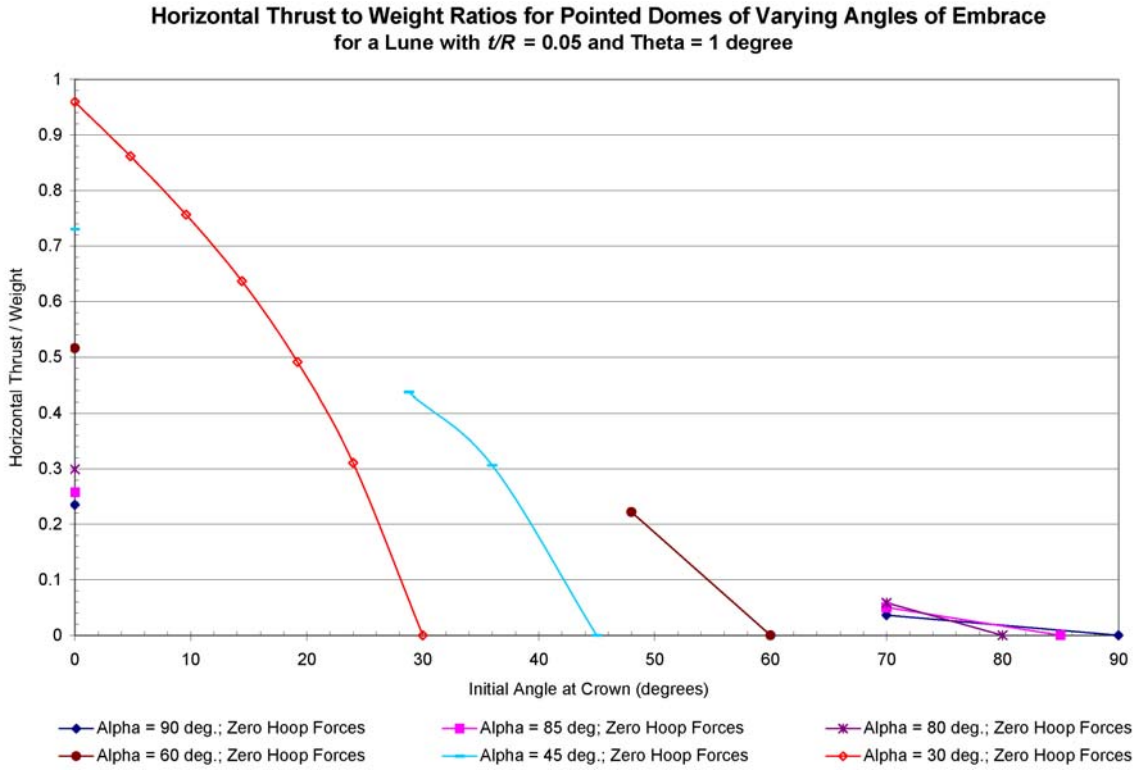

Figure 4.12. Minimum horizontal thrust for a pointed dome with $t/R = 0.05$ without hoop force transfer between lunes. Gaps in the curves indicate that the modified thrust line program could not find a satisfactory thrust line for the corresponding δ values.

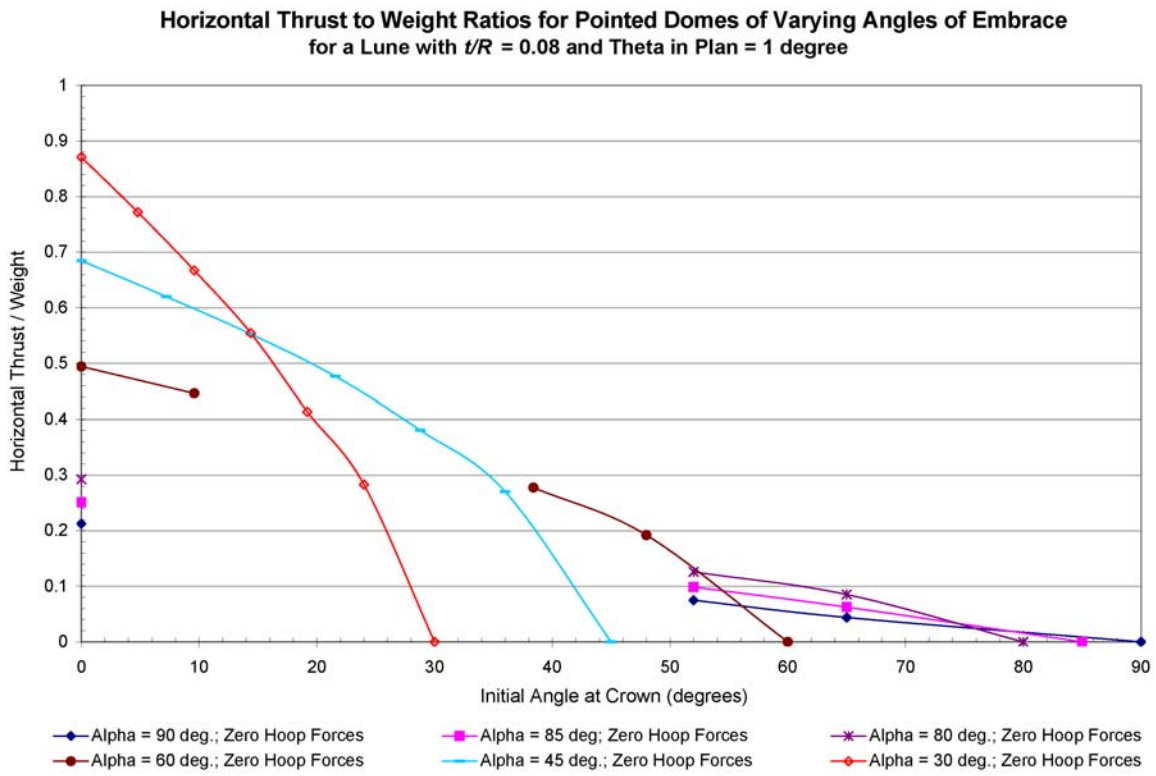

Figure 4.13. Minimum horizontal thrust for a pointed dome with $t/R = 0.08$ without hoop force transfer between lunes. Gaps in the curves indicate that the modified thrust line program could not find a satisfactory thrust line for the corresponding δ values.

Thus, hoop forces are imperative in the stability of many pointed dome geometries with $t/R \leq 0.08$ and $45° < \alpha \leq 90°$; this latter range includes the embrace angles for many existing structures. If the dome cannot develop hoop forces, perhaps due to meridional cracks from crown to base, then the propping force at the centerline is insufficient to maintain the stability of the individual lunes. Near the crown of the dome, the masonry units need compressive hoop forces to prevent failure. Interestingly, in spherical domes with the same t/R ratios, hoop forces are not required for stability. The near-horizontal orientation of the voussoirs in the cap of a spherical dome enables the thrust line to remain within its effective thickness.

4.3. Applications of the Minimum Thrust-to-Weight Ratio in Pointed Domes

Applications of the minimum thrust-to-weight ratio for pointed dome geometries parallel the applications for spherical domes. One may calculate the minimum thrust required for dome stability from Figs. 4.2 to 4.10. The similarity between the analyses including and excluding hoop forces results in interchangeable use of the charts; again, one must be mindful of the

increased range of stable geometries when hoop forces develop in the dome. However, should the existing structure in question be standing, then stability is obviously not in question. If the dome exhibits increasing meridional cracks, then the question of stability is imperative.

Equation 3.1 calculates the horizontal thrust at the base of the dome in units of force per length of circumference.

Interpolating and Extrapolating the Minimum Thrust

For $\theta \leq 45°$, the relatively linear relationship between δ and H/W naturally leads to an expression, derived from a series of linear regression equations, to estimate H/W as a function of δ and α, in radians:

$$\frac{H}{W} = 0.551\delta - 1.061\frac{\delta}{\alpha} - 0.615\alpha + 1.164 \qquad \text{for } \delta < \alpha \tag{4.1}$$

The minimum thrust of a dome portion with different values of θ may be estimated from Eqs. 3.3 and 3.4, although the change in thrust with respect to θ is minimal for the geometries studied. For $1° \leq \theta \leq 45°$, one may also interpolate between Figs. 4.2 and 4.10. Again, this study of minimum thrust is theoretical and dependent on the material and geometry assumptions stated in this and previous chapters. The accuracy of the results for different parameters is unknown.

To illustrate the different methods to estimate H/W, the author applied the methods to the dome of Farag Ibn Barquq. The dome's parameters are: $t/R = 0.44$, $\alpha = 83°$, and $\delta = 10°$. From Eq. 4.1, the estimated H/W ratio is:

$$\frac{H}{W} = 0.551 \cdot 0.175 - 1.061 \cdot \frac{0.175}{1.449} - 0.615 \cdot 1.449 + 1.164 = 0.24$$

Interpolating for $\alpha = 83°$ and $\theta = 15°$ in Figs. 4.3, 4.4, 4.6, and 4.7, the author estimated H/W as 0.25. Chapter 5 compares these estimated ratios with the ratio attained in the specific case study of the dome of Farag Ibn Barquq.

Estimating the Minimum Thrust through Equilibrium Equations

Similar to spherical domes, one can use static equilibrium equations to approximate the minimum thrust of pointed domes. Assuming a pin support at the midpoint of the lune's bottom edge, and a vertical roller support at the extrados at the crown against the dome's centerline, the minimum horizontal reaction, H, may be estimated with Eq. 3.6. However, while this equation may provide a good estimate of minimum thrust, it and other equations alone reveal nothing about the dome's stability.

The Half-Dome as a Buttress

Fig. 4.14 shows the minimum thrust for a half-pointed dome structure calculated with the same methodology as that for spherical half-domes. As δ approaches α, assumed as 90 degrees, H/W decreases rapidly. Thus, the minimum thrust-to-weight ratio of a pointed half-dome structure will always be lower than the ratio of a spherical half-dome structure.

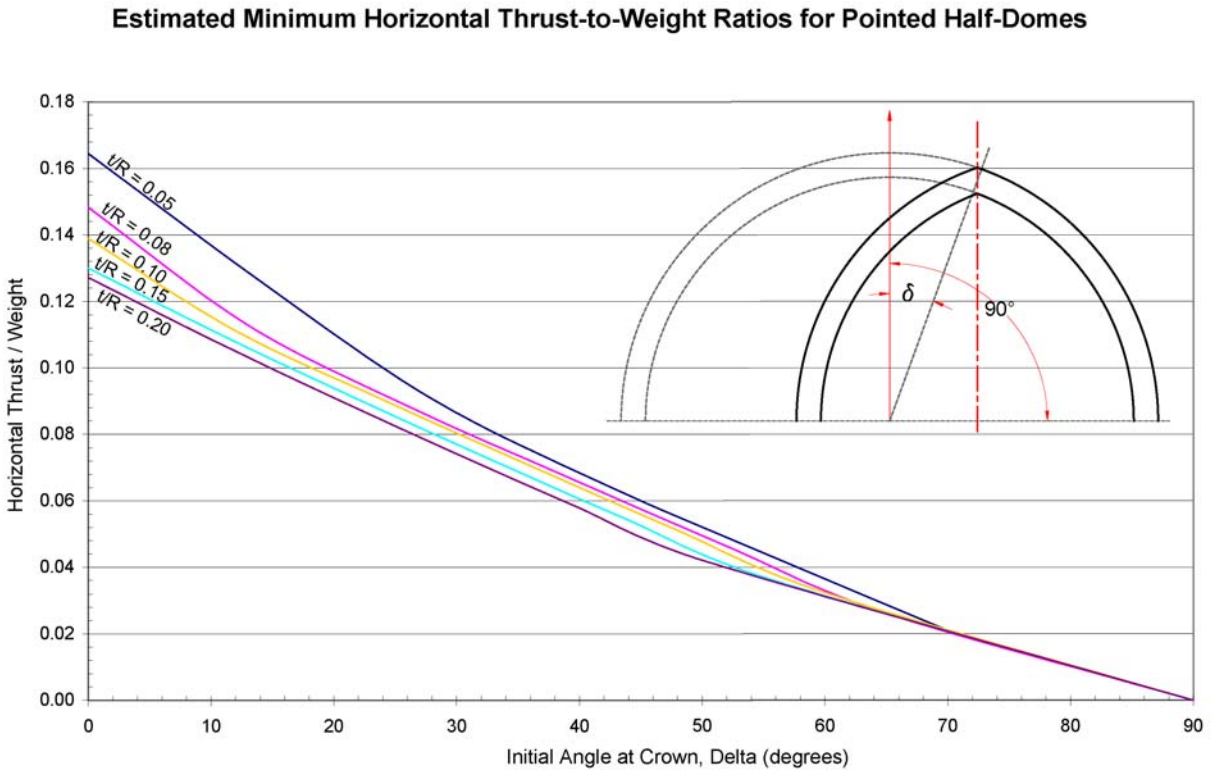

Figure 4.14. Minimum thrust of a pointed dome buttress with $\alpha = 90°$

Stability of the Support Structure

The minimum thrust-to-weight ratio may be used to determine if and where the thrust line exits the support structure under the dome, assuming no tensile resistance in either structure. Eq. 2.6 provides the *x*-coordinate of the first point of thrust line segment entering the support structure, where $\beta = \alpha - \frac{\pi}{180}$ and $\gamma = \alpha$, in radians. Eq. 3.7 locates the *y*-coordinate of the thrust line with respect to the median height of the dome (Fig. 3.20), where *k*-values for a lune with $\theta = 1°$ and $\alpha = 90°$, are listed in Table 4.1. Eq. 3.8 estimates the vertical distance, with respect to the median dome height, at which the thrust line exits the support wall. Chapter 5 illustrates this technique**.**

Table 4.1. Values of *k*, the vertical distance from the median rise of the dome to the final thrust line point in the dome, divided by the median height of the dome for a pointed dome lune with $\theta = 1°$ and $\alpha = 90°$

	Thickness-to-Radius Ratio				
Initial Angle at Crown (deg.)	**0.05**	**0.08**	**0.10**	**0.15**	**0.20**
70	0.91	0.94	0.99	0.98	0.99
56	1.00	0.98	0.99	1.00	1.00
42	1.00	0.99	1.00	1.00	1.00
28	1.00	1.00	1.00	1.00	1.00
14	0.99	1.00	1.00	1.00	1.00
0	0.93	1.00	1.00	1.00	1.00

Internal Force Comparison to the Membrane Theory

The internal hoop force values provide insight to the stability of a pointed masonry dome with meridional cracks. For a lune with $\theta = 22.5°$ and $t/R = 0.05$ under axisymmetrical self-weight loads only, the author compared the φ-locations at where hoop forces become zero from the modified thrust line analyses, to the locations of the transition point between compressive and tensile hoop forces predicted by the membrane theory equations (Fig. 4.15).

The modified thrust line method predicts that compressive hoop forces are not required for many locations of $\varphi < \alpha$. In other words, meridional cracks may occur in these regions on the dome surface without compromising stability, barring severe material degradation or other significant structural defects. The membrane theory equations provide information only on whether hoop forces are tensile or compressive hoop forces.

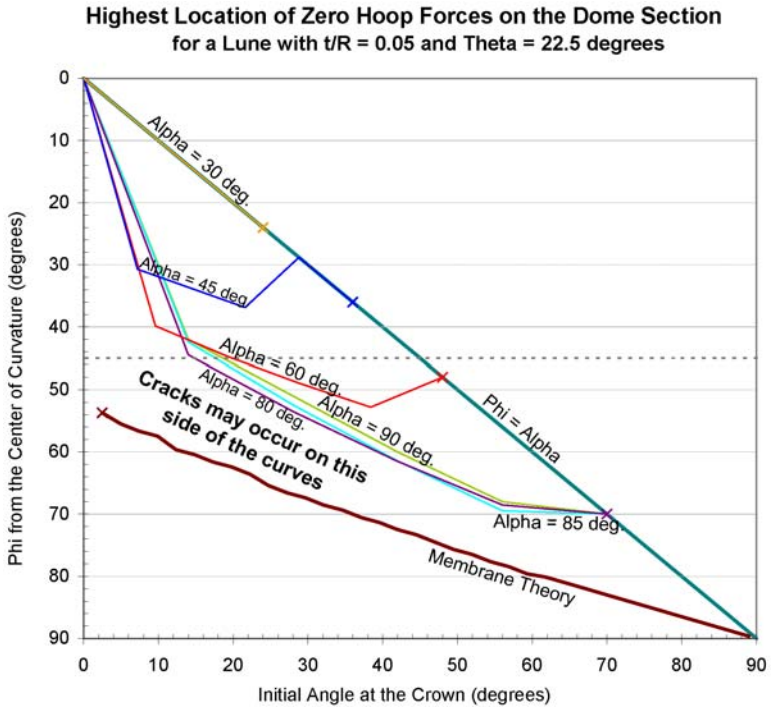

Figure 4.15. A pointed dome with meridional cracks between the curves and a horizontal line through $\varphi = \alpha$ is theoretically stable. Unless noted otherwise, curves are from the modified thrust line analyses. The "Membrane Theory" curve marks only the transition point between compressive and tensile hoop forces.

4.4. Comparison between Results for Spherical and Pointed Domes

The minimum thrust-to-weight ratio results reveal several similarities and differences between the structural behaviors of spherical and pointed domes. As the angle of embrace of either dome type increases, the minimum thrust-to-weight ratio decreases. For hemispherical domes, *H/W* tapers to approximately 0.20 to 0.25; for pointed domes with an embrace angle of 90 degrees, *H/W* tapers to between 0.25 and theoretically zero for truncation angles between 0 to 90 degrees, respectively. With all other geometric parameters equal, the pointed dome will have a lower minimum thrust-to-weight ratio than the spherical dome.

For both dome types, the minimum thrust-to-weight ratio is inversely related to the thickness-to-radius ratio. For a given *t/R*, the range in *H/W* values narrows as the embrace angle increases, and the domes become deeper. As an example, for a spherical dome with $\alpha = 30°$, *H/W* is 0.95 for $t/R = 0.05$, and 0.65 for $t/R = 0.20$. For a pointed dome with $\alpha = 30°$, *H/W* varies between 0.86 and 0.56 for the previous *t/R* ratios, respectively, and for $\delta = 5°$. However, when $\alpha = 80°$, the range in *H/W* values decreases to 0.02 for spherical domes, and 0.03 for pointed domes.

The relationship between H/W and α is relatively linear for spherical and pointed domes. The plan angle of a lune under study has a minimal impact on the value of H/W for both dome types.

From the geometries studied, the range of stable geometries increases when hoop forces develop between lunes; the presence of hoop forces is more significant in pointed domes than in spherical domes. If t/R is or exceeds 0.05, and possibly lower, spherical domes with an embrace angle between 0 and 90 degrees are theoretically stable. However, several pointed dome geometries with $t/R = 0.05$, and even 0.08, are unstable without hoop forces (Figs. 4.12 and 4.13). As a result, when analyzing pointed domes with relatively low t/R, one must be mindful that hoop force development may be crucial for stability.

The regions in which meridional cracks may develop without detriment to the dome's stability correlate with the greater dependence on hoop forces of pointed domes with the small t/R ratios (Figs. 3.21 and 4.15). For spherical domes with embrace angles less than 85 degrees, meridional cracks can occur anywhere between the base and crown of the dome surface; even hemispherical domes can experience cracks in most of their surfaces, with complete integrity required only in the cap. However, cracks are permissible in only limited regions of the surface of pointed domes before they negatively impact the structural stability.

4.5. Chapter Summary

This chapter discussed the minimum thrust values of masonry domes with pointed geometries and their relevant applications to structural behavior. By including hoop forces in analyses for pointed domes, the modified thrust line method finds satisfactory thrust line solutions that satisfy limit state conditions that could not be achieved with the membrane theory or existing analysis methods evaluated in this thesis. The author demonstrated that while the presence or absence of hoop forces in pointed domes does not significantly change the value of the minimum thrust, hoop forces are critical in the stability of many pointed dome geometries with thickness-to-radius ratios equal to or less than 0.08. The chapter concluded by comparing structural insights revealed from the spherical and pointed dome analyses. The next chapter will demonstrate the use of the modified thrust line method in specific thin-shell spherical and pointed masonry dome case studies.

Chapter 5. Case Studies

This section discusses the application of the modified thrust line method to existing thin-shell masonry domes for which current analysis methods cannot satisfactorily explain their stability, or would be overly complex to use. The author analyzed two case studies with unconventional and structurally daring geometries: first, a pointed dome constructed in the period of Mamluk rule (1250-1517 A.D.) in Cairo, Egypt; and second, a spherical thin-shell dome in Dover, England, in which the author participated in both design validation and to a lesser extent, construction. Both case studies compare results to results using two other analysis methods: one that assumes no hoop force development, or arch behavior, in the domes, and one that assumes membrane theory conditions.

5.1. Dome of Farag Ibn Barquq, Cairo, Egypt

In Cairo, Egypt, during a period of profuse construction from 1250 to 1517 A.D., workers built an estimated 400 brick and stone masonry domes on the mausoleums of sultans and emirs (Cipriani 2005). More than 200 pointed masonry domes continue to stand 500 to 750 years after their construction (Cipriani and Lau 2006). These intricately decorated and expeditiously erected Mamluk domes represent some of the most daring structures in the world. To this day, the stability of some of these domes remains unclear. Though Creswell (1959) and Kessler (1976) have documented the dimensions of the domes, no written sources or drawings describing the design or construction processes of the Mamluk complexes are known to exist (Cipriani 2005).

The progression of the structural geometries and decorative carving from earlier to later domes suggests an accruement of structural design knowledge through experience. For example, brick domes, which appeared early in the Mamluk period, are typically between 13 and 23 ft in diameter and between 13 and 25 ft in height, while stone masonry domes, built later the in period, are between 26 and 33 ft in diameter and between 25 and 36 ft in height (Cipriani 2005). Also, the typical thickness of the domes decreases from between 1.3 and 1.6 ft for brick domes to between 1.0 and 1.4 ft for stone domes (Ibid.). This study focuses on one exception to these size generalizations: the dome on Mausoleum of Sultan Farag Ibn Barquq, one of the most structurally daring domes that stands today.

Geometry and Features

The Mausoleum of Sultan Farag Ibn Barquq was constructed between approximately 1398 and 1411 (Fig. 5.1).

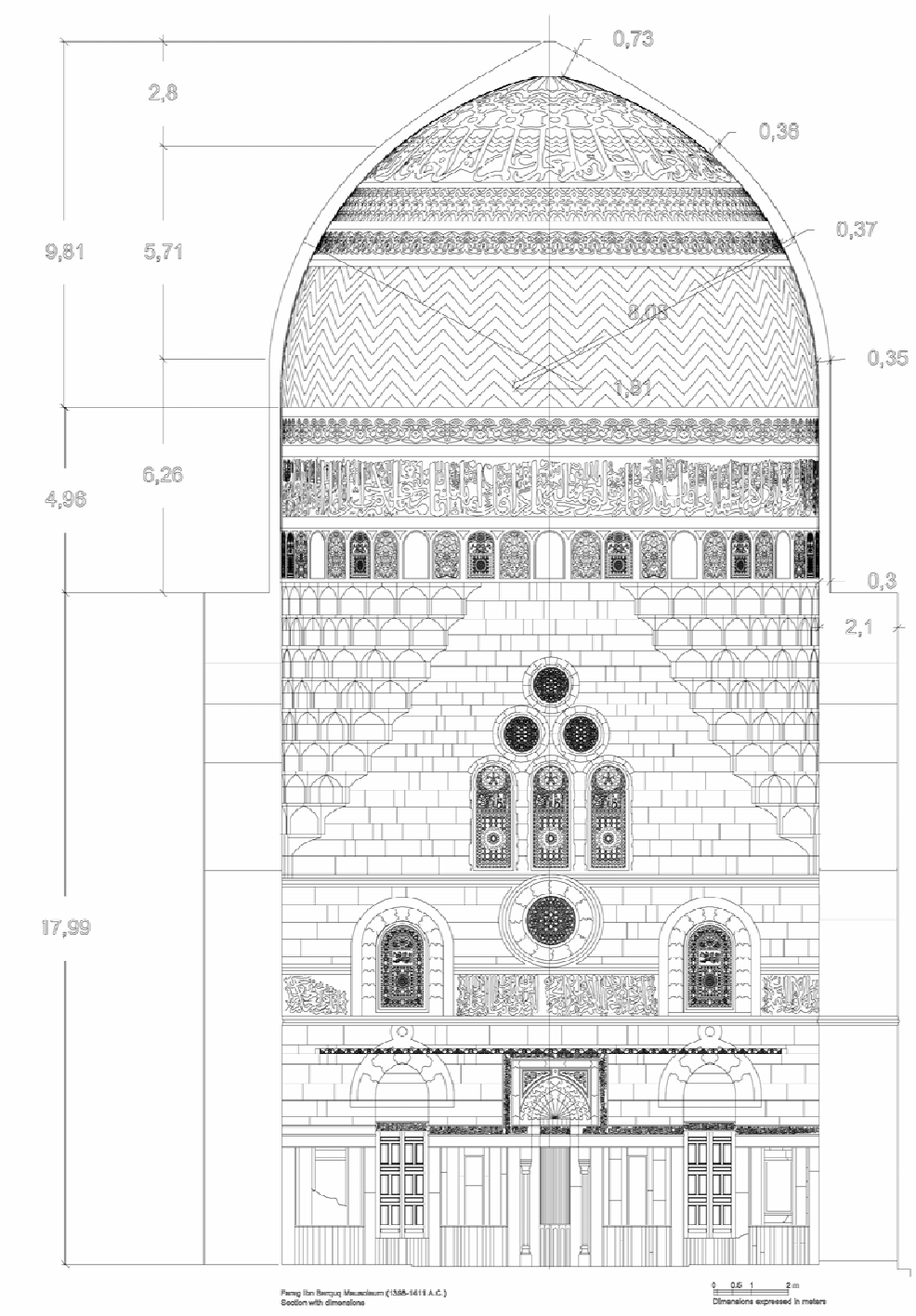

Figure 5.1. Dimensions in meters of the dome and drum and mausoleum of Farag Ibn Barquq (from Cipriani 2005)

Table 5.1 lists the approximate geometric parameters of the complex's thin stone masonry dome.

Table 5.1. Geometric Parameters for the Dome of Farag Ibn Barquq

Median radius of curvature, a (ft):	27
Rise from springing (ft):	32
Span at base (ft):	47
Thickness, t (ft):	1.2
Thickness-to-Radius:	0.045
Angle at crown (deg.):	10

The dome is a single-shell construction for $25° < \varphi < 83°$; above $\varphi = 25°$, the shell splits into a double-shell construction to the pointed crown. Stone rubble fills the space between the shells, and a hollow lead pinnacle extends above the pointed crown. While this adds some surcharge to the crown, it was assumed negligible compared to the weight of the solid stone voussoirs.

In recent restoration work, preservationists have not found evidence of metal tension reinforcement, such as a continuous hoop ring, in the dome itself. Cipriani (2005) observed various dovetail cuts in deconstructed masonry voussoirs that may have permitted wood inserts to temporarily hold the masonry together until the rings were completed. The presence of tensile reinforcement in the drum, the cylindrical support wall under the dome, remains unknown. To be conservative, the author assumed that the dome and drum lack any means of tensile reinforcement in the subsequent structural analyses.

Structural Analyses

The author investigated the stability of the dome of Farag Ibn Barquq using three different methods: traditional thrust line analysis assuming zero hoop forces or arch conditions, the membrane theory, and the modified thrust line analysis. The study analyzed the dome as a lune with $\theta = 15°$ under uniform axisymmetrically loads only, and an assumed material unit weight of the stone of 150 pcf.

Zero Hoop Forces

This traditional thrust line analysis method is incorporated in the program created in *Cabri II*, and assumes that the dome acts as a radial series of independent lunes that do not transfer hoop forces between adjacent lunes, but do thrust against their complementing lune. This method has

two unknown variables: the horizontal thrust at the crown and base of each lune, and the initial eccentricity, or starting point, of the thrust line at the crown. The shape of the thrust line depends on the fixed length of the load line and, more importantly, the unknown length of the horizontal segment on the force polygon representing the thrust. Without hoop forces development between lunes, the analysis did not find a satisfactory thrust line that fit completely within the section (Fig. 5.2).

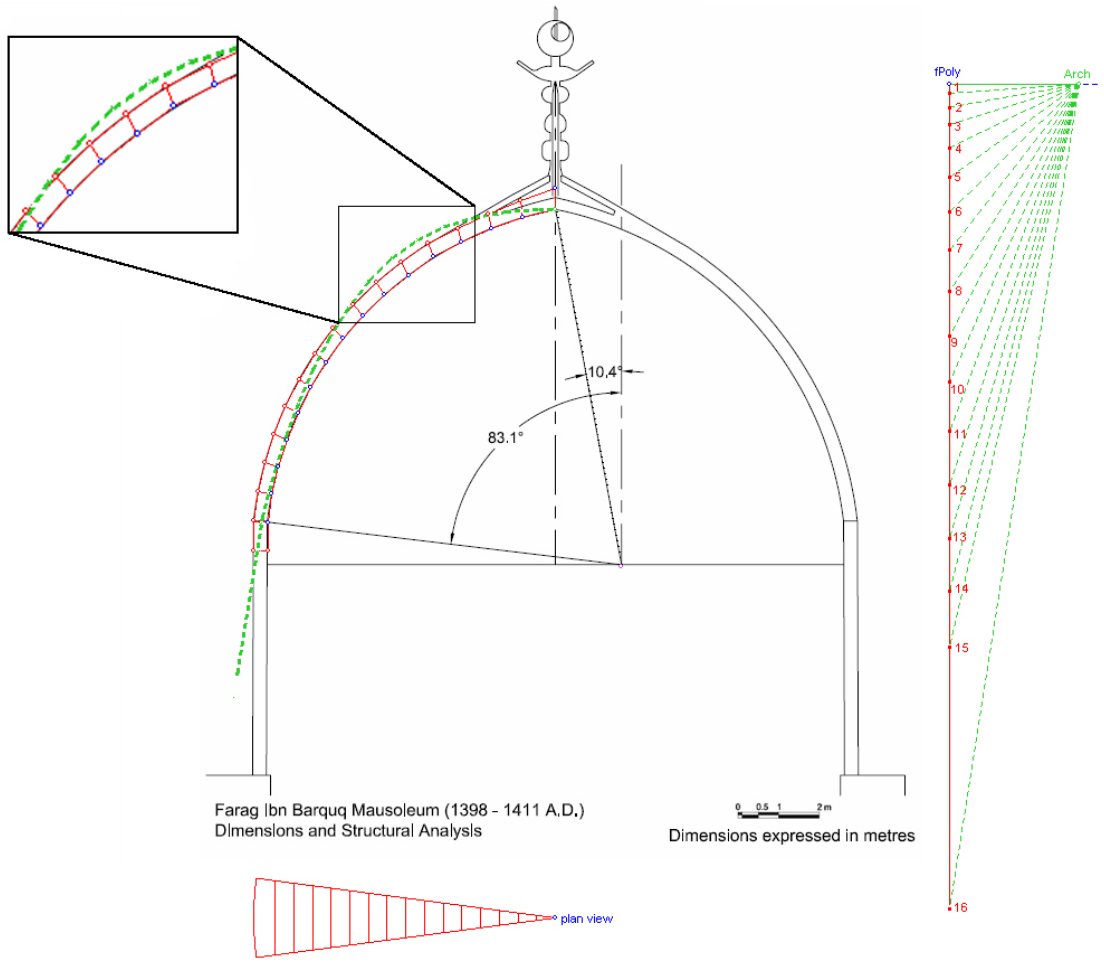

Figure 5.2. The thrust line does not fit within thickness of the dome of Farag Ibn Barquq without hoop forces.

Because the thrust line exits the dome section, the dome of Farag Ibn Barquq would not stand without hoop forces development. In this sense, it is a more daring dome than other well-known domes such as St. Peter's in Rome, or St. Paul's in London, in which it is possible to demonstrate that these domes would stand as a series of independent arches.

Membrane Theory

The membrane theory equations for pointed domes, given in Section 2.3, assume the line of thrust acts at the median surface of the dome; thus, the thrust line will always lie within the dome section. However, internal forces required to constrain the thrust line to this location may not satisfy limit state assumptions. The internal meridional and hoop forces in the dome of Farag Ibn Barquq as determined by the membrane theory (Eqs. 2.3 and 2.4) are shown in Fig. 5.3.

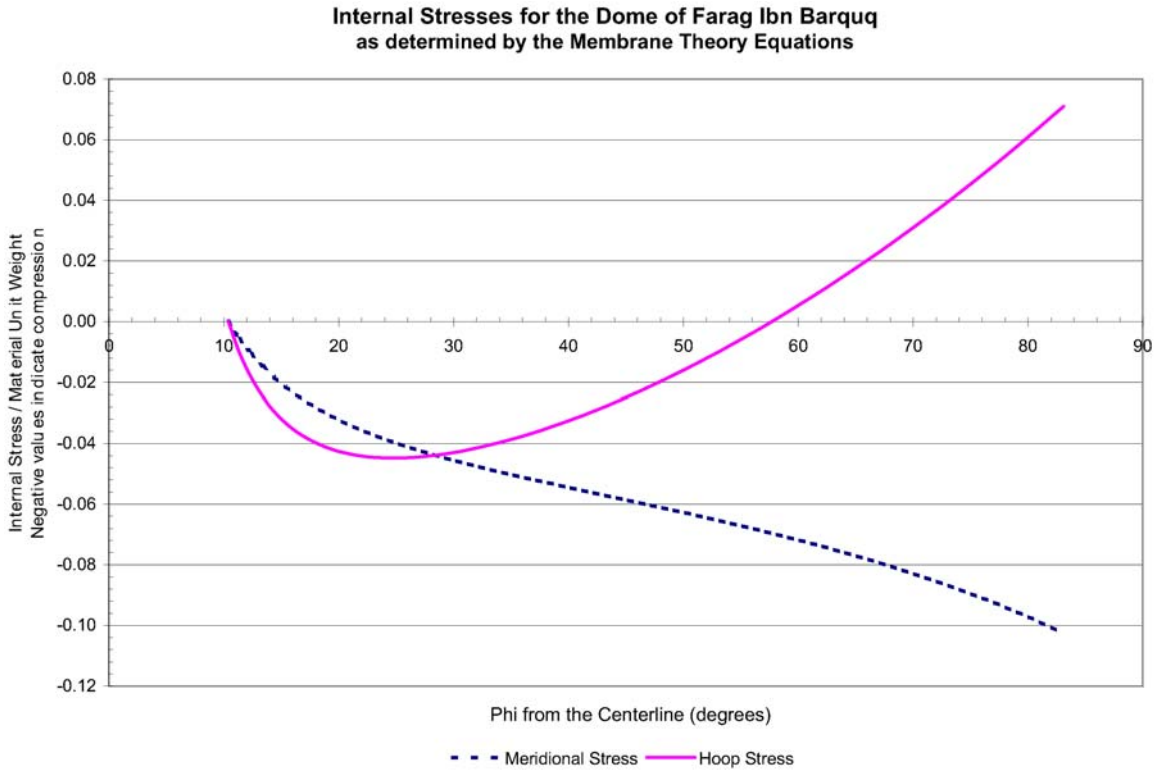

Figure 5.3. Internal stresses in the dome of Farag Ibn Barquq per the membrane theory. Hoop forces become tensile at $\varphi = 58°$ from the dome's center axis of revolution.

The membrane theory equations calculate tensile hoop forces for $58° < \varphi < 83°$, and a horizontal thrust at the base of the lune of 8.4% of its weight. At the base of the dome, tensile hoop stresses of about 7% of the material unit weight are required to prevent dome instability. Existing cracks in the dome, albeit minor, preclude tensile hoop forces of any magnitude from developing. Therefore, the membrane theory does not explain the stability of the dome.

Using the interactive geometry software program based on Wolfe's graphical analysis method to meet limit analysis (Section 2.2), the author appended an alternative no-tensile force thrust line

to the thrust line at the median surface in the base of the dome. This combined thrust line nearly fits within the dome section, but still exits the dome just prior to the dome's transition to the drum (Fig. 5.4). This solution would be satisfactory if the base of the dome was thickened to accommodate the thrust line; however architectural drawings do not indicate this.

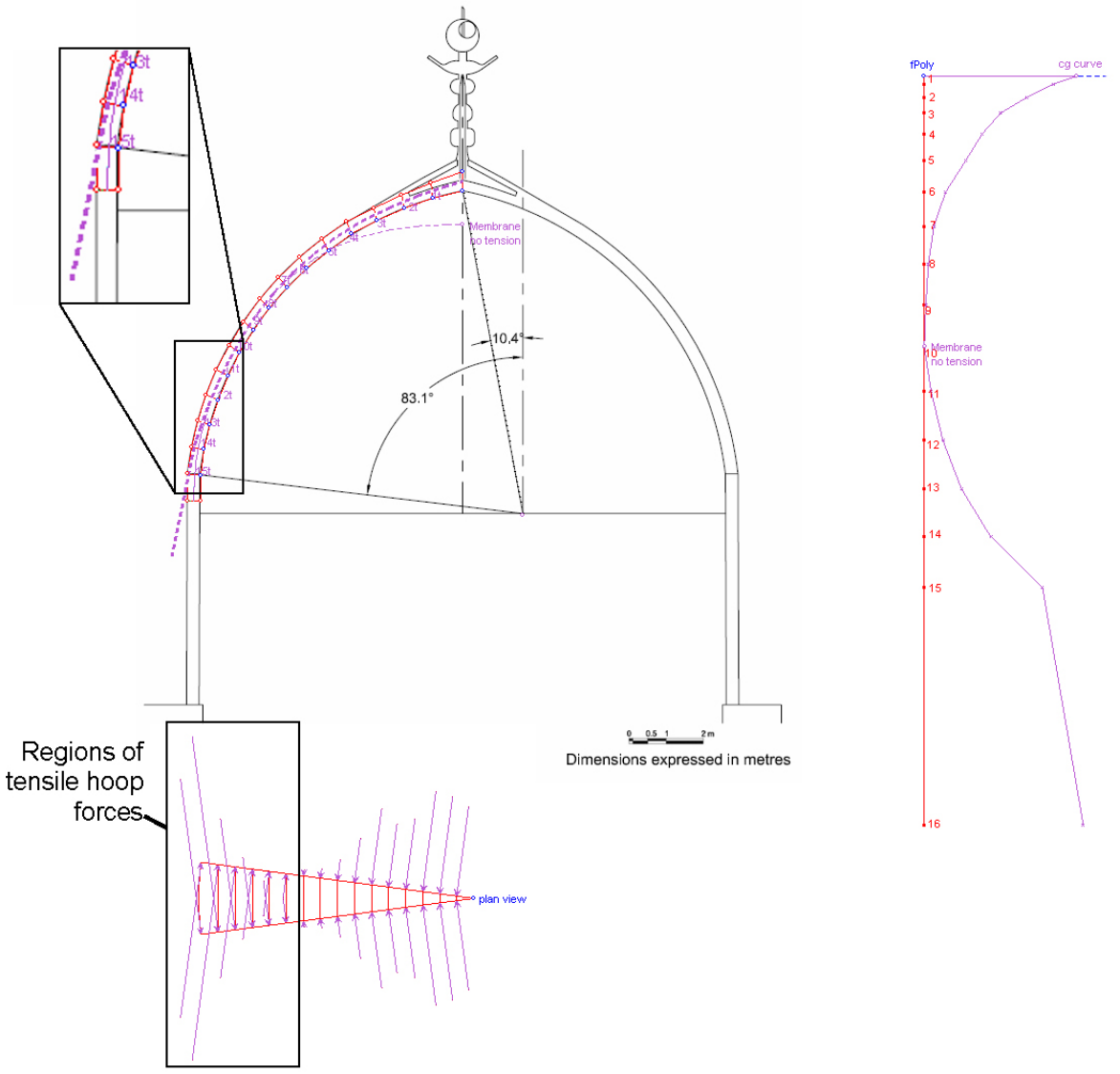

Figure 5.4. The thrust line generated by the graphical membrane theory method exits the dome section at the base of the dome at the transition to the support wall. Note: On the plan view of the dome, the tensile hoop forces shown do not actually exist because the alternative thrust line construction nullifies hoop forces at the base of the dome.

Modified Thrust Line

The two previous analyses failed to explain the stability of the dome of Farag Ibn Barquq. However, both the interactive geometry and numerical spreadsheet-based modified thrust line analysis programs found satisfactory thrust lines that remained within the structure's section to varying degrees (Figs. 5.5 and 5.6).

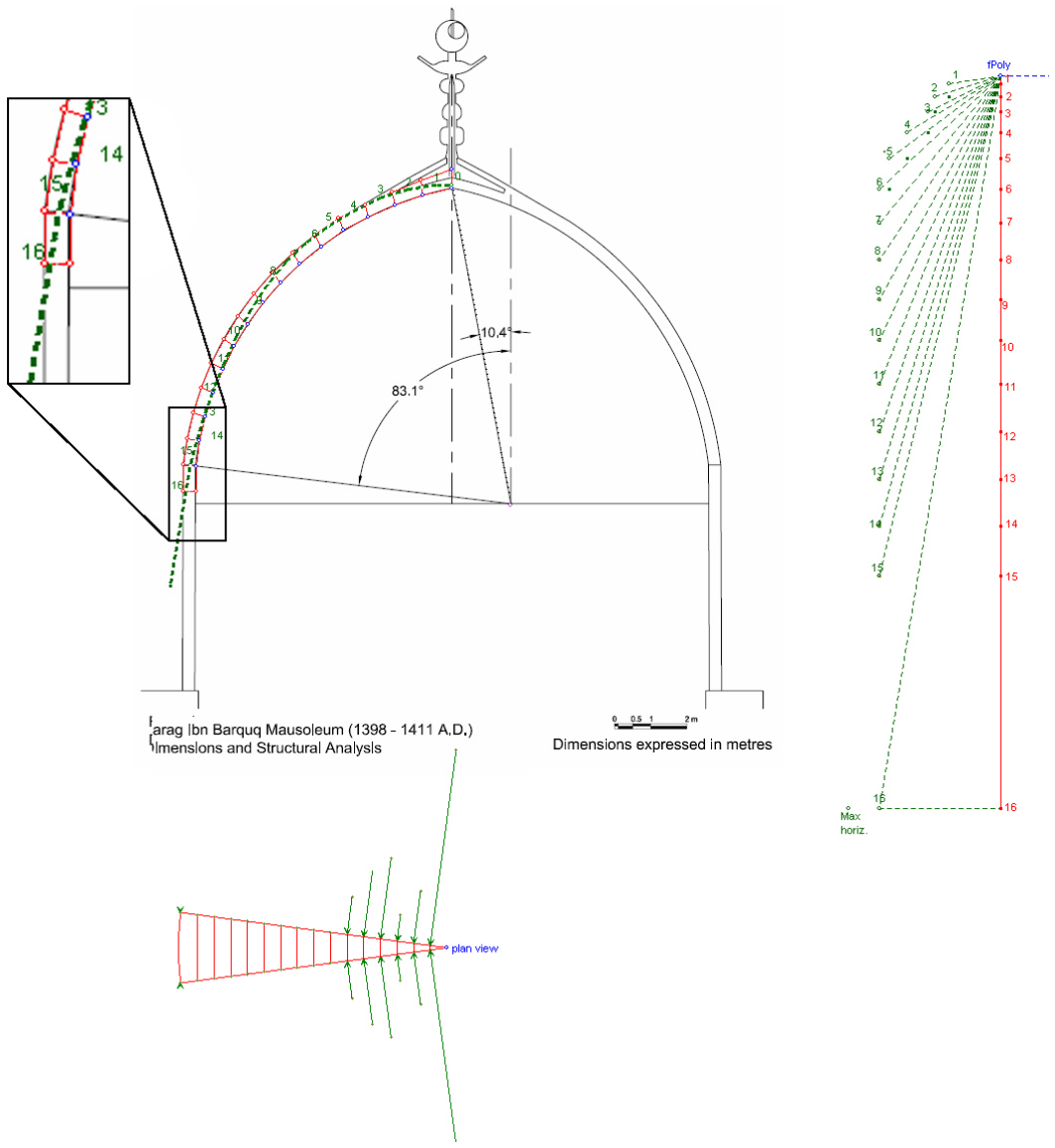

Figure 5.5. The modified thrust line method finds a satisfactory thrust line for the dome of Farag Ibn Barquq. The solution requires compressive hoop forces to develop in the dome cap.

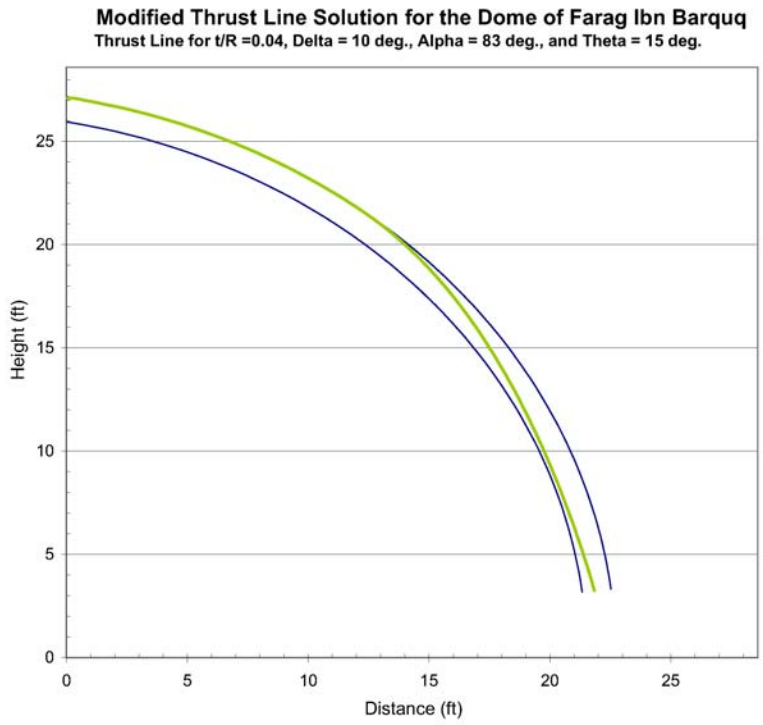

Figure 5.6. The thrust line generated by the numerical modified thrust-line program satisfies equilibrium and limit state conditions (here, the thrust line is allowed to approach a minimum of 0.*01a* to the dome's surfaces).

The thrust line generated by the *Visual Basic* spreadsheet program divided the lune into 90 voussoirs, significantly higher than the 16 divisions the interactive geometry program used in its analysis. This, coupled with the former program's ability to specify exact tolerances to the lune's surfaces, resulted in a smoother thrust line curve that enters the support structure under the dome with a steeper slope.

The internal forces associated with both thrust line solutions are only compressive (Fig. 5.7).

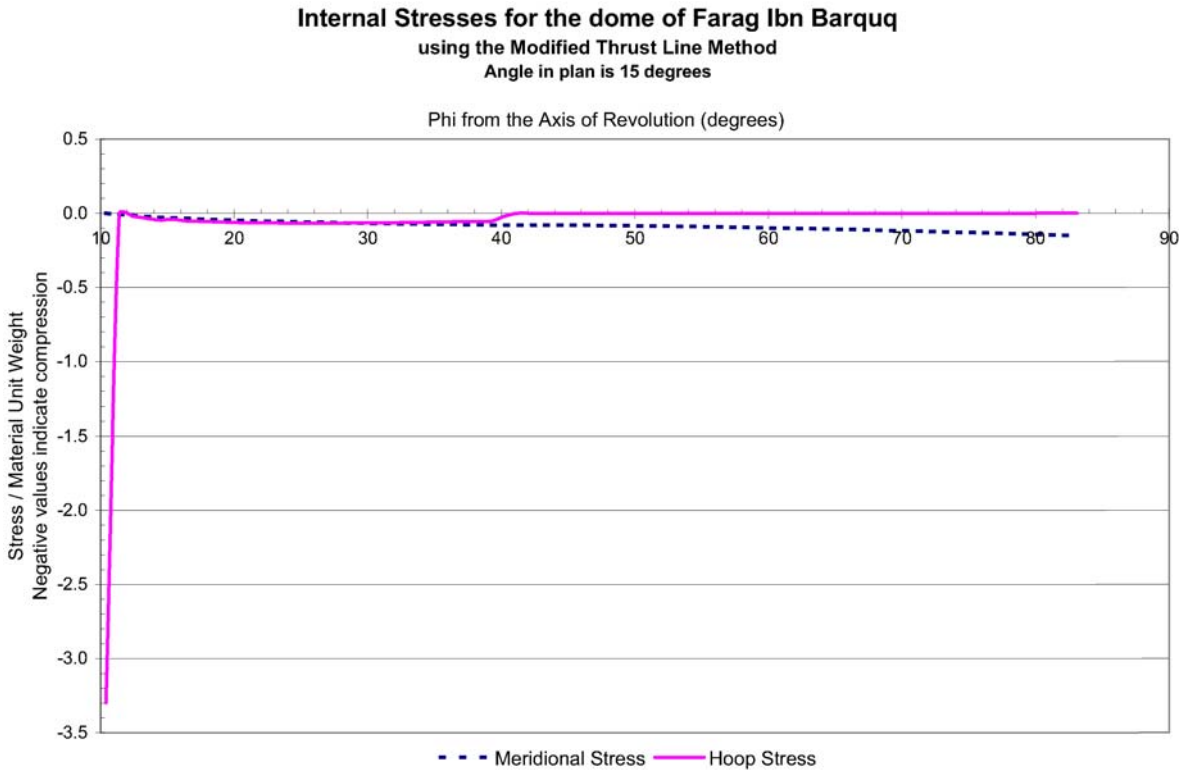

Figure 5.7. From the modified thrust line analysis, one possible combination of internal forces that satisfy equilibrium of the dome of Farag Ibn Barquq

The thrust line solution shown in Fig. 5.6 estimates each lune in the dome experiences an outward thrust equal to 24% its weight, which coincides exactly with the *H/W* prediction made with the linear regression equation, and closely to the prediction made by interpolating from the charts in Chapter 4. From Eq. 3.1, assuming a unit weight of the stone masonry of 150 pcf, the thrust at the base of the dome is:

$$H = \frac{0.24 \cdot W_{lune}}{a\theta(\sin\alpha - \sin\delta)} = \frac{0.24 \cdot 21797}{27 \cdot \frac{15\pi}{180}(\sin 83° - \sin 10°)} = 905 \frac{lbs}{ft}$$

where W_{lune} is calculated from Eq. 2.5.

Though this solution demonstrates that the dome is capable of standing on its own, the stability of the drum under the dome remains unexplained. In the most favorable conditions, the thrust line shown in Fig. 5.5 exits the masonry in the supporting drum, which suggests that the

supporting structure is insufficient. With the procedure described from Section 3.3 and the thrust line in Fig. 5.6, the exit location of the thrust line in the drum may be calculated:

$$W_{wall} = a\theta\rho(\sin\alpha - \sin\delta)\cdot height_{wall}\cdot t_{wall} = 27\cdot\frac{15\pi}{180}\cdot 150\cdot(\sin 83^\circ - \sin 10^\circ)\cdot 20.5\cdot 1 = 21360\,lbs$$

$$x_{ext.wall} = (a-t)(\sin\alpha - \sin\delta) + t_{wall} = \left(27 - \frac{1.1}{2}\right)(\sin 83^\circ - \sin 10^\circ) + 1.1 = 22.8\,ft$$

Substituting these values into Eq. 3.8:

$$y_{exit} = -\frac{21797 + 21360}{21797\cdot 0.24}(22.8 - 21.8) + 23.9 = 16.4\,ft$$

where 21.8 ft is the *x*-coordinate of the center of gravity of the voussoir at the base of the dome, and 23.9 ft is the vertical distance between the median rise of the dome and the *y*-coordinate of the thrust line at $x = 21.8$ ft. The modified thrust line method predicts the thrust line exits the drum 16.4 ft below the base of the dome, or 4.1 ft above the base of the 20.5 ft high drum. Since the dome stands today, the structure must have the means to resist the horizontal thrust transferred into the drum. The combined gravity loads of the dome and wall at the point in the wall where the thrust line exits is:

$$\frac{W_{lune} + \frac{16.4}{20.5}W_{wall}}{Length_{wall}} = \frac{21797 + 0.80\cdot 21360}{5.8} = 6704\frac{lbs}{ft}$$

The horizontal thrust of 905 lbs/ft is about 13% of the gravity load of the dome and drum portion. If an indirect tensile capability develops from friction between the stones, and the friction coefficient for the stone masonry is equal to or greater than 0.13, then friction might resist the thrust as a series of stone tension rings acting in the drum. A typical conservative estimate of the friction coefficient for stone is 0.5, suggesting that such tension forces could develop. However, this would require the drum to be completely intact and without vertical cracks or window openings that would preclude the development of stone tension rings. Given

that Cairo is a region of significant seismicity, it is unlikely that the drum stands only because of friction. Such frictional forces could easily be reduced in a moderate earthquake, yet the dome has stood for many centuries. It is possible that tension rings of iron or wood remain hidden in the fabric of the stone drum, though this is an area for future research.

By deriving a satisfactory thrust line within the dome and most of its support drum, the modified thrust line method demonstrated how the dome of Farag Ibn Barquq stands.

5.2. The Domes of Pines Calyx™, Dover, England

The Pines Calyx™, a sustainable event and conference center in Dover, England, was the product of numerous design, engineering and construction collaborations that included St. Margaret Bay's Trust[7], Cameron Taylor Engineers, and the Massachusetts Institute of Technology. The author had the privilege of participating in the design validation of the two domes of the Pines Calyx, constructed in 2005 and 2006. The upper and lower domes are spherical shallow domes constructed of thin clay masonry tiles similar to that used in traditional Spanish timbrel vaulting, which is also known as Guastavino or Catalan vaulting. A reinforced concrete ring beams resists the outward thrust at the base of each dome, so that the orientation of the thrust line in the domes becomes a vertical gravity load vector, which is transferred easily to the vertical support structure under the domes.

Geometry and Features

Table 5.2 summarizes the geometric parameters of the masonry domes of the Pines Calyx:

Table 5.2. Geometric parameters for the upper and lower domes of the Pines Calyx

	Upper	Lower
Median radius of curvature, a (ft):	43	43
Maximum rise from springing (ft):	4.3	4.3
Span of the dome (ft):	38	38
Thickness, t (ft):	0.33	0.33
Thickness-to-Radius:	0.0076	0.0076
Angle at oculus opening (deg.):	4	5
Angle of embrace (deg.):	26	26

[7] Information on the Pines Calyx is available at www.baytrust.org.uk/html/pines_calyx.html. Additional information and press coverage is available in Parker (2005) and "UK Sees" (2005).

Though the thickness-to-radius ratio of the domes is smaller than that of the Mamluk dome case study, the shallow embrace angle and tension ring beams would suggest that membrane theory assumptions lead to a satisfactory solution.

However, a number of architectural features on the domes complicate the structural analysis. Each dome has a circular oculus at its crown that tapers into a "basal sun tube". Both domes are incomplete: the upper dome surface has a lens-shaped cutout while the lower dome intersects the cylindrical support wall of the upper dome (Fig. 5.8). A parapet wall traces the lens-shaped cutout, applying a concentrated line load on the upper dome edge. Finally, preliminary design loads included an asymmetrical live load case on the domes.

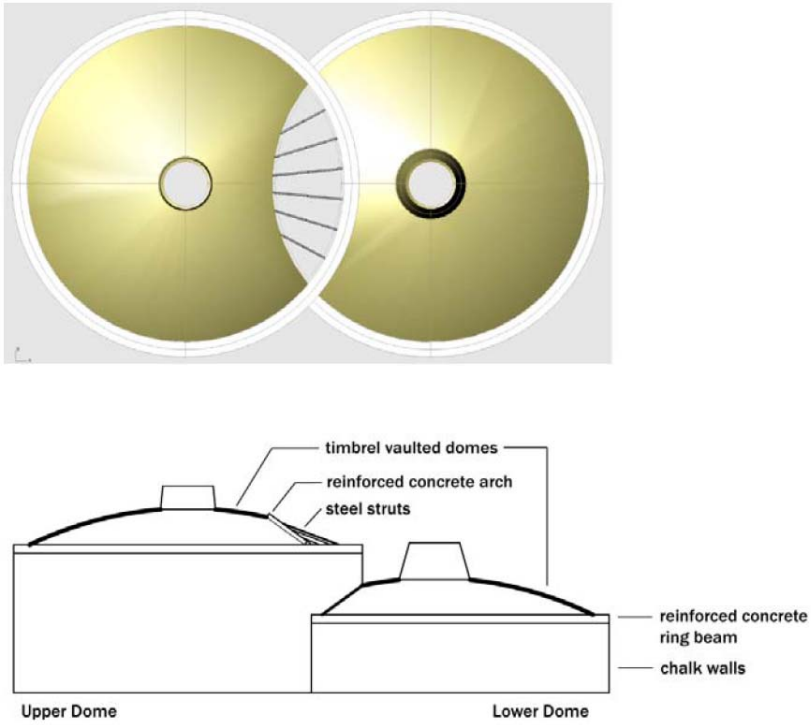

Figure 5.8. Plan and elevation views of the double domes of the Pines Calyx, Dover, England (from Ochsendorf et al. 2005, and courtesy of Michael Ramage)

Structural Analyses

The study relied on a combination of the membrane theory analysis, to evaluate the domes under axisymmetrical load conditions assuming no cutouts other than the oculi, and the modified thrust

line analysis to evaluate the domes' structural stability under asymmetrical live loads[8]. The latter method was vital in the study because the membrane theory is invalid under asymmetrical load conditions due to the introduction of shear and bending internal forces in the membrane plane. The author used the following factored loads in the structural analyses (Table 5.3):

Table 5.3. Factored loads for the upper and lower domes of the Pines Calyx

Uniform Load for Upper and Lower Dome	**kN/m^2**	**Load Factor**	**Factored Ld (kN/m^2)**
Self-weight: dead load of three layers of tile and mortar	2.4	1.4	3.3
Combined dead load: self weight and overburden	8.9	1.4	12.4
Live load	4.9	1.6	7.8
Combined dead load and live load	13.8		**20.3**
Concentrated Load at Oculus	**kN/m**	**Load Factor**	**Factored Load (kN/m)**
Line load at Upper Dome oculus:	1.8	1.4	**2.6**
Line load at Lower Dome oculus:	2.5	1.4	**3.5**

Membrane Theory

Under axisymmetrical factored loads, the membrane theory equations calculate only compressive stresses in the domes, with a maximum stress of approximately 350 psi (2.41 N/mm^2), less than 6% of the crushing strength of the tile (Ochsendorf et al. 2005) (Figs. 5.9 & 5.10).

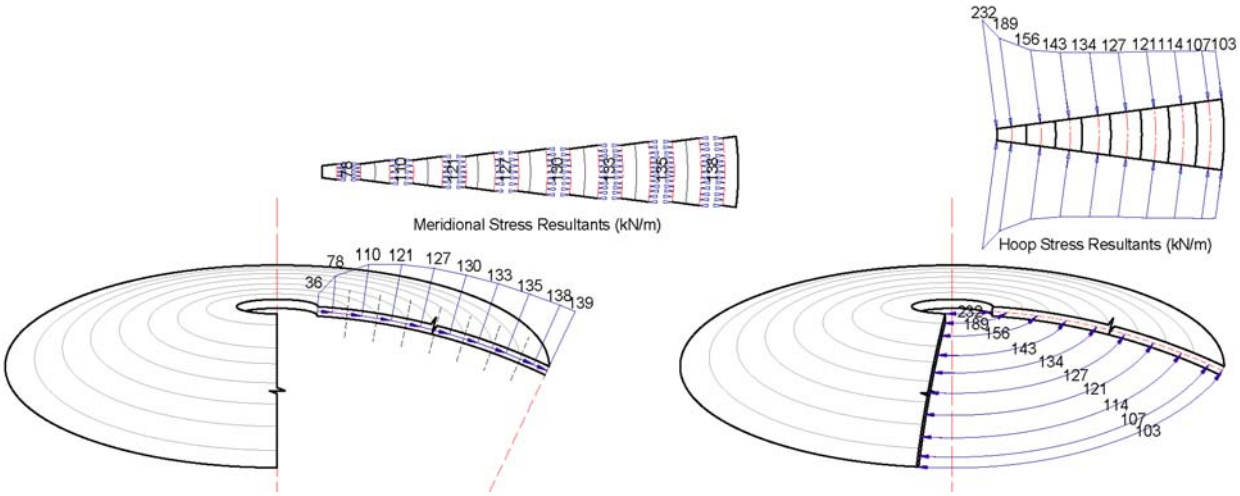

Figure 5.9. Internal meridional and hoop stress resultants in units of kN/m for the upper dome of the Pines Calyx (Ochsendorf et al. 2005)

[8] Comprehensive structural analyses for the Pines Calyx domes are available in the report "The Calyx Domes: Structural Design and Analysis" (Ochsendorf et al. 2005).

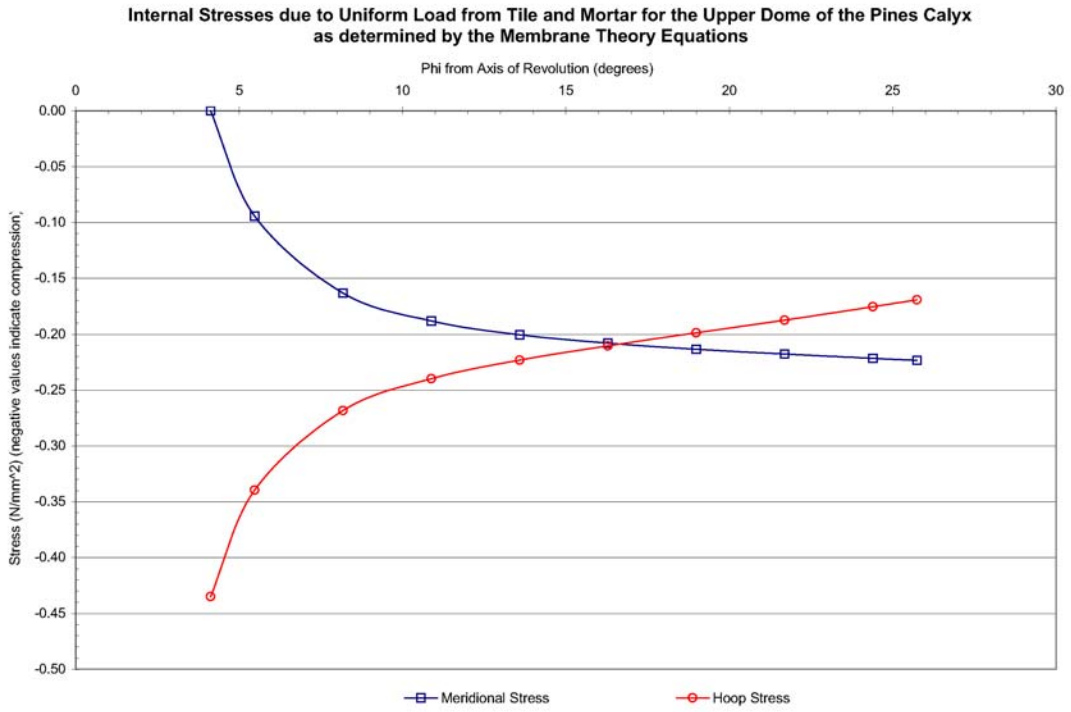

Figure 5.10. Internal stresses calculated from the membrane theory for the upper dome of the Pines Calyx. Stress values for the lower dome are similar.

The horizontal thrust at the bases of both domes is about 188% of the vertical gravity loads on the domes. The high percentage is due to the shallow geometries of the domes.

Modified Thrust Line

Using the interactive geometry software, *Cabri II*, the author created a program based on the modified thrust line analysis to address the most challenging aspect of the Pines Calyx structural analysis: the axisymmetrical dead loads and asymmetrical live load case[9]. Few existing analysis methods contend with asymmetrical loading in domes. The program, based on the modified thrust line method determined a satisfactory thrust line under the most extreme asymmetrical loading case: maximum live load on one-half of the dome, and zero live load on the other half. The lune profile used in the program consisted of two complementary wedges that span the full dome diameter, and are separated at the crown by the oculus. To simulate the asymmetrical load condition, the program used different surcharge values on each lune half. Two force polygons,

[9] Live load conditions on the Pines Calyx have since been withdrawn due to numerous factors that accompanied the permitting of pedestrian traffic on the domes' surfaces.

representing the respective loads on both halves of the lune, were combined to generate the final thrust line (Fig. 5.11).

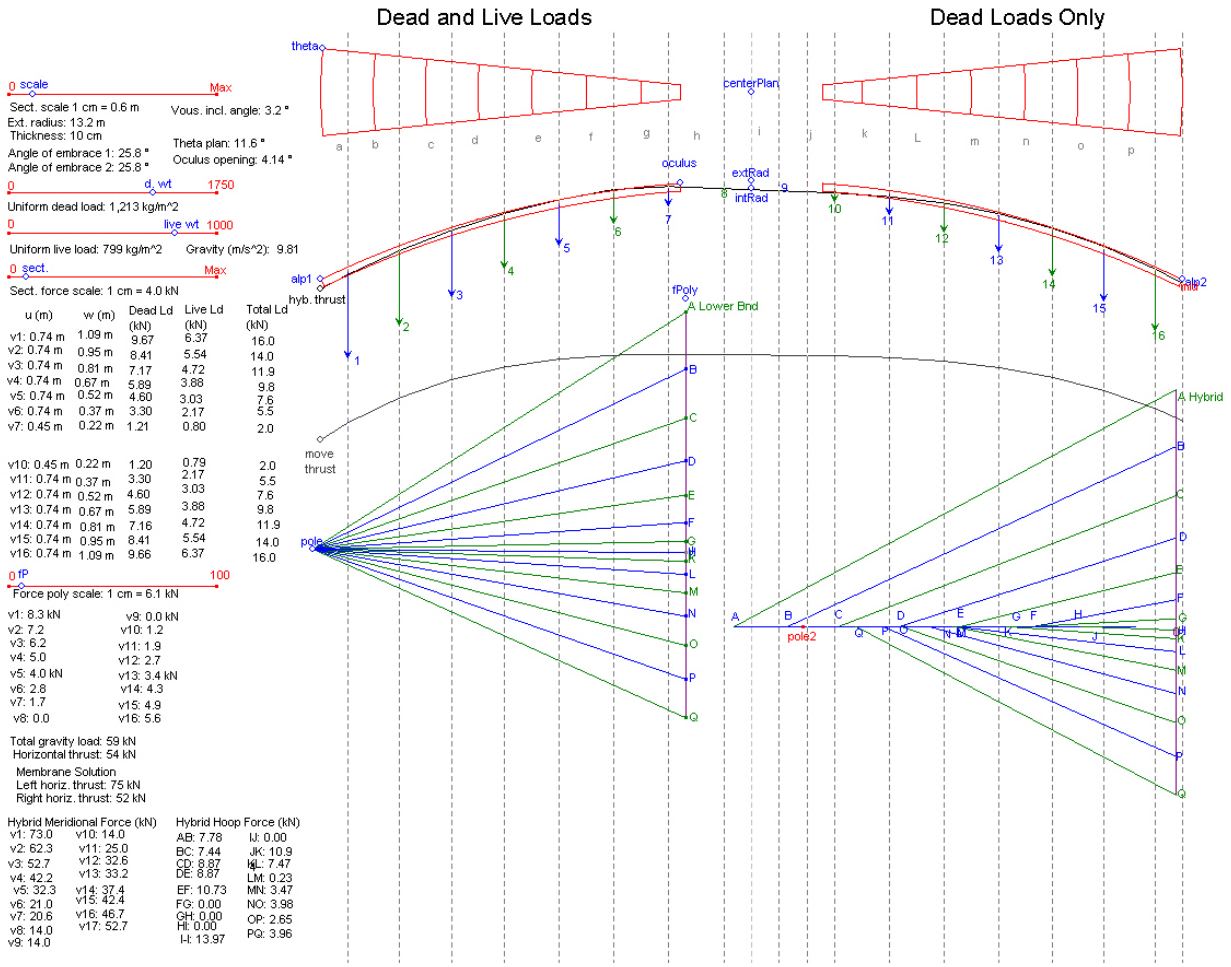

Figure 5.11. The graphics-based modified thrust line theory solution for an asymmetrical load case. The thrust line is satisfactory in both halves of the wedge-shaped lune, assumed to span the full diameter of the dome.

The horizontal thrust for the half-lune supporting live and dead loads is 195% of its gravity loads. The lune's counterpart, which supports only dead loads, has a thrust of only 111% its gravity loads. Not surprisingly, the half dome supporting the higher load thrusts more than its counterpart.

Under asymmetrical loading, it was not possible to attain a satisfactory thrust line without hoop forces.

By deriving satisfactory lower bound solutions using the membrane theory and the modified thrust line method, which also met material strength limits, the author and this work contributed to the validation of the design of the Pines Calyx domes (Fig. 5.12).

Figure 5.12. The interior of the lower dome of the Pines Calyx near the end of its construction (photograph courtesy of Michael Ramage)

5.3. Chapter Summary

The modified thrust line theory proved valuable in the analysis of two masonry domes whose unconventional and daring geometries could not be satisfactorily explained with existing analysis methods. The modified thrust line method's versatility in analyzing domes with various geometry, material, and load parameters, provides a significant advantage over existing analysis methods, which would require time-consuming modifications to analyze custom dome parameters, without assurance that much useful information will be revealed in their solutions. The numerous methods by which to estimate the minimum thrust-to-weight ratio listed in Chapters 3 and 4 proved accurate for the pointed dome of Farag Ibn Barquq.

Chapter 6. Upper Bound Limits

The previous chapters discussed lower bound applications of the modified thrust line method, and existing lower bound analysis methods such as the membrane theory. The upper bound or critical load capacity of masonry structures is difficult to quantify for numerous reasons, including variability in material composition and construction. In the past century, several authors have attempted to predict the plastic limits of domes, but these methods remain largely unproven, untested, and most importantly, not applicable to masonry construction. This chapter examines the potential use of the modified thrust line method to predict upper bound limits in the case of two experiments in which two small-scale masonry dome were loaded to failure by a concentrated load at the crown (Fig. 6.1).

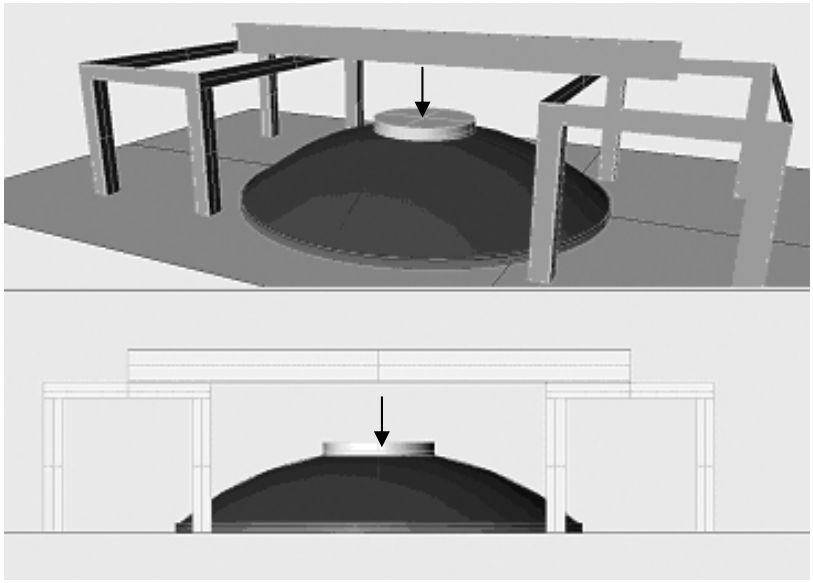

Figure 6.1. Load configuration for the AAC domes (figure courtesy of Michael Ramage)

6.1. Theoretical Limits and the Modified Thrust Line Method

Following limit state conditions, the modified thrust line method assumes a dome is unstable if a thrust line cannot fit within its effective thickness. The upper bound limit is the maximum load capacity of the structure prior to failure; any additional load causes the thrust line to exit the dome's thickness and create a collapse mechanism. The unique value of this load limit is found in accordance with the upper bound theorem (Heyman 1995). Due to the large self-weight of

masonry and the relatively low live loads, it is uncommon for masonry domes to be overloaded to the point of collapse although some instances of historical collapses have occurred (Fig. 6.2).

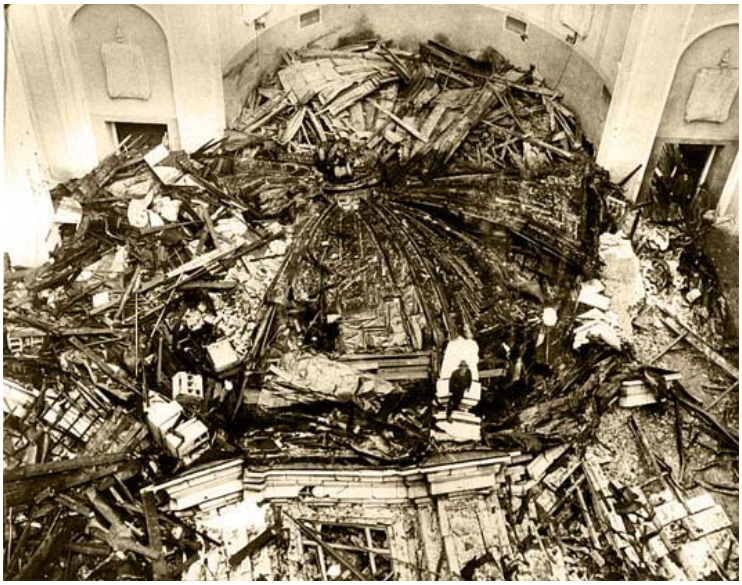

Figure 6.2. The steel-supported masonry dome of St. James Cathedral, Seattle, collapsed in 1916 after a snowstorm; figure from St. James Cathedral (2006).

The author used the upper bound principles to explore the potential of the modified thrust line method to predict the upper bound limits of two small-scale thin shell masonry domes that were loaded to collapse by a concentrated load at the crown[10]. Using the interactive geometry program, the author increased the surcharge loads on a representative lune section until a satisfactory thrust line was no longer found.

Dome Geometry

The masonry domes were constructed of mid-grade TruStone aerated autoclaved concrete (AAC) TS 3 tiles supplied by TruStone America[11], and United States Gypsum Company[12] (USG 1997) Hydrocal White Gypsum Cement. TruStone's published unit weight for the AAC tile is 37 pcf (TruStone America 2005). Assuming 40:100 parts water:gypsum in weight, the author calculated

[10] The construction and load test of the first AAC dome was in collaboration with the research of Michael Ramage (2005), a fellow architecture graduate student at MIT.
[11] TruStone America, a manufacturer of aerated autoclaved concrete, is currently located in Providence, RI. More information is available at www.truestoneamerica.com.
[12] Information on the United States Gypsum Company and its products is available at www.usg.com.

the dry unit weight of the gypsum mortar as 94 pcf (USG 1997). The author estimated the dome composition as 85% AAC tiles and 15% mortar, resulting in a monolithic unit weight of 46 pcf.

The domes consisted of a single layer of 1.25 in. thick tiles cut no larger than 4 x 8 in. They were constructed without centering, and with building techniques and methods similar to those used for timbrel vault structures. Table 6.1 lists the design geometries of the two domes.

Table 6.1. Design geometries of the AAC domes

	Dome 1	Dome 2
Angle of Embrace (deg.)	45.0	60
Med. Radius of Curvature (ft)	5.0	4.1
Thickness (in.)	1.25	
Thickness-to-radius ratio	0.021	0.025
Height (ft)	1.5	2.1
Median Span (ft)	7.0	
Deviation of As-Built Dome from Design Radius of Curvature (in.)	+/- 1.0	+/- 2.0
Deviation of As-Built Dome from Design Radius of Curvature as % of Design Radius	+/- 1.7%	+/- 4.1%

One steel tension ring, fabricated with an inside diameter of 86.8 in. (7.2 ft), was used to resist the outward thrust at the base of both domes. The author documented the as-built geometries of the domes. The design and as-built dome sections were used to approximate their deviation from the design radius of curvature (Table 6.1, Figs. 6.3 and 6.4).

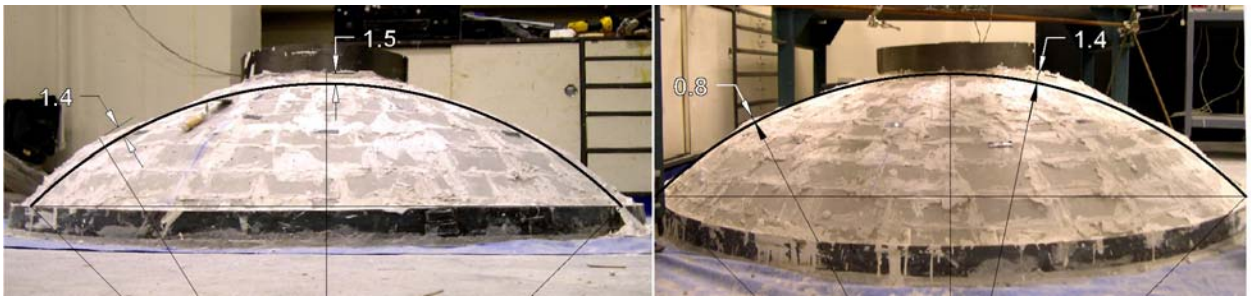

Figure 6.3. Comparison of design and as-built geometry of Dome 1 (dimensions shown in inches)

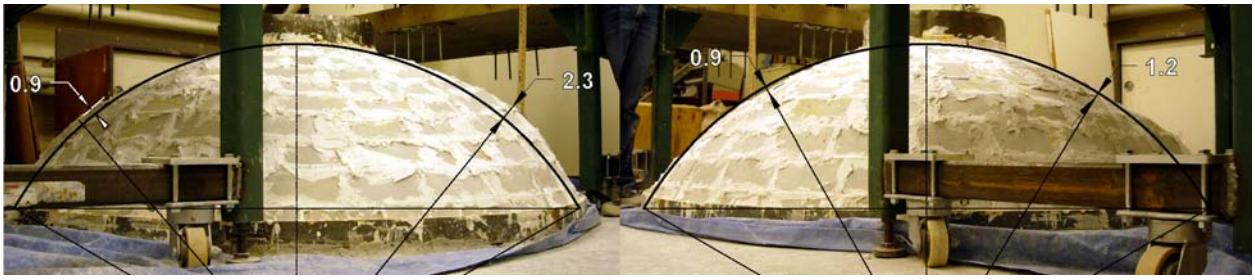

Figure 6.4. Comparison of design and as-built geometry of Dome 2 (dimensions shown in inches)

Critical Load Predictions

The author predicted the upper bound limits of the domes as a function of direct tensile strength using three different analysis methods: the membrane theory, plastic limit (Save et al. 1997), and the modified thrust line. The predicted failure loads shown in Figs. 6.5 and 6.6 include the concentrated applied load, surcharge weight of a cylindrical plaster load pad on the dome crown, and the load test equipment. The plaster load pad was cast to distribute the point load at the crown, applied by a single load cell, that would cause a punching failure. At the base, the tiles were encased in a gypsum mortar bed in the steel tension ring angle.

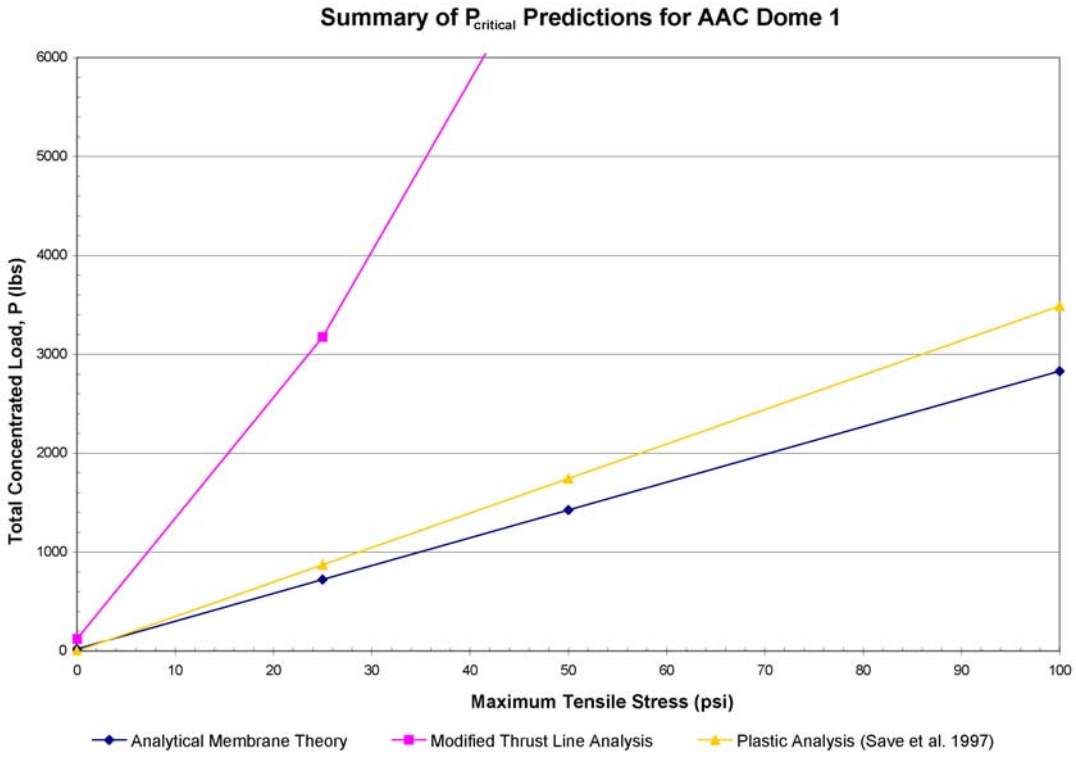

Figure 6.5. Predictions for total critical load, including applied and surcharge loads, for Dome 1 as a function of material tensile strength

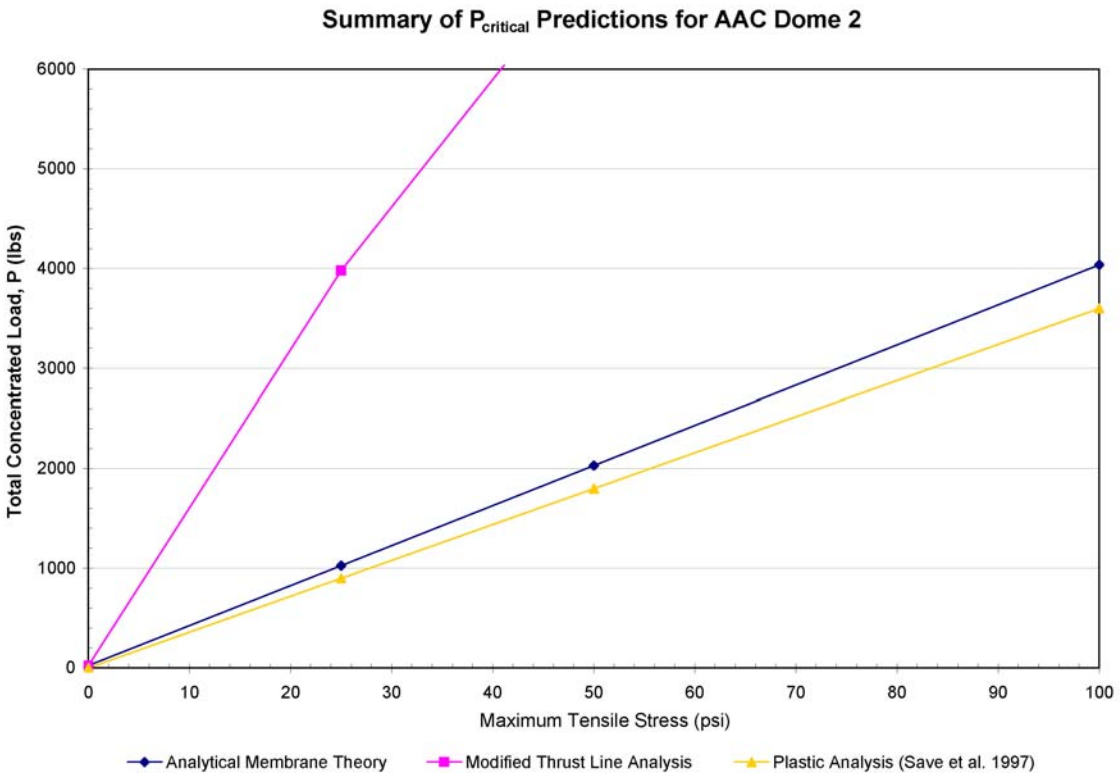

Figure 6.6. Predictions for total critical load, including applied and surcharge loads, for Dome 2 as a function of material tensile strength

Interestingly, all three methods predicted the domes would not stand even under only the concentrated load of the plaster load pad without tensile capacity in the masonry. For the membrane theory and modified thrust line analyses, the author assumed the applied point load was uniformly distributed on the surface area of the load pad. The plastic method of analysis by Save et al. (1997) predicts the critical uniform load distributed over the horizontal projected area of the spherical reinforced concrete dome. Given that the domes discussed here have little ductility and are loaded with a point load rather than a uniform distributed load, this method is not directly applicable, but was included in the study for comparison. In addition, to attain a value from this method, one must select a φ-value of the topmost hinge circle of the collapse mechanism. After conducting the load tests, the author retroactively used the φ-value from the data to obtain the values shown in Figs. 6.5 and 6.6. Without prior knowledge on where the hinge circle occurs, as in the case of any existing stable domes, this method would be difficult to apply to masonry structures, thus further decreasing the potential of the this method to predicting the ultimate load capacity of masonry domes.

In the modified thrust line method, the thrust line's ability to deviate from the dome's median radius induces bending in the structure due to the moment generated by axial forces at an eccentric distance away from the section's neutral axis (Fig. 6.7).

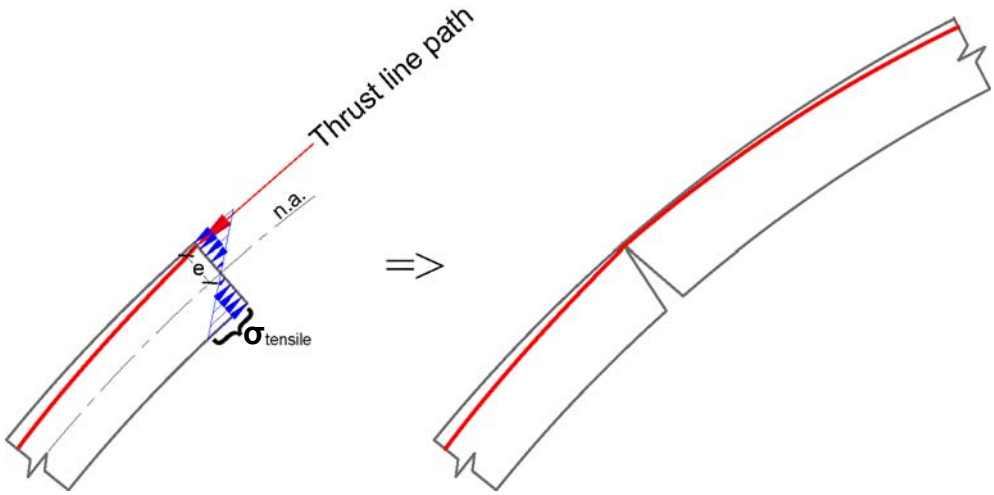

Figure 6.7. The eccentricity of the thrust line location with respect to the neutral axis of the dome section may produce tensile stresses due to bending in the structure, and create a hinge.

At one extreme, the superposition of compressive stresses due to bending and axial meridional forces can cause localized crushing in the thrust line path. At the other extreme, the tensile stresses due to bending forces may cause the masonry to move apart and form a hinge in the structure away from the thrust line path. As a result, the modified thrust line analysis will tend to overestimate the critical load because it does not account for the contribution of bending forces to the failure of a dome. Instead, the analysis currently assumes that the structure has not already failed in bending where the thrust line is in close proximity to the extrados or intrados, and that the structure will experience local crushing and form hinge lines.

The author conducted two additional analyses with the modified thrust line method whose predictions are discussed later in this chapter. The first incorporates the middle-third rule, which assumes the thrust line remains within the middle-third of the dome section. The second analysis assumes the thrust line cannot deviate beyond an eccentric distance from the neutral axis of the dome section that is determined by the modulus of rupture of the masonry. Though this work has discussed the middle-third rule's inapplicability to a brittle, nonlinear-elastic material, scale effects increase the masonry's reliance on its tensile properties for stability.

Scale Effects

The small size of the experimental dome structures relative to the sizes of actual dome structures introduces scale effects into the challenge of predicting upper bound limits. As a result, the tensile strength of the masonry in the AAC domes has a greater role in resisting the applied loads than if the domes were full size. If a proportionally-sized load pad and applied load was placed on dome ten times greater than the test domes, the larger dome will have greater opportunity to develop internal compressive forces in its volume to resist the load, due to Galileo's square-cube law[13], and rely less on tensile strength, an unreliable factor in masonry structures.

6.2. Material Strength Properties

Though limit state analysis assumes infinite compression strength and zero tensile strength, in reality, the AAC masonry construction has a finite crushing limit and tensile capacity, which are significant in predicting upper bound limits. These material properties limit the magnitudes of the internal forces in the dome, which translate to geometric limits in the force polygons in the modified thrust line method (Fig. 6.8).

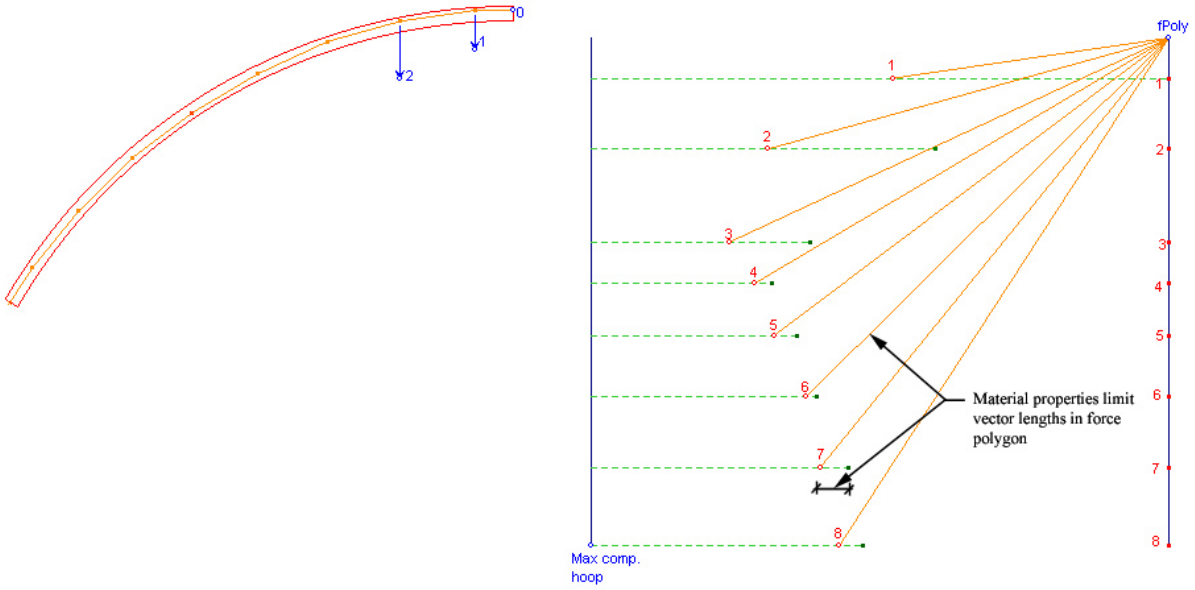

Figure 6.8. Material strength properties limit internal force values, which translate into vector lengths in the force polygon for the modified thrust line method.

[13] Galileo's square-cube law states: "When an object undergoes a proportional increase in size, its new volume is proportional to the cube of the multiplier and its new surface area is proportional to the square of the multiplier" (Wikipedia 2006).

The author determined the average compressive and tensile strengths of the AAC/gypsum mortar masonry by conducting material load tests in compression, bending and direct tension. The cure time of the gypsum mortar ranged from about two weeks to two months. On average, samples that cured for a shorter duration had a higher modulus of rupture, although the range of strengths for all samples was similar regardless of mortar cure time. The relatively large standard deviations for all the material tests reinforce the notion that masonry construction is not homogeneous, but heterogeneous in composition, such as the gypsum mortar proportions, and construction technique. Detailed testing procedures and results may be found in Appendix E. Table 6.2 summarizes the material strength properties of the masonry.

Table 6.2. Average strengths of AAC tile masonry (standard deviation in parentheses)

	Bonded AAC and Hydrocal	AAC Tile Only
Compressive Strength (psi)	336 (41)	396 (35)
Flexural Tensile Strength (psi)	50 (20)	63 (16)
Direct Tensile Strength (psi)	23 (11)	52 (14)

TruStone's published compressive strength for non-bonded AAC is 600 psi (TruStone 2005). USG's published dry compressive strength for the gypsum mortar is about 6700 psi, assuming 40:100 parts water to gypsum (USG 1997). From the load tests, the average crushing strength of the assembly of these two materials was about 340 psi, 44% lower than the published values for the AAC alone.

On average, the bonded AAC tiles had a lower modulus of rupture than the AAC tile alone. Therefore, failure due to bending stresses in the structure, which manifests into cracks in the hoop direction, is more likely to occur at the joint-to-tile interface than through the masonry tile. The author did not find literature on the tensile capacities of the AAC tile or gypsum mortar by the manufacturers.

The average tensile strength of 23 psi for the bonded specimens is lower than the average strength of the AAC tile alone. During the material tests, failure in the bonded samples occurred at the mortar-to-tile interface, but not through the mortar. Because the average tensile strength is lower than the modulus of rupture, a dome structure constructed of AAC tiles and gypsum mortar will likely first fail in areas that experience direct tension, such as in the hoop direction,

which results in radial cracks that divide the dome into independent lunes. The dome will then fail in bending and form hinge circles around the dome.

6.3. Load Tests

In addition to the point load applied by the load cell, the domes carried the surcharge weight of the plaster load pad and load test equipment. The plaster consistency was approximately 70:100 parts water to gypsum mortar for a unit weight of 66 pcf. For Dome 1, the total surcharge weight of the plaster load pad and steel equipment was 54 lbs. For Dome 2, the total surcharge weight was 74 lbs. These surcharge loads are included in the load values plotted in Figures 6.5 and 6.6.

Two linear variable differential transformers (LVDTs), placed approximately 180 degrees apart on the top surface of the load pads on the crowns of the domes, monitored their downward displacement with the applied load.

Dome 1

Overall, the load-displacement relationship of Dome 1 demonstrated the brittle behavior of the AAC masonry in which the dome experienced small plastic deformations before abrupt failure (Fig. 6.9)[14].

[14] The gradual decrease in total load supported coupled with the gradual increase of displacement shown in Figure 6.9 result from the mechanics the load cell; the loss of contact between the dome and the load cell, as the dome displaced downward, reduce the applied load exerted by the load cell, and allows for the dome to stabilize. If the ultimate load on the dome remained constant, as in most real-life live loads, the dome's failure would be abrupt, as expected for brittle materials.

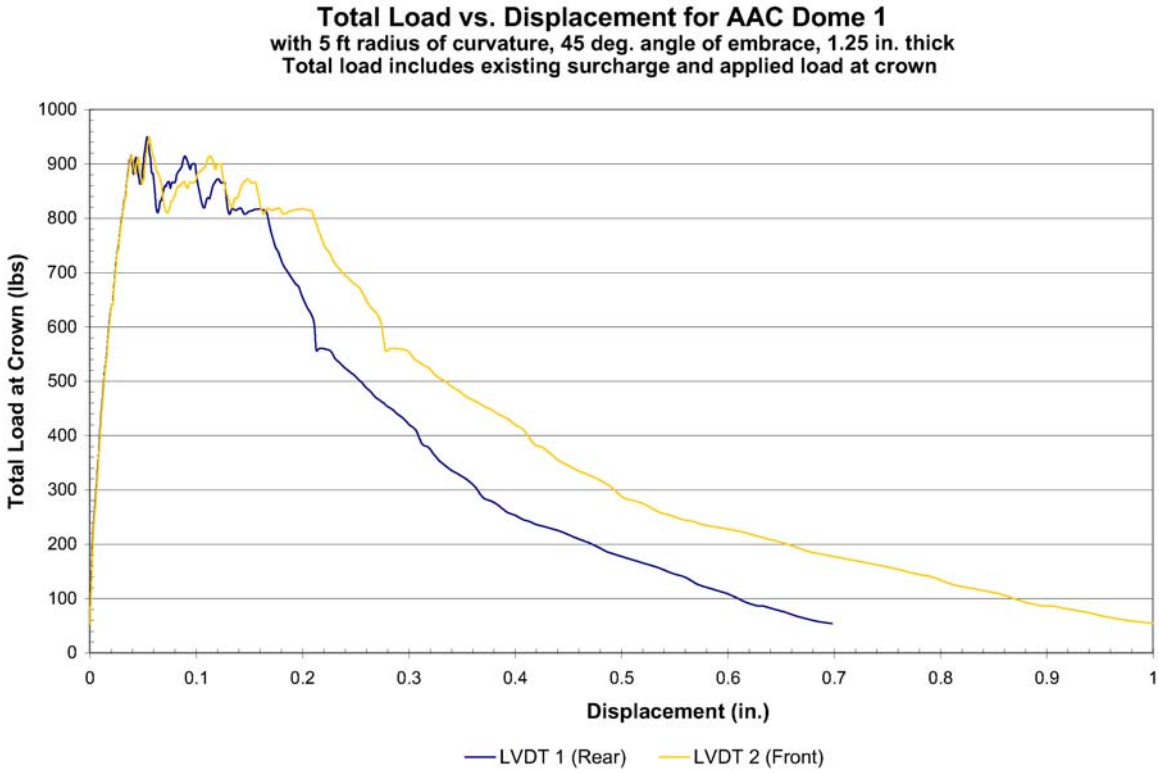

Figure 6.9. Total applied and surcharge load on the crown versus displacement for Dome 1

The load-displacement relationship was linear until the total applied load reached about 920 lbs with an average displacement of 0.04 in., at which the dome developed hairline cracks in the meridional direction. Dome 1 was not unloaded to permit potential recovery of deformation. The dome supported a maximum load of 950 lbs with a displacement of about 0.06 in., at which point additional displacement caused a drop in the applied load on the dome. The dome briefly had a plastic response in which the total supported load vacillated between 800 and 900 lbs with increasing displacement. The dome experienced minimal creep at about 800 lbs with a change in displacement of 0.03 in. At this point, overt meridional cracks appeared due to the added displacement, and the displacement of the crown increased while the total load the dome could support steadily decreased. When the crown had displaced about 0.25 in., the total supported load briefly hovered at 560 lbs, after which visible hinge circles appeared (Fig. 6.10).

Figure 6.10. Dome I: Cracks in the hoop direction, or hinge circles, created the collapse mechanism after displacement exceeded 0.5 in.

On average, the dome deformed about 0.85 in. total before collapsing relatively symmetrically. Individual lunes formed three hinges before failing: the middle hinge which formed on the intrados occurred approximately at $\varphi = 23°$; the upper hinge at the extrados appeared to occur at $\varphi = 12°$ from the photograph documentation; the final hinge circle occurred near the base of the dome at $\varphi = 41°$.

Dome 2

For the load test of Dome 2, the overall load-displacement relationship demonstrated the brittle behavior of the masonry in which the dome experienced small plastic deformations before abrupt failure (Fig. 6.11).

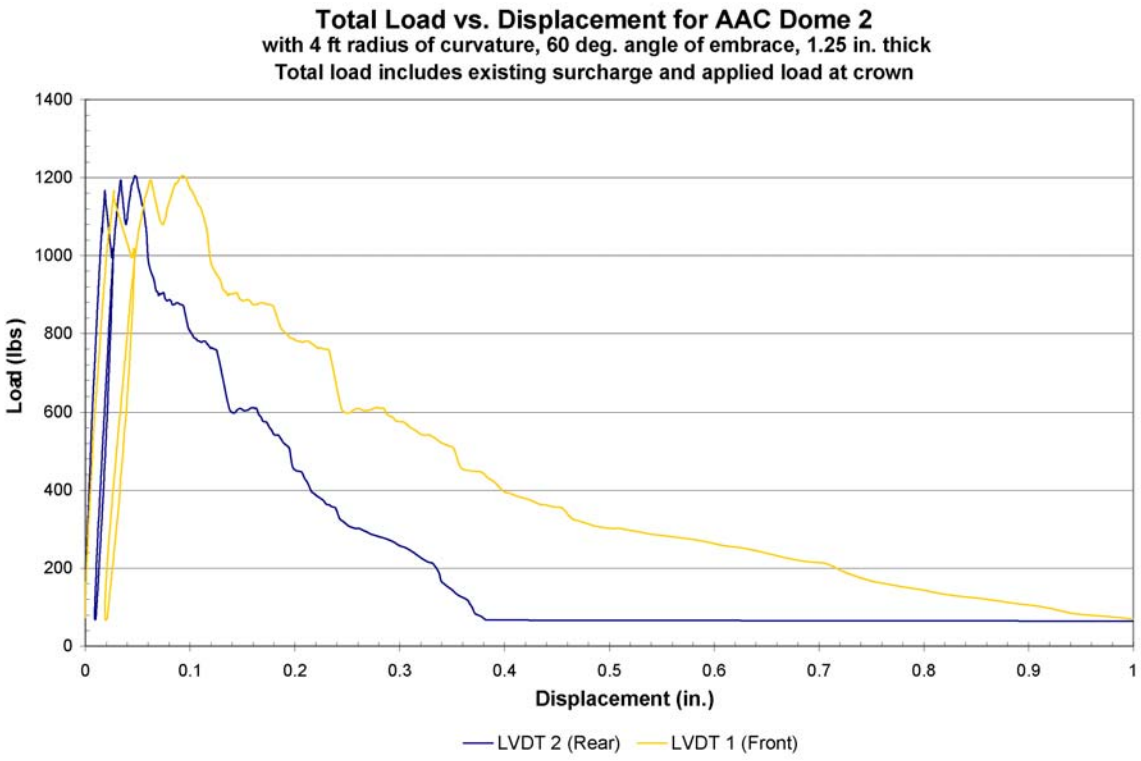

Figure 6.11. Total applied and surcharge load at the crown versus displacement for Dome 2

The initial load-displacement relationship was linear elastic until the first significant meridional crack occurred at a total load of 1170 lbs with an average deformation of 0.023 in. The dome experienced some minor creep before it was unloaded to only the weight of the existing surcharge of the load pad and test equipment. As the load was removed, the dome recovered only 0.01 in. in displacement, affirming the masonry's brittle behavior and associated plastic deformations. As the load was reapplied, the displacement again was linear elastic and parallel to the initial linear-elastic curve.

The dome recovered to surpass its initial load to a total ultimate load of 1205 lbs. As the supported load vacillated between 1050 and 1200 lbs, the dome had a semi-plastic and semi-elastic response in which additional load gradually increased displacement, but intermediate recovery after additional cracking and displacement was linear elastic. The dome again reached its ultimate load with a displacement of about 0.075 in. The impact of the dome's as-built asymmetrical construction became evident, when one-half of the dome exhibited significant meridional cracks while the other half had no overt meridional cracks.

Visible hinge circles appeared on the cracked half of the dome when the average displacement reached 0.1 in. and total supported load was 900 lbs. Meridional and hoop cracks and crown displacement continued to increase while the total load that the dome supported decreased. At an average total displacement of 0.25 in., and an applied load of 575 lbs, a continuous hinge circle formed on one half of the dome. After this half displaced 0.96 in., it collapsed (Fig. 6.12). The other half of the dome remained standing.

Figure 6.12. Half of Dome 2 collapsed when total displacement of the crown reached almost 1 in.

The asymmetrical response likely resulted from significant asymmetrical construction aberrations from the design geometry. On the failed half, the individual lunes formed three hinges prior to failure: the middle hinge on the intrados occurred at approximately $\varphi = 40°$; the upper hinge appeared at approximately $\varphi = 15°$; a third hinge circle at approximately $\varphi = 57°$, near the base of the dome.

Load Tests Comparison

Dome 2 supported a maximum load at the crown that was 27% greater than the load supported by Dome 1. This may seem contradictory based on the membrane theory principle that a dome

with zero tensile capacity will fail under self-weight if $\alpha > 51.8°$. However, from Chapter 3, under a uniform axisymmetrical load, such as self-weight, and limit state conditions, the modified thrust line method demonstrated that the minimum thrust-to-weight ratio actually decreases as α and t/R increases for spherical dome geometries. As a result, loads in Dome 2 can be transferred in a more vertical path to its support than in Dome 1 (Fig. 6.13).

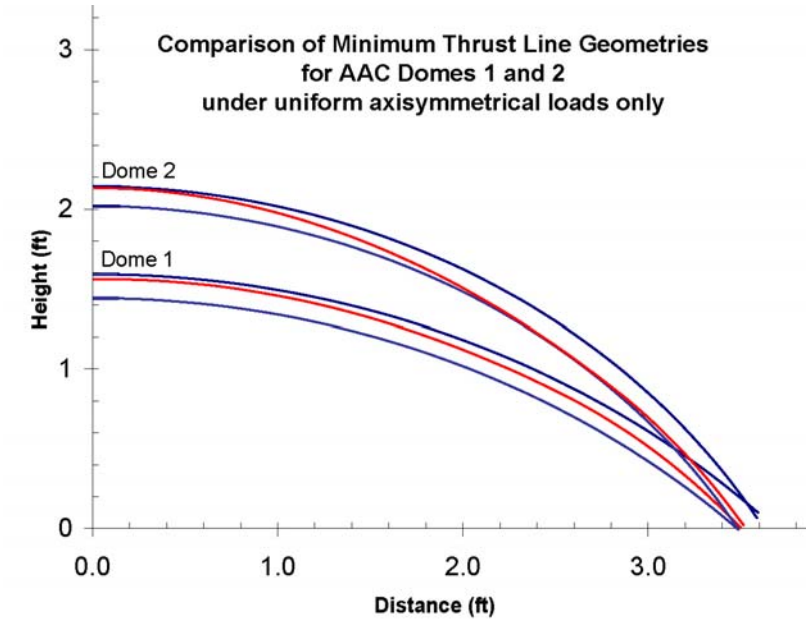

Figure 6.13. The thrust line of the dome with a larger embrace angle can assume a more vertical orientation at the base.

A concentrated load at the crown requires nearby masonry voussoirs to develop large compressive hoop forces to resist failure in shear and inward rotation, and thus further increases the thrust-to-weight ratio: the thrust line moves closer to the extrados. The larger dome construction with a greater number of rings will have more opportunity to develop compressive and tensile hoop forces that work together to resist the applied load. To summarize, Dome 2 was larger than Dome 1 in terms of surface area and volume, and had a slightly greater t/R ratio that worked to its advantage.

Review of Load Predictions

Figures 6.14 and 6.15, modified from the previous Figs. 6.5 and 6.6, plot the results of the load tests with the prediction lines from other analysis methods discussed below.

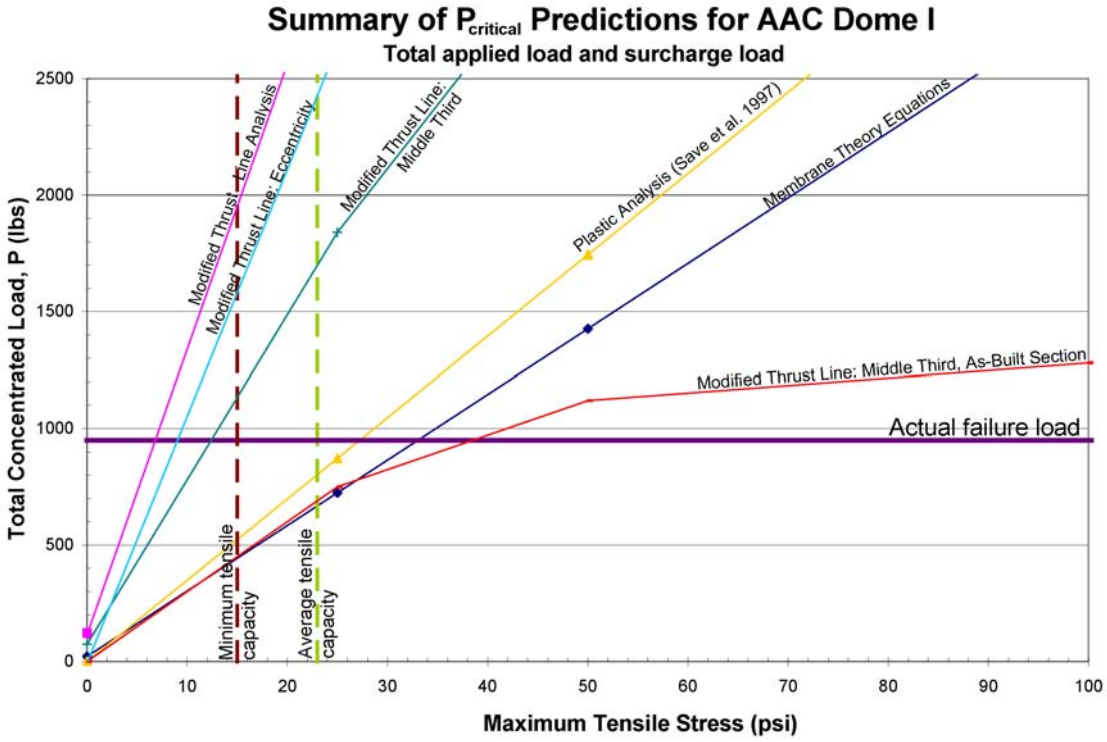

Figure 6.14. Comparison of predicted and actual total load results for AAC Dome 1

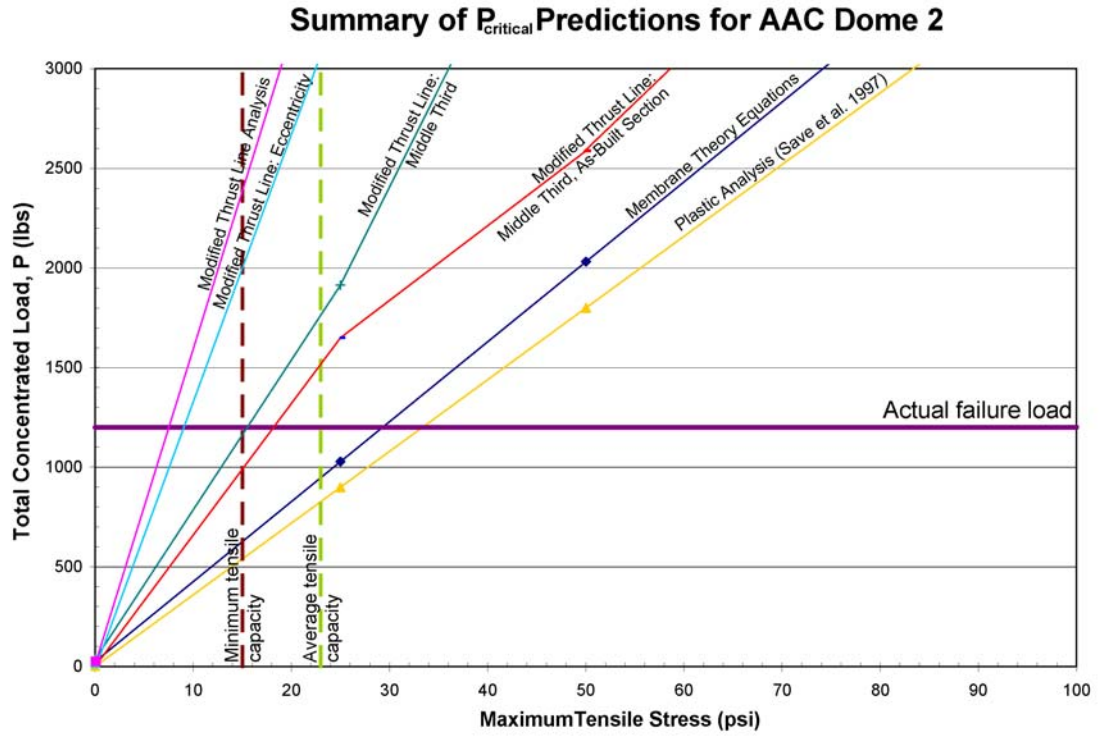

Figure 6.15. Comparison of predicted and actual total load results for AAC Dome 2

Predictions from Initial Analysis Methods

From the initial three prediction methods, assuming a governing strength of 23 psi in direct tension for the AAC/gypsum mortar bonded samples, the plastic limit analysis and the membrane theory predictions were about equal in accuracy. For Dome 1, the plastic limit analysis method predicted a failure load of 800 lbs versus 950 lbs (16% difference); for Dome 2, this method predicted a failure load of 800 lbs versus 1200 lbs (33% difference). However, the usefulness of this method to predict the critical load of any masonry dome remains uncertain because the propriety of this method to construction materials and load conditions other than what was assumed in its derivation is not discussed by the authors.

The derivation of the membrane theory allows an analyst to evaluate the specific load case of a concentrated load at the crown in accordance with the experiment. For Dome 1, the membrane theory calculated that internal tensile hoop forces exceed 23 psi when the total concentrated load applied on the crown is 660 lbs. This is about 30% lower than the actual collapse load of 950 lbs. For Dome 2, the membrane theory calculated the critical concentrated load as 935 lbs, which is about 22% lower than the actual collapse load of 1200 lbs. Construction aberrations play a significant role in the ultimate strength of the domes, as particularly visible in Dome 2, where one half of the dome was virtually unaffected by the load test and the collapse of its counterpart.

Assuming the limiting strength of the domes is due to direct tension only, and that the thrust line can occupy the entire thickness of the dome, the modified thrust line method overestimated the load capacities of the domes: for Dome 1, the prediction was about 232% greater than the actual failure load; for Dome 2, the prediction was about 230% greater. These large overestimations may result from the heterogeneous composition of the masonry: Due to the wide range of strength values from the material tests, one could argue that the lowest, instead of the average, strength values will govern the failure of the structure. In this case, the error of reduces to approximately 100% for both domes.

Predictions from Additional Analysis Methods

The author explored three potential adjustments to the modified thrust line method based on different material behavior assumptions due to larger role of scale effects in these tests. The first

examined the role of eccentricity. In general, for masonry structures, the thrust line can occur anywhere within the thickness of the dome to no detriment other than potential local crushing. Due to scale effects, the bending stresses generated by the eccentricity of the thrust line from the median dome surface influenced the failure of these domes. The curves, "Modified Thrust Line: Eccentricity," on Figs. 6.14 and 6.15 permitted the thrust line to deviate only a distance, *e*, from the median radius where *e* is:

$$e = \frac{t}{3}\left[\frac{2\sigma_r \theta t a \sin\phi_i}{M_i} + 1\right] \tag{6.1}$$

and *t* is equal to one-half the dome's thickness, and σ_r is the average modulus of rupture shown in Table 6.2. Assuming the direct tensile strength of the domes as 23 psi and the average σ_r of 50 psi, this analysis still overestimated the critical loads of Domes 1 and 2 by 153% and 149%, respectively, which suggests the material's reaction was affected by elasticity.

The "Modified Thrust Line: Middle Third" curves further decreased the maximum distance between the thrust line and median radius to 1/6 the effective thickness on either side of the median surface. This analysis assumes the masonry behaved perfectly linear-elastically. This analysis overestimated the critical loads of Domes 1 and 2 by 79% and 45%, respectively; hence the masonry acts somewhere between a brittle, no-tension material and a linear-elastic material.

Finally, aberrations in the as-built geometry from the design geometry will affect the structure's load capacity, as the asymmetrical collapse of Dome 2 demonstrated. If construction was perfect, the domes would likely support more load due to reduced internal shear and bending stresses from asymmetry. The author conducted an additional modified thrust line analysis using the middle-third rule and assuming that the most deformed section of the dome, where notable failure first occurred in both the load tests, will govern the load capacity (Figs. 6.14 and 6.15). The "Modified Thrust Line: Middle Third, As-Built Section" curves underestimated the critical load of Dome 1 by 23% and overestimated the critical load of Dome 2 by 25%. Though on average, this method produced the lowest difference from the actual critical loads, it is subject to minor interpretation errors due to inherent limits of the graphics-based output.

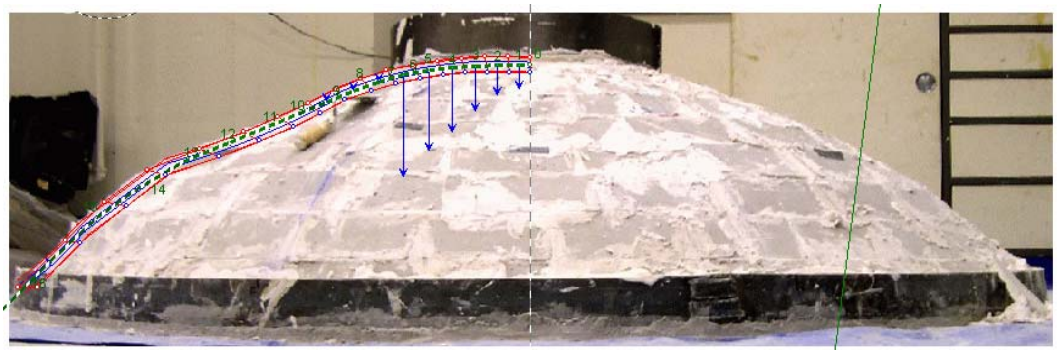

Figure 6.16. The modified thrust line method was applied to the section with the greatest aberration from the design geometry under a total load at the crown of approximately 750 lbs and a direct tensile strength of 25 psi.

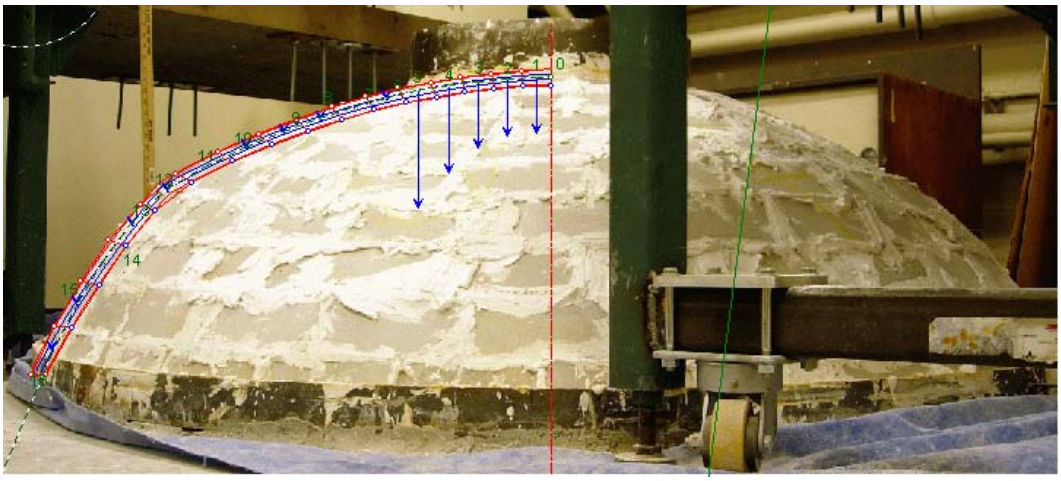

Figure 6.17. The modified thrust line method was applied to the section with the greatest aberration from the design geometry under a total load at the crown of approximately 1650 lbs and a direct tensile strength of 25 psi.

6.4. Chapter Summary

Based on the two empirical dome case studies, the modified thrust line method currently well overestimates the upper bound limit of masonry domes while the membrane theory and plastic limit analyses slightly underestimate the limit. Factors such as masonry composition, construction, and material and geometry discrepancies, influence the upper bound limits of any structure. The author demonstrated the versatility of the modified thrust line method to account for such factors. The small-scale of the two domes subjects the load tests to scale effects, which increases the roles of tensile and flexural strengths in resisting applied loads than in real-size masonry domes. Further study is required to fully understand these considerations when applying the modified thrust line method as an upper bound analysis.

Chapter 7. Conclusions

Previous studies in the structural behavior of masonry domes had limited success in evaluating the three-dimensional capabilities and the structural limits of domes. In general, these studies, as well as existing structural analysis methods for masonry domes, reduced the role of internal hoop forces in the stability and capacities of domes. In addition, existing analytical methods fix the values of internal forces, thus limiting the analysis to find only one solution when potentially infinite solutions exist.

This thesis introduced the modified thrust line analysis as a new graphical method to analyze the equilibrium of masonry domes. This versatile method, which allows internal meridional and hoop forces to attain a range of values, can be applied to domes with conventional or non-conventional axisymmetrical geometries, the latter of which are often too complex to analyze with existing graphical, analytical, or numerical analysis methods.

The flexibility offered by graphical analysis led to solutions for the minimum thrust of domes, a previously unknown structural parameter. By combining different internal force values, the author identified the theoretical thrust lines that correspond to the minimum thrust of spherical and pointed domes. From the results, many insights into the structural behavior of masonry domes became apparent.

First, geometry is significant to the minimum thrust-to-weight ratio of spherical and pointed domes. The minimum thrust-to-weight ratio is inversely related to the thickness-to-radius ratio. For two domes with all other geometric parameters equal, the thrust of the thicker dome will be a lower percentage of its weight than the thinner dome. The minimum thrust-to-weight ratio is also inversely related to the embrace angle of the dome. A dome with an embrace angle near or equal to 90 degrees will have a lower minimum thrust-to-weight ratio than a shallow dome.

With all other geometric parameters equal, a pointed dome will have a lower minimum thrust-to-weight ratio than a spherical dome. The minimum thrust of a hemispherical dome portion, equal to or smaller than one-eighth of the complete dome, is approximately 20 to 25% of its weight, regardless of t/R. For pointed domes with an embrace angle of 90 degrees, as the truncation angle

increases from 0 to 90 degrees, increasing the dome's steepness, the minimum thrust-to-weight ratio decreases from between 20% and 25% to zero.

Several methods were described to estimate the minimum thrust-to-weight ratio. One can interpolate the ratio from the plots included in the main body and appendices of this thesis. For spherical domes with embrace angles greater than π/3 in radians, the minimum thrust-to-weight ratio may also be approximated by $\frac{H}{W} = -0.583\alpha + 1.123$, where α is the embrace angle in radians. For pointed domes, this equation is $\frac{H}{W} = 0.551\,\delta - 1.061\,\frac{\delta}{\alpha} - 0.615\,\alpha + 1.164$, where δ, the truncation angle in radians, is less than α. Basic static equilibrium equations may also be used. However, equation-based estimates reveal nothing about the stability of the domes.

The Mamluk dome case study demonstrated these methods produce accurate and precise estimates. Thus, one who estimates the minimum thrust-to-weight ratio rather than conducting the modified thrust line analysis will likely achieve a reasonable result.

Hoop forces are critical in the stability of spherical dome geometries with thickness-to-radius ratios less than 0.05, and embrace angles greater than 22 degrees when $t/R = 0.01$; when t/R increases to 0.04, hoop forces are critical when embrace angles exceed 50 degrees. Without hoop forces, the modified thrust line analyses did not achieve satisfactory thrust line solutions for these dome geometries.

Hoop forces are critical in the stability of several pointed dome geometries with thickness-to-radius ratios less than or equal to 0.08, which is higher than the ratio for spherical domes. As a result, when using equations to estimate the minimum thrust of thin-shell pointed domes, one must be mindful that hoop forces may be critical to the overall stability of the dome.

From the internal force values corresponding to the thrust lines producing the minimum thrust, the modified thrust line method identified regions in which the presence of meridional cracks in a dome's surface does not impact the dome's stability. For $t/R = 0.05$, spherical domes may exhibit meridional cracks higher in its surface than pointed domes.

By neglecting hoop forces, previous studies derived minimum thicknesses of masonry domes that were similar to values derived in this thesis. However, previous studies typically determined these limits by assuming the dome conditions at incipient collapse, while this study derived these values under stable equilibrium states. In this study, hoop forces were critical in that they increase the range of stable dome geometries, and provide insight to their role in dome stability, as in the discussion of meridional cracks in the dome.

This thesis also discussed applications of the minimum thrust in the stability of half-dome buttresses. For a hemispherical half-dome structure, the minimum thrust-to-weight ratio lies between 0.18 and 0.12 for thickness-to-radius ratios between 0.05 and 0.20, respectively. This is comparable to Heyman's estimated thrust-to-weight of the complete dome ratio of 0.068 (Heyman 1977). For a pointed half-dome structure with an embrace angle of 90 degrees, the minimum thrust-to-weight ratio is inversely related to the truncation angle. For $\delta = 0°$, the ratio ranges from 0.17 to 0.12 for t/R between 0.05 and 0.20, respectively, to zero for $\delta = \alpha$.

The modified thrust line method provides insight to the stability of the support structure under a dome. The case study of the support structure under the dome of Farag Ibn Barquq demonstrated how minimum thrust-to-weight ratios inform the geometry of thrust line in the support structure.

In its current state, the modified thrust line method overestimates the critical load capacity of masonry domes based on empirical tests conducted on two small-scale domes. Scale effects, due to the domes' small sizes, likely increased the masonry's reliance on tensile strength, which is an unreliable material property for masonry. Due to the flexibility proffered by modified thrust line theory, the author also made upper bound predictions by applying the middle-third rule, and evaluating the as-built geometry of the domes. These modifications brought the estimates to within 25% of the actual failure loads of both domes. In conclusion, upper bound analyses have many complexities unique to the different load conditions and construction materials. The modified thrust line method currently does not account for all possible factors.

7.1. Future Work

This thesis is only the starting point for the modified thrust line method, or any other new analysis method for masonry dome structures. The ability of internal forces to vary in magnitude presents many new potential equilibrium states for masonry domes. The range of values in which meridional and hoop forces can attain, and corresponding thrust line shapes, should be validated in additional empirical tests, perhaps involving dry-constructed domes and adaptable support conditions. With the basic methodology already programmed, one may naturally extend the modified thrust line program to analyze domes with varying thickness, surcharge loads, asymmetrical loads and geometry, voussoir divisions, and thrust line tolerances to dome surfaces. In addition, one should incorporate checks on limits to equilibrium due to the ability or inability of friction in the masonry to prevent sliding failure of the voussoirs.

The stability of the support structure of Farag Ibn Barquq remains unanswered. One may continue this investigation by verifying the surcharge loads at the crown, the material weights of the dome and drum masonry, and the impacts on thrust line geometry. Additional field work may be conducted to confirm or refute the presence of tensile reinforcement in the drum.

Finally, one may continue to study the potential of the modified thrust line method in predicting upper bound limits of masonry domes. Future considerations may include the relation between bending and direct tensile force development in the dome, the behavior of real-scale masonry domes, among other factors. A great deal of work remains in applying this new method to existing masonry domes to gain an improved understanding of their relative stability.

7.2. Thesis Summary

In this thesis, the author introduced the modified thrust line analysis as a method by which to assess the equilibrium of masonry domes. This method was used to identify the minimum thrusts of spherical and pointed dome geometries, which have many relevant applications in design, analysis, and preservation. Using interactive geometry software, the author also automated graphical analysis methods to output solutions in real-time, expediting the traditionally laborious process. These methods have the potential to unveil a wide range of information on the structural abilities of masonry domes.

References

Ameida, J. C., Lourenço, P. B., & Barros, J. A. 2002. Characterization of brick and brick-mortar interface under uniaxial tension. In Santos, F., et al., (Eds.), *Proceedings of the 7th International Seminar on Structural Masonry*, pp. 67-76. Belo Horizonte, Brasil: Centro Federal de Educaçâo Tecnològica de Minas Gerais.

American Society for Testing and Materials. 2005. Standard Test Methods for Sampling and Testing Brick and Structural Clay Tile (ASTM C67-03a). *Annual Book of ASTM Standards*, *04.05.* West Conshohocken, PA: ASTM International.

Anselmi, C., De Roas, E., & Fino. L. Limit analysis of masonry structures. In Lourenço, P. B. and Roca, P. (Eds.), *Historical Constructions: Proceedings of the 3rd International Seminar*, pp. 545-550. Guimarães, Portugal: University of Minho.

Billington, D. P. 1982. *Thin shell concrete structures.* New York: McGraw-Hill Book Co.

Cipriani, B. 2005. *Development of Construction Techniques in the Mamluk Domes of Cairo* [Master's Thesis]. Cambridge, MA: Massachusetts Institute of Technology.

Cipriani, B., & Lau, W. W., 2006. Construction techniques in medieval Cairo: The domes of Mamluk mausolea. In Dunkeld, M., Campbell, J. W., Louw, H., Tutton, M., Addis, B., & Thorne, R. (Eds.), *Proceedings of the Second International Congress on Construction History*, *2*, pp. 695-716. Exeter, U.K.: Short Run Press.

Crave Services. No date. Gol Gumbaz. *Mohan's Holiday Pictures*. Retrieved from: http://www.craveservices.com/photos/index.htm?bijapur.htm&right.

Creswell, K.A.C. 1959. The Muslim architecture of Egypt. Oxford: Clarendon Press.

D'Ayala, D, 2001. Limit state analysis of hemispherical domes with finite friction. In Lourenço, P. B. and Roca, P. (Eds.), *Historical Constructions: Proceedings of the 3rd International Seminar*, pp. 617-626. Guimarães, Portugal: University of Minho.

Dunn, W. 1904. Notes on the stresses in framed spires and domes. *J. Royal Institute of British Architects, 11*, 63-73, 108-112.

Dunn, W. 1908. The principles of dome construction: I and II. *J. Royal Institute of British Architects, 23*, 401-412.

Eddy, H. T. 1877. *New constructions in graphical statics*. New York: D. Van Nostrand.

Farshad, M. 1992. *Design and analysis of shell structures.* Netherlands: Kluwer Academic Publishers.

Hanser, D. 2003. Minoan Society. In *Arch 2003: Architecture and Society*. Retrieved from http://hanser.ceat.okstate.edu/2003/new%20pages%2001/2003mt8sldb.htm.

Heyman, J. 1977. *Equilibrium of shell structures*. Oxford: Oxford University Press.

Heyman, J. 1982. *The masonry arch*. West Sussex, England: Ellis Horwood Limited.

Heyman, J. 1995. *The stone skeleton*. Cambridge: Cambridge University Press.

Heyman, J. 1996. *Arches, vaults and buttresses*. Hampshire, Great Britain: Variorum.

Hodge, Jr., P.G., & Lakshmikantham, C. 1963. Limit analysis of shallow shells of revolution. *J. Applied Mechanics: Series E, 30*(2), 215-218.

Huerta, S. 2003. The mechanics of timbrel vaults: A historical outline. In A. Becchi (Ed.) *Essays on the History of Mechanics*, pp. 89-133. Boston: Birkhauser Verlag.

Kessler, C. 1976. The carved masonry domes of medieval Cairo [AARP/Art and Archaeology Research Papers]. Cairo: The American University in Cairo Press.

Lévy, M. 1888. *La statique graphique et ses applications aux constructions*, *IV Partie*. Paris: Gautheir-Villars, Imprimeur-Libraire.

Livsley, R. K. 1992. A computational model for the limit analysis of three-dimensional masonry structures. *Meccanica, 27*, 161-172.

Melaragno, M. 1991. *An introduction to shell structures: The art and science of vaulting*. New York: Van Nostrand Reinhold.

Ochsendorf, J. A., Ramage, M. H., & Lau, W. W. 2005. The Calyx domes: Structural design and analysis [Report]. Cambridge, MA: Massachusetts Institute of Technology.

O'Dwyer, D. 1999. Funicular analysis of masonry vaults. *Computers & Structures, 73*, pp. 187-197.

Oppenheim, I. J., Gunaratnam, D. J., & Allen, R. H. 1989. Limit state analysis of masonry domes. *Journal of Structural Engineering, 115*, 868-882.

Paradiso, M., Rapallini, M., & Tempesta, G. Masonry domes. Comparison between some solutions under no-tension hypothesis. In *Proceedings of the First International Congress on Construction History*, pp. 1571-1581. Madrid: Instituto Juan de Herrera, Escuela Técnica Superior de Arquitectura.

Parker, D. 2005, Sept. 8. New age thinking. *New Civil Engineer*, pp. 16-17.

Peña, F. 2005. Correlation between tensile strength and the collapse mechanism of brick masonry constructions. In C. Modena, P. B. Lourenco & P. Roca (Eds.), *Structural Analysis of Historical Constructions, 2,* pp. 1165-1174. London: A.A. Balkema Publishers.

Rankine, W. J. M. 1904. *A manual of applied mechanics.* 17th ed. London: C. Griffin and Co., Ltd.

Robison, E. C. 1988. St. Peter's dome: The Michelangelo and Della Porta designs. In *Domes from Antiquity to Present: Proceedings of the IASS – MSU International Symposium*. Istanbul: Mimar Sinan University, pp. 253-260.

Save, M. A., Massonnet, C. E., & de Saxce, G. 1997. *Plastic limit analysis of plates, shells and disks.* Amsterdam: Elsevier Science.

Schwedler, J. W. 1851. *Theorie der Brückenbalkensysteme*. In *Zeitschrift für Bauwesen*, *1*, pp. 114-123, 162-173, 265-278.

St. James Cathedral. 2006. The Great Dome. In *Centennial of St. James Cathedral Parish*. Retrieved on May 23, 2006 from http://www.stjames-cathedral.org/main.htm.

TruStone America. 2005. *Physical properties*. Retrieved April 20, 2006, from http://www.trustoneamerica.com/properties.html.

UK sees its first use of Guastavino vaulting. 2005, August 9. *New Civil Engineer*, p. 12.

United States Gypsum Company. 1997. *Industrial plasters and gypsum cements: versatile products for countless industrial applications* [Brochure]. Chicago, Illinois.

Walling, Dianne. 2006. Module 4: The Aegean World. In *Art 100: History and Appreciation of Art.* Retrieved from http://mil.ccc.cccd.edu/classes/art100/module4.htm.

Square-cube law. 2006, March 8. In *Wikipedia, The Free Encyclopedia*. Retrieved May 23, 2006, from http://en.wikipedia.org/w/index.php?title=Square-cube_law&oldid=42835343.

Wolfe, W. S. 1921. *Graphical Analysis: A text book on graphic statics*, New York: McGraw-Hill Book Co., pp. 250-253.

Parameter Definitions

a, a	Median radius of curvature
C	Constant
c	Minimum horizontal thrust-to-weight ratio, H/W
e	Eccentricity, or the distance between the thrust line path and the neutral axis or median radius of the dome
H	Horizontal thrust, in units of force
H_i	Hoop force resultant at voussoir i, in units of force
H_{net}, H_{total}	Total horizontal thrust of the dome, or lune, at the base and at the crown
H/W	Minimum thrust-to-weight ratio for the lune or dome portion under study
h	Horizontal thrust, in units of force per length
h_i	In force polygon, cumulative thrust in voussoir i, in units of force
$height_{wall}$	Height of the support wall between the extrados and intrados of the dome
i	Counting variable in series
j	Counting variable in series
k	Ratio of the median rise of a dome to the vertical distance to the final thrust line point in the dome
M_i	Meridional force resultant at voussoir i, in units of force
MOR	Modulus of rupture
N_φ, N_ϕ	Internal meridional stress resultant, in units of force per length
N_θ, N_θ	Internal hoop force resultant, in units of force per length
n	Final counting variable or total number of objects in a series

n.a.	Neutral axis
r	The radius of curvature of the dome's extrados: the sum of the median radius of curvature and half the effective thickness of the dome
r'	The radius of curvature of the dome's intrados: the difference between the median radius of curvature and half the effective thickness of the dome
t	One-half the effective thickness of a dome section
t_{wall}	Thickness of the support structure wall under the dome
t/R	Ratio of the total effective thickness to the radius of curvature
W, W_n, W_θ	Total weight of the lune under study, which is equal to the cumulative weight from crown to voussoir n, or the sum of the weights of smaller lunes comprising the lune
W_{dome}	Weight of the dome under study, with a plan angle of 360 degrees
W_{wall}	Weight of the wall segment with a plan angle equal to θ of the dome portion under study
W_i	Cumulative weight of lune from crown to voussoir i
w, w_i	Self-weight, in units of force per area in context of membrane theory; otherwise, self-weight of an individual component in units of force
x	Coordinate with reference to the orientation of the x-axis; with reference to force polygon, the n^{th} letter of the alphabet where n is the total number of voussoirs
x_{cg} , x_{cg_i}	Horizontal distance between the center of curvature and the center of gravity of a lune or a voussoir i
$x_{cg\,lune}$	Horizontal distance between the center of curvature and the center of gravity of a lune
x_e , x_{e_i}	Horizontal distance between a reference origin and a point on the extrados, which may align with the centroid of voussoir i
$x_{ext.wall}$	Horizontal distance between a reference origin and the exterior face of a support structure

x_i, x_{i_i}	Horizontal distance between a reference origin and a point on the intrados, which may align with the centroid of voussoir *i*
x_{TL}, x_{TL_i}	Horizontal coordinate of the thrust line relative to a reference origin for voussoir *i*, or the i^{th} *x*-coordinate of the thrust line
y	Coordinate with reference to the orientation of the *y*-axis
y_{exit}	Vertical coordinate of the thrust line relative to a reference origin at where a thrust line exits a support structure under a dome
y_{TL}, y_{TL_i}	Vertical coordinate of the thrust line relative to a reference origin for voussoir *i*, or the i^{th} *y*-coordinate of the thrust line
α	Angle of embrace, or the maximum φ from the dome's centerline to bottom edge
β	Angle from the dome's centerline to the top face of a voussoir
γ, γ	Angle from the dome's centerline to the bottom face of a voussoir
δ	Angle from the dome's centerline at which the arc of a pointed dome begins
δ_{max}	Maximum angle from the dome's centerline at which the arc of a pointed dome begins
ρ	Material unit weight in units of force per volume
σ_H	Hoop stress
σ_M	Meridional stress
σ_r	Flexural tensile stress or average modulus of radius
$\sigma_{tensile}$	Tensile stress
φ, ϕ, ϕ_i	Angle with respect to the dome's centerline or vertical axis of rotation
θ	Angle of a dome portion or lune viewed in plan
θ'	Angle in plan of an individual lune comprising a larger lune or dome

Appendices

Appendix A. The Membrane Theory

The membrane theory equations are derived by considering equilibrium of either an infinitesimal element of the dome, or equilibrium of the entire dome structure. Using the former approach, consider an element in an axisymmetrical loaded spherical dome that is defined by two adjacent hoop rings and two adjacent meridians (Fig. A.1) (Heyman 1977).

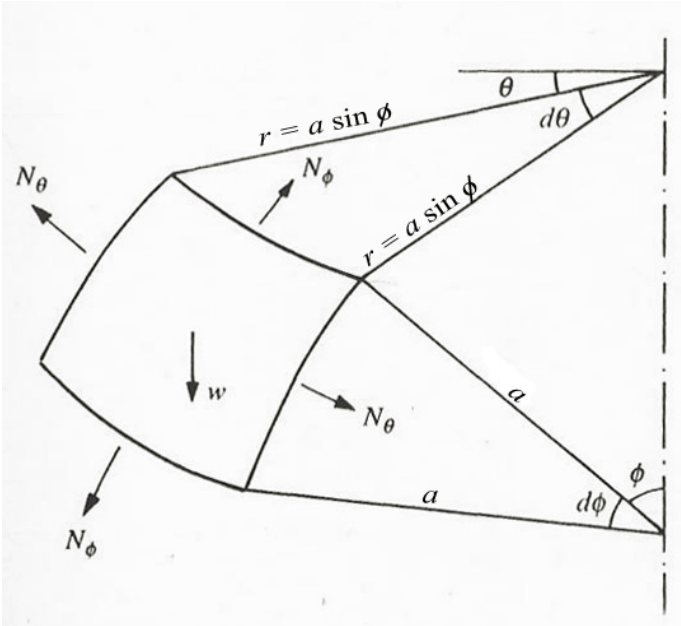

Figure A.1. The membrane theory considers equilibrium of an infinitely small particle located on the median radius of a dome (modified from Heyman 1977).

The meridional force resultant, N_φ, and the radius in plan, $a\sin\phi$, increase with respect to φ by a value of $\frac{d}{d\phi}N_\phi r\, d\theta d\phi$. Hoop forces are coplanar and perpendicular to the element's edges.

Resolving forces into normal and tangential components with respect to the element, equilibrium equations may be written for the element (Heyman 1977):

In the tangential direction:

$$\frac{d}{d\phi}\left(N_\phi r\right)d\theta\, d\phi - N_\theta\, a\, d\phi\, d\theta\, \cos\phi = -w\, r\, d\theta\, a\, d\phi \sin\phi$$

Substitute $a\sin\phi$ for r:

$$\frac{d}{d\phi}\left(N_\phi \sin\phi\right) - N_\theta \cos\phi = -w a \sin^2\phi \qquad \text{(A.1.)}$$

In the normal direction:

$$\left(N_\phi \, r \, d\theta\right) d\phi + N_\phi \, a \, d\phi \, d\theta \sin\phi = -w \, r \, d\theta \, a \, d\phi \cos\phi$$

Substitute $a \sin\phi$ for *r*:

$$N_\phi + N_\theta = -w a \cos\phi \qquad \text{(A.2.)}$$

In the θ direction, an identity is obtained due to the axisymmetrical geometry. Using Eqs. A.1 and A.2 to solve for N_φ:

$$N_\phi = -\frac{w a \left(\cos\phi + C\right)}{\sin^2\phi}$$

When $\varphi = 0°$, the constant of integration must equal -1 for N_φ to remain finite. Thus, the meridional stress resultant is found by:

$$N_\phi = -\frac{w a}{1 + \cos\phi} \qquad \text{(A.3.)}$$

From Eq. A.2, the hoop stress resultant, N_θ, is found by:

$$N_\theta = w a \left[\frac{1}{1 + \cos\theta} - \cos\phi\right] \qquad \text{(A.4.)}$$

A similar procedure may be used to derive the membrane theory equations for pointed domes (Billington 1982).

Appendix B. Modified Thrust Line Method for Spherical Domes

This appendix contains the program the author wrote and used to conduct the theoretical analyses for spherical domes. The program was written for *Visual Basic for Application with Excel*, *version 6.3*, by Microsoft Corporation. The author wrote a similar program for the analysis of pointed domes.

```
Option Explicit

Private Sub cmdButtonActivate_Click()

    Dim i As Integer                                        'i is the trial number from 1 to 30

    For i = 1 To 30
        If (i = 1 Or i = 11 Or i = 21) Then                 'User must input initial row of parameters
            Call SetUpInitialParameters(i)
        Else
            Call ChangeParameters(i)
        End If
        Cells(SHROW + i, "A") = i                           'List trial number
        Call AddAnalysisSheet(i)
        FormatCellsHeadings                                 'Alignment and headings in place
        Call NumberVousColumn(i)
        DomeDefine
        Call AddChartSheet(i)         'Plot coordinates of the dome extrados and intrados -- add thrust
line later
        DetermineYLimits
        Call CalcWeight(i)
        Call StartThrustLine(i)
        Call CalcInternalForces(i)
    Next i

End Sub

Private Sub cmdButtonReset_Click()
'Erase analyses and clear parameter data

    Dim i As Integer
    Dim data As Range

    For i = 1 To 30
        Sheets("Analysis" & i).Delete
        Charts("Section" & i).Delete
        Sheets("IntForces" & i).Delete
    Next i

    Set data = Sheets("Summary").Range("A6:N100")
    data.ClearContents
```

```
End Sub

Private Sub cmdButtonSummary_Click()

    Dim SHROW As Integer
    Dim tRValue As Single

    SHROW = 5
    tRValue = Range("D6").Value

    Sheets("Summary").Select
    Cells(SHROW + 1, "A").Select
    Selection.EntireRow.Insert
    Selection.EntireRow.Interior.ColorIndex = 35
    Selection.EntireRow.Interior.Pattern = xlSolid
    Cells(SHROW + 1, "E").FormulaR1C1 = "0"
    Cells(SHROW + 1, "K").FormulaR1C1 = "0"
    Cells(SHROW + 1, "I").FormulaR1C1 = "0"
    Cells(SHROW + 1, "L").FormulaR1C1 = "0"
    Cells(SHROW + 12, "A").Select
    Selection.EntireRow.Insert
    Cells(SHROW + 23, "A").Select
    Selection.EntireRow.Insert
    Cells(SHROW + 1, "A").Select
    Selection.EntireRow.Copy
    Cells(SHROW + 12, "A").Select
    ActiveSheet.Paste
    Cells(SHROW + 23, "A").Select
    ActiveSheet.Paste
    Application.CutCopyMode = False
    Charts.Add
    With ActiveChart
        .ChartType = xlXYScatterSmooth
        .SeriesCollection.NewSeries
        .SeriesCollection(1).Name = "=""Theta = 1 deg.; Zero Hoop Forces"""
        .SeriesCollection(1).XValues = "=Summary!R6C5:R16C5"
        .SeriesCollection(1).Values = "=Summary!R6C9:R16C9"
        .SeriesCollection.NewSeries
        .SeriesCollection(2).Name = "=""Theta = 22.5 deg.; Zero Hoop Forces"""
        .SeriesCollection(2).XValues = "=Summary!R17C5:R27C5"
```

```
    .SeriesCollection(2).Values = "=Summary!R17C9:R27C9"
    .SeriesCollection.NewSeries
    .SeriesCollection(3).Name = "=""Theta = 45 deg.; Zero Hoop Forces"""
    .SeriesCollection(3).XValues = "=Summary!R28C5:R38C5"
    .SeriesCollection(3).Values = "=Summary!R28C9:R38C9"
    .SeriesCollection.NewSeries
    .SeriesCollection(4).Name = "=""Theta = 1 deg.; With Hoop Forces"""
    .SeriesCollection(4).XValues = "=Summary!R6C5:R16C5"
    .SeriesCollection(4).Values = "=Summary!R6C11:R16C11"
    .SeriesCollection.NewSeries
    .SeriesCollection(5).Name = "=""Theta = 22.5 deg.; With Hoop Forces"""
    .SeriesCollection(5).XValues = "=Summary!R17C5:R27C5"
    .SeriesCollection(5).Values = "=Summary!R17C11:R27C11"
    .SeriesCollection(6).Name = "=""Theta = 45 deg.; With Hoop Forces"""
    .SeriesCollection(6).XValues = "=Summary!R28C5:R38C5"
    .SeriesCollection(6).Values = "=Summary!R28C11:R38C11"
    .Location Where:=xlLocationAsNewSheet, Name:="Summary Chart"
End With
With ActiveChart
    .HasTitle = True
    .ChartTitle.Characters.Text = "Minimum Horizontal Thrust for t/R = " & tRValue
    .Axes(xlCategory, xlPrimary).HasTitle = True
    .Axes(xlCategory, xlPrimary).AxisTitle.Characters.Text = "Angle of Embrace (degrees)"
    .Axes(xlValue, xlPrimary).HasTitle = True
    .Axes(xlValue, xlPrimary).AxisTitle.Characters.Text = "Horizontal Thrust/Weight per Lune"
    .HasLegend = True
    .Legend.Select
    With Selection
        .Position = xlBottom
        .Border.LineStyle = xlNone
        .Width = 750
        .Left = 50
    End With
    .Axes(xlCategory).Select
    With Selection
        .MinorTickMark = xlOutside
        .MinimumScale = 0
        .MaximumScale = 90
        .MinorUnit = 5
        .MajorUnitIsAuto = True
    End With
```

```
    End With
    ActiveChart.PlotArea.Select
    Selection.Interior.ColorIndex = xlNone
    ActiveChart.SeriesCollection(4).Select
    With Selection
        .Border.ColorIndex = 43
        .MarkerForegroundColorIndex = 43
        .MarkerStyle = xlX
        .Smooth = True
        .MarkerSize = 5
    End With
    ActiveChart.SeriesCollection(3).Select
    With Selection
        .Border.ColorIndex = 45
        .MarkerBackgroundColorIndex = 45
        .MarkerForegroundColorIndex = 45
        .MarkerStyle = xlTriangle
        .Smooth = True
        .MarkerSize = 5
    End With

End Sub

Option Explicit

Public a As Single          'median radius of curvature in ft
Public t As Single          'half of the thickness in ft
Public tR As Single         'The thickness to radius of curvature ratio
Public alpha As Single      'Angle of embrace between 0 and 90 degrees
Public rho As Single        'material unit weight in lbs/ft^3
Public theta As Single      'Included angle in plan so arc length of base included = 1 ft
Public maxCS As Single      'Maximum compression stress in units of psi
Public numVous As Integer   'Number of voussoirs equal to alpha in degrees
Public vousAngle As Single  'The number of radians per voussoir division of the dome section
Public vousPhi() As Single  'The value of phi in radians for the bottom face of each voussoir i
Public r As Single          'The radius to the extrados: r = a + t
Public rPrime As Single     'The radius to the intrados: r = a - t
Private theta1, theta2 As Single        'Three values of theta in plan will be analyzed
Private theta3 As Single        'Theta values in degrees

Const PI = 3.141593
```

```
Public SHROW, AHROW As Integer     'The number of rows by which to offset worksheet "Summary"
                                   'The number of rows by which to offset worksheets "Analysis#" and
"IntForces#"
Public moveStartTolerance As Single     'The increment by which to increase the start point of the thrust
line
Public initTLTolerance As Single        'The closest distance (ft) to which the thrust line can approach
the extrados _
                                           can increase or decrease

Public Sub SetUpInitialParameters(initTrial As Integer)
'Augment so that 30 trials are run with varying theta from theta = 1, 22.5 and 45 degrees

    Dim i As Integer
    Dim initAlpha As Single     'Let the first alpha value = 5 deg.
    initAlpha = 5               'Arbitrary

    'Set the theta in plan values (in degrees); arbitrarily assigned
    theta1 = 1
    theta2 = 22.5
    theta3 = 45

    'Set up the header rows
    SHROW = 5
    AHROW = 8

    Sheets("Summary").Select
    rho = Range("B4").Value
    maxCS = (Range("D4").Value) * 144    'Convert psi into psf
    a = Range("B6").Value
    tR = Range("D6").Value
    t = a * tR / 2
    Range("C6").Value = 2 * t
    r = a + t
    rPrime = a - t

    moveStartTolerance = Range("F4").Value                  'Set the increment by which the start point
moves
    initTLTolerance = Range("H4").Value                     'Set initial thrust line tolerance

    Cells(SHROW + initTrial, "E").Value = initAlpha  'For trials 1, 11 and 21, alpha will be 5 degrees
    alpha = Application.WorksheetFunction.Radians(Cells(SHROW + initTrial, "E").Value)
```

```
    Select Case initTrial
        Case Is = 1
            Cells(SHROW + initTrial, "F").Value = theta1
        Case Is = 11
            Cells(SHROW + initTrial, "F").Value = theta2
        Case Is = 21
            Cells(SHROW + initTrial, "F").Value = theta3
    End Select

    theta = Application.WorksheetFunction.Radians(Cells(SHROW + initTrial, "F").Value)

    'Fill in the a, thickness, and tR values for rows 11 and 21
    If (initTrial <> 1) Then
        For i = 2 To 4
            Cells(SHROW + initTrial, i).Value = Cells(SHROW + 1, i).Value
        Next i
    End If

End Sub

Public Sub ChangeParameters(trial As Integer)
'Need to write procedure to increment parameter in question
'Work with varying alpha and theta

    Dim alpInc1 As Integer
    Dim alpinc2 As Integer

    alpInc1 = 5                 'increment alpha either 5 degrees
    alpinc2 = 10                'increment alpha by 10 degree intervals

    Sheets("Summary").Select
    Cells(SHROW + trial, "B").Value = Cells(SHROW + 1, "B").Value       'the radius of curvature will not
change from a
    Cells(SHROW + trial, "C").Value = Cells(SHROW + 1, "C").Value       'the thickness of the dome will not
change from 2t
    r = a + t                                                           'outer and inner radii do not
change
    rPrime = a - t
    Cells(SHROW + trial, "D").Value = 2 * t / a                         'the thickness to radius ratio
```

```
    'Vary the alpha value in degrees
    If (trial = 2 Or trial = 12 Or trial = 22) Then
        Cells(SHROW + trial, "E").FormulaR1C1 = ("=R[-1]C+" & alpInc1)
    Else
        Cells(SHROW + trial, "E").FormulaR1C1 = ("=R[-1]C+" & alpinc2)
    End If

    alpha = Application.WorksheetFunction.Radians(Cells(SHROW + trial, "E").Value)  'reset the alpha
variable

    'Vary theta
    Select Case trial
        Case Is < 11
            Cells(SHROW + trial, "F").Value = theta1
        Case 11 To 20
            Cells(SHROW + trial, "F").Value = theta2
        Case Is > 21
            Cells(SHROW + trial, "F").Value = theta3
    End Select

    theta = Application.WorksheetFunction.Radians(Cells(SHROW + trial, "F").Value)

End Sub

Public Sub AddAnalysisSheet(trial As Integer)

    Sheets("Summary").Select
    Sheets.Add
    With ActiveSheet
        .Move After:=Sheets("Summary")
        .Name = "Analysis" & trial
        .Move After:=Sheets("Summary")       'Worksheets class does not include Chart sheets
        .Select
    End With

End Sub

Public Sub FormatCellsHeadings()
    Cells.HorizontalAlignment = xlCenter
    Cells.VerticalAlignment = xlCenter
    Range("A1").Value = "Modified Thrust Line Analysis for Masonry Domes"
```

```
    Range("A2").Value = "Radius of Curvature (ft):"
    Range("A3").Value = "Angle of Embrace (deg.):"
    Range("A4").Value = "Thickness (ft):"
    Range("A5").Value = "Material Unit Weight (lbs/ft^3):"
    Range("A6").Value = "Theta (deg.):"
    Range("D2").Value = "Max. Stress (psi):"
    Range("D3").Value = "Thrust Line Tol. (ft):"
    Range("A1:E7").Font.Bold = True
    Range("A1").HorizontalAlignment = xlLeft
    With Range("A2:A6, D2:D6")
        .Columns.AutoFit
        .HorizontalAlignment = xlRight
    End With
    Range("A7").Value = "Phi(degrees)"
    Range("B7").Value = "X extrados (ft)"
    Range("C7").Value = "Y extrados (ft)"
    Range("D7").Value = "X intrados (ft)"
    Range("E7").Value = "Y intrados (ft)"
    Range("F7").Value = "X CG & TL (ft)"
    Range("G7").Value = "Y CgE (ft)"
    Range("H7").Value = "Y TL (ft)"
    Range(" I7").Value = "Y CgI (ft)"
    Range("J7").Value = "Horiz. Dist HT(lbs)"
    With Range("B7:J7")
        .WrapText = True
        .ColumnWidth = "10"
        .Font.Bold = True
    End With
    Range("B2:B6").NumberFormat = "0.0"
    Cells(AHROW, 1).Select
    ActiveWindow.FreezePanes = True

End Sub

Public Sub ListParameters(trial As Integer)
'List parameters in individual "Analysis" spreadsheets

    Sheets("Analysis" & trial).Select
    Range("B2").Value = a
    Range("B3").Value = Application.WorksheetFunction.Degrees(alpha)
    Range("B4").Value = t * 2
```

```
    Range("B5").Value = rho
    Range("B6").Value = Application.WorksheetFunction.Degrees(theta)
    Range("E2").Value = maxCS / 144     'Convert psf to psi
    Range("E3").Value = tLTolerance

End Sub

Public Sub NumberVousColumn(trial As Integer)
'Determine the array size for the number of voussoirs and subsequent parameters.
'Establish vousPhi values, the phi value in radians of the bottom face of each voussoir

    Dim i As Integer
    Dim tempAlphaDeg As Integer

'For processing time's sake, limit the max. number of voussoirs to 30; _
numVous can be, and should be, INCREASED for greater accuracy

    tempAlphaDeg = Round(Application.WorksheetFunction.Degrees(alpha))
    numVous = Application.WorksheetFunction.Max(30, tempAlphaDeg)

    ReDim vousPhi(numVous)
    vousAngle = alpha / numVous     'Calculate vousAngle: the number of radians per voussoir

    For i = 0 To numVous
        vousPhi(i) = i * vousAngle
        Cells(i + AHROW, "A").Value = Application.WorksheetFunction.Degrees(vousPhi(i))
    Next

    Range("A" & AHROW & ":A" & (AHROW + numVous)).NumberFormat = "0.0"

End Sub

Public Sub AddIntForceSheet(trial As Integer)
    Worksheets.Add
    With ActiveSheet
        .Move After:=Sheets("Analysis" & trial)
        .Name = "IntForces" & trial
        Cells.HorizontalAlignment = xlCenter
        Cells.VerticalAlignment = xlCenter
        Range("A1:A7").Font.Bold = True
        Range("A1").HorizontalAlignment = xlLeft
```

```
        Range("A1").Value = "Modified Thrust Line Analysis for Masonry Domes (continued)"
        Range("A3").Value = "Weight of One Lune (lbs):"
        Range("A4").Value = "Total Weight of Dome (ft):"
        Range("A3:A4").ColumnWidth = 24
        Range("C4").Value = "should equal"
        Range("A7").Value = "Phi (degrees)"
        Range("B7").Value = "Meridional Force (lbs)"
        Range("C7").Value = "Hoop Force (lbs)"
        Range("D7").Value = "Meridional Stress (psi)"
        Range("E7").Value = "Hoop Stress (psi)"
        With Range("B7:F7")
            .Font.Bold = True
            .WrapText = True
            .ColumnWidth = 12
        End With
        Range("A" & AHROW & ":E" & numVous + AHROW).NumberFormat = "0.0"
    End With

End Sub

Option Explicit
Const PI = 3.141593
Public beta As Single                       'The upper bound phi angle defining the voussoir
Public gamma As Single                      'The lower bound phi angle defining the voussoir
Public xE() As Single, yE() As Single       'Determine the coordinates of the dome extrados
Public xI() As Single, yI() As Single       'Determine the coordinates of the dome intrados
Public xCg() As Single                      'Determine the x-coordinate of the center of gravity; y-
coordinate not needed
Public w() As Single                        'Determine the cumulative weights of voussoirs
Public phiCgE() As Single, phiCgI() As Single   'The phi angle on the extrados/intrados with the xCg(i)
coordinate
Public yCgE() As Single, yCgI() As Single       'The y-coordinates on the extrados/intrados with the xCg(i)
coordinate
Public xCGLune As Single                    'The x-coordinate center of gravity of one lune
Public hMax() As Single                     'The max. horiz. component of force on the force polygon for
each voussoir

Public Sub DomeDefine()
    Dim i As Integer
    Dim vousWt As Single                    'Wt of individual voussoir to be added to growing weight
    Dim phi As Single                       'Average phi angle to send to functions GetMaxHDist
```

```
    Dim tempH As Single                     'the previous value of maximum horizontal distance
    Dim tempPhi0 As Single                  'the angle of the oculus, as applicable; for now, set equal to
zero
    ReDim xE(numVous), yE(numVous)          'Redimension arrays to the number of included degrees
    ReDim xI(numVous), yI(numVous)
    ReDim xCg(numVous), w(numVous)          'w is the cumulative weight along each voussoir
    ReDim hMax(numVous)                     'hMax is the total horizontal distance on the force polygon
'Locate the coordinates defining the dome center of gravity, wt. of ea. voussoir, and _
 call a function to get maximum horizontal distance
    For i = 0 To numVous
        Call DefineExtraIntra(i)    'Locate the coordinates defining the dome extrados and intrados
        If i <> 0 Then
            beta = vousPhi(i) - vousAngle               'beta is the upper phi-angle from the centerline
            gamma = vousPhi(i)                          'gamma is the lower phi-angle from the dome
centerline
            phi = (beta + gamma) / 2                    'average of beta and gamma in radians
            xCg(i) = (3 / 16) * (r ^ 4 - rPrime ^ 4) / (r ^ 3 - rPrime ^ 3) * (2 * gamma - Sin(2 * gamma) -
2 * beta + _
                     Sin(2 * beta)) / (Cos(beta) - Cos(gamma)) * Sin(theta / 2) / (theta / 2)
            vousWt = (Cos(beta) - Cos(gamma)) * rho * (r ^ 3 - rPrime ^ 3) / 3 * theta
            w(i) = w(i - 1) + vousWt
            If i = 1 Then
                tempH = 0
            Else
                tempH = hMax(i - 1)
            End If
            hMax(i) = GetMaxHDistance(w(i), phi, tempH)

        End If
    Next

    tempPhi0 = 0
    xCGLune = (3 / 16) * (r ^ 4 - rPrime ^ 4) / (r ^ 3 - rPrime ^ 3) * (2 * alpha - Sin(2 * alpha) - 2 *
tempPhi0 + _
                     Sin(2 * tempPhi0)) / (Cos(tempPhi0) - Cos(alpha)) * Sin(theta / 2) / (theta / 2)

End Sub

Public Sub DefineExtraIntra(i As Integer)
'Define the extrados and intrados coordinates of the dome section
        xE(i) = (a + t) * Sin(vousPhi(i))
```

```
        Cells(i + AHROW, "B").Value = xE(i)
        yE(i) = (a + t) * Cos(vousPhi(i))
        Cells(i + AHROW, "C").Value = yE(i)
        xI(i) = (a - t) * Sin(vousPhi(i))
        Cells(i + AHROW, "D").Value = xI(i)
        yI(i) = (a - t) * Cos(vousPhi(i))
        Cells(i + AHROW, "E").Value = yI(i)
End Sub

Public Function GetMaxHDistance(ByVal tempWt As Single, phi As Single, tempH As Single) As Single
'Determine the maximum horizontal distance (hoop compression) and meridional force to set limits based on
material strength
'This function is in a loop, so values are constantly replaced
'Material stresses are in general very low, and will not be approached in the solution; perhaps this
function is unnecessary

    Dim htMaxMerid As Single    'the max. horizontal thrust distance determined by meridional stress
    Dim htMaxHoop As Single     'the max. horizontal thrust distance determined by hoop stress
    Dim mM As Single            'the maximum meridional force in units of lbs
    Dim mH As Single            'the maximum hoop force in units of lbs
    Dim maxHTDist As Single     'the maximum horizontal distance on the force polygon

    mM = maxCS * a * theta * Sin(phi) * 2 * t    'compression stress times the voussoir area in section
taken through center _
                                                    of curvature of dome; theta varies with phi
    htMaxMerid = (mM ^ 2 - tempWt ^ 2) ^ 0.5     'the max horizontal thrust distance based on meridional
stress _
                                                 this function assumes that max merid will be > tempWt
based on material limits
    mH = maxCS * 2 * t * a * vousAngle          'compression stress times the voussoir area in section
where dPhi = alpha/numV
    htMaxHoop = 2 * Sin(theta / 2) * mH + tempH  'the max horiz. thrust dist. based on hoop stress added to
previous hMax value

    If htMaxMerid < htMaxHoop Then              'Use the more conservative value of horizontal distance on
force polygon
        maxHTDist = htMaxMerid
    Else
        maxHTDist = htMaxHoop
    End If
```

```
    GetMaxHDistance = maxHTDist

End Function

Public Sub DetermineYLimits()
'Determine the max/min y of the thrust line coordinates at x = xCg(i)
    Dim i As Integer
    ReDim yCgE(numVous), yCgI(numVous)
    ReDim phiCgE(numVous), phiCgI(numVous)

    'For i = zero on the dome centerline, yCge and yCgi are on the dome's extrados/intrados
    yCgE(0) = a + t
    yCgI(0) = a - t

    For i = 1 To numVous
        If (xCg(i) <= (a - t) * Sin(alpha)) Then
            phiCgE(i) = Application.WorksheetFunction.Asin(xCg(i) / (a + t))    'find the phi at x = xCg
and y on intra/extrados
            phiCgI(i) = Application.WorksheetFunction.Asin(xCg(i) / (a - t))
            yCgE(i) = (a + t) * Cos(phiCgE(i))                                  'find the y-coordinate
limits
            yCgI(i) = (a - t) * Cos(phiCgI(i))
        Else                                                                    'for more complete domes
where xCg passes the base of the dome
            phiCgE(i) = Application.WorksheetFunction.Asin(xCg(i) / (a + t))    'find the phi at x = xCg
and y on intra/extrados
            yCgE(i) = (a + t) * Cos(phiCgE(i))                                  'find the y-coordinate
upper limit
            phiCgI(i) = alpha
            yCgI(i) = xCg(i) / Tan(phiCgI(i))
        End If
    Next

End Sub

Option Explicit
    Public tLTolerance As Single                    'Dynamic thrust line tolerance to dome surfaces
    Public xTL() As Single, yTL() As Single         'Thrust line coordinates
    Public m() As Single                            'Slope of thrust line segment and meridional segment on
forcePolygon
```

```
    Public hT() As Long, hNet() As Single           'hT = Dynamic horiz. distance on force polygon
representing cumul. _
                                                    horizontal thrust hNet = difference between hT(i) and
ht(i-1)
    Public finalCheck As Boolean                    'Final yTLValues are satisfied; all checks are
satisfied
    Const PI = 3.141593

Public Sub StartThrustLine(trial As Integer)                'Draw the thrust line with calls to various
values
    Dim i As Integer                                        'i is the voussoir level
    ReDim xTL(numVous + 1), yTL(numVous + 1)
    ReDim m(numVous)
    ReDim hT(numVous), hNet(numVous)

    Sheets("Analysis" & trial).Select

    i = 1
    Call StartPoint(i)
    ListKnownCoordinates                    'List known coordinates: extrados, intrados, xCenterGravity,
yCgE and yCgI

    For i = 1 To numVous
        xTL(i) = xCg(i)                     'X-coordinates of line of thrust will always coincide with
centers of gravity
    Next i

    Call DetermineHTLimits(yTL(0))


'if the previous two zero hoop analyses for alpha > 5 deg. did not find a solution, then jump to next theta
iteration

    If (trial <> 1 And trial <> 2 And trial <> 11 And trial <> 12 And trial <> 21 And trial <> 22) Then
        If (Sheets("Summary").Cells(trial + SHROW - 2, "I").Value <> "" And _
            Sheets("Summary").Cells(trial + SHROW - 1, "I").Value <> "") Then
            Call ZeroHoopEstimate(yTL(0), trial)     'Establish a minimum ht(numVous) based on assumption
of zero hoop forces
        ElseIf (Sheets("Summary").Cells(trial + SHROW - 2, "I").Value <> "" And _
            Sheets("Summary").Cells(trial + SHROW - 1, "I").Value = "") Then
```

```
            Call ZeroHoopEstimate(yTL(0), trial)     'Establish a minimum ht(numVous) based on assumption
of zero hoop forces
        End If
    Else
        Call ZeroHoopEstimate(yTL(0), trial)     'Establish a minimum ht(numVous) based on assumption of
zero hoop forces
    End If

'Begin analysis with hoop forces
    i = 1
    tLTolerance = initTLTolerance                                    'Set initial thrust line tolerance

'if the previous two hoop analyses for alpha > 5 deg. did not find a solution, then jump to next theta
iteration

    Do
        Call ListParameters(trial)                          'List dome parameters in Analysis sheet
        Call StartPoint(i)                    'Reset the StartPoint from the ZeroHoopEstimate function
        If (trial <> 1 And trial <> 2 And trial <> 11 And trial <> 12 And trial <> 21 And trial <> 22) Then
            If (Sheets("Summary").Cells(trial + SHROW - 2, "K").Value <> "" And _
                Sheets("Summary").Cells(trial + SHROW - 1, "K").Value <> "") Then
                Call DrawThrustLine(yTL(0), trial)      'Determine the rest of the points based on known
yTL(0) and yTL(1)
            ElseIf (Sheets("Summary").Cells(trial + SHROW - 2, "K").Value <> "" And _
                Sheets("Summary").Cells(trial + SHROW - 1, "K").Value = "") Then
                Call DrawThrustLine(yTL(0), trial)      'Determine the rest of the points based on known
yTL(0) and yTL(1)
            End If
        Else
            Call DrawThrustLine(yTL(0), trial)      'Determine the rest of the points based on known yTL(0)
and yTL(1)
        End If

        If (finalCheck = False) Then
            tLTolerance = tLTolerance + 0.01
        End If

    Loop Until (finalCheck = True Or tLTolerance > tR)

    If (finalCheck = False) Then
        Sheets("Summary").Select
```

```
        Cells(trial + SHROW, "J").Value = "No Sol'n"
        Exit Sub
    End If

End Sub

Public Sub StartPoint(i As Integer)
'Determine the start point of the thrust line. Initially start just under the extrados at the crown
'Reset StartPoint after ZeroHoopEstimate procedure has run

    Dim startTolerance As Single        'How far away from the extrados should the initial pt. of the
thrust line begin?

    startTolerance = 0.01               'Can reduce or increase; arbitrary

    xTL(0) = 0                  'Initial coordinate of thrust line - will always be 0 for complete dome
    yTL(0) = a + t              'Initial coordinate of thrust line at extrados - will vary a-t < yTL < a+t

    m(i - 1) = 0            'For no applied loads, zero slope from centerline to xCg(1), yTL(1)
    yTL(i) = yTL(i - 1)     'yTL(1) and yTL(0) will always be equal

    If (yTL(i) >= yCgE(i) Or yTL(i) <= yCgI(i)) Then        'if the start point lies outside the dome
section
        yTL(i - 1) = yCgE(i) - startTolerance     'yTL(0) must be lowered to less than the limiting y-value
of yCge(1)
    End If

End Sub

Public Sub DrawThrustLine(initTLPt As Single, trial As Integer)
'Starting from the first voussoir, begin iterating values of hT(level) from zero to htMax(level), which
will depend on _
what ht(value) limits the thrust line from exceeding the extrados, or other constraints per routine
EstHTLimits
'initPt sent in from Sub StartPoint or MoveStartPoint

    Dim nLevel As Integer               'The current level from 0 to numVous
    Dim hTMax As Long                   'The maximum ht value given a certain level
    Dim i As Long                       'The range of possible integer htValues for ht(1): 1st pt on thrust
line
```

```
    yTL(1) = initTLPt                   'Set yTL(1) equal to yTL(0), the initial pt of the thrust line

    For nLevel = 1 To numVous
        hTMax = EstHTLimit(nLevel)
        finalCheck = False                          'Reset the finalCheck value
        Call RemainderForcePoly(nLevel, hT(nLevel - 1), hTMax, trial)
            'nLevel is the current level; ht(nLevel-1) is the starting point of the next ht())
        If finalCheck = True Then
            Call ListHTValues(trial)
            Sheets("Summary").Cells(trial + SHROW, "J").Value = hT(numVous)
            'List HT/Wt. ratio in summary sheet if finalCheck = true
            Sheets("Summary").Cells(trial + SHROW, "K").Value = hT(numVous) / w(numVous)
            Sheets("Summary").Cells(trial + SHROW, "L").FormulaR1C1 = "=MIN(RC[-3],RC[-1])"
            Call ListTLCoordinates(trial)               'List thrustline coordinates
            Call PlotThrustLine(trial)                  'Plot thrust line
            Exit Sub                                    'This stops the MoveStartPoint function from being
called
        End If

    'if the final thrust line point exceeds the extrados or the thrust line is complete without finalCheck
= true, _
     and the initial point of the thrust line can still be lowered then move the start point
        If ((xTL(numVous + 1) > xE(numVous) Or nLevel = numVous) And initTLPt - moveStartTolerance >= a -
t) Then
            Call MoveStartPoint(initTLPt)
            Call DrawThrustLine(yTL(0), trial)
            If (finalCheck = True) Then
                Exit Sub
            End If
        ElseIf (initTLPt - moveStartTolerance < a - t) Then
            Exit Sub
        End If
    Next nLevel

End Sub

Public Sub RemainderForcePoly(level As Integer, hTPrev As Long, hTMax As Long, trial As Integer)
'Recursive function to find the remaining values of hT(i) between ht(1) and ht(numVous)

    Dim hTStart As Long                 'The min. ht value for voussoir level 1 -- the max. of jMinD or
htPrev+1 (equal to 0)
```

```
    Dim i As Long                       'The range of htValues for each level - integers for NOW - maybe
change into DO loop
    Dim j As Integer                    'The number of voussoir levels

    If (level = 1) Then
        hTStart = Application.WorksheetFunction.Max(jMinD, hTPrev + 1)
    Else
        hTStart = hTPrev + 1
    End If

    For i = hTStart To hTMax                'Increase as integers FOR NOW
        hT(level) = i
        For j = (level + 1) To numVous      'Increase as integers FOR NOW
            hT(j) = i
        Next j
'Call ListHTValues(trial)
        CheckYTLValues                      'all ht values from levels from 1 to numVous are full, run
checks
'Call ListTLCoordinates(trial)
        If (finalCheck = True) Then
            Exit Sub
        End If

        If (level < numVous) Then
            'If the thrust line will exceed the extrados if this ht(level) continues to increase, then move
to next hTvalue
            If (yTL(level + 1) + tLTolerance >= yCgE(level + 1)) Then 'And xTL(numVous + 1) < xI(numVous))
                Exit For
            End If
        End If

        If (xTL(numVous + 1) > xE(numVous)) Then      'If the final thrust line point exceeds extrados,
then move start point
            Exit For
        End If

    Next i

End Sub

Option Explicit
```

```
Public Function EstHTLimit(ByVal n As Integer) As Long
'Establish the maximum horizontal distance on the thrust line for each n level; n is always greater than 0
'For this program version, remove constraint tempHT2 based on hNet such that hoop forces can jump back and
forth

    Dim tempHT1 As Single               'based on force polygon slope at previous n level
    'Dim tempHT2 As Single               'based on hNet of previous n level
    Dim tempHT3 As Single               'based on compression strengths at prev. n level; due to small area
for init. vous. _
                                         ASSUME that crushing does not occur per limit state assumptions,
and because _
                                         internal stresses do not approach material limits
    'Only voussoir 1 is unlimited by previous horiz. distance values
    If (n = 1) Then
        EstHTLimit = jMax
    Else
        hNet(n - 1) = hT(n - 1) - hT(n - 2) 'Establish hNet of previous ht values
        tempHT1 = w(n) / w(n - 1) * hT(n - 1)
        'tempHT2 = hT(n - 1) + hNet(n - 1)
        'tempHT3 = hMax(n)                  'TEMPORARILY DISABLE THIS CHECK
        EstHTLimit = Int(Application.WorksheetFunction.Min(tempHT1)) ', tempHT2))  'Establish limit as min.
of 2 options
    End If

End Function

Public Sub CheckYTLValues()
'All hT(levels) are filled and meet hTConstraints; w(levels) are known; _
 hNet(levels) are known: need to check yThrust Line values

    Dim i As Integer                                    'the voussoir level
    Dim checkYTL As Boolean                             'Check thrust line points against dome
intrados/extrados

    checkYTL = False

    For i = 1 To numVous
        m(i) = -w(i) / hT(i)                            'the slopes on the force polygon; m(i)
establishes the location _
                                                            of yTL(i+1)
```

```
        'The initial point, yTL(1) is known; find other points for v.levels 2 to numVous
        If (i > 1) Then
            yTL(i) = m(i - 1) * (xTL(i) - xTL(i - 1)) + yTL(i - 1) 'almost completed y-array except for
v.Level = numVous + 1
        End If
    Next i

    For i = 1 To numVous
        If (yTL(i) < yCgE(i) And yTL(i) > yCgI(i)) Then
            checkYTL = True
        Else
            checkYTL = False
            Exit For
        End If
    Next i

   Call TLFinalPoint(numVous + 1, checkYTL)

End Sub

Public Sub TLFinalPoint(finalI As Integer, checkPrevious As Boolean)
'TL points from 0 to numVous are known. Check the final point TL(numVous + 1)
'Extend the thrust line to the base of the dome

    xTL(finalI) = (yTL(numVous) - m(numVous) * xTL(numVous)) / (1 / Tan(alpha) - m(numVous)) 'Solve for x-
coordinate

    'Redefine yTL(finalI), which must satisfy criteria
    yTL(finalI) = xTL(finalI) / Tan(alpha)

'MsgBox ("m(numVous)=" & m(numVous) & "; xtl(" & finalI & ")=" & xTL(finalI))
'check that final point is within dome; if all yTL values satisfy conditions for voussoir = 1 to numVous+1
then
    If (checkPrevious = True And xTL(finalI) >= xI(numVous) And xTL(finalI) <= xE(numVous)) Then
        finalCheck = True
    Else
        finalCheck = False
    End If

End Sub
```

```
Public Sub MoveStartPoint(prevYTL As Single)

    If (prevYTL - moveStartTolerance >= a - t) Then                  'if yTL(0) is greater than y = a, then
move down by 0.1 ft
        yTL(0) = prevYTL - moveStartTolerance                          'decrease yTL(0) by 0.1
    End If
'MsgBox ("MoveStartPoint; yTL(0) =" & yTL(0))

End Sub

Option Explicit
Public jMinA As Long, jMax As Long              'The min. and max. HTdistance for level(numVous) for arch
analysis
Public jMinD As Long                            'The min. HTdistance for level(numVous) for dome analysis


Public Sub DetermineHTLimits(initTLPt)
'Determine the initial minimum and maximum estimated values of horizontal thrust for Zero Hoop Force case

    jMinA = Int(MinHTNumVous(initTLPt))      'Estimate the min. horizontal thrust distance possible based
fitting yTL(2) in dome

    jMax = Int(MaxHTnumVous)                'Estimate the max. horiz. thrust assuming TL starts at (0, a)
based on equil.

End Sub

Public Function MinHTNumVous(ByVal firstYTL As Single) As Single
'Estimate the min. horizontal thrust distance possible based fitting yTL(2) in dome and knowing yTL(1) and
yCgI(2)
'Used only in zeroHoopForce estimates

    Dim maxSlope1 As Single
    Dim tempHTMin1 As Single
    Dim tempHTMin2 As Single

    maxSlope1 = Abs((yCgI(2) - firstYTL) / (xTL(2) - xTL(1)))            'This is a negative slope!
    tempHTMin1 = w(1) / maxSlope1

'Estimate the min. horizontal distance of ht(numVous) assuming the horizontal thrust is applied at (0,
yTL(0)), _
```

```
solving for zero moment about a pin support at the base, and dividing value by an arbitrary value to reduce
the range _
of possible values for ZERO HOOP FORCE analysis

    Dim arbValue As Integer
    arbValue = 4

    tempHTMin2 = Abs((w(numVous) * (a * Sin(alpha) - xCGLune) / (firstYTL - a * Cos(alpha))) / arbValue)

'Let the minimum value at which the zero hoop force condition begins equal to the maximum of the two
estimated minimums
    MinHTNumVous = Application.WorksheetFunction.Max(tempHTMin1, tempHTMin2, 1)

'Set the min. value at which with hoop force analysis begins by using thrust line slope estimates
    If (tempHTMin1 >= 1) Then
        jMinD = Int(tempHTMin1)
    Else
        jMinD = 1
    End If

End Function

Public Function MaxHTnumVous() As Single
'Determine maximum estimated horiz. thrust based on equilibrium assuming HT acts at rPrime (0, a-t)

    Dim tempMax As Single

    'Max. thrust = moments about support; assume pin connection
    tempMax = Abs(w(numVous) * (a * Sin(alpha) - xCGLune) / ((a - t) - a * Cos(alpha)))
    MaxHTnumVous = Application.WorksheetFunction.Max(tempMax, 1)

End Function

Public Sub ZeroHoopEstimate(initTLPt As Single, trial As Integer)
'Establish a more accurate estimate for a min. value of hT(numVous) - the horizontal thrust - by running a
test _
 for zero hoop force conditions first.

    Dim i As Integer            'The voussoir level from 1 to numVous
    Dim j As Long               'The value of hT for all voussoirs from 1 to numVous
```

```
    Dim zeroHoopMin As Long     'The min. HT value as determined by assuming zero hoop forces - Integer FOR
NOW
    Dim zHoopCheck As Boolean   'To expedite zeroHoop estimate, use Boolean to determine whether any pt. _
                                   on the thrust line exceeds the extrados; if true, move start pt.
    finalCheck = False
    yTL(1) = initTLPt           'set the initial value of yTL based on the initial start point

    'Fill the hT array with the same value (assumes zero hoop forces).
    For j = jMinA To jMax
        For i = 1 To numVous
            hT(i) = j
        Next i
        CheckYTLValues                              'The ht array is full
'Call ListHTValues(trial)
        If (finalCheck = True) Then
            zeroHoopMin = j
            Sheets("Summary").Cells(trial + SHROW, "H").Value = zeroHoopMin
            Sheets("Summary").Cells(trial + SHROW, "I").Value = zeroHoopMin / w(numVous)
            Exit For
        End If
        zHoopCheck = True
     'If any pt. of the thrust line exceeds extrados, then move start point; increasing the ht value beyond
will not fit _
     the thrust line into the section for the case of zero hoop forces
        For i = 1 To (numVous - 1)
            If (yTL(i + 1) >= yCgE(i + 1)) Then
                zHoopCheck = False
                Exit For
            End If
        Next i
        If (zHoopCheck = False) Then
            Exit For
        End If
    Next j

    'If a solution has not been found using zero hoop assumptions, move the start point by 0.1 and redo the
loop.

    If (finalCheck = False And initTLPt - moveStartTolerance >= a - t) Then
        Call MoveStartPoint(initTLPt)
        Call ZeroHoopEstimate(yTL(0), trial)
```

```
    ElseIf (finalCheck = False And initTLPt - moveStartTolerance < a - t) Then         'No solution
assuming zero hoop forces
        Sheets("Summary").Cells(trial + SHROW, "H").Value = "No Sol'n"
    End If

End Sub

Option Explicit
Public merid() As Single                        'An array to store the meridional forces
Public hoop() As Single                         'An array to store the calculated internal hoop forces
Public mStress() As Single                      'Check on meridional stresses do not exceed max.
compressive stress
Public hStress() As Single                      'Check on hoop stresses do not exceed max. hoop stress
Public wtLune As Single                         'The total weight of the lune in question
Public tWeight As Single                        'The total weight of the dome in question - use as a check
Public checkTWt As Single                       'Numerical calc. of total dome weight
Const PI = 3.141593

Public Sub CalcWeight(trial As Integer)
'Serves as a check on dome weight

    Charts("Section" & trial).Select

    Call AddIntForceSheet(trial)

    Dim tempPhi0 As Single                          'The angle of the oculus opening at the crown; equals
zero for now

    Sheets("IntForces" & trial).Select

    wtLune = w(numVous)
    tWeight = wtLune * (2 * PI / theta)             'Total weight of dome, theta in radians
    tempPhi0 = 0
    checkTWt = (2 * PI) * rho * (r ^ 3 - rPrime ^ 3) / 3 * (Cos(tempPhi0) - Cos(alpha))
    Range("B3").Value = wtLune
    Range("B4").Value = tWeight
    Range("D4").Value = checkTWt
    Range("B3, B4, D4").NumberFormat = "0"
    Range("B3:D4").ColumnWidth = "15"

    Sheets("Summary").Select
```

```
    Cells(SHROW + trial, "G").Value = w(numVous)


End Sub

Public Sub CalcInternalForces(trial As Integer)
'Calculate the internal meridional and hoop forces after all checks have been made for the dome
'w(i) should remain the same throughout the program
'Parameters that are finalized are hT(i) distances

    ReDim merid(numVous), hoop(numVous)
    ReDim mStress(numVous), hStress(numVous)
    Dim i As Integer                                    'The voussoir level

    'Do not calculate internal forces if a hoop force thrust line solution is not found
    If (finalCheck <> True) Then
        Exit Sub
    End If

    Sheets("IntForces" & trial).Select

    For i = 0 To numVous
        If (i <> 0) Then
            merid(i) = (w(i) ^ 2 + hT(i) ^ 2) ^ 0.5         'On force polygon, merid. force is the
hypotenus of legs w(i) and ht(i)
                                                            'Meridional force at values of phi degrees =
integer
            mStress(i) = merid(i) / (a * Sin(vousPhi(i)) * theta * 2 * t) / 144
                                                            'Meridional force / plan area, covert to psi
            hNet(i) = hT(i) - hT(i - 1)                     'Calculate net horiz. force by subtracting
accruing hT(i) distances
            hoop(i) = hNet(i) / (2 * Sin(theta / 2))        'Calculate the hoop resultant
            hStress(i) = hoop(i) / (2 * t * a * vousAngle) / 144   'hoop resultant force / section area
converted to psi
        ElseIf (i = 0 Or i = numVous) Then                  'At phi = alpha, hoop force area is 1/2 trib.
section area; recalculate
            hNet(i) = hT(numVous)                           'At phi=0, the horiz. thrust is equal to the
total distance of hT
            hoop(i) = hNet(i) / (2 * Sin(theta / 2))        'Calculate the hoop resultant
            hStress(i) = hoop(i) / (0.5 * 2 * t * a * vousAngle) / 144 'hoop resultant force / 1/2 trib.
section area
```

```
        End If

        Cells(i + AHROW, "A").Value = Application.WorksheetFunction.Degrees(vousPhi(i))
        Cells(i + AHROW, "B").Value = merid(i)
        Cells(i + AHROW, "C").Value = hoop(i)
        Cells(i + AHROW, "D").Value = mStress(i)
        Cells(i + AHROW, "E").Value = hStress(i)
    Next i

End Sub
    Option Explicit

Public Sub AddChartSheet(trial As Integer)
'Draw the extrados and intrados of the dome
    Dim xERange As String, yERange As String
    Dim xIRange As String, yIRange As String
    Dim alphaDeg As Integer, thetaDeg As Integer

    xERange = "R8C2:R" & (numVous + AHROW) & "C2"
    yERange = "R8C3:R" & (numVous + AHROW) & "C3"
    xIRange = "R8C4:R" & (numVous + AHROW) & "C4"
    yIRange = "R8C5:R" & (numVous + AHROW) & "C5"

    Sheets("Summary").Select
    alphaDeg = Cells(trial + SHROW, "E").Value
    thetaDeg = Cells(trial + SHROW, "F").Value
    Sheets("Analysis" & trial).Select
    Charts.Add
    With ActiveChart
        .Move After:=Sheets("Analysis" & trial)
        .Name = "Section" & trial
        .ChartType = xlXYScatterSmoothNoMarkers
        .SeriesCollection.NewSeries
        .SeriesCollection.NewSeries
        .SeriesCollection(1).XValues = "=Analysis" & trial & "!" & xERange
        .SeriesCollection(1).Values = "=Analysis" & trial & "!" & yERange
        .SeriesCollection(1).Name = "=""Extrados"""
        .SeriesCollection(2).XValues = "=Analysis" & trial & "!" & xIRange
        .SeriesCollection(2).Values = "=Analysis" & trial & "!" & yIRange
        .SeriesCollection(2).Name = "=""Intrados"""
        .Location Where:=xlLocationAsNewSheet
```

```
        .PlotArea.Select
            Selection.Width = 460
            Selection.Width = 460
        .HasLegend = True
        .Legend.Position = xlRight
        .Legend.Border.LineStyle = xlNone
        .HasTitle = True
        .ChartTitle.Characters.Text = "Thrust Line for t/R =" & tR & ", Alpha = " & alphaDeg & " deg., and
Theta = " & thetaDeg & " deg."
        .Axes(xlCategory, xlPrimary).HasTitle = True
        .Axes(xlCategory, xlPrimary).AxisTitle.Characters.Text = "Distance (ft)"
        .Axes(xlValue, xlPrimary).HasTitle = True
        .Axes(xlValue, xlPrimary).AxisTitle.Characters.Text = "Height (ft)"
        With ActiveChart.Axes(xlCategory)
            .TickLabels.NumberFormat = "0.0"
            .MinimumScale = 0
            .MaximumScale = a + t + 2
        End With
        With ActiveChart.Axes(xlValue)
            .TickLabels.NumberFormat = "0.0"
            .MinimumScale = 0
            .MaximumScale = a + t + 2
        End With
    End With

End Sub

Public Sub ListKnownCoordinates()
'The proper worksheet should already be selected.

    Dim i As Integer

    For i = 0 To numVous
        Cells(i + AHROW, "F").Value = xCg(i)
        Cells(i + AHROW, "G").Value = yCgE(i)
        Cells(i + AHROW, "I").Value = yCgI(i)
    Next

    Range("B" & AHROW & ":I" & (numVous + AHROW + 1)).NumberFormat = "0.000"
End Sub
```

```
Public Sub ListHTValues(trial As Integer)
'For progress checking, list HT in-progress values

    Dim i As Integer

    For i = 0 To numVous
        Sheets("Analysis" & trial).Cells(i + AHROW, "J").Value = hT(i)
    Next

End Sub

Public Sub ListTLCoordinates(trial As Integer)
'Input x- and y-values of thrust line into excel chart
Dim i As Integer

    Worksheets("Analysis" & trial).Select
    For i = 0 To numVous
        Cells(i + AHROW, "H").Value = yTL(i)
    Next

    'Plot the final base point of the thrust line
    Cells(1 + numVous + AHROW, "F").Value = xTL(numVous + 1)
    Cells(1 + numVous + AHROW, "H").Value = yTL(numVous + 1)

'PlotThrustLine

End Sub

Public Sub PlotThrustLine(trial As Integer)
'Plot the thrust line coordinates
Dim xCGRange As String, yTLRange As String

    xCGRange = "R8C6:R" & (numVous + AHROW) & "C6"
    yTLRange = "R8C7:R" & (numVous + AHROW) & "C7"

Charts("Section" & trial).Select
    With ActiveChart
        '.SeriesCollection.NewSeries
        '.SeriesCollection.NewSeries
        '.SeriesCollection.NewSeries
```

```
        .SeriesCollection(3).XValues = "=Analysis" & trial & "!R8C6:R" & (1 + numVous + AHROW) & "C6"
'include last point of thrust line
        .SeriesCollection(3).Values = "=Analysis" & trial & "!R8C8:R" & (1 + numVous + AHROW) & "C8"
        .SeriesCollection(3).Name = "=""Thrust Line"""

        '.SeriesCollection(4).XValues = "=Analysis" & trial & "!R8C6:R" & (numVous + AHROW) & "C6"
        '.SeriesCollection(4).Values = "=Analysis" & trial & "!R8C7:R" & (numVous + AHROW) & "C7"
        '.SeriesCollection(4).Name = "=""CgExtrados"""

        '.SeriesCollection(5).XValues = "=Analysis" & trial & "!R8C6:R" & (numVous + AHROW) & "C6"
        '.SeriesCollection(5).Values = "=Analysis" & trial & "!R8C9:R" & (numVous + AHROW) & "C9"
        '.SeriesCollection(5).Name = "=""CgIntrados"""

        .Legend.Left = 484
        .Legend.Top = 220
        .Legend.Width = 110
    End With

End Sub
```

Appendix C. Estimate of Minimum Thrust for Spherical Domes

Using the coefficients determined by equations 3.3 and 3.3, the author estimated the minimum thrust for a lune with $\theta = 45°$ from the thrust results for a lune with $\theta' = 1°$ (Fig. A.2). From Fig. 3.16, the multiplier coefficient for a lune comprised of $n = 45$ lunes with $\theta' = 1°$ is 43.9. Thus, the change in H divided by the change in weight is 43.9/45 = 0.975. The estimated minimum thrust-to-weight ratio is the product of 0.975 and the H/W values shown in Fig. 3.2. The difference between the estimates and the values shown in Fig. 3.4, and divided by the latter, results in the error in predicting the minimum horizontal thrust using smaller lunes to estimate a larger lune.

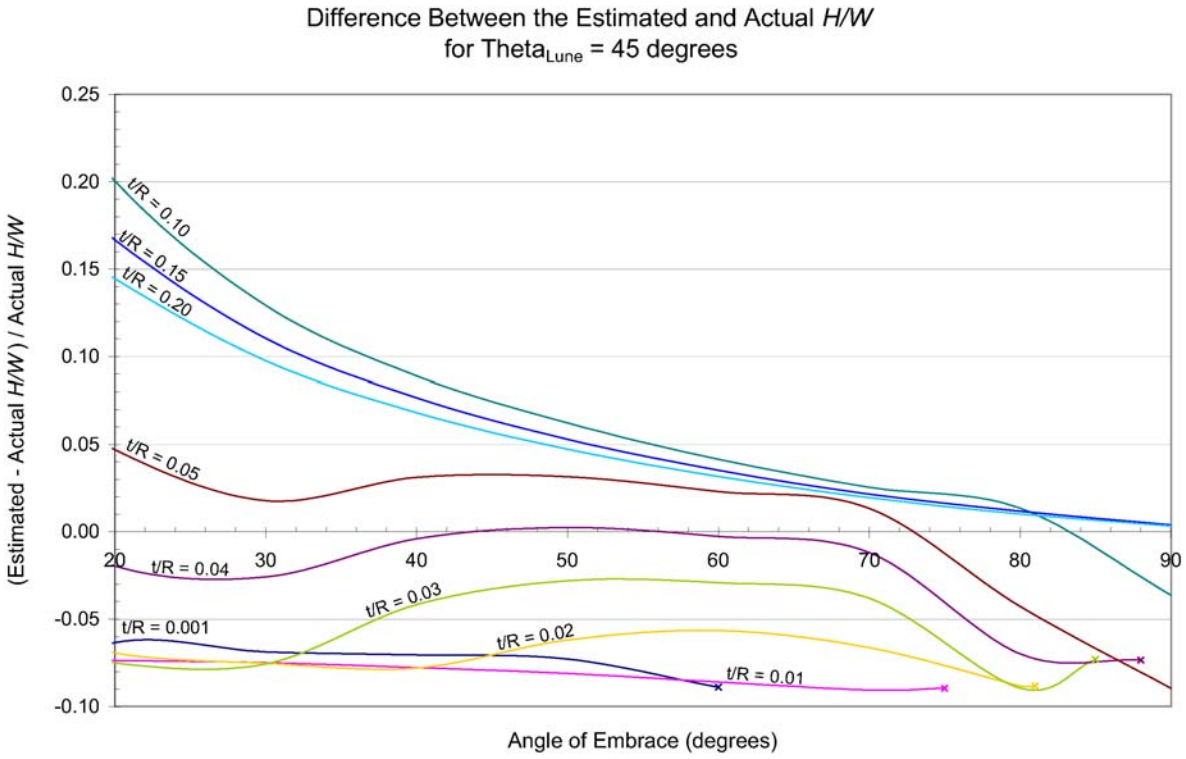

Figure A.2. The percent difference between the minimum thrust-to-weight ratio calculated by the modified thrust line program for $\theta = 45°$, and the ratio estimated by 45 lunes with $\theta = 1°$

Appendix D. Minimum Thrust-to-Weight Ratio for Pointed Domes with Two Centers of Curvature

This appendix contains the summary charts for all pointed dome geometries that the author investigated using the modified thrust line method, and assuming that hoop forces can oscillate between increasing and decreasing from the crown to base of the dome.

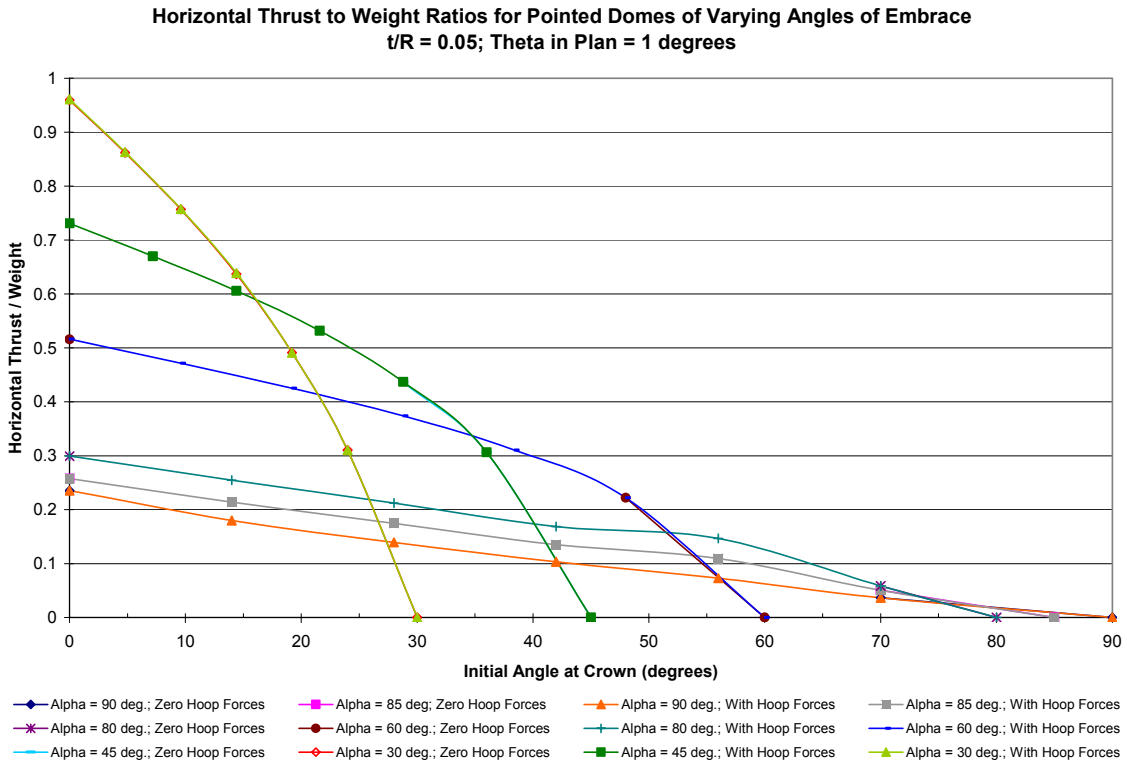

Figure A.3. The minimum horizontal-thrust-to-weight ratio for pointed domes with $t/R = 0.05$, and $\theta = 1°$

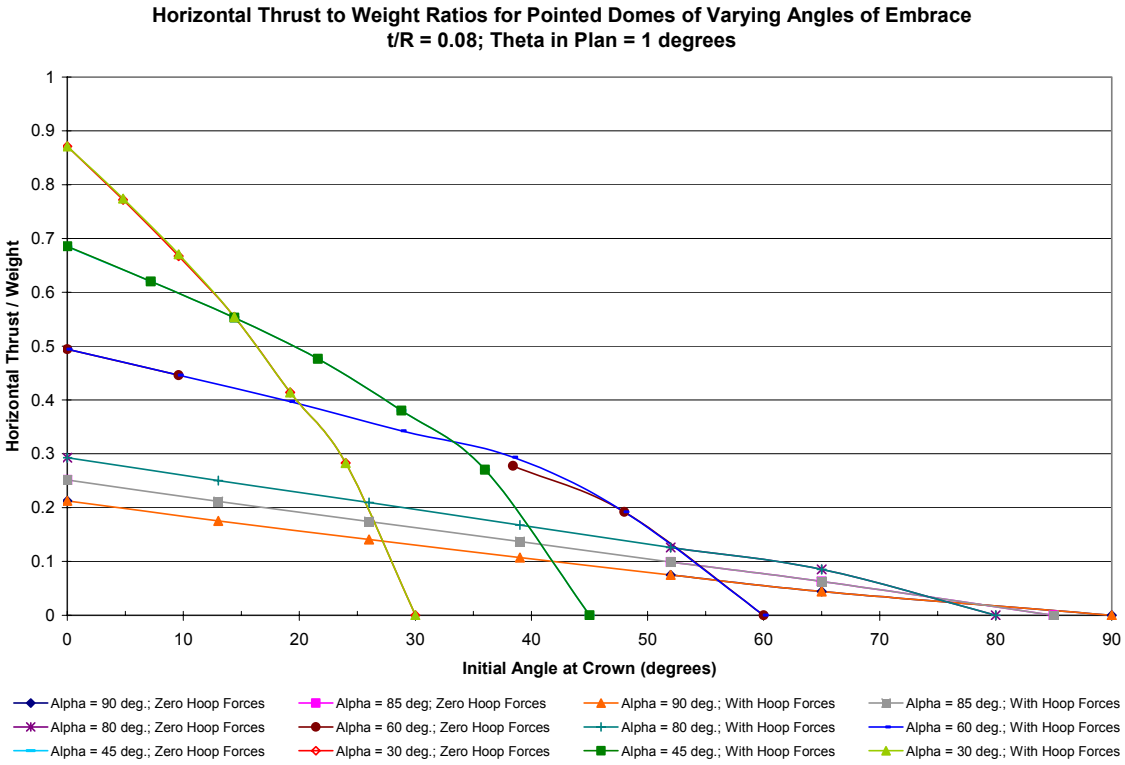

Figure A.4. The minimum horizontal-thrust-to-weight ratio for pointed domes with $t/R = 0.08$, and $\theta = 1°$

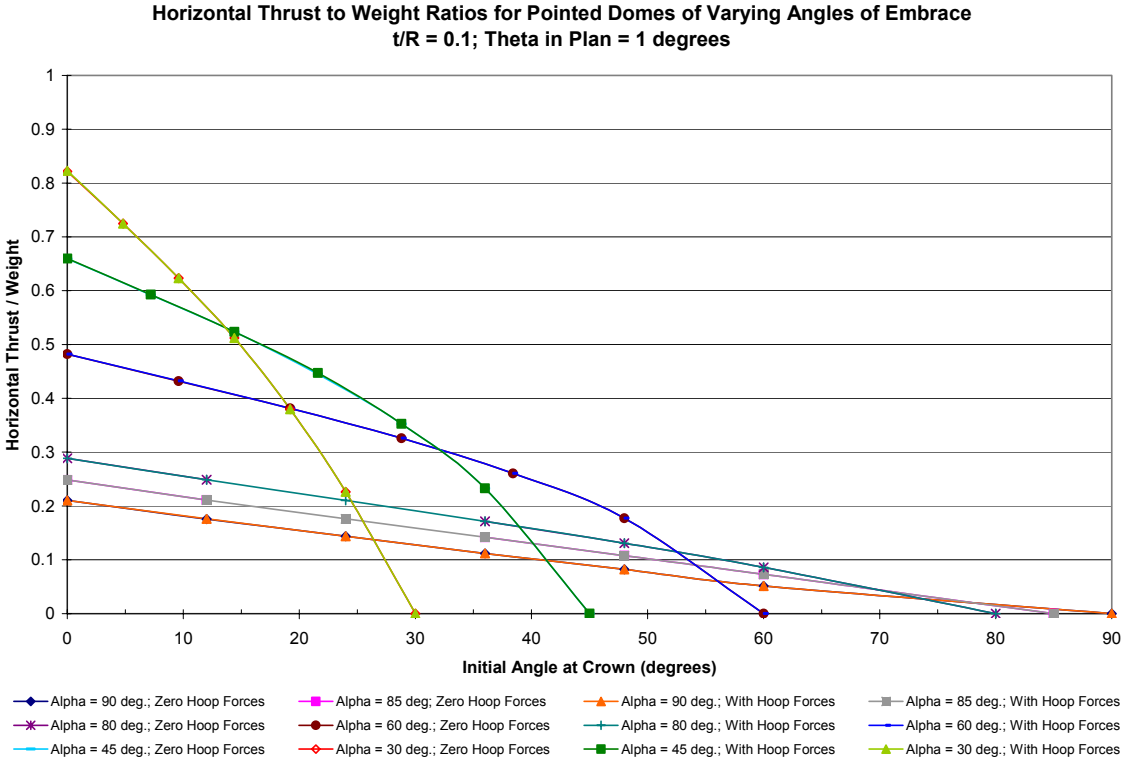

Figure A.5. The minimum horizontal-thrust-to-weight ratio for pointed domes with $t/R = 0.10$, and $\theta = 1°$

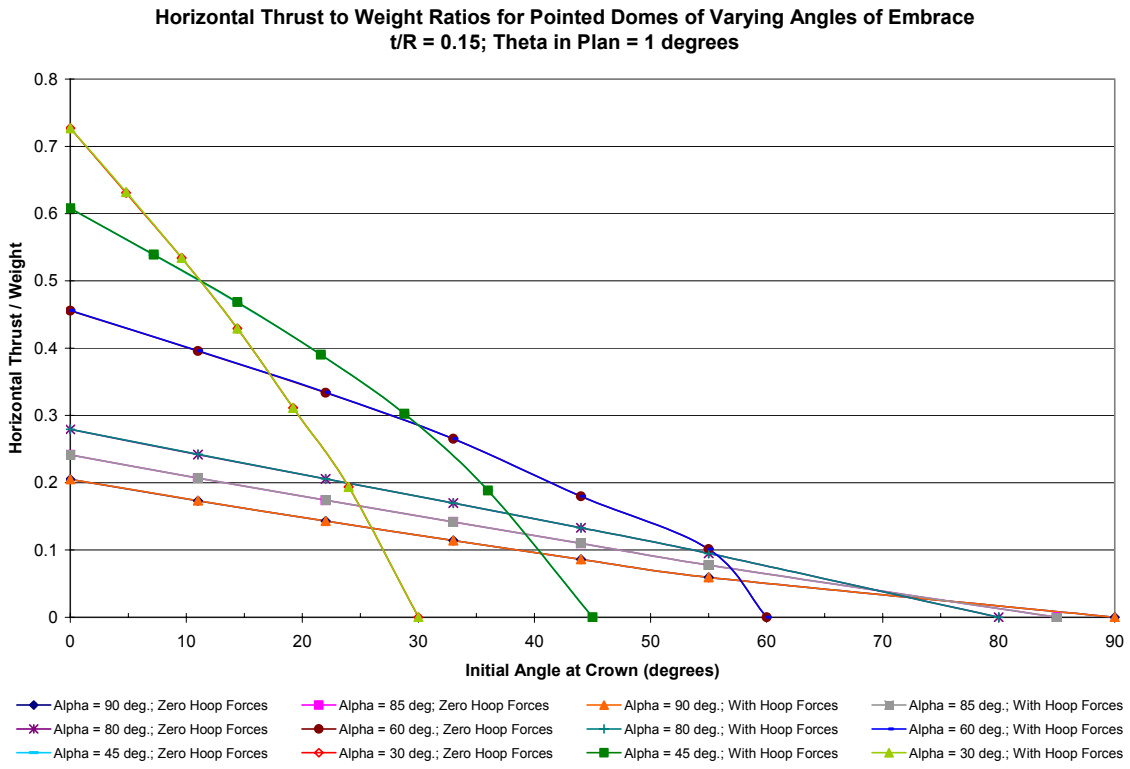

Figure A.6. The minimum horizontal-thrust-to-weight ratio for pointed domes with $t/R = 0.15$, and $\theta = 1°$

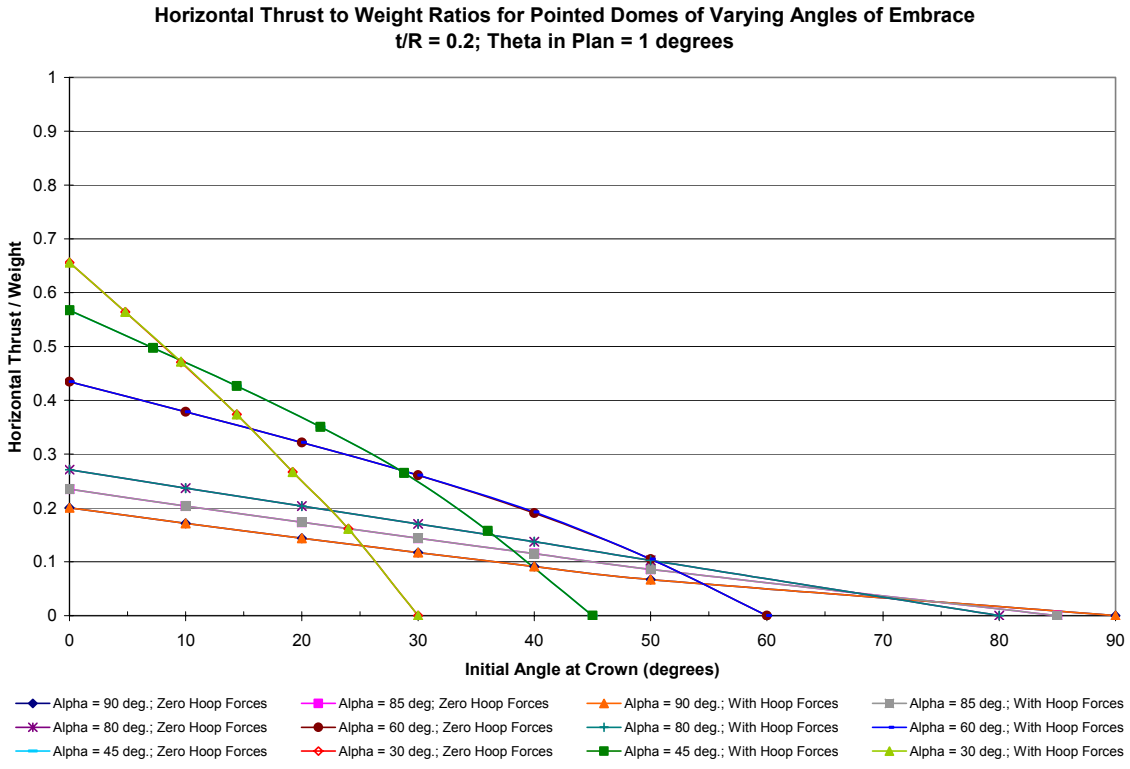

Figure A.7. The minimum horizontal-thrust-to-weight ratio for pointed domes with $t/R = 0.20$, and $\theta = 1°$

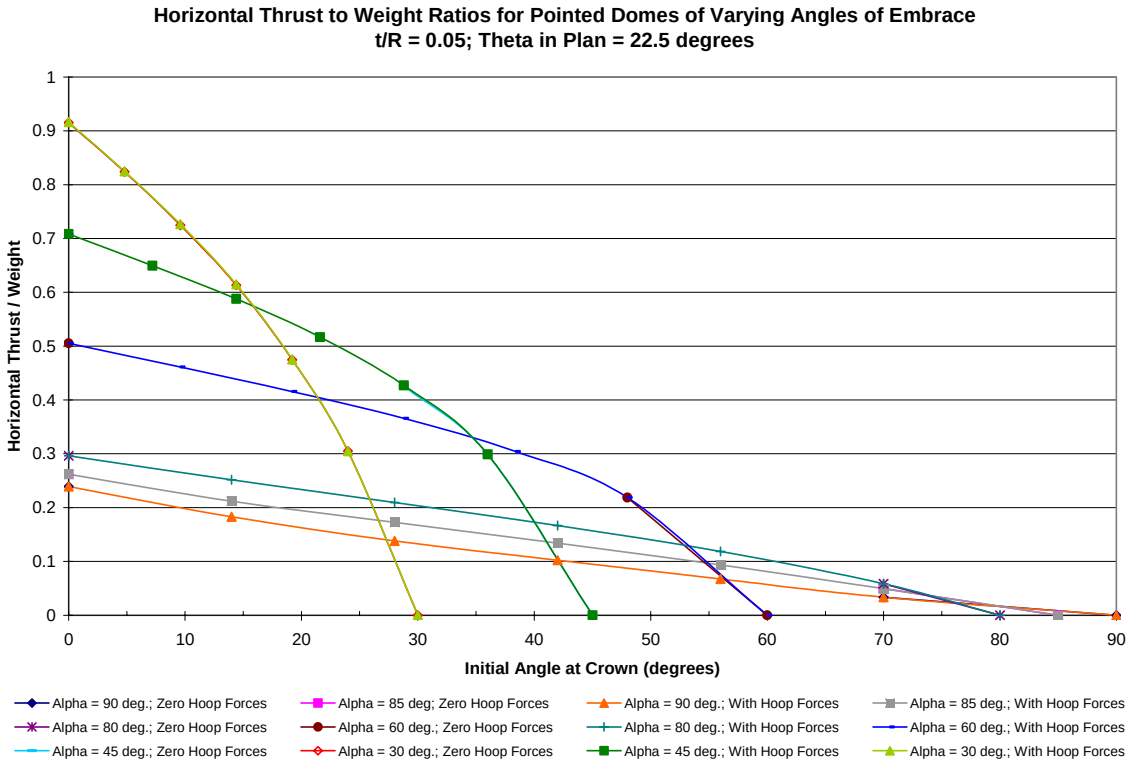

Figure A.8. The minimum horizontal-thrust-to-weight ratio for pointed domes with t/R = 0.05, and θ = 22.5°

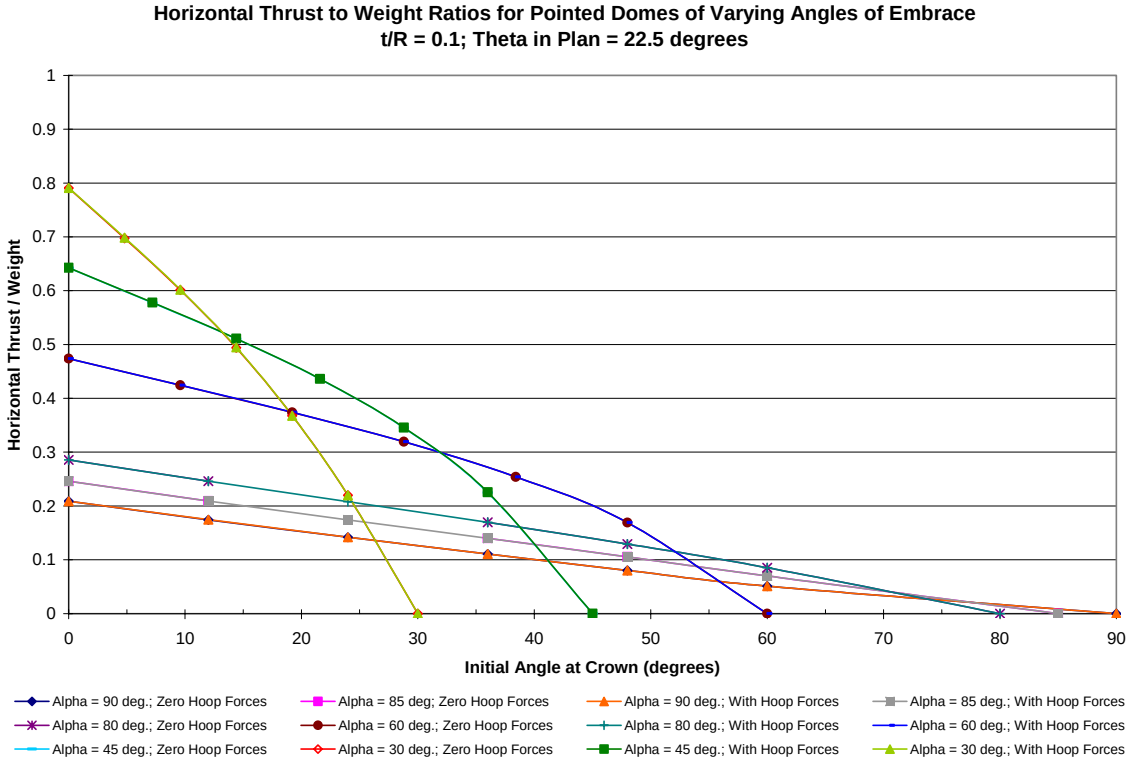

Figure A.9. The minimum horizontal-thrust-to-weight ratio for pointed domes with t/R = 0.10, and θ = 22.5°

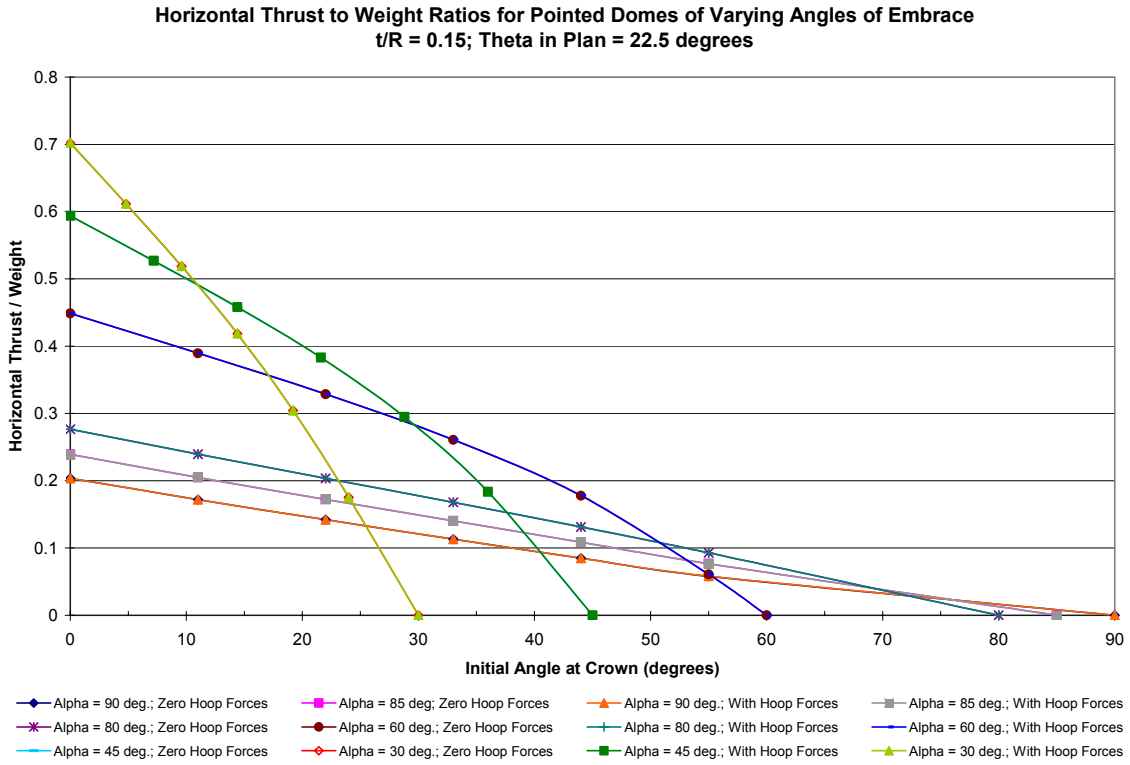

Figure A.10. The minimum horizontal-thrust-to-weight ratio for pointed domes with $t/R = 0.15$, and $\theta = 22.5°$

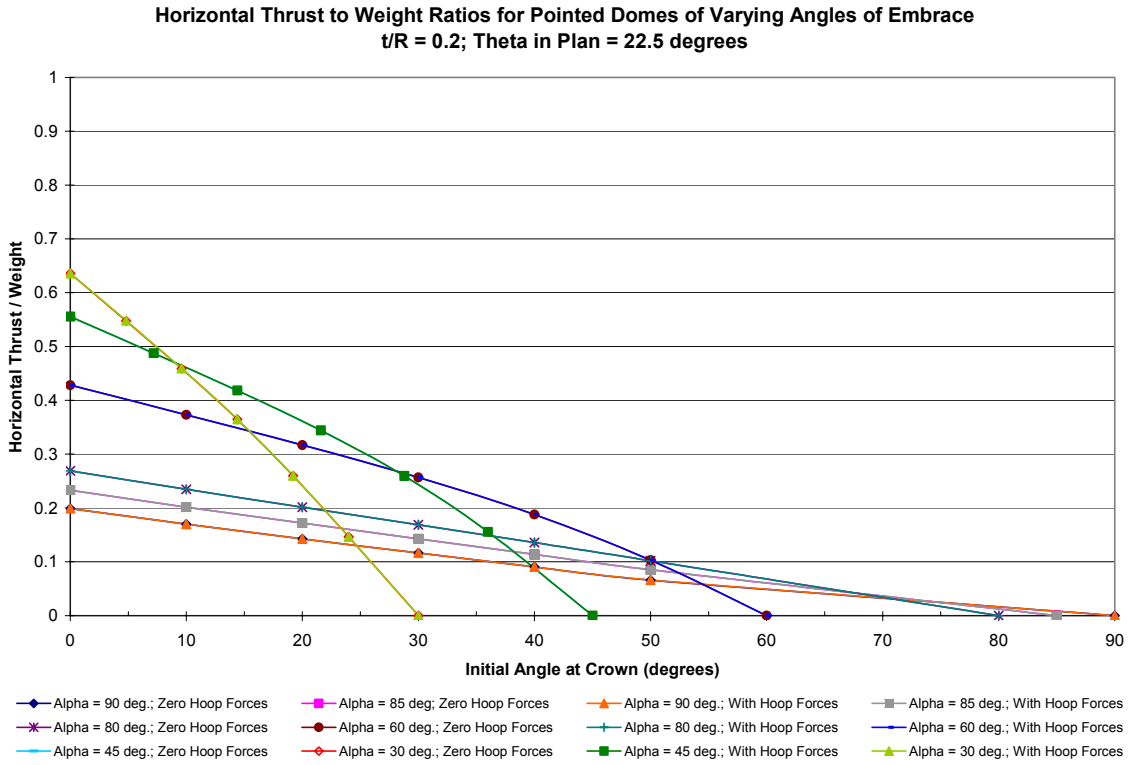

Figure A.11. The minimum horizontal-thrust-to-weight ratio for pointed domes with $t/R = 0.20$, and $\theta = 22.5°$

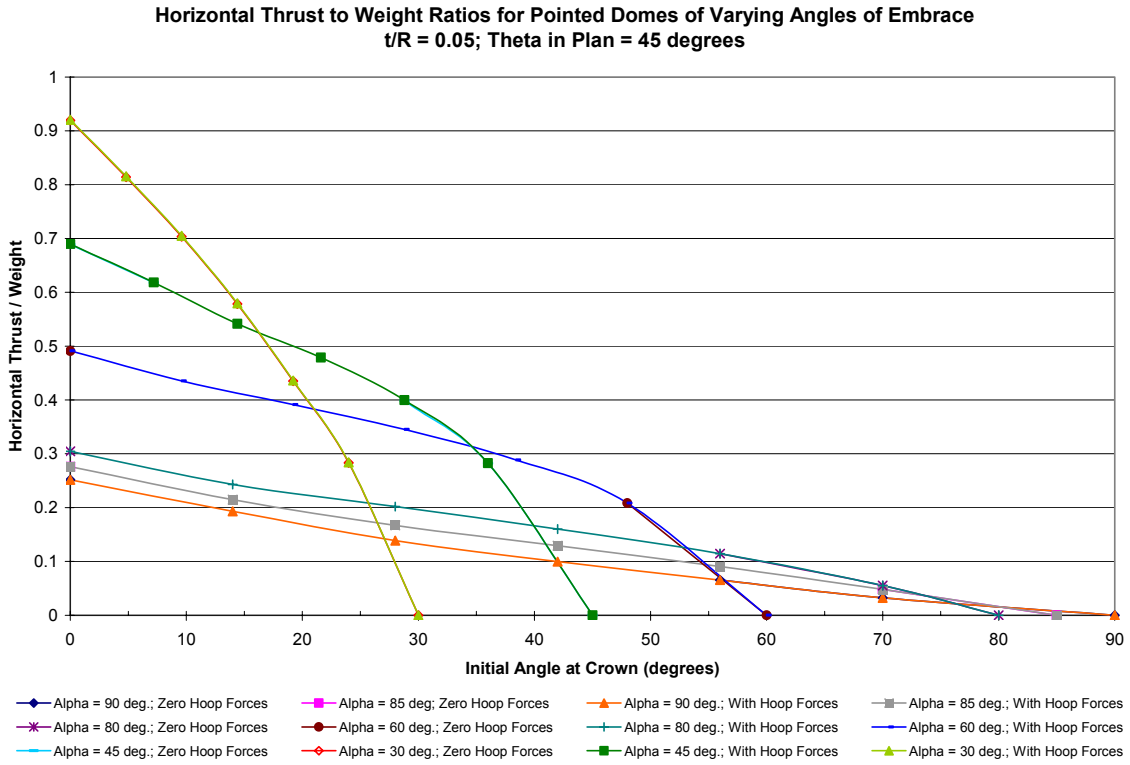

Figure A.12. The minimum horizontal-thrust-to-weight ratio for pointed domes with $t/R = 0.05$, and $\theta = 45°$

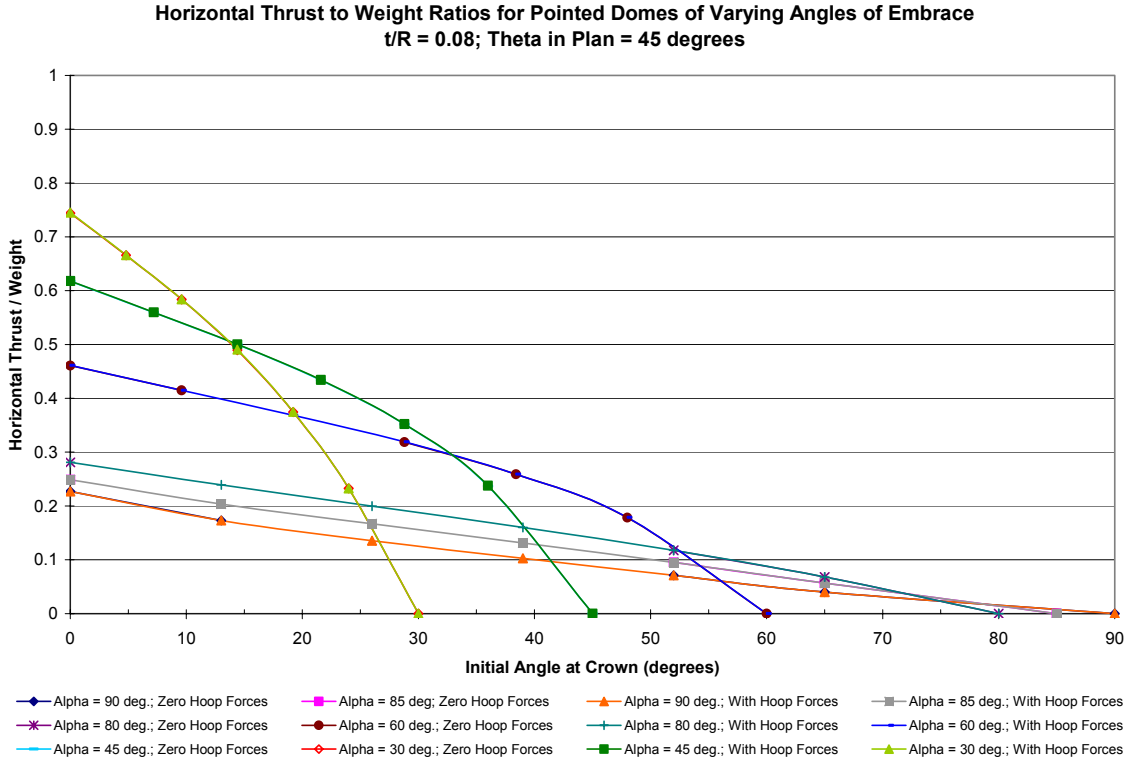

Figure A.13. The minimum horizontal-thrust-to-weight ratio for pointed domes with $t/R = 0.08$, and $\theta = 45°$

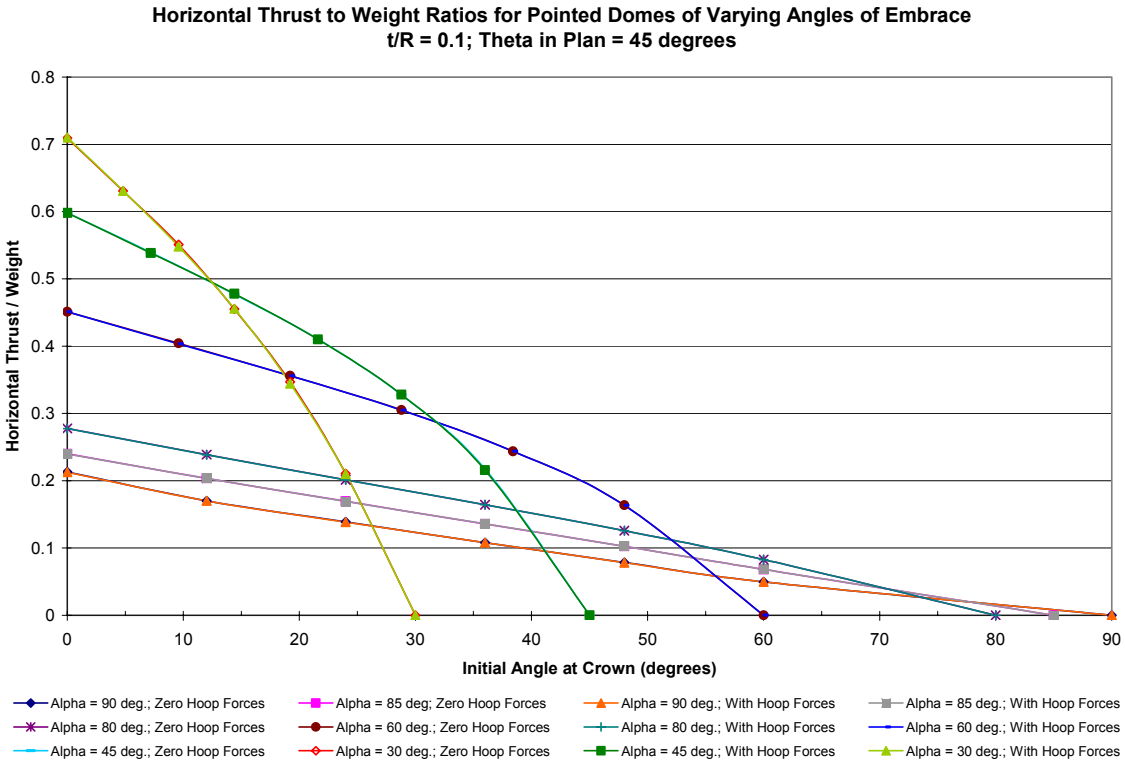

Figure A.14. The minimum horizontal-thrust-to-weight ratio for pointed domes with $t/R = 0.10$, and $\theta = 45°$

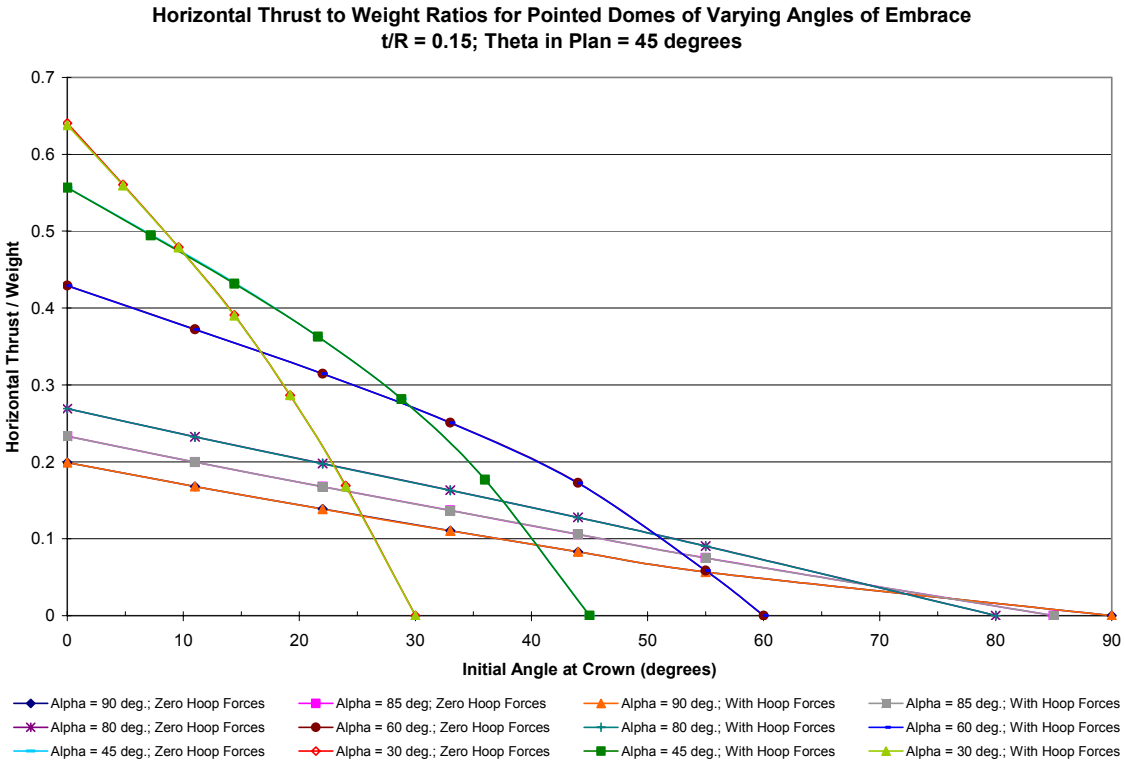

Figure A.15. The minimum horizontal-thrust-to-weight ratio for pointed domes with $t/R = 0.15$, and $\theta = 45°$

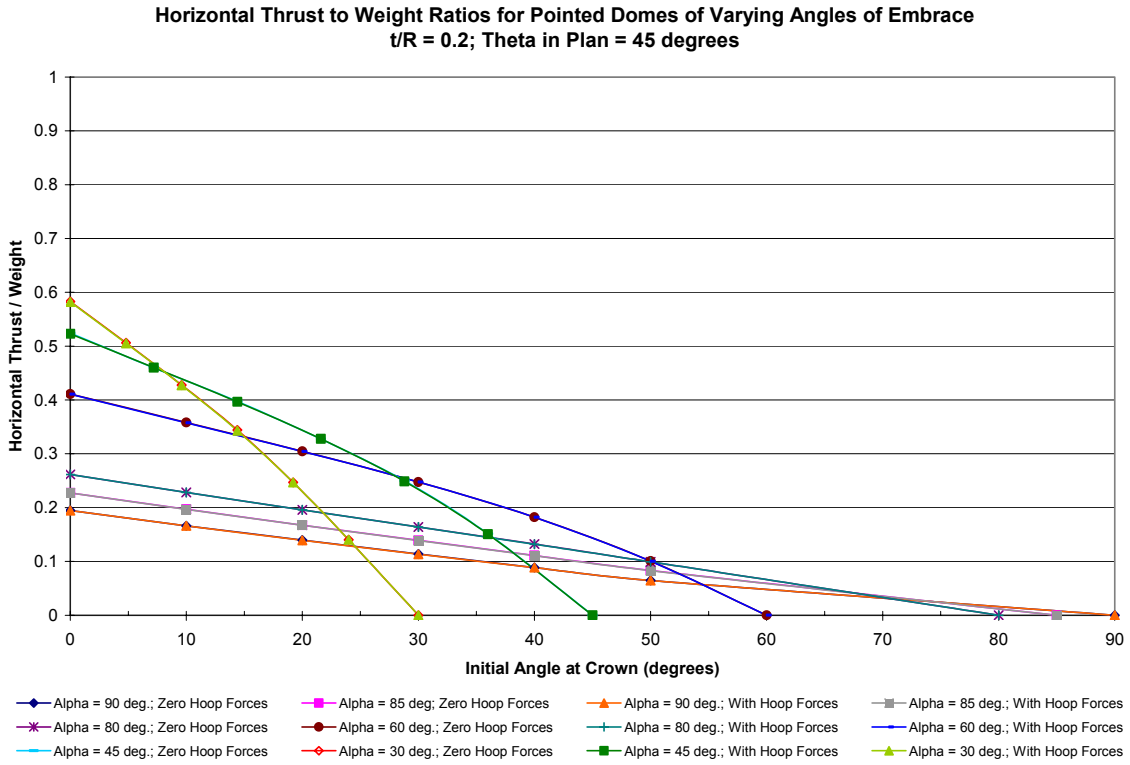

Figure A.16. The minimum horizontal-thrust-to-weight ratio for pointed domes with $t/R = 0.20$, and $\theta = 45°$

Material Tests of AAC Tile and USG Hydrocal Gypsum Mortar

Compressive Strength

The author tested two bonded samples and three non-bonded specimens in compression (Table A.1). The author modified the testing procedure from ASTM C67, "Sampling and Testing Brick and Structural Clay Tile," to reflect the difference in specimen material and geometry (Fig. A.17) (ASTM 2005). The bonded samples consisted of two 4 x 4 x 8 AAC blocks with a ¼ ± ⅛ in. gypsum mortar joint. The non-bonded samples were one 4 x 4 x 8 AAC block. Table A.1 summarizes the compressive test results.

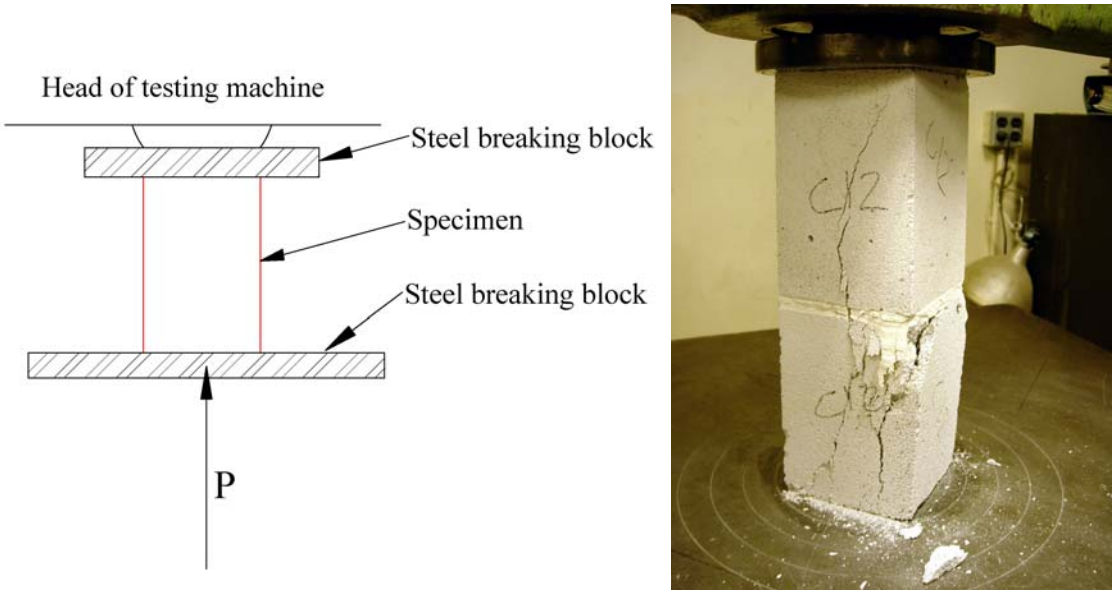

Figure A.17. Left: Schematic compression test shown for non-bonded AAC block. Right: Bonded AAC tile-and-mortar sample loaded to failure in compression

Table A.1. Summary of Compression Test Results for Aerated Autoclaved Concrete Domes

Cross-Section Dimensions		Wet AAC face			No Bond		
W (in.)	L (in.)	Specimen	App. Load (lbs)	Ult. Stress (psi)	Specimen	App. Load (lbs)	Ult. Stress (psi)
4	4	D10	≠		G10	5711	357
4	4	D11	4921	308	G11	6809	426
4	4	D12	5844	365	G12	6500	406
			Average (psi):	336		Average (psi):	396

≠ The specimen's top and bottom faces were too unparallel to safely perform the compression test. The sample was not tested.

Flexural Strength

The author tested twelve AAC wet face/gypsum mortar bonded samples and five non-bonded AAC block samples by four-point loading to determine the average flexural strength, or modulus of rupture (Table A.2). The author modified the test procedure was modified from ASTM C67, "Sampling and Testing Brick and Structural Clay Tile" (ASTM 2005). Due to the precut tile dimensions and variations in the tile or mortar dimensions, the four applied loads were not located at the third-points of the specimen, but instead, centered about the mortar joint (Figs. A.18 and A.19). The bonded specimens were constructed from two 6 x 12 tiles, 1, 2 and 4 in. thick, and a ¼ ± ⅛ in. gypsum mortar joint; the non-bonded samples consisted of one 6 x 24 block, 1, 2 and 4 in. thick. Table A.2 summarizes the flexural test results.

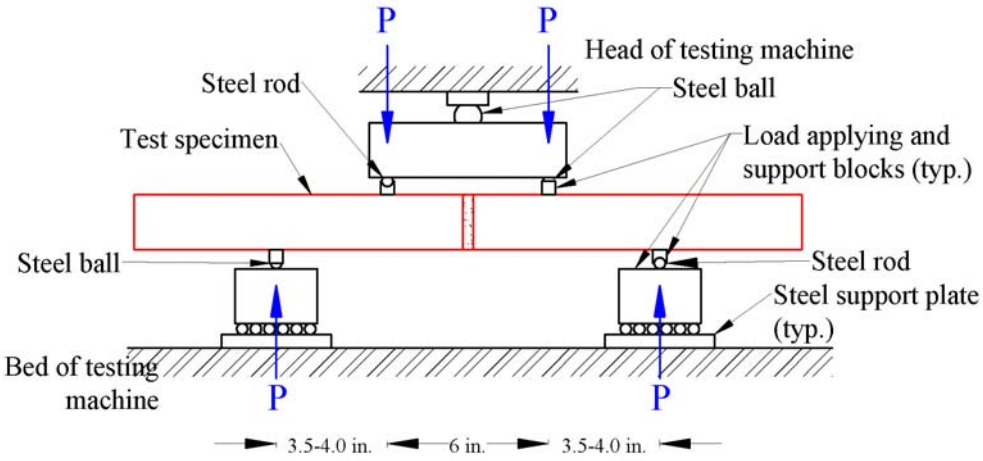

Figure A.18. Schematic of flexural test set up with 6 x 24 x 2 in. bonded specimen shown (roughly to scale)

Figure A.19. Photograph of flexural test for bonded AAC/gypsum mortar specimen

Table A.2. Summary of Flexural Test Results for Aerated Autoclaved Concrete Domes

		USG Hydrocal on Wet AAC face			No Bond		
Cross-Section Dimensions		Specimen	Total Load (lbs)	MOR (psi)	Specimen	Total Load (lbs)	MOR (psi)
W (in.)	H (in.)						
6	1	**D1**	17.1	60	**G1**	╪	
6	1	**D2**	9.2	32	**G2**	24.4	85
6	1	**D3**	20.2	71	**G3**	19.1	67
6	2	**D4**	╪		**G4**	63.3	55
6	2	**D5**	37.3	33	**G5**	74.9	66
6	2	**D6**	53.8	47	**G6**	49.4	43
6	4	**D7**	146.1	32			
6	4	**D8**	176.4	39			
6	4	**D9**	187.4	41			
			Average (psi):	**44**		**Average (psi):**	**63**

╪ The sample was broken prior to testing. The sample was not tested.

Direct Tensile Strength

The relationship between the flexural bond strength and tensile bond strength of masonry is not well known (Ameida, et al. 2002); therefore to ascertain the tensile strength of the AAC tile masonry, the author conducted direct tension tests on six[15] bonded wet face/gypsum mortar AAC tile specimens and three non-bonded AAC tile specimens. The test procedure was modeled on a direct tensile bond strength test methods for a brick couplet outlined by Ameida (Ibid.) (Fig. A.20). Five bonded specimens consisted of two 4 x 4 x 1.25 in. tiles mortared together; the final specimen used two 4 x 8 x 1.25 in. tiles. The non-bonded samples consisted of one 4 x 4 x 1.25 in. tiles. Table A.3 summarizes the direct tensile test results.

[15] The author conducted two additional direct tensile tests on bonded specimens, but did not monitor movement of the specimens during epoxy curing. When the epoxy contracted during cure, specimens were inadvertently loaded in tension and subsequently failed when additional load was applied during testing. These results are not included.

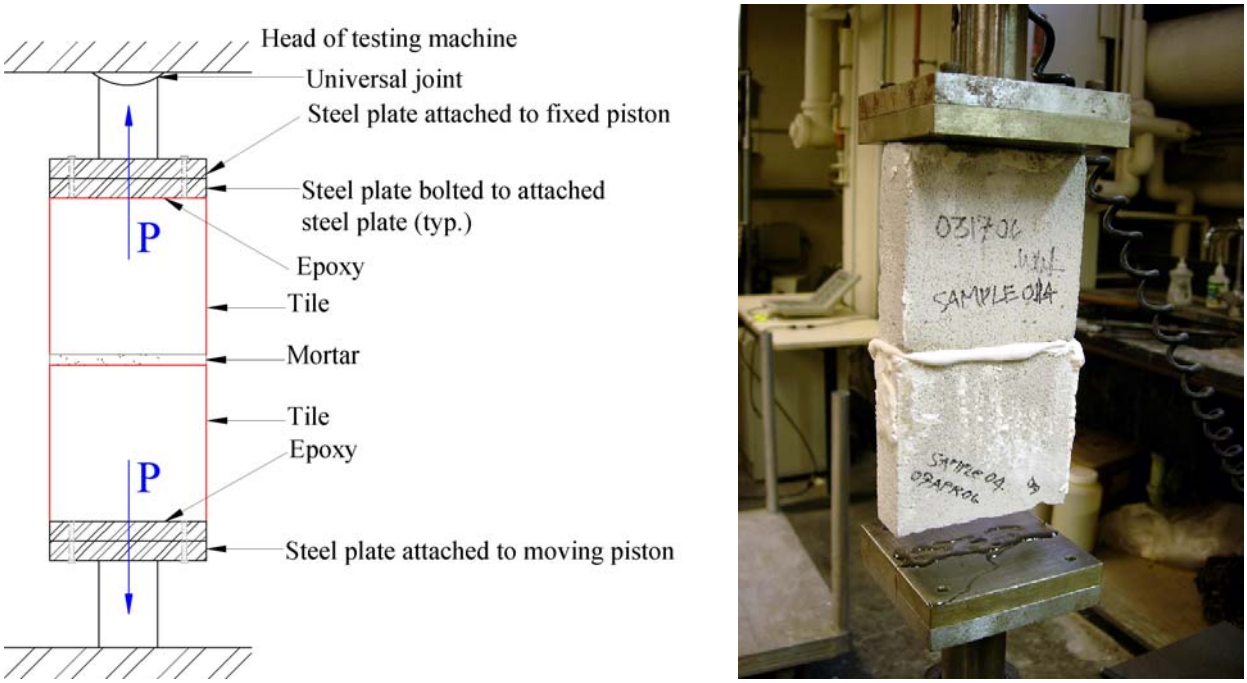

Figure A.20. Left: Direct tension test set-up with two 4 x 4 x 1.25 AAC tiles bonded by a gypsum mortar joint. Right: To minimize unintentional bending forces during testing, the specimens were lowered into an epoxy bed on the lower steel plate in the testing machine.

Table A.3. Summary of Direct Tension Test Results for Aerated Autoclaved Concrete Domes

	Specimen	Tile Dimension (in.)	Load Rate (in./min)	Ult. Tensile Load (lbs)	Tensile Stress (psi)
Bonded	1	4x4x1.25	0.5	67	13
	2	4x4x1.25	0.1	195	39
	3	4x4x1.25	0.1	115	23
	4	4x4x1.25	0.1	74	15
	5	4x4x1.25	0.1	74	15
	6	4x8x1.25	0.1	158	32
				Average (psi):	**23**
Tile only	7	4x4x1.25	0.1	315	63
	8	4x4x1.25	0.1	285	57
	9	4x4x1.25	0.1	185	37
				Average (psi):	**52**